ABSTRACT

Title of Dissertation: MODEL FOLLOWING CONTROL STRATEGIES AND HUMAN INTERFACE TECHNIQUES FOR THE TREATMENT OF TIME DELAY DURING TELEOPERATION

Sarah Hall, Doctor of Philosophy, 2004

Dissertation directed by: Associate Professor Robert M. Sanner
Department of Aerospace Engineering

Teleoperation of remotely located space/underwater vehicles requires the human operator to interact with time delayed vehicle responses to issued commands. This often results in the adoption of a "move and wait" strategy whereby the vehicle operator waits to view the results of the previous command before issuing the next command. This work investigates combining a command display (CD) located at the operator control station with a model following controller residing on the remote vehicle to allow the teleoperator to interact with the vehicle in a more seamless manner in time delayed environments.

Command displays differ from more traditional predictive displays in two major ways. First, in a CD system, a trajectory tracking controller is located on the remote vehicle; the teleoperator interacts with an ideal kinematic model

of the vehicle at the control station, with the controller forcing the vehicle to fly the indicated trajectory. Second, model information resides on board the vehicle controller in a CD. In a predictor display system the prediction model is located at the control station.

The utility of implementing a CD on a full 6 DOF dynamic simulation of an underwater remotely operated vehicle (UROV) is examined. The task involves 18 subjects maneuvering the UROV through an obstacle course. Sensitivity of the CD to model accuracy is addressed, i.e. does implementation of a vehicle controller capable of adaptation in the presence of model uncertainty improve performance. Successful implementation of an adaptive CD is demonstrated.

Results indicate that the CD is instrumental in improving performance for teleoperated systems with signal transmission delays as seen by decreased completion times, improved accuracy and more consistent use of hand controllers. In addition, the CD proves surprisingly robust to model inaccuracy when time delay is present. On the other hand, results indicate that implementation of a CD may be contraindicated in the absence of time delay. There is evidence that discrepancies between the actual and desired vehicle due to controller accuracy may have confused the test subjects. Task completion times are higher and subjects are less accurate when the CD is implemented with no time delay.

MODEL FOLLOWING CONTROL STRATEGIES AND HUMAN INTERFACE TECHNIQUES FOR THE TREATMENT OF TIME DELAY DURING TELEOPERATION

by

Sarah Hall

Dissertation submitted to the Faculty of the Graduate School of the
University of Maryland at College Park in partial fulfillment
of the requirements for the degree of
Doctor of Philosophy
2004

Advisory Committee:

Associate Professor Robert M. Sanner, Chairman/Advisor
Associate Professor David L. Akin
Adjunct Professor Craig R. Carignan
Assistant Professor Benjamin Shapiro
Associate Professor Paul J. Smith

DEDICATION

To my families: both West and East coast.

ACKNOWLEDGEMENTS

It's been quite a ride and I've met many incredible people along the way. Many thanks Dave for the chance to be a member of the lab and and the opportunity to participate in so many exciting activities. It is with great sorrow that I relinquish my "Dive Queen" crown to... Brian? Rob, I am indebted to you for your patience and guidance throughout this process (not to mention all the proofreading!). Thanks also to the remaining members of my committee: Craig, Dr. Shapiro and Dr. Smith who spent countless hours patiently explaining the subtleties involved with statistical analysis to me.

Kiwi and Glen, thanks so much for your friendship and invaluable assistance with programming. I have learned much from both of you. Suneel and Brook, my comrades in arms, you have been excellent sounding boards and great friends. I can only hope that I have given back a fraction of what I've gained from you.

Applause and much appreciation are due all of my test subjects: Cat, Daniel, Dave, Emily, Eric, Jamie, Jeff B., Jeff C., Jeff S., Kristin, Matt, Meg, Mike, John, Pete, Rob, Suneel, Tony, Vegard and Wendy. You volunteered many long hours to help me and I am grateful.

I'd also like to thank my family in California including my sister-in-law, Brenda, who provided a home away from home and starred in the roles of head cheerleader and enthusiastic proofreader. In addition many thanks to my adopted family in Maryland. I consider myself fortunate to have found such a fantastic circle of friends in Maryland.

GO TERPS!!!!

TABLE OF CONTENTS

LIST OF TABLES

LIST OF FIGURES

Chapter 1

Introduction

The combination of greater computational capability and miniaturization of associated hardware permits increasingly complex remote operations in the space and underwater environments. However, for humans to successfully perform remote operations in such environments the issue of time delayed operation must be addressed. Two available strategies include teleoperation, in which a human operator interacts directly with the vehicle, or fully autonomous operation of a vehicle. Both approaches have advantages and disadvantages associated with them. Teleoperation enables a human operator to have more direct input during vehicle operations which provides flexibility to the system particularly when addressing unplanned scenarios which may arise during a mission. As an example, consider an underwater vehicle scanning the seabed for a debris field. A human operator can quickly decide to adjust the course if something of interest appears at the edge of the screen.

Unfortunately, teleoperation under time delay can be frustrating to the human operator, and if the time delay is great enough, destabilizing to the system. Autonomous operations require less human interaction on an immediate basis and are unaffected by time delay since all control decisions occur onboard the

vehicle. However, they may not be as immediately adaptable to unexpected events as teleoperated vehicles with current state of the art.

This thesis provides a bridge between teleoperation and autonomous operation of a remote vehicle while addressing the time delay issue. A command display is implemented which assists time delayed teleoperation by appearing to remove time delay from the operator loop. The command display is coupled with autonomous controllers which reside on the vehicle, thus reducing the effect of time delay in the vehicle loop. This composite system will be evaluated on a six degree of freedom (DOF) simulation of a free-flying vehicle performing canonical maneuvering tasks.

With a command display the pilot interacts with a kinematic simulation of the vehicle which provides immediate visual feedback of the vehicle state resulting from operator commands. There is an implicit trust issue associated with this arrangement. For optimal performance the operator must be confident that the actual vehicle will accurately track the displayed state. If this trust isn't present, the pilot will interact directly with the (time-delayed) state of the actual vehicle and the communication link delays will be reinserted into the pilot feedback loop. Several different controllers are included in this study to investigate the effect of model accuracy on pilot performance.

1.1 The Time Delay Issue

Time delay poses a challenge which must be addressed for successful long distance remote operations. Transmission delays occur when commands are sent over great distances, and are typical of remotely operated vehicles such as those used in space or for deep underwater operations. Figure 1.1 shows a simplified block

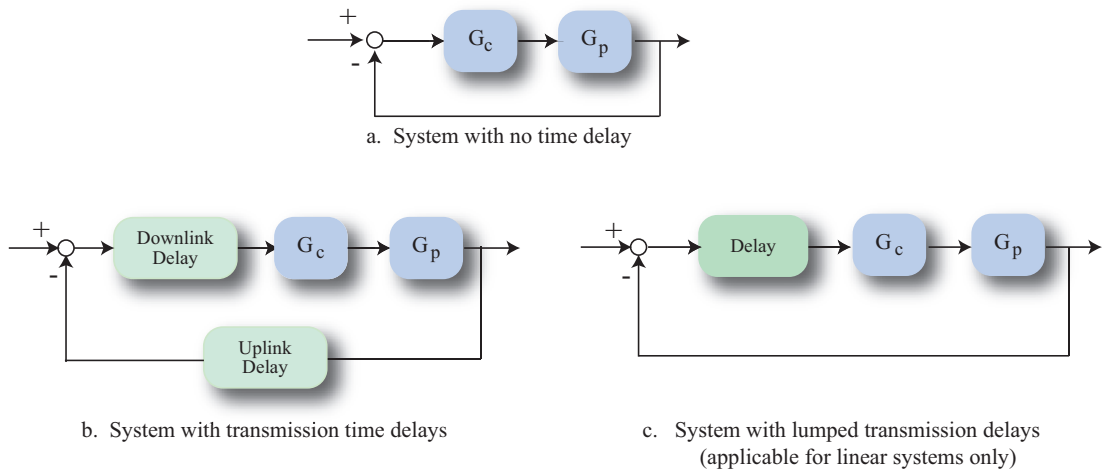

Figure 1.1: Simplified Block Diagrams Demonstrating Placement of Transmission Time Delays.

diagram to demonstrate where signal transmission time delays typically enter a system. Transmission delays actually reside in both the communications uplink and downlink when signals are transmitted from the control station to the vehicle as shown in Figure 1.1b. However, since stability criteria for linear systems are not reliant on whether delay elements exist in the forward or feedback loop (Sheridan, 1993, pg. 593), it is often easier to lump these delays together as shown in Figure 1.1c when the stability of linear systems is addressed. Time delay affects system stability by appearing as pure negative phase in the feedback loop. If the time delay is great enough, a system which exhibits stable performance under conditions of no time delay can become unstable as a result of the addition of too much negative phase to the system.

Even if the system is stable, overall performance can suffer due to time delay if the task is visually oriented with a human operator issuing commands. Early studies performed by Ferrell (1965) and Sheridan and Ferrell (1963) at MIT

examined the effect time delay had on visual tasks involving master and slave manipulators. During their experiments, they discovered that by far the most common method adopted by test subjects to compensate for the transmission delay was to use a "move and wait" strategy, whereby the subject would move the master arm open loop and wait for visual feedback from the slave arm at the work site. While this strategy presents one approach to dealing with time delay, it is not necessarily a satisfactory solution to the problem; as task difficulty increases, so does the amount of time required to complete the task since the "move and wait" strategy depends on the number and duration of operator commands.

1.2 Dealing with Time Delay

1.2.1 Internal Prediction

One method of compensating for time delay is to provide the system operator with extensive training on the system to be used. This essentially "trains" the human to anticipate the effect of delay. As observed in Warner (1969, pg. 12-13)

> The human operator has shown considerable talent in predicting the response of fairly complicated systems with which he has had a great deal of training. The tossing of a ball to a target is an example in which his experience has given him predictive abilities which are usually sufficient. However, we may note that as the distance or duration of the toss is increased, his accuracy worsens, in part due to the deterioration of his predictive abilities. This type of behavior is represented in the predictive model of the human operator proposed by Sheridan (1966) in which, conceptually at least, a fast-time analog model of the

> controlled element is formed by the operator. This model is necessarily not perfect; therefore prediction accuracy will deteriorate with increases in the required prediction span. Hence, a common strategy in throwing a ball at a target is to throw it hard. This has the effect of shortening the required prediction time span, and allowing an inaccurate model to produce less error.

While the tossing of a ball against a wall represents a relatively simple task, it provides an illustration of the role of a human as a predictor. Humans develop internal models for all systems they interact with. Thus, with sufficient training, they are able to form an internal prediction about how a system will respond to their commands. Unfortunately, the incorporation of non-negligible time delay into a task disrupts this internal model and results in a rapid decrease in operator performance, even for simple tracking tasks. Even relatively short time delays of less than a second can cause a complete breakdown of the operator's internal model to the point where the "move and wait" type strategy is adopted. While this may enable the operator to complete the task eventually, it is probable that the time required to do so will become prohibitive.

Studies have been conducted to determine the effect time delay has on the human operator performance. Warrick (1949) used a compensatory pursuit tracking experiment to examine the effect transmission control lags had on operator performance for time delays ranging from 0 to 0.32 seconds. It was discovered that operators had an increasingly difficult time maintaining their cursor on the target as time delay increased. Even when subjects were unable to determine if a time lag existed, it appeared that their performance suffered from the case in which no delay was involved. Studies performed by Conklin (1957) also indicate

decrease in performance as time delay increases.

1.2.2 Computer Assisted Prediction

1.2.2.1 Prediction Displays

In the 1960s efforts were undertaken to develop methods to allow the human operator to better perform tasks in which time delay is a factor. Due to computer limitations of the time, control of such systems was manual. A seemingly natural solution was to supplement the human's internal model with some sort of immediate visual feedback through the use of a *predictive* display. The immediate feedback provided by a computer-based predictor would decrease the mental workload of the operator by reducing his need to rely upon and constantly update his internal model.

A schematic representation of a predictor display is illustrated in Figure 1.2. Operator commands are transmitted to both the predictor model and the actual vehicle. The predictor model is a dynamics based representation of the vehicle which extrapolates the expected system response at an accelerated rate and displays the results on the predictor display. The actual system response is also displayed to the operator after the requisite time delays. Early predictor systems implemented rudimentary system "models" consisting of a Taylor series extrapolation of the dynamics.

Figure 1.3 demonstrates that even crude predictions are of assistance to an operator. This study comparing effectiveness of various orders of Taylor series predictors on a third order undamped system was performed by Bernotat and Widlok (1966b) on skilled subjects. This system had no time delay and used a fast time model to predict system performance into the future. The measure of

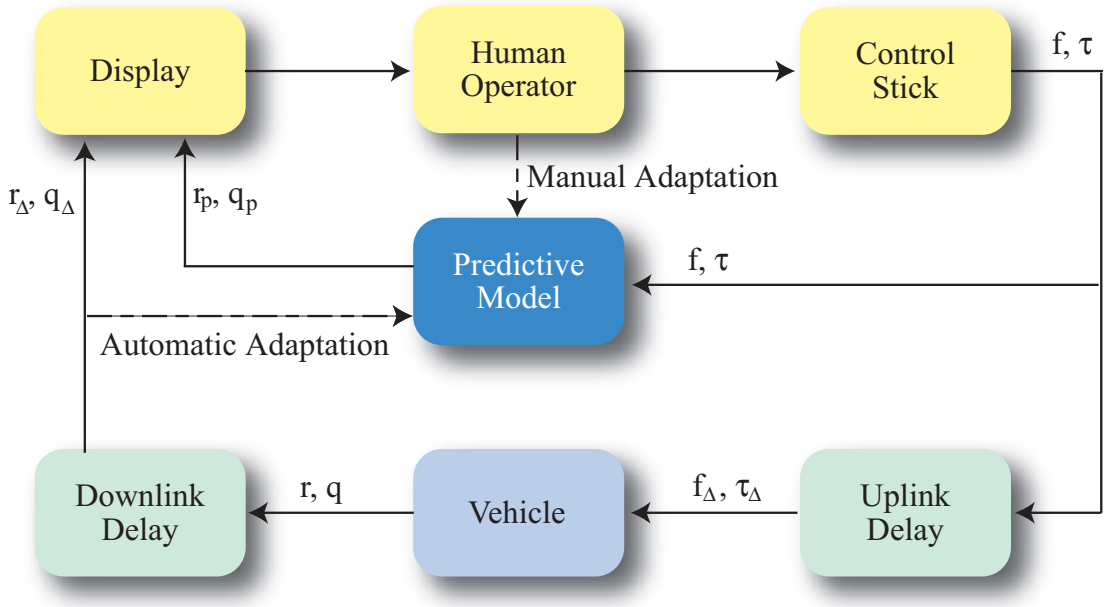

Figure 1.2: Predictor Display Block Diagram.

performance was error as determined by the root mean square of the difference between the actual and command values for the controlled variable.

$$\tilde{\epsilon} = \sqrt{\frac{1}{T}\int_0^T (x_A - x_C)^2 dt}$$

Baseline performance consists of a zero order Taylor series corresponding to no prediction display and results in a mean error of 5.3. Improvement over this baseline is evident with the other three levels of prediction although the degree of improvement is dependent on the order of the predictor model and the amount of time a prediction is projected into the future.

While the predictor display aids the system operator, its utility is dependent on the system model. If the dynamics associated with the controlled system are quite complex, for example, a detailed dynamic model may not be known (e.g. to account for complex fluid effects). In addition, if system dynamics change

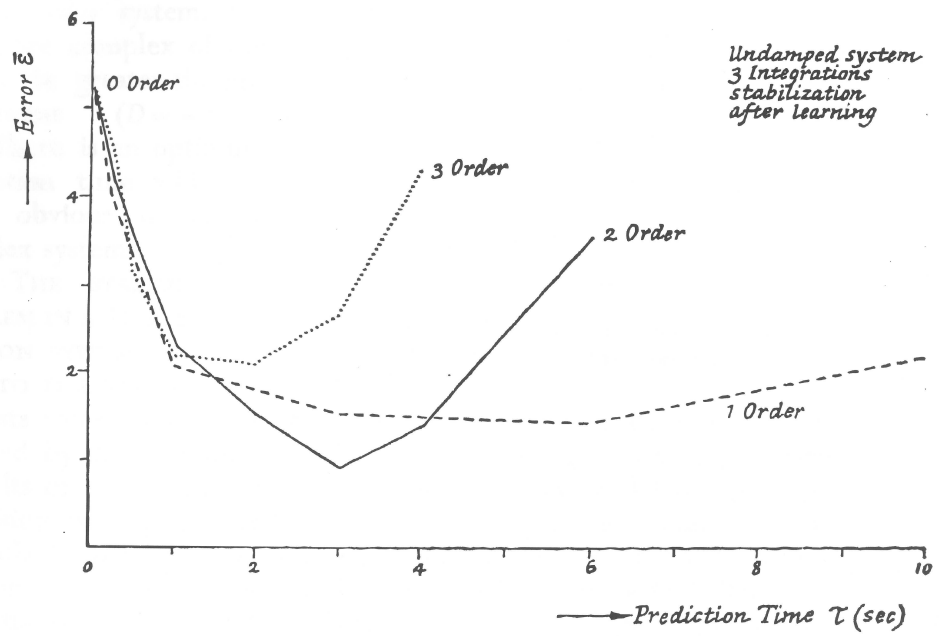

Figure 1.3: Influence of Prediction Time and Order of the Prediction Display. From Bernotat and Widlok (1966b).

suddenly during operation, the predictor model will no longer agree with the dynamic model. Preliminary studies implementing *adaptive predictive* displays was conducted in the early 1970's to address these issues and will be reviewed in Chapter 2.

1.2.2.2 Command Displays

While predictor displays have proven useful in time delayed teleoperation the technology has a major shortcoming associated with it. If the actual vehicle dynamics change it may become necessary to update the predictor model to reflect this. In order for an adaptive predictor to autonomously correct for errors in the assumed model the local prediction must be synchronized in time with the delayed vehicle data. This synchronization can be difficult when the amount of time delay is not known exactly.

A time stamped record of all the predictor states must be maintained so that the predictor model is updated with the time delayed vehicle information at the correct time. However, if the length of the time delay is either unknown or variable it can become difficult to adapt the predictor model to the current vehicle dynamics.

Advances in computer capabilities and miniaturization have permitted more sophisticated techniques to be developed to deal with time delays associated with remote operations. One such technology which avoids the complications associated with predictive displays is a *command* display system shown in Figure 1.4. A primary difference between a command display and a predictive display lies in the placement and type of model each system uses. The model used in a *predictive* display is a model of the vehicle dynamics which resides at the control station. The model in a *command* display, however, resides onboard the vehicle in the controller. This collocation of the model with the vehicle makes adaptation of the model insensitive to time delay.

Another difference between the two display methodologies concerns the inputs. In a predictor display system, the human operator provides control inputs such as forces and torques to the vehicle. In a command display system, the operator interacts with a simple kinematic vehicle model to generate an idealized desired trajectory. It is this trajectory that is fed back to the operator in real time as well as transmitted to the vehicle via the appropriate time delays. It is the duty of an autonomous controller onboard the vehicle to accurately track this desired trajectory. Thus the operator essentially plays a video game with the "desired" vehicle motion in real time and is removed from the time delayed vehicle feedback loop. In addition, since the feedback tracking controller resides

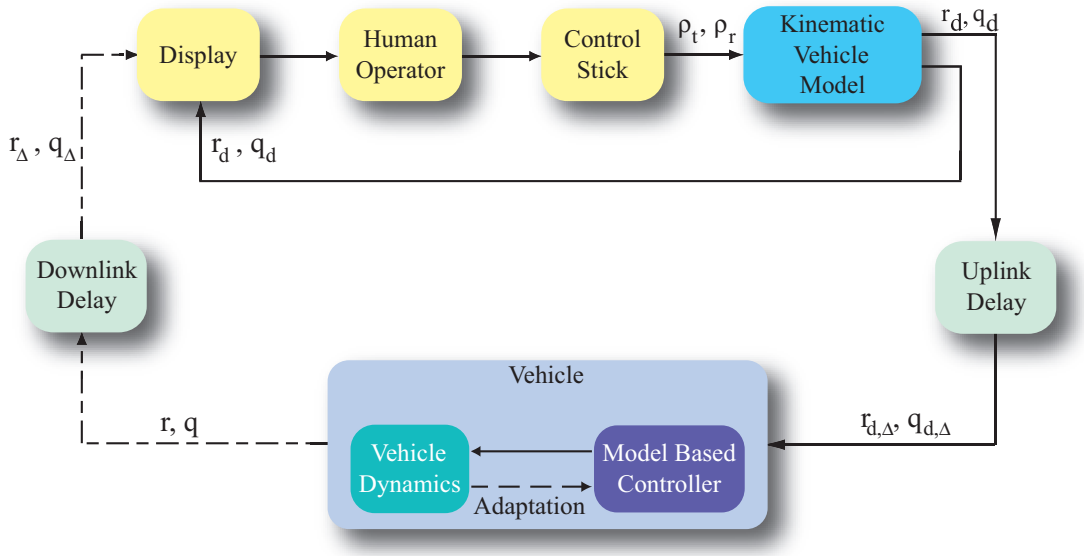

Figure 1.4: Command Display Block Diagram.

on the vehicle, the tracking control loop doesn't experience time delay. If the controller can ensure perfect, or near perfect, tracking, the actual motion of the vehicle will be a time delayed version of the "video game" desired trajectory. Table 1.1 provides a quick reference on the differences between the predictor and command display technologies.

Previous research with command display systems has been performed by Lane

Display Technology	**Location of Vehicle Model**	**Vehicle Inputs**
Predictor	Control Station	$\mathbf{f}$, $\boldsymbol{\tau}$
Command	Vehicle Controller	$\boldsymbol{r}_d, \boldsymbol{q}_d$

Table 1.1: Summary of Differences between Predictor and Command Display Technologies.

(2000) at the University of Maryland using a kinematic computer simulation of the seven degree of freedom Ranger robotic manipulator developed in the Space Systems Lab. Pilot studies compared *predictive* and *command* displays for time delayed systems. While most earlier *predictive* display systems used the prediction model to project vehicle performance to some future time, Lane's predictor model was used to provide real time feedback to the operator. One problem inherent with such a predictive display results from the fact that while pilot generated commands are sent simultaneously to both the predictive model and the actual dynamic system there is no guarantee that they are received by each system in the same amount of time (disregarding any time delay present in the system due to remote operations. This leads to calibration errors in the system. As a result, Lane utilized the *command* display system for his main experiments. Subjects performed much better in trials with the command display when time delay was present than when no command display was available.

Command display systems are now possible due to advances in control technology within the past ten years resulting in the development of a class of *model following* controllers. These controllers incorporate knowledge of vehicle parameters into the control law. The ability to place these more sophisticated control systems at the remote site allows for better system performance in situations where model uncertainty may exist. Work on this type of controller has been conducted by Fjellstad and Fossen (1994); Fjellstad et al. (1992) and Fossen and Sagatun (1991) for application to underwater remotely operated vehicles, and by Egeland and Godhavn (1994) for control of a rigid spacecraft.

1.3 Scope of This Dissertation

To date, an asymmetry exists in the research of predictive/command displays. As can be seen in Figure 1.5 the concept of a predictive system originated in the 1950s with Ziebolz and Paynter (1953). During the 1960s and early 1970s predictor systems were more fully investigated for systems with time delay. Some of the final work in predictive displays during this time involved adaptive predictive displays. No further work in this area is evident until renewed interest arose fueled by the possibility of ground controlled space telerobotics. Research in this area extended through the mid 1990s.

Command display technology was introduced by Lane in the late 1990s. As explained previously, in a command display system the operator is effectively removed from the vehicle loop and interacts with a simple kinematic model of the vehicle in real time. As of yet, there has been no research conducted in the area of an *adaptive command* display. Such a system pairs a vehicle level adaptive controller with the command display technology. This body of work focuses on several issues previously studied for predictor displays but not yet fully investigated with the newer command display technology. The effects of model errors and the possibility of adaptively compensating for model inaccuracies are specifically addressed.

This thesis extends the state of the art in the area of command displays in several ways. It

- clearly delineates the difference between *predictive* and *command* displays,
- utilizes full 6 DOF commanded control for vehicle maneuvers,
- analyses the effect of controller accuracy on the *command* display paradigm,

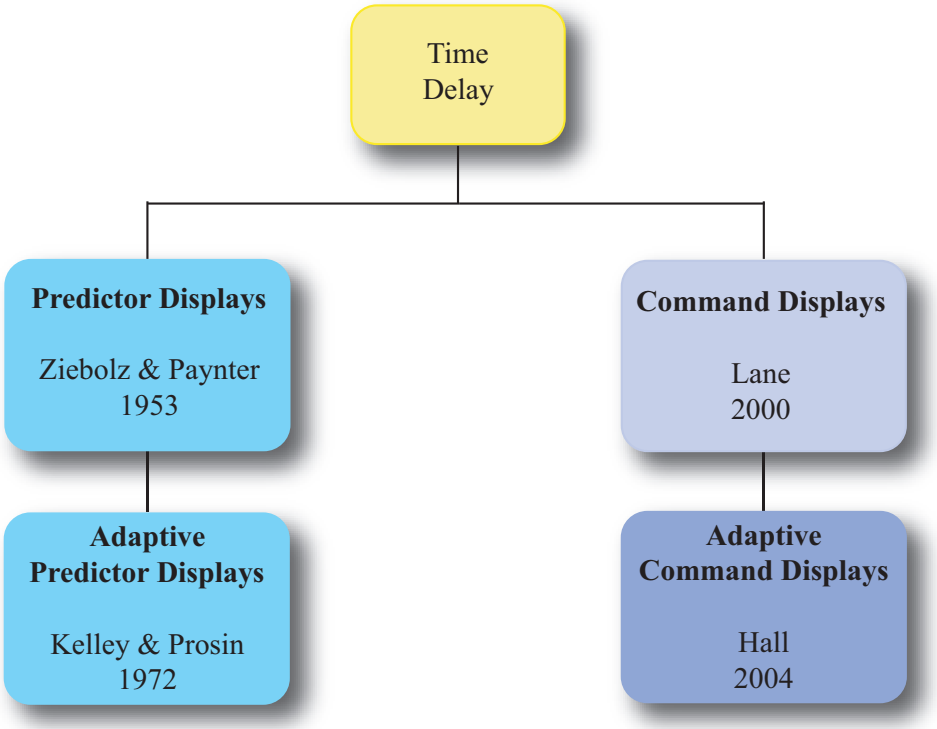

Figure 1.5: Technology for Coping With Time Delay

- determines whether model adaptation is possible in a *command* display system ,
- determines if adaptation in the presence of model uncertainty increases performance and
- addresses the sensitivity of the *command* display paradigm to model accuracy.

The central hypothesis of this thesis is that more capable controllers should allow an operator to place more trust in the real time kinematic simulation and to rely less on the possibly time delayed actual vehicle information. To this end, nonlinear and adaptive controllers should provide superior performance over a

'PD' controller.

Because the Space Systems Lab currently does not have position sensing technology in the Neutral Buoyancy Facility, tests with an actual flight vehicle such as SSV could not be conducted. Thus, a full six degree of freedom dynamic simulation of a free-flying vehicle was developed to provide a test platform for the command display technology issues addressed in this thesis. This simulation was based on SCAMP SSV, a second generation maneuverable camera platform.

1.4 Organization

This thesis is divided into seven chapters. Chapter 2 provides extensive detail of the history of the development of predictor displays and command displays. Chapter 3 develops the necessary dynamic equations of motion for coupled six degree of freedom motion of a rigid vehicle as well as the three controllers used in this work: the 'PD'-like controller, the nonlinear controller and the adaptive nonlinear controller. Chapter 4 provides a description of the computer simulation interface and details the kinematic, dynamic, and graphical computer simulations used in this work. In order to determine the factors most relevant to address in the main study, a pilot study with two test subjects was undertaken. Chapter 5 details this process and presents the pilot study results. Chapter 6 details the main study. Conclusions and future work are discussed in Chapter 7.

Chapter 2

Background

2.1 Overview

Through training, humans develop an internal model of any system with which they interact. With sufficient training, they are able to form an internal prediction about how a system will respond to their commands. The act of driving a car is such an example. The inputs of a student driver (clutch, gas pedal, and steering wheel) may cause the car to move in a jerky manner. As the student gains experience, he develops an intuitive feel for the reaction to his inputs and his driving becomes smoother. In essence he understands the model of the vehicle and can better predict the outcome of his commands. This anticipatory behavior of humans is discussed in Poulton (1957) and Adams (1961). Two studies of prediction in tracking tasks are presented by Gottsdanker (1952, 1955).

Depending on the complexity of the task, this internal model may not be complete enough to provide adequate performance. For instance, a sudden alteration in the system dynamics may result in a discrepancy between the actual system and the internal model. Extending the car example presented above, consider someone driving onto a sheet of black ice or attempting to use the brakes after

driving through a puddle. If the driver doesn't realize he needs to account for the ice or wet brakes he may expect the car to behave in the same manner prior to the disturbance, possibly resulting in an accident.

Disruption in the internal model of the human also occurs when communications delays are incorporated into the system, such as those seen in Figure 1.1 in Chapter 1. Transmission delays occur when commands must be sent over great distances, and are typical of remotely operated vehicles such as those used in space or for deep underwater operations. Early experiments in time delayed operations by Warrick (1949) found that even time delays as small as 60 ms adversely affected subject performance, even if the subjects were unaware of the transmission delay. Sheridan and Ferrell (1963) examined the effect time delay had on visual tasks involving master and slave manipulators (see also Ferrell (1965)). During their experiments, they discovered that by far the most common method adopted by test subjects to compensate for the transmission delay was to implement a "move and wait" strategy, whereby the subject would move the master arm open loop and wait for the visual feedback at the work site. While this strategy presents an approach to dealing with time delay, it is not necessarily a satisfactory solution to the problem; as task difficulty increases, so does the amount of time required to complete the task since the "move and wait" strategy depends on the number and duration of open loop moves.

The remainder of this chapter details concepts developed to address time delayed operations with humans in the loop. The predictor display is discussed and then the more recently developed command display is addressed.

2.2 History of External Predictor Systems

The concept of the predictor system originated with Ziebolz and Paynter (1953) concerning automatic control systems, i.e. those processes which do not involve a human operator in the control loop. They proposed a system which would consist of a computer operating on a time-scale much faster than the actual process occurred. This computer would, at specified intervals, use the current plant variables as its input; it would then calculate the state of the plant at some future time using these current variables. This could offer the controller the opportunity to readjust the gain settings if for some reason the desired parameters were to vary more than the permissible amount.

Ziebolz and Paynter's concept was extended to human in the loop systems in the late 1950s when efforts were undertaken to develop methods to allow the human operator to better perform tasks in which time delay is a factor. Due to computer limitations of the time, control of such systems was manual. Thus, a seemingly natural solution was to supply the system operator with some type of immediate visual feedback through the use of a predictive display. Such immediate feedback through the use of an external predictor would decrease the mental workload of the operator by decreasing his need to rely upon and constantly update his internal model. Some of the earliest work with predictor displays was conducted in the area of submarine controls by Berbert and Kelley (1962) and Kelley (1958, 1960a,b, 1962). While these vehicles do not have signal transmission delays associated with their control systems, they tend to have long dynamic lags which result in large response times. Kelley found that with a predictor instrument a novice could learn to operate a complex control system as well or better than even the most highly skilled operator using standard indicators

in just a short amount of time. This was due to the fact that since the predictor effectively displayed the system dynamics to the operator not as much time was required to develop an internal model of the system. Other work in the application of predictor displays to submarines can be found in McLane and Wolf (1965, 1966, 1967).

In addition to his work with submarines, Kelley et al. (1964) also investigated the application of predictive displays to the control of space vehicles. In this study several different display types were considered. For attitude change or stabilization maneuvers, there was no significant difference in fuel consumption among the various display types. However, when requested to perform attitude tracking or hold maneuvers, performance with the predictor display required 20% less fuel and resulted in 59% less error (RMS) than did the next best display.

Kelley et al. (1966) also investigated whether training with a predictor system would prove beneficial in a simulated orbital docking task obtaining mixed results. They concluded that a combination of control skills training and predictive training appeared more effective than either training method alone. In addition, it was determined that the test techniques used in the project were nonoptimal; it was difficult to separate prediction tasks from control tasks.

The application of predictor displays to the area of orbital rendezvous was investigated by McCoy and Frost (1965, 1966, 1967). They compared the more traditional on-line prediction to off-line prediction, in which an operator could place test inputs into the predictor system and see the results before actually sending the commands to the vehicle. In a simulated Gemini rendezvous task, fuel usage with the off-line predictor was 7-24% less than with the on-line predictor.

During the 1960s the use of predictor systems for planetary rovers was also

investigated. While the remote operation of earth vehicles involves little to no signal transmission delay, the same cannot be said about planetary rovers. An operator of a remote lunar rover would encounter a round trip signal time delay of approximately 2.6 seconds for direct line of sight operations. This prompted an investigation into the handling characteristics of a rover type vehicle as it encountered increasing time delays. One such early study performed by Adams (1962) examined time lags of up to three seconds on tracking and vehicle control to demonstrate the rapid deterioration that occurred in tracking ability as time delay increased. With no time delay, highly trained operators were off course only 2% of the time. Time off course increased to 15% with 0.5 seconds of delay and the vehicle was considered uncontrollable with two seconds of delay since the subjects were off course 75% of the time.

The results of the Adams study prompted Arnold and Braisted (1964) and Braisted (1964) to examine how a predictor display might improve the remote tracking task. This predictor display differed from the more utilized Kelley type predictor in that the prediction was made one round trip into the future only. With this predictor display they were able to successfully maintain control of the Adams vehicle with 2.6 seconds of time delay at about 7 ft per second which was over twice the speed at which Adams found the vehicle to be uncontrollable without benefit of a predictor display. Leslie et al. (1966) extended the Braisted type predictor to a simulated vehicle maneuvering on varying terrain. Other investigation into the benefit of predictor displays was conducted by Kelley (1969) who adapted his fast-time computer model prediction system to lunar/planetary rovers.

There appears to be little work in the area of prediction displays from the

early 1970s until the mid 1980s when Noyes (1984) conducted a study of the first graphic based predictor display for telemanipulation to see if this would aid in time delayed teleoperation. His predictor operated in a manner similar to that of Arnold and Braisted, in that it computed the position of the arm one time delay period in advance. The display consisted of a 'wire-frame' line drawing representing the 'present' configuration of the manipulator arm and was generated by control inputs to a kinematic model of the arm. The predictor display was superimposed on the video picture of the actual arm which was time delayed.

In an attempt to examine a range of tasks which an operator might encounter, two different types of experiments were run. The first task, to pick up blocks and place them in a bin, involved both manipulation and motion. Scoring for this task consisted of time to completion. If all blocks were successfully placed in the box, the score was the actual completion time. A penalty time was incurred for blocks which missed the box. The second task, to trace a predetermined path, involved only motion. Scoring for this task was based on RMS error and time to completion. It was found that the use of undelayed simulated predictor graphics improved subject performance by 50-150% over operation without graphics.

Mar (1985) used Noyes's telemanipulator graphics overlay system to investigate performance of a predictor display on a three-dimensional, time delayed manipulation task. Time delays varying from 0-5.0 seconds were considered. Task completion time served as the measure of performance, with subjects being instructed to complete the task as quickly as possible without making errors. Subjects were able to complete the task 15-20% more quickly when the predictor was used. While subjects still tended to use a "move and wait" strategy with the

predictor, "the number of waiting periods for feedback on the video monitor was reduced and longer distances were covered in each motion" (Mar, 1985, pg. 28). Sometimes subjects demonstrated the ability to combine several motions when using the predictor.

Some work with predictive displays was also undertaken in Japan around this time. Matsumoto (1992) performed experiments using a predictor model which simulated the kinematics and dynamics of a manipulator in real time and displayed a graphical overlay over the actual arm. A 5 DOF manipulator was used to examine the effect that time delays ranging up to 8 seconds would have on pick and place tasks and hole insertion tasks. For the pick and place tasks, use of the predictor display enabled task completion with times only 40-60% greater than the no time delay cases. When no predictor display was available to the operator, it was found that task completion time increased at a rate of approximately 22 seconds for each second increase of time delay. Operation of the joy stick was smooth when used in conjunction with the predictor display; subjects adopted the "move and wait" strategy when no predictor was available. It was also found that the precision of the predictor display was not of high enough quality to be of much assistance in the hole insertion task.

During the mid to late 1980s, the concept of using telemanipulators to perform satellite servicing activities became important. This body of work deals almost exclusively with the prediction of force feedback to the operator, which is not part of the current study. The interested reader is referred to Ferrell (1966), Sheridan (1972), Black (1971), Pennington (1983), Buzan (1989), Kim (1990, 1996), Kim and Bejczy (1991, 1993), Kim et al. (1994), Bejczy and Kim (1990a,b), Bejczy and Kim (1990b), Bejczy et al. (1995), Hannaford and Kim (1989) and Hannaford

(1994) for more information.

2.2.1 Adaptive Predictor Systems

Predictor displays are useful in manual control situations because they preclude the operator from having to rely so heavily on his internal model of the system. The predictor provides the operator the opportunity to receive immediate visual information regarding his inputs to the system. A drawback to the predictor display is that its utility is only as good as the system model. Kelley and Prosin (1971) investigated the utility of an adaptive predictor display in systems in which the vehicle dynamics were altered to varying degrees. "The principle of the adaptive display is to show an operator a path or time history of the output of the controlled element, and a prediction trace of the future of the same variables generated by a fast-time model.... The nature and extent of the departure of the two paths provide diagnostic information regarding the kind of change that has taken place. And the adjustment of the model so that errors in prediction are eliminated completes the adaptive process. The adjustment of the physical model externalizes the adaptive process within the operator." (Kelley and Prosin, 1971, pg. 4). The model adaptation for these experiments was not automatic; rather, the operator manually adjusted parameters to update the predictor model.

The first experiment was performed to determine if the predictor trace on the display would more readily enable an operator to determine whether or not a "stability augmentation failure" had occurred in his system. It was discovered that the predictor, "while of no particular value in reducing the mean time to detect gross failures, did cause a significant alteration in the distribution of the time scores, allowing for significantly quicker detections. Further, the predictor

was of significant value in allowing the subject to adapt to a severely degraded, unstable tracking system." (Kelley and Prosin, 1971, pg. 19). Without the predictor display, the system virtually always went out of control after the failure whereas the subject was able to maintain some sort of control in about half the cases in which the predictor display was implemented.

The next experiment extended the first to determine if an adaptive display would not only assist an operator in the determination of a "stability augmentation failure" but also in diagnosing the extent of the failure. "The second experiment clearly demonstrated that, in simulated failures of a less drastic nature, the presence of adaptive predictor information aided the subject in detecting possible failures or changes in system dynamics. Small changes especially were detected much more quickly with than without the adaptive display." (Kelley and Prosin, 1971, pg. 19). Subjects were also able to much more accurately predict the extent of the failure with the display than without.

Kelley and Prosin (1971) also examined whether an adaptive display might aid in the detection of changes in a control element which were not immediate, but rather occurred over the span of several minutes (such as those due to fuel consumption or changes in trim as a result of a severe temperature gradient). It was found that once again, an adaptive predictor display improved performance. Subjects were "significantly better able to adjust or trim the system with the predictor than with the standard display, and at the same time showed less tracking performance decrement." (Kelley and Prosin, 1971, pg. 43).

A final experiment described in the 1971 report investigated the performance of an adaptive predictor display that adapted automatically to large, moderately fast changes in the dynamics such as those that might occur in a VSTOL aircraft

as it transitions from cruise to hover. Results indicated that while the adaptive predictor display did not improve performance greatly in either mode alone, it does assist an operator during the transitions of the dynamic modes.

Cheng (1991) examined the use of an adaptive predictor for towed submersibles, which are passive underwater vehicles; they are positioned solely via a cable which tethers them to the mother ship. Because these cables may extend for thousands of meters, there are long dynamic lags associated with such systems. Cheng modeled the tow cable as a spring mass system with damping. Adaptation occurred automatically and was implemented in the following manner; after the states of the submersible vehicle were estimated, the predictor adjusted the spring and damping values of the cable via a least-squares method with exponential data-weighting technique to provide for minimum modeling error. System behavior was then simulated at an accelerated rate and displayed to the operator. Cheng's model was implemented in a computer simulation for both a one-dimensional longitudinal tracking task and two-dimensional tracking experiments. Tracking performance was found to improve by around 60% when the adaptive predictor display was used for the one-dimensional tracking task. It was also determined that the duration of the prediction span seemed not to affect control performance; for a given cable length tracking performance was almost identical regardless of the length of prediction.

Cheng's two-dimensional task required the subjects to follow a two-dimensional trajectory. To simplify the task, control subjects were only required to adjust lateral thrust for the surface ship; the forward thrust was fixed at 75% full power. The same prediction time spans and cable lengths of 1,200 and 2,000 meters were used for this series of tests. The same normalized RMS error was

used to evaluate performance. Performance improvements of as much as 50% were seen when the predictor was used. In addition, the predictor span appeared to have some effect on operator performance for this series of tests. From this series of tests it was concluded that length of prediction could affect performance; however, it should be noted that performance with any of the predictor spans indicated a vast improvement over performance without any prediction.

A final experiment performed by Cheng investigated control capability for curved maneuvers. In this task, subjects were instructed to intersect three targets consecutively. Subjects had control of both lateral and longitudinal thrust for the surface ship. Only one pass was allowed at a target and time limits to reach each target were implemented. The same prediction span and cable lengths were used as for the previous experiment. Performance measures for this series of experiments included the success rate for attaining each target and completion time. Success rates to reach targets 2 and 3 improved by about 100% with the use of the predictor display for the 1,200 meter cable, and by about 50% for the 2,000 meter cable. In addition, predictor span appeared to more dramatically affect performance for this type of task than seen previously; performance for the 1,200 meter cable was best with the shortest prediction span and decreased to about 75% of that for the longest prediction span. In addition, operating with the longer cable increased task difficulty. When no predictor display was used, subjects appeared not to be able to reach the third target. Subjects were able to attain the second target 80% of the time for the 3 and 6 minute prediction span whereby performance decreased to only 40% success rate for the 10 minute prediction span. Performance figures for the third target were similar to those for the second. While the use of a predictor display did not demonstrate a significant

difference in the amount of time required to attain target 2, execution time to attain target 3 decreased by approximately 3 minutes if a predictor was used.

2.2.2 Extrapolation Type Predictor Systems

In summarizing the history of prediction displays, there is one other type of predictor that was investigated during the early years of this field and should be mentioned. This alternate method of prediction is termed an extrapolation predictor. Rather than base the prediction on a more complete dynamic model of the vehicle, only the system output information is extrapolated into the future using a Taylor series expansion. Work on this type of predictor was performed by several researchers including Bernotat (1971), Bernotat and Widlok (1966a,b) and Dey (1969, 1971a,b). Dey believed that while the dynamic model based fast-time predictors, such as those developed by Kelly, performed better in cases with prediction times on the order of several seconds, the extrapolation type predictor could be valuable for situations in which short prediction times were required. To this end, he investigated first and second order Taylor series expansions of a third order acceleration system such as might be found in one axis on a VTOL aircraft. While both first and second order predictors improved pilot performance, the second order predictor which provided acceleration information proved more beneficial than the first order predictor which only provided rate information.

Cheng (1991) compared the performance of an extrapolation predictor with that of a fast-time model in his work and found that the fast-time model resulted in better performance. For example, if the RMS prediction error is compared for performance with the 1,200 meter cable and 10 minute prediction span, it is found that the extrapolation method results in an error (200 m) that is a magnitude

of order greater than that arising through the use of the fast-time model (15 m). While this type of predictor could be expected to alleviate some of the mental load placed on a system operator, it suffered from several drawbacks. First, the predictions from an extrapolation type predictor were not as accurate as those for model based predictors since they depend on current vehicle status only. Second, an extrapolation type predictor was only useful for short time delays (as is evidenced by Cheng's work which involves predictor times which span minutes, not seconds). Thus, interest in this method soon waned. It is mentioned here only for completeness.

2.3 Command Displays

A potentially significant problem with a predictive display arises in what Lane (2000) termed calibration errors. The information rate of the predictor display loop is different from that of the time delayed loop in which the time delay may be unknown/variable. Thus it is necessary to keep a time stamped table of the predictor information to maintain calibration between the two systems, otherwise errors will creep into the scene shown to the operator. The command display system conceived of by Lane (2000) at the University of Maryland (and introduced in Chapter 1) avoids this calibration issue. In a command display system the operator issues higher level commands to the vehicle such as a trajectory to follow. It is the responsibility of the controller onboard the remote vehicle to follow these commands.

Lane developed a computer simulation of the Ranger 7 DOF right dexterous manipulator. Note that his work did not contain any dynamic models; rather both the command and "actual" arm were kinematic models. Preliminary tests

compared subject performance using a predictor display to a command display in a modified Fitts' Law task for time delays ranging from 0 to 6 seconds. Results for average task completion time indicate the predictive display was only half as effective at alleviating the effects of time delay as the command display, due to the calibration errors that creep into the predictive display. Thus, the majority of Lane's further testing did not include a predictor display.

Lane tested a number of different variables in his experiments including manipulator speed, sampling rate and varying amounts of time delay. While dynamics were not specifically addressed in his work, he did make an effort to examine the effects of errors in the system, introducing both random and fixed offset errors into the system. The erroneous command displays, while still more useful than no command display, showed decreased benefit as error increased.

Lane found that throughout his experiments, time delay was a critical parameter in subject performance. A linear relationship was discovered between completion time and time delay throughout the series of tests. The command display was successful in eliminating up to 91% of completion time increases resulting from the presence of time delay in the system. In addition, subjects used the command display to detect and correct impacts more rapidly than when the command display was unavailable.

Command display technology is relatively new and has not been analyzed as extensively as the predictor display. The goal of this thesis is to close this gap by

- examining the effect of model accuracy,
- examining the possibility of adaptive model tuning and
- performing more comprehensive testing of the command display paradigm

with realistic dynamic models and tasks.

2.4 Summary

This chapter has endeavored to provide a background into the technology of predictor and command displays. Other strategies exist for dealing with time delayed systems but are not applicable to this body of work. Some of these strategies include completely autonomous control, supervisory control (Backes, 1992, 1994; Backes et al., 1996), shared control (Hayati and Venkataraman, 1989) and teleprogramming (Funda, 1991; Paul et al., 1992). This is by no means an exhaustive list but should provide a starting point for the interested reader.

Chapter 3

Dynamics and Control of Rigid Spacecraft

3.1 Equations of Motion

The two governing equations of motion for a rigid body consist of first, the kinematic equations which describe motion of a vehicle independent of the forces causing that motion and second, the dynamic equations which describe the accelerations of a body as a result of forces applied to that body. In their most general form, the equations of motion of a six DOF rigid body vehicle can be represented in the following manner

$$\boldsymbol{H}(\boldsymbol{\eta})\dot{\boldsymbol{\nu}} + \boldsymbol{C}(\boldsymbol{\eta},\boldsymbol{\nu})\boldsymbol{\nu} + \boldsymbol{E}(\boldsymbol{\eta},\boldsymbol{\nu}) = \boldsymbol{u} \tag{3.1}$$

$$\dot{\boldsymbol{\eta}} = \boldsymbol{J}(\boldsymbol{\eta})\boldsymbol{\nu} \tag{3.2}$$

where Equation (3.1) presents the dynamics in Hamiltonian form. $\boldsymbol{H} \in \mathcal{R}^{6x6}$ represents the generalized mass matrix, $\boldsymbol{C} \in \mathcal{R}^{6x6}$ describes the accelerations (Coriolis, centripetal, etc.) caused by the relative motion of the various degrees of freedom, and $\boldsymbol{E} \in \mathcal{R}^{6}$ represents the generalized forces and torques applied to the system by the environment. The control forces and torques supplied by the vehicle are denoted by $\boldsymbol{u}$.

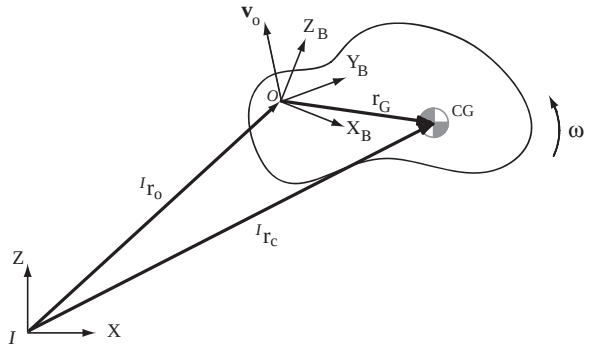

Figure 3.1: Coordinate Frame Definitions for a Rigid Body.

The vehicle kinematics are described in Equation (3.2) where $\boldsymbol{J(\eta)} \in \mathcal{R}^{7x6}$ transforms the body-fixed coordinate frame (B-frame) to the inertial coordinate frame (I-frame). In addition, $\boldsymbol{\eta}$ represents the vehicle configuration variables with respect to some fixed reference frame, usually the I-frame, and $\boldsymbol{\nu}$ is a vector containing the generalized velocity variables.

$$\boldsymbol{\eta} = \begin{bmatrix} {}^{I}\boldsymbol{r}_o \\ \boldsymbol{q} \end{bmatrix} \tag{3.3}$$

The configuration variables defining vehicle position and orientation are shown in Figure 3.1. ${}^{I}\boldsymbol{r}_o$ represents the position of the origin of the vehicle frame of reference to the inertial frame of reference. Description of the vehicle orientation is somewhat more ambiguous. While numerous methods are available to describe the attitude of a vehicle, many of these representations may experience singularities for some vehicle orientations. One method which avoids these singularities is the Euler axis and angle parameterization which is based upon the fact that for any given B-frame orientation only a single rotation about a specific axis is required to align it with the I-frame. This angle, known as the Euler angle, represents the smallest angular distance between the two frames. The axis about

which the rotation takes place is called the Euler axis. Unfortunately, while this method is singularity free, it may prove cumbersome for real-time computations since it involves computation of trigonometric functions. Fortunately there exists an alternative method of attitude representation which is much less computationally expensive but is still based upon the Euler axis/angle formulation. This method implements a quaternion which is a four element vector formulated from the Euler method such that

$$\boldsymbol{q} = \begin{bmatrix} \boldsymbol{\epsilon} \\ \eta \end{bmatrix} = \begin{bmatrix} \sin\frac{\varphi}{2}\boldsymbol{a} \\ \cos\frac{\varphi}{2} \end{bmatrix}$$

where $\boldsymbol{q}$ is the quaternion, $\boldsymbol{a}$ is the Euler axis, and φ is the Euler angle (Wertz, 1978, pg. 414).

The velocity variables are defined as follows, where ${}^{B}\boldsymbol{v}_o$ describes the translational velocity of the origin of the body frame with respect to the body frame and ${}^{B}\boldsymbol{\omega}$ the rotational velocity of the vehicle with respect to the body frame.

$$\boldsymbol{\nu} = \begin{bmatrix} {}^{B}\boldsymbol{v}_o \\ {}^{B}\boldsymbol{\omega} \end{bmatrix} \tag{3.4}$$

The above dynamic and kinematic equations are more fully detailed in the following sections. For the rest of this chapter, the relevant frame for a variable is superscripted immediately prior to the variable as shown above.

3.1.1 Kinematic Equations of Motion

Equation (3.2) above can be represented in its corresponding translational and rotational components as

$$\dot{\boldsymbol{\eta}} = \begin{bmatrix} {}^{I}\dot{\boldsymbol{r}}_o \\ \dot{\boldsymbol{q}} \end{bmatrix} = \begin{bmatrix} \boldsymbol{R}_{ib}(\boldsymbol{q}) & \boldsymbol{0}_{3\,\mathrm{x}\,3} \\ \boldsymbol{0}_{4\,\mathrm{x}\,3} & \boldsymbol{J}_r(\boldsymbol{q}) \end{bmatrix} \begin{bmatrix} {}^{B}\boldsymbol{v}_o \\ {}^{B}\boldsymbol{\omega}_b \end{bmatrix} \tag{3.5}$$

where $\boldsymbol{r}_o \in \mathcal{R}^3$ describes the position of the origin of the vehicle frame in the I-frame coordinates, $\boldsymbol{q}$ describes the vehicle orientation with respect to a fixed reference frame and $\boldsymbol{v}$ and $\boldsymbol{\omega}$ are the translational and rotational velocities respectively as measured in the B-frame.

The rotation matrix $\boldsymbol{R}_{bi}$ transforms the linear velocity from the I-frame to the B-frame and is defined in terms of Euler parameters as

$$\boldsymbol{R}_{bi}(\boldsymbol{q}) = (\eta^2 - \boldsymbol{\epsilon}^T\boldsymbol{\epsilon})\boldsymbol{I} + 2\boldsymbol{\epsilon}\boldsymbol{\epsilon}^T - 2\eta\boldsymbol{S}(\boldsymbol{\epsilon}). \tag{3.6}$$

Because it is an orthogonal matrix $\boldsymbol{R}_{bi}^{-1} = \boldsymbol{R}_{bi}^T = \boldsymbol{R}_{ib}$. In addition

$$\dot{\mathbf{R}}_{bi} = -\boldsymbol{S}({}^B\boldsymbol{\omega})\boldsymbol{R}_{bi}. \tag{3.7}$$

$\boldsymbol{S}$ provides a convenient matrix representation of the cross product vector such that $\boldsymbol{a}$ x $\boldsymbol{b} = \boldsymbol{S}(\boldsymbol{a})\boldsymbol{b}$ where $\boldsymbol{S}(\boldsymbol{a}) = -\boldsymbol{S}(\boldsymbol{a})^{\boldsymbol{T}}$ is a skew-symmetric matrix defined as

$$\boldsymbol{S} = \begin{bmatrix} 0 & -a_3 & a_2 \\ a_3 & 0 & -a_1 \\ -a_2 & a_1 & 0 \end{bmatrix}.$$

$\boldsymbol{J}_r(\boldsymbol{q})$, the rotational portion of the kinematics defined in Equation (3.2), relates the angular velocities to the quaternion

$$\boldsymbol{J}_r(\boldsymbol{q}) = \frac{1}{2}\begin{bmatrix} \eta\boldsymbol{I} + \boldsymbol{S}(\boldsymbol{\epsilon}) \\ -\boldsymbol{\epsilon}^T \end{bmatrix}.$$

3.1.2 Dynamics

The dynamics as described in Equation (3.1) can be written in vector form

$$m\left({}^B\dot{\boldsymbol{v}}_o + {}^B\boldsymbol{\omega} \times {}^B\boldsymbol{v}_o + {}^B\dot{\boldsymbol{\omega}} \times \boldsymbol{r}_G + {}^B\boldsymbol{\omega} \times \left({}^B\boldsymbol{\omega} \times \boldsymbol{r}_G\right)\right) = {}^B\boldsymbol{f}_o$$

$$\boldsymbol{H}_o\,{}^B\dot{\boldsymbol{\omega}} + {}^B\boldsymbol{\omega} \times \left(\boldsymbol{H}_o\,{}^B\boldsymbol{\omega}\right) + m\boldsymbol{r}_G \times \left({}^B\dot{\boldsymbol{v}}_o + {}^B\boldsymbol{\omega} \times {}^B\boldsymbol{v}_o\right) = {}^B\boldsymbol{\tau}_o$$

where $\boldsymbol{r}_G$ is the distance from the body center of mass to the origin of the B-frame and $\boldsymbol{H}_o$ is the inertia matrix about the origin of the B-frame. Recast into the Hamiltonian form Equation (3.1)

$$\boldsymbol{H}(\boldsymbol{\eta}) = \begin{bmatrix} m\boldsymbol{I} & -m\boldsymbol{S}(\boldsymbol{r}_G) \\ m\boldsymbol{S}(\boldsymbol{r}_G) & \boldsymbol{H}_o \end{bmatrix} \tag{3.8}$$

$$\boldsymbol{C}(\boldsymbol{\eta}, \boldsymbol{\nu}) = \begin{bmatrix} m\boldsymbol{S}({}^B\boldsymbol{\omega}) & -m\boldsymbol{S}({}^B\boldsymbol{\omega})\boldsymbol{S}(\boldsymbol{r}_G) \\ m\boldsymbol{S}(\boldsymbol{r}_G)\boldsymbol{S}({}^B\boldsymbol{\omega}) & -\boldsymbol{S}(\boldsymbol{H}_o^B\boldsymbol{\omega}) \end{bmatrix} \tag{3.9}$$

Notice that C is a skew symmetric matrix. If the center of mass of the vehicle coincides with the B-frame coordinate origin, $\boldsymbol{H}$ and $\boldsymbol{C}$ reduce to

$$\boldsymbol{H}(\boldsymbol{\eta}) = \begin{bmatrix} m\boldsymbol{I} & 0 \\ 0 & \boldsymbol{H}_o \end{bmatrix} \tag{3.10}$$

$$\boldsymbol{C}(\boldsymbol{\eta}, \boldsymbol{\nu}) = \begin{bmatrix} m\boldsymbol{S}({}^B\boldsymbol{\omega}) & 0 \\ 0 & -\boldsymbol{S}(\boldsymbol{H}_o^B\boldsymbol{\omega}) \end{bmatrix} \tag{3.11}$$

where $\boldsymbol{H}$ is now a constant, symmetric, positive definite matrix.

3.1.3 External Forces and Torques

The external forces and torques acting upon an underwater vehicle are different from those acting upon a space vehicle. Space vehicles must compensate for gravity gradient forces, solar pressure, and aerodynamic drag. While underwater vehicles are also affected by gravity, they operate in an environment that is much more viscous than space resulting in much larger drag forces and torques that are highly nonlinear and coupled. These environmental forces and torques can be broken up into their component parts

$$\boldsymbol{E} = \boldsymbol{E}_d + \boldsymbol{E}_g + \boldsymbol{E}_b \tag{3.12}$$

where $\boldsymbol{E}_d$ represents drag forces and torques, $\boldsymbol{E}_g$ forces and torques arising due to gravity and $\boldsymbol{E}_b$ forces and torques due to vehicle buoyancy effects.

A commonly used approach in modeling vehicle drag is to consider that the vehicle is symmetric about all three axes, and is undergoing uncoupled motion. In addition, terms of greater than second order are ignored (Fossen, 1994, pg. 43). This allows use of the following second order model to approximate water drag effects on the vehicle.

$$\boldsymbol{E}_d = \begin{bmatrix} \boldsymbol{f}_d \\ \boldsymbol{\tau}_d \end{bmatrix} = \begin{bmatrix} \boldsymbol{C}^B_{d_v} \boldsymbol{v}_o |^B \boldsymbol{v}_o| \\ \boldsymbol{C}^B_{d_\omega} \boldsymbol{\omega} |^B \boldsymbol{\omega}| \end{bmatrix} \tag{3.13}$$

where $\boldsymbol{C}_{d_v} \in \mathcal{R}^{3x3}$ is a diagonal matrix which contains the translational coefficients of drag with units of $\frac{kg}{m}$ and $\boldsymbol{C}_{d_\omega} \in \mathcal{R}^{3x3}$ is a diagonal matrix containing the rotational coefficients of drag and has units of $kg\,m^2$.

The underwater environment results in additional forces acting on the vehicle which are not present in space vehicles. These forces, termed hydrostatic forces, arise because in addition to the gravitional force acting upon the center of mass of the vehicle, the water exerts an upward force on the vehicle which acts at the center of buoyancy. Figure 3.2 presents a schematic of the vehicle with the associated buoyancy and gravitational forces represented.

Using this figure as a guide, the buoyancy and gravitational forces on the vehicle can be written as

$$\begin{aligned} \boldsymbol{f}_b &= b\boldsymbol{R}_{bi}(-{}^I\hat{\boldsymbol{k}}) \\ \boldsymbol{f}_g &= mg\boldsymbol{R}_{bi}\,{}^I\hat{\boldsymbol{k}} \end{aligned}$$

where g is the gravitational constant and b is the magnitude of the buoyancy

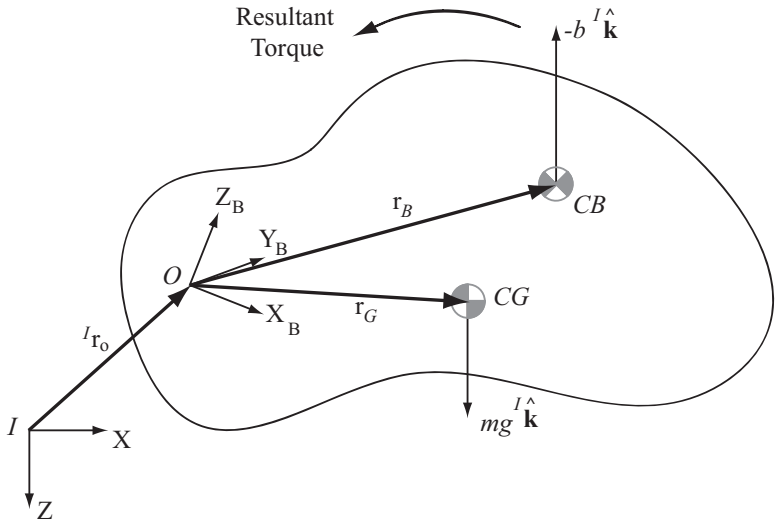

Figure 3.2: Forces Acting on a Submersible Vehicle.

force. The above equations rewritten in B-frame coordinates are

$$\begin{aligned} \boldsymbol{f}_b &= -b\,{}^B\hat{\boldsymbol{k}} \\ \boldsymbol{f}_g &= mg\,{}^B\hat{\boldsymbol{k}} \end{aligned}$$

where ${}^B\hat{\boldsymbol{k}}$ is the z component of the inertial vector rotated into the body frame. It should be noted that if the vehicle is depth neutral, $b = mg$.

Since the vehicle center of gravity does not often coincide with the coordinate origin of the B-frame a resultant torque must be accounted for.

$$\begin{aligned} \boldsymbol{\tau}_g(\boldsymbol{q}) &= \boldsymbol{r}_G \times \boldsymbol{f}_g \\ &= mg\,(\boldsymbol{r}_G \times {}^B\hat{\boldsymbol{k}}) \end{aligned}$$

$\boldsymbol{r}_G$ is the location of the center of gravity with respect to the origin of the B-frame as seen in Figure 3.2.

Generally the vehicle center of mass and center of buoyancy do not coincide with each other, resulting in a torque which rotates the vehicle until the center

of buoyancy resides directly above the center of gravity. This can also be seen in Figure 3.2. The external torque acting upon the vehicle due to the buoyancy force is

$$\begin{aligned} \boldsymbol{\tau}_b(\boldsymbol{q}) &= \boldsymbol{r}_b \times \boldsymbol{f}_b \\ &= -b\,(\boldsymbol{r}_b \times {}^B\hat{\boldsymbol{k}}) \end{aligned}$$

where $\boldsymbol{r}_b$ represents the location of the point of application of the buoyancy force with respect to the origin of the B-frame.

The environmental forces and torques due to gravity and buoyancy effects on the vehicle can be rewritten in matrix form as

$$\boldsymbol{E}_g = \begin{bmatrix} \boldsymbol{f}_g \\ \boldsymbol{\tau}_g(\boldsymbol{q}) \end{bmatrix} = \begin{bmatrix} mg\,{}^B\hat{\boldsymbol{k}} \\ mg\,\boldsymbol{S}({}^B\hat{\boldsymbol{k}})\boldsymbol{r}_G \end{bmatrix} \tag{3.14}$$

and

$$\boldsymbol{E}_b = \begin{bmatrix} \boldsymbol{f}_b \\ \boldsymbol{\tau}_b(\boldsymbol{q}) \end{bmatrix} = \begin{bmatrix} -b\,{}^B\hat{\boldsymbol{k}} \\ -b\boldsymbol{S}({}^B\hat{\boldsymbol{k}})\boldsymbol{r}_b \end{bmatrix}. \tag{3.15}$$

3.2 Control Algorithms

The following sections discuss the error metrics involved in tracking control followed by the three controllers implemented in this study: a 'PD' like controller; a nonlinear controller; and an adaptive nonlinear controller. For a more detailed presentation of the material presented here consult Sanner (2001).

3.2.1 Tracking Control Error Metrics

There are three frames of reference which must be considered to follow a commanded 6 DOF trajectory: the inertial, or reference frame; the body frame; and

the desired frame. These three frames are shown in Figure 3.3. The desired

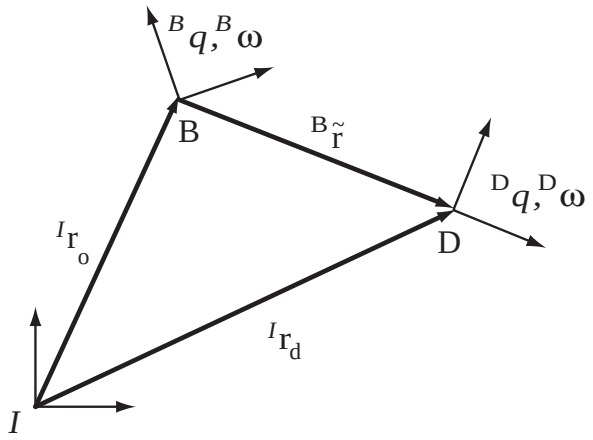

Figure 3.3: Coordinate Frame Representations

velocities as shown in Equation (3.16) can be supplied by either a pilot or an artificial intelligence planning system.

$$\boldsymbol{\nu}_d = \begin{bmatrix} {}^{I}\boldsymbol{v}_d \\ {}^{D}\boldsymbol{\omega}_d \end{bmatrix} \tag{3.16}$$

Desired position and orientation are obtained by integrating

$$\dot{\boldsymbol{\eta}}_d = \begin{bmatrix} {}^{I}\dot{\boldsymbol{r}}_d \\ \dot{\boldsymbol{q}}_d \end{bmatrix} = \begin{bmatrix} {}^{I}\boldsymbol{v}_d \\ \boldsymbol{J}_r(\boldsymbol{q}_d)^{D}\boldsymbol{\omega}_d \end{bmatrix}. \tag{3.17}$$

The discrepancy between the desired and actual vehicle/body frames results in the error metrics used by the controllers. If the D-frame kinematics are specified as in Equation (3.17) and the actual vehicle variables $\boldsymbol{\eta}$ and $\boldsymbol{\nu}$ are specified as in Equations (3.3) and (3.4), then the error in vehicle configuration, $\tilde{\boldsymbol{\eta}}$, is defined as

$$\tilde{\boldsymbol{\eta}} = \begin{bmatrix} {}^{B}\tilde{\boldsymbol{r}} \\ \tilde{\boldsymbol{\epsilon}} \end{bmatrix} = \begin{bmatrix} \boldsymbol{R}_{bi}(\boldsymbol{q})({}^{I}\boldsymbol{r}_o - {}^{I}\boldsymbol{r}_d) \\ \tilde{\boldsymbol{\epsilon}} \end{bmatrix}. \tag{3.18}$$

$\tilde{\boldsymbol{\epsilon}}$ represents the vector portion of the error quaternion $\tilde{\boldsymbol{q}}$. The error quaternion corresponds to the rotation required to bring the actual attitude described in the B-frame into alignment with the desired attitude expressed in the D-frame and is defined as

$$\tilde{\boldsymbol{q}} = \boldsymbol{Q}(\boldsymbol{q}_d^{-1})\boldsymbol{q} \tag{3.19}$$

with

$$\boldsymbol{Q}(\boldsymbol{q}_d^{-1}) = \begin{bmatrix} \eta_d \boldsymbol{I} - \boldsymbol{S}(\boldsymbol{\epsilon}_d) & -\boldsymbol{\epsilon}_d \\ \boldsymbol{\epsilon}_d^T & \eta_d \end{bmatrix}.$$

The accompanying velocity errors, $\tilde{\boldsymbol{\nu}}$, which describe the difference between desired and actual velocities can be written as

$$\tilde{\boldsymbol{\nu}} = \begin{bmatrix} {}^B\tilde{\boldsymbol{v}} \\ {}^B\tilde{\boldsymbol{\omega}} \end{bmatrix} = \begin{bmatrix} {}^B\boldsymbol{v}_o - \boldsymbol{R}_{bi}(\boldsymbol{q})^I\boldsymbol{v}_d \\ {}^B\boldsymbol{\omega} - \boldsymbol{R}_{bd}(\tilde{\boldsymbol{q}})^D\boldsymbol{\omega}_d \end{bmatrix}$$

which can be rewritten in a more convenient form as

$$\tilde{\boldsymbol{\nu}} = \boldsymbol{\nu} - \boldsymbol{T}(\boldsymbol{q}, \boldsymbol{q}_d)\boldsymbol{\nu}_d \tag{3.20}$$

where $\boldsymbol{\nu}$ are the actual vehicle velocities in the B-frame, $\boldsymbol{\nu}_d$ are the desired velocities and $\boldsymbol{T}$, the appropriate rotation matrices as shown below.

$$\boldsymbol{T}(\boldsymbol{q}, \boldsymbol{q}_d) = \begin{bmatrix} \boldsymbol{R}_{bi}(\boldsymbol{q}) & \boldsymbol{0} \\ \boldsymbol{0} & \boldsymbol{R}_{bd}(\tilde{\boldsymbol{q}}) \end{bmatrix}$$

If a "reference velocity", $\boldsymbol{\nu}_r$, is defined as

$$\boldsymbol{\nu}_r = \boldsymbol{T}(\boldsymbol{q}, \boldsymbol{q}_d)\boldsymbol{\nu}_d - \lambda\tilde{\boldsymbol{\eta}}$$

then a composite error metric can be defined as the difference between the actual and the reference velocity.

$$\begin{aligned} \boldsymbol{\sigma} &= \boldsymbol{\nu} - \boldsymbol{\nu}_r \\ &= \tilde{\boldsymbol{\nu}} + \lambda\tilde{\boldsymbol{\eta}} \end{aligned} \tag{3.21}$$

where $\lambda > 0$.

3.2.2 'PD' Control

One of the simplest controllers to implement for these systems is a 'PD'- like controller. Let the control input

$$\boldsymbol{u} = -\boldsymbol{K}_d\tilde{\boldsymbol{\nu}} - \boldsymbol{K}_p\tilde{\boldsymbol{\eta}} = -\boldsymbol{K}_d\boldsymbol{\sigma} \tag{3.22}$$

where $\boldsymbol{K}_d$ is a positive definite diagonal gain matrix and $\boldsymbol{K}_p = \boldsymbol{K}_d\lambda$ with $\lambda > 0$ scalar.

This controller is similar in structure to the classical linear PD controller often used but neither the proportional nor the derivative terms are linear in the controller used in Equation (3.22). For instance, note that the since the error measure for spacecraft angular velocity is a reflection of the nonlinear kinematics associated with the vehicle, it is not actually the derivative of the error measure for spacecraft attitude. An advantage of the 'PD'-like controller is that it is easily implemented.

If position regulation is desired

$$\begin{aligned} \boldsymbol{q}_d &= \text{constant} \Rightarrow {}^D\boldsymbol{\omega}_d = 0 \\ \boldsymbol{r}_d &= \text{constant} \Rightarrow {}^I\boldsymbol{v}_d = 0 \end{aligned}$$

and environmental disturbances are ignored ($\boldsymbol{E} = 0$), the dynamic equation becomes

$$\boldsymbol{H}\dot{\boldsymbol{\nu}} + \boldsymbol{C}\boldsymbol{\nu} = -\boldsymbol{K}_d\tilde{\boldsymbol{\nu}} - \boldsymbol{K}_p\tilde{\boldsymbol{\eta}}. \tag{3.23}$$

Then it can be shown that the above 'PD'-like control law is globally asymptotically stable in the sense of Lyapunov. Choose as a Lyapunov function

$$\boldsymbol{V} = \frac{1}{2}\tilde{\boldsymbol{\nu}}^T\boldsymbol{H}\tilde{\boldsymbol{\nu}} + K_p\left[||\tilde{\boldsymbol{\epsilon}}||^2 + (\tilde{\eta} - 1)^2 + ||{}^I\tilde{\boldsymbol{r}}||^2\right] \tag{3.24}$$

and note that since the desired velocities are identically zero $\tilde{\boldsymbol{\nu}} = \boldsymbol{\nu}$. For the stability proof, consider K_p to be scalar. Taking the derivative of $\boldsymbol{V}$:

$$\dot{\boldsymbol{V}} = \boldsymbol{\nu}^T H \dot{\boldsymbol{\nu}} + K_p \left[2\tilde{\boldsymbol{\epsilon}}^T \dot{\tilde{\boldsymbol{\epsilon}}} + 2(\tilde{\eta} - 1)\dot{\tilde{\eta}} + {}^I\tilde{\boldsymbol{r}}^T \left(\frac{d}{dt} {}^I\tilde{\boldsymbol{r}} \right) \right].$$

Substituting $\boldsymbol{H}\dot{\boldsymbol{\nu}}$ from Equation (3.23) along with

$$\dot{\tilde{\eta}} = -\frac{1}{2} \tilde{\boldsymbol{\omega}}^T \boldsymbol{\epsilon} \tag{3.25}$$

and noting that since $\boldsymbol{C}$ is a skew symmetric matrix $-\boldsymbol{\nu}^T \boldsymbol{C} \boldsymbol{\nu} = \boldsymbol{0}$ results in

$$\begin{aligned} \dot{\boldsymbol{V}} &= \boldsymbol{\nu}^T \left[-\boldsymbol{C}\boldsymbol{\nu} - \boldsymbol{K}_d \tilde{\boldsymbol{\nu}} - K_p \tilde{\boldsymbol{\eta}} \right] + K_p \left[\tilde{\boldsymbol{\epsilon}}^T \tilde{\boldsymbol{\omega}} + {}^I\tilde{\boldsymbol{r}}^T {}^I\tilde{\boldsymbol{v}} \right] \\ &= -\boldsymbol{\nu}^T \boldsymbol{K}_d \boldsymbol{\nu} - K_p \boldsymbol{\nu}^T \tilde{\boldsymbol{\eta}} + K_p \tilde{\boldsymbol{\epsilon}}^T \tilde{\boldsymbol{\omega}} + K_p {}^I\tilde{\boldsymbol{r}}^T ({}^I\tilde{\boldsymbol{v}}) \end{aligned} \tag{3.26}$$

It can further be shown that $\dot{\boldsymbol{V}}$ simplifies to

$$\begin{aligned} \dot{\boldsymbol{V}} &= -\boldsymbol{\nu}^T \boldsymbol{K}_d \boldsymbol{\nu} \\ &\leq 0 \end{aligned} \tag{3.27}$$

since

- from Equations (3.4) and (3.18)

$$-K_p \boldsymbol{\nu}^T \tilde{\boldsymbol{\eta}} = -K_p \left[{}^B\boldsymbol{v}^T {}^B\tilde{\boldsymbol{r}} + \boldsymbol{\omega}^T \tilde{\boldsymbol{\epsilon}} \right],$$

- the final term of Equation (3.26) can be transformed into the B-frame

$$\begin{aligned} K_p ({}^I\tilde{\boldsymbol{r}})^T ({}^I\tilde{\boldsymbol{v}}) &= K_p (\boldsymbol{R}_{bi}^T {}^B\tilde{\boldsymbol{r}})^T (\boldsymbol{R}_{bi}^T {}^B\tilde{\boldsymbol{v}}) \\ &= K_p^B \tilde{\boldsymbol{r}}^T (\boldsymbol{R}_{bi} \boldsymbol{R}_{bi}^T) {}^B\tilde{\boldsymbol{v}} \\ &= K_p^B \tilde{\boldsymbol{r}}^T {}^B\tilde{\boldsymbol{v}}. \end{aligned}$$

Since $\dot{\boldsymbol{V}}$ is not a function of the complete state of $\boldsymbol{V}$, asymptotic stability cannot be guaranteed by using Lyapunov's direct method. Rather, use of LaSalle's invariant set theorem (Khalil, 1996, pg. 115) allows us to show (almost) global asymptotic stability via

$$\tilde{\eta} \rightarrow 0 \text{ as } t \rightarrow \infty. \tag{3.28}$$

As mentioned previously, 'PD'-like controllers ignore the environmental dynamics associated with the $\boldsymbol{E}$ matrix in Equation (3.1). The gains $\boldsymbol{K}_p$ and $\boldsymbol{K}_d$ can be "tuned" with "disturbances" in mind through the use of semi-classical techniques (e.g. step response); however, if the environmental dynamics are understood system performance can be improved by including them in the control law. In addition, 'PD' control may be insufficient to ensure adequate performance and stability if a tracking task is required. For example, consider a system with some unknown disturbance $\boldsymbol{d}(t)$. If $\boldsymbol{d}(t)$ is bounded, it can be seen from Sanner (2001) that the position accuracy is

$$\|^I \tilde{\boldsymbol{r}}_o \|_{rms} \leq \frac{\| \boldsymbol{d} \|_{rms}}{K_d' \lambda}$$

and pointing accuracy can be expressed as

$$\| \tilde{\boldsymbol{\epsilon}} \|_{rms} \leq \frac{\| \boldsymbol{d} \|_{rms}}{K_d' \lambda}$$

where K_d' is the smallest eigenvalue of $\boldsymbol{K}_d$. Greater accuracy and/or larger disturbance rejection can be achieved by increasing the gains. Unfortunately, this may lead to saturation of the control actuators and so may not be feasible. Two control methods which take environmental disturbances into account and demonstrate good tracking ability are discussed in the following sections.

3.2.3 Model-Based Control

If the system parameters and dynamics are well known, it is possible to implement a nonlinear feedback controller using this information. If the control input as shown in Equation (3.29)

$$\boldsymbol{u} = \boldsymbol{H}(\boldsymbol{\eta})\dot{\boldsymbol{\nu}}_r + \boldsymbol{C}(\boldsymbol{\eta},\boldsymbol{\nu})\boldsymbol{\nu}_r + \boldsymbol{E}(\boldsymbol{\eta},\boldsymbol{\nu}) - \boldsymbol{K}_d\boldsymbol{\sigma} \tag{3.29}$$

is substituted into Equation (3.1) the closed loop dynamics can be rewritten as

$$\boldsymbol{H}(\boldsymbol{\eta})\dot{\boldsymbol{\sigma}} + \boldsymbol{C}(\boldsymbol{\eta},\boldsymbol{\nu})\boldsymbol{\sigma} + \boldsymbol{K}_d\boldsymbol{\sigma} = \boldsymbol{0} \tag{3.30}$$

$$\tilde{\boldsymbol{\nu}} + \lambda\tilde{\boldsymbol{\eta}} = \boldsymbol{\sigma}. \tag{3.31}$$

As with the 'PD' controller, $\boldsymbol{K}_d$ is positive definite.

The above closed loop system can be shown to be globally stable and capable of asymptotically perfect tracking by using a Lyapunov-like analysis (Khalil, 1996; Slotine and Li, 1991). Much of the following derivation is from (Sanner, 2001). Consider the quadratic, positive definite function of $\boldsymbol{\sigma}$

$$\boldsymbol{V} = \frac{1}{2}\boldsymbol{\sigma}^T\boldsymbol{H}\boldsymbol{\sigma} \tag{3.32}$$

with $\boldsymbol{V}$ lower bounded, radially unbounded ($\boldsymbol{V} \to \infty$ as $||\boldsymbol{\sigma}|| \to \infty$) and continuously differentiable. The derivative can be written as

$$\dot{\boldsymbol{V}} = \boldsymbol{\sigma}^T\boldsymbol{H}\dot{\boldsymbol{\sigma}} + \frac{1}{2}\boldsymbol{\sigma}^T\dot{\boldsymbol{H}}\boldsymbol{\sigma}. \tag{3.33}$$

Substituting $\boldsymbol{H}\dot{\boldsymbol{\sigma}}$ from Equation (3.30) and rearranging terms results in

$$\dot{\boldsymbol{V}} = -\boldsymbol{\sigma}^T\boldsymbol{K}_d\boldsymbol{\sigma} + \frac{1}{2}\boldsymbol{\sigma}^T(\dot{\boldsymbol{H}}. - 2\boldsymbol{C})\boldsymbol{\sigma}$$

Because $\boldsymbol{H}$ is a constant matrix, $\dot{\boldsymbol{H}} = \boldsymbol{0}$. Earlier it was demonstrated that $\boldsymbol{C}$ is skew symmetric. Therefore the second term is a quadratic function of a skew

matrix which is identically equal to zero. Thus,

$$\dot{\boldsymbol{V}} = -\boldsymbol{\sigma}^T \boldsymbol{K}_d \boldsymbol{\sigma}. \tag{3.34}$$

Since $\boldsymbol{K}_d$ is a constant positive definite matrix, $\dot{\boldsymbol{V}}$ is a negative definite function of $\boldsymbol{\sigma}$. If the Lyapunov function is upper and lower bounded such that

$$\lambda_{min}(\boldsymbol{K}_d)||\boldsymbol{\sigma}||^2 \leq \boldsymbol{V}(\boldsymbol{\sigma}) \leq \lambda_{max}(\boldsymbol{K}_d)||\boldsymbol{\sigma}||^2$$

where λ_{min} and λ_{max} represent the minimum and maximum eigenvalues of $\boldsymbol{K}_d$ respectively and $\dot{\boldsymbol{V}}$ is upper bounded as demonstrated by

$$\dot{\boldsymbol{V}} \leq \lambda_{min}||\boldsymbol{\sigma}||^2$$

then by Theorem 3.8 and Corollary 3.4 of (Khalil, 1996), $\boldsymbol{\sigma} \rightarrow \mathbf{0}$ exponentially fast from any initial condition.

Briefly digressing, let us define $\mathcal{L}_\infty$ as the space of all bounded functions and $\mathcal{L}_2$ the space of all square integrable functions. Consider a function s.

- s is considered bounded and thereby $s \in \mathcal{L}_\infty$ if

$$||s||_{\mathcal{L}_\infty} = \sup_{t \geq 0} ||s(t)|| < \infty$$

- $s \in \mathcal{L}_2$ if

$$||s||_{\mathcal{L}_2} = \sqrt{\int_0^\infty s^T(t)s(t)dt} < \infty$$

With the above definitions in mind it is now evident that

1. $\boldsymbol{\sigma} \in \mathcal{L}_\infty$ since
   - $\boldsymbol{V}$ is a positive definite function of $\boldsymbol{\sigma}$
   - $\dot{\boldsymbol{V}} \leq \mathbf{0} \Rightarrow \boldsymbol{V}(t) \leq \boldsymbol{V}(t_o) < \infty$

2. $\boldsymbol{\sigma} \in \mathcal{L}_2$ since

- $||\boldsymbol{\sigma}||_{\mathcal{L}_2} = \int_0^t ||\boldsymbol{\sigma}(\tau)||^2 d\tau \leq -\frac{1}{k_o} \int_0^t \dot{\boldsymbol{V}}(\tau) d\tau = \frac{1}{k_o} [\boldsymbol{V}(0) - \boldsymbol{V}(t)]$
- $\frac{1}{k_o} [\boldsymbol{V}(0) - \boldsymbol{V}(t)] \leq \frac{1}{k_o} \boldsymbol{V}(0)$ is finite since $\boldsymbol{V} \geq 0$ always
- as $t \to \infty \quad ||\boldsymbol{\sigma}||_{\mathcal{L}_2} \leq \frac{1}{k_o} \boldsymbol{V}(0) < \infty$

which will be useful later.

In order to demonstrate asymptotically perfect tracking it is also necessary to show that $\tilde{\boldsymbol{r}} \to \mathbf{0}$ and $\tilde{\boldsymbol{\epsilon}} \to \mathbf{0}$. This is most easily accomplished by addressing the translational and rotational equations separately.

$$\boldsymbol{\sigma} = \begin{bmatrix} \boldsymbol{\sigma}_t \\ \boldsymbol{\sigma}_r \end{bmatrix}$$

First, consider the translational portion. From Equation (3.31) it can be shown

$${}^B\tilde{\boldsymbol{v}} + \lambda {}^B\tilde{\boldsymbol{r}} = \boldsymbol{\sigma}_t$$

which can be rewritten in the I-frame as

$${}^I\dot{\tilde{\boldsymbol{r}}} + \lambda {}^I\tilde{\boldsymbol{r}} = \boldsymbol{R}^T(\boldsymbol{q})\boldsymbol{\sigma}_t. \tag{3.35}$$

Since it has been previously demonstrated that $||\boldsymbol{\sigma}|| \to \mathbf{0}$ exponentially fast and

$$||\boldsymbol{R}^T(\boldsymbol{q})\boldsymbol{\sigma}_t|| = [-\boldsymbol{\sigma}_t \boldsymbol{R}(\boldsymbol{q})\boldsymbol{R}^T(\boldsymbol{q})\boldsymbol{\sigma}_t]^{\frac{1}{2}} = ||\boldsymbol{\sigma}_t||,$$

$||\boldsymbol{\sigma}_t|| \to \mathbf{0}$ exponentially.

Equation (3.35) is a stable, first order linear differential equation driven by an exponentially decaying input. Therefore, ${}^I\tilde{\boldsymbol{r}} \to \mathbf{0}$ exponentially fast which implies that ${}^B\tilde{\boldsymbol{r}} \to \mathbf{0}$ exponentially fast.

Next, to consider the rotational portion of Equation (3.31), begin with

$$\tilde{\boldsymbol{\omega}} + \lambda \tilde{\boldsymbol{\epsilon}} = \boldsymbol{\sigma}_r. \tag{3.36}$$

In order to prove stability and asymptotic tracking, it must be shown that

$$\tilde{\boldsymbol{\epsilon}} \in L_\infty \quad \text{and} \quad \tilde{\boldsymbol{\epsilon}} \to \mathbf{0}$$

$$\tilde{\boldsymbol{\omega}} \in L_\infty \quad \text{and} \quad \tilde{\boldsymbol{\omega}} \to \mathbf{0}.$$

The boundedness condition shall be addressed first. As before, since $\boldsymbol{\sigma}$ is bounded and $\boldsymbol{\sigma} \to \mathbf{0}$ exponentially, the same holds true for the subvector $\boldsymbol{\sigma}_r$. Because $\tilde{\boldsymbol{\epsilon}}$ is the vector portion of $\tilde{\boldsymbol{q}}$, the error quaternion, and by definition $||\tilde{\boldsymbol{q}}|| = 1$, $\tilde{\boldsymbol{\epsilon}}$ is bounded. The boundedness of $||\tilde{\boldsymbol{\omega}}||$ is implied because

$$\begin{aligned} ||\boldsymbol{\sigma}_r|| &= \left[(\tilde{\boldsymbol{\omega}} + \lambda\tilde{\boldsymbol{\epsilon}})^T(\tilde{\boldsymbol{\omega}} + \lambda\tilde{\boldsymbol{\epsilon}})\right]^{\frac{1}{2}} \\ &= \left[||\tilde{\boldsymbol{\omega}}||^2 + \lambda^2||\tilde{\boldsymbol{\epsilon}}||^2 + 2\lambda\tilde{\boldsymbol{\omega}}^T\tilde{\boldsymbol{\epsilon}}\right]^{\frac{1}{2}} \end{aligned} \tag{3.37}$$

and it was shown above that $\boldsymbol{\sigma}_r \in \mathcal{L}_\infty$ and $\tilde{\boldsymbol{\epsilon}} \in \mathcal{L}_\infty$.

To show that $\tilde{\boldsymbol{\epsilon}} \to \mathbf{0}$ and $\tilde{\boldsymbol{\omega}} \to \mathbf{0}$ a somewhat abstract form of Barbalat's lemma (Sanner, 1997) can be implemented. This lemma states that if a function $f(t)$ is such that

1. $f \in \mathcal{L}_\infty \cap \mathcal{L}_2$
2. $\dot{f} \in \mathcal{L}_\infty$

then $f(t) \to 0$ as $t \to \infty$.

Addressing the first portion of Barbalat's lemma, it has already been demonstrated above that $\tilde{\boldsymbol{\epsilon}} \in \mathcal{L}_\infty$ and $\tilde{\boldsymbol{\omega}} \in \mathcal{L}_\infty$. To show that $\tilde{\boldsymbol{\epsilon}} \in \mathcal{L}_2$ and $\tilde{\boldsymbol{\omega}} \in \mathcal{L}_2$ begin with Equation (3.37) and recall that $\tilde{\boldsymbol{\omega}}^T\tilde{\boldsymbol{\epsilon}} = -2\dot{\tilde{\eta}}$.

$$\begin{aligned} \int_0^t ||\boldsymbol{\sigma}_r(\tau)||^2 d\tau &= \int_0^t ||\tilde{\boldsymbol{\omega}}(\tau)||^2 dt + \lambda^2 \int_0^t ||\tilde{\boldsymbol{\epsilon}}(\tau)||^2 d\tau + 2\lambda \int_0^t \tilde{\boldsymbol{\omega}}^T(\tau)\tilde{\boldsymbol{\epsilon}}(\tau) d\tau \\ &= \int_0^t ||\tilde{\boldsymbol{\omega}}(\tau)||^2 d\tau + \\ &\qquad \lambda^2 \int_0^t ||\tilde{\boldsymbol{\epsilon}}(\tau)||^2 d\tau - 4\lambda\left[\tilde{\eta}(t) - \tilde{\eta}(0)\right]. \end{aligned} \tag{3.38}$$

Now

- $\tilde{\eta}$ is the scalar portion of the quaternion,
- $4\lambda\left[\tilde{\eta}(t) - \tilde{\eta}(0)\right]$ is finite since $||\tilde{\eta}|| \leq 1$ for any t and
- as $t \to \infty$, since it has been shown that $||\boldsymbol{\sigma}_r|| \in \mathcal{L}_2$ and the constant term in Equation (3.38) is finite,
  - $||\tilde{\boldsymbol{\epsilon}}||_{\mathcal{L}_2} < \infty$
  - $||\tilde{\boldsymbol{\omega}}||_{\mathcal{L}_2} < \infty$

which satisfies the first portion of Barbalat's lemma.

To show that $\tilde{\boldsymbol{\epsilon}} \to 0$ using Barbalat's lemma, it is necessary to show that $\dot{\tilde{\boldsymbol{\epsilon}}} \in \mathcal{L}_\infty$. By examining Equation (3.39)

$$\dot{\tilde{\boldsymbol{\epsilon}}} = \frac{1}{2}[\tilde{\eta}\boldsymbol{I} + \boldsymbol{S}(\tilde{\boldsymbol{\epsilon}})]\tilde{\boldsymbol{\omega}} \tag{3.39}$$

it can be seen that in fact $\dot{\tilde{\boldsymbol{\epsilon}}} \in \mathcal{L}_\infty$ because we have already shown

- $\tilde{\boldsymbol{\epsilon}} \in \mathcal{L}_\infty$ and $\tilde{\eta} \in \mathcal{L}_\infty$
- $\tilde{\boldsymbol{\omega}} \in \mathcal{L}_\infty$

Thus the second portion of Barbalat's lemma is satisfied and $\tilde{\boldsymbol{\epsilon}} \to 0$.

Since it has been shown that $\boldsymbol{\sigma}_r \to \mathbf{0}$ and $\tilde{\boldsymbol{\epsilon}} \to \mathbf{0}$ it follows from Equation (3.36) that $\tilde{\boldsymbol{\omega}} \to \mathbf{0}$.

3.2.4 Adaptive, Nonlinear Control

One of the objectives of this thesis is to evaluate operator performance under conditions of time delay for a vehicle with model terms that may not be well

understood. It is proposed that implementation of an adaptive controller on such a system will improve system performance in a manner similar to that found by (Kelley and Prosin, 1971) with adaptive predictive displays. If vehicle parameters contained in the model are uncertain, but are known to remain either constant or to change only incrementally, a linearly parameterized adaptive controller can be used. Suppose now,

$$\boldsymbol{u} = \hat{\boldsymbol{H}}(\boldsymbol{\eta})\dot{\boldsymbol{\nu}}_r + \hat{\boldsymbol{C}}(\boldsymbol{\eta},\boldsymbol{\nu})\boldsymbol{\nu}_r + \hat{\boldsymbol{E}}(\boldsymbol{\eta},\boldsymbol{\nu}) - \boldsymbol{K}_d\boldsymbol{\sigma} \tag{3.40}$$

where $\hat{\boldsymbol{H}}, \hat{\boldsymbol{C}}$ and $\hat{\boldsymbol{E}}$ are estimates of the actual parameters contained in $\boldsymbol{H}, \boldsymbol{C}$ and $\boldsymbol{E}$. If $\boldsymbol{u}$ is now substituted into the system dynamics as expressed in Equation (3.1) the closed loop dynamics become

$$\boldsymbol{H}\dot{\boldsymbol{\sigma}} + \boldsymbol{C}\boldsymbol{\sigma} + \boldsymbol{K}_d\boldsymbol{\sigma} = (\hat{\boldsymbol{H}} - \boldsymbol{H})\dot{\boldsymbol{\nu}}_r + (\hat{\boldsymbol{C}} - \boldsymbol{C})\boldsymbol{\nu}_r + (\hat{\boldsymbol{E}} - \boldsymbol{E}).$$

The right hand side of the above equation can be written in a more condensed form

$$\boldsymbol{H}\dot{\boldsymbol{\sigma}} + \boldsymbol{C}\boldsymbol{\sigma} + \boldsymbol{K}_d\boldsymbol{\sigma} = \boldsymbol{Y}(\boldsymbol{\eta},\boldsymbol{\nu},\boldsymbol{\nu}_r,\dot{\boldsymbol{\nu}}_r)\tilde{\boldsymbol{a}} \tag{3.41}$$

where $\boldsymbol{Y}$ is a matrix containing known functions of $\boldsymbol{\eta},\boldsymbol{\nu},\boldsymbol{\nu}_r$ and $\dot{\boldsymbol{\nu}}_r$ which are determined by the (known) functional forms of $\boldsymbol{H}$, $\boldsymbol{C}$ and $\boldsymbol{E}$. $\tilde{\boldsymbol{a}}$ represents the difference between the estimated vehicle parameters $\hat{\boldsymbol{a}}$ and the actual physical parameters, $\boldsymbol{a}$.

$$\tilde{\boldsymbol{a}} = \hat{\boldsymbol{a}} - \boldsymbol{a}$$

Equation (3.40) can now be rewritten as

$$\boldsymbol{u} = \boldsymbol{Y}\hat{\boldsymbol{a}} - \boldsymbol{K}_d\boldsymbol{\sigma}. \tag{3.42}$$

To create a real-time adjustment strategy for the estimate, $\hat{\boldsymbol{a}}$, a Lyapunov-like

stability analysis can again be employed. Define

$$\boldsymbol{V} = \frac{1}{2}\boldsymbol{\sigma}^T \boldsymbol{H}\boldsymbol{\sigma} + \frac{1}{2}\tilde{\boldsymbol{a}}^T \boldsymbol{\Gamma}^{-1}\tilde{\boldsymbol{a}} \tag{3.43}$$

where $\boldsymbol{V}$ is once again a positive definite funciton. Taking the derivative of $\boldsymbol{V}$ and substituting $\boldsymbol{H}\dot{\boldsymbol{\sigma}}$ from Equation (3.41) leads to

$$\dot{\boldsymbol{V}} \leq -\boldsymbol{K}_d||\boldsymbol{\sigma}||^2 + \boldsymbol{\sigma}^T \boldsymbol{Y}\tilde{\boldsymbol{a}} + \frac{1}{2}\tilde{\boldsymbol{a}}^T \boldsymbol{\Gamma}^{-1}\dot{\tilde{\boldsymbol{a}}}.$$

Since the actual parameter values are constant, $\dot{\tilde{\boldsymbol{a}}} = \dot{\hat{\boldsymbol{a}}}$ which causes $\dot{\boldsymbol{V}}$ to become

$$\dot{\boldsymbol{V}} \leq -\boldsymbol{K}_d||\boldsymbol{\sigma}||^2 + \boldsymbol{\sigma}^T \boldsymbol{Y}\tilde{\boldsymbol{a}} + \frac{1}{2}\tilde{\boldsymbol{a}}^T \boldsymbol{\Gamma}^{-1}\dot{\hat{\boldsymbol{a}}}.$$

Choosing as the adaptation law

$$\dot{\hat{\boldsymbol{a}}} = -\boldsymbol{\Gamma}\boldsymbol{Y}^T \boldsymbol{\sigma} \tag{3.44}$$

where $\boldsymbol{\Gamma}$ is a positive definite, diagonal matrix of learning gains reduces $\dot{\boldsymbol{V}}$ to

$$\dot{\boldsymbol{V}} \leq -\boldsymbol{K}_d||\boldsymbol{\sigma}||^2, \tag{3.45}$$

demonstrating that $\boldsymbol{\sigma} \rightarrow \boldsymbol{0}$ is more complex than for the nonlinear controller. Now $\dot{\boldsymbol{V}}$ is only negative semidefinite, since it is no longer a function of the full state vector. In other words, $\boldsymbol{V}$ is a function of $\boldsymbol{\sigma}$ and $\tilde{\boldsymbol{a}}$ but $\dot{\boldsymbol{V}}$ is a function only of $\boldsymbol{\sigma}$. Therefore $\dot{\boldsymbol{V}}$ could equal zero regardless of the value of $\tilde{\boldsymbol{a}}$. Once again, Barbalat's lemma provides a tool to show that $\boldsymbol{\sigma} \rightarrow \boldsymbol{0}$ even though $\dot{\boldsymbol{V}}$ is only negative definite. This is developed in Slotine and Li (1991, pg.123).

Once convergence of $\boldsymbol{\sigma}$ has been shown the proofs that ${}^I\tilde{\boldsymbol{r}} \rightarrow \boldsymbol{0}$ and $\tilde{\boldsymbol{\epsilon}} \rightarrow \boldsymbol{0}$ follow as for the nonlinear controller. Note that convergence of ${}^I\tilde{\boldsymbol{r}}$ and $\tilde{\boldsymbol{\epsilon}}$ does not necessarily imply convergence of parameter estimates $\tilde{\boldsymbol{a}}$ to their actual values $\boldsymbol{a}$. The adaptation mechanism finds parameters which drive the tracking error to

zero, but it is possible that many vectors of controller parameters can accomplish this in addition to the true parameter vector, $\boldsymbol{a}$ (Slotine and Li, 1991, pg.331). In order for $\hat{\boldsymbol{a}} \rightarrow \boldsymbol{a}$ the reference signal must satisfy certain requirements termed "persistency of excitation" conditions. These conditions essentially ensure that the reference signal is complex enough that all degrees of freedom are sufficiently exercised and can be summarized as

$$\int_{t}^{t+T} \boldsymbol{Y}^T(\tau)\boldsymbol{Y}(\tau)\mathrm{d}\tau \geq \alpha \boldsymbol{I}$$

where $\boldsymbol{Y}$ is the matrix described previously in Equation (3.41) and α and T are positive constants Sanner (2001). Nevertheless, even if the "persistency of excitation" conditions are not satisfied the nonlinear adaptive controller results in stable performance with theoretically perfect tracking for systems in which the primary uncertainty is due to unknown vehicle parameter values.

3.2.4.1 Adaptation Considerations

In practice, if additional disturbances occur which are unaccounted for in the model terms, then it may become necessary to temporarily halt adaptation. Such disturbances could include collisions with objects in the environment, thruster saturation, currents in the water or sensor noise. There are several instances in which adaptation will temporarily cease.

The first occurs due to the possibility that a parameter estimate could become unbounded. The adaptation law in Equation (3.44) can be adjusted as follows

$$\dot{\hat{a}}_i = P(-\boldsymbol{\Gamma}_i \boldsymbol{Y}_{i,\cdot}^T \boldsymbol{\sigma}, \hat{a}_i, \hat{a}_{i,min}, \hat{a}_{i,max}) \tag{3.46}$$

where P is a "projection operator" which prevents the parameter estimates from becoming unbounded when unplanned disturbances occur, and is defined as in

Ioannou and Sun (1996) such that

$$P(x, y, z_l, z_u) = \begin{cases} x & \text{if} \begin{cases} z_l < |y| < z_u \\ \text{or } y \leq z_l \text{ and } x > 0 \\ \text{or } y \geq z_u \text{ and } x < 0 \end{cases} \\ 0 & \text{else} \end{cases} \tag{3.47}$$

Essentially, adaptation takes place on a parameter as long as $a_{i,min} \leq \hat{a}_i \leq a_{i,max}$. If $\hat{a}_i$ exceeds the allowed bounds its value is reset to the appropriate upper or lower bound until it once again resides in the allowable adaptation range.

The second instance in which adaptation temporarily ceases involves the magnitude of the translational and rotational portions of the error metric, $||\boldsymbol{\sigma}_t||$ or $||\boldsymbol{\sigma}_r||$. As the controller attempts to compensate for the forces and torques resulting from unmodeled disturbances acting on the vehicle, $||\boldsymbol{\sigma}_t||$ or $||\boldsymbol{\sigma}_r||$ may become too large. Adaptation in the simulation halts if *both*

$$\begin{aligned} ||\boldsymbol{\sigma}_t|| &> \boldsymbol{\sigma}_{t,max} \\ ||\boldsymbol{\sigma}_r|| &> \boldsymbol{\sigma}_{r,max}. \end{aligned}$$

These limits were obtained by first examining the values for $||\boldsymbol{\sigma}_t||$ or $||\boldsymbol{\sigma}_r||$ arising from the automatic trajectory generator and then iteratively adjusting them for performance with a human pilot.

A third consideration when using an adaptative controller concerns available control. Control actuators on physical systems are limited in the amount of control authority they are able to supply. Thruster saturation has been included in the SSV dynamic simulation to more provide a more realistic evaluation of the usefulness of an adaptive controller with a command display. While no mechanism was included to specifically stop adaptation during thruster saturation, this is

addressed indirectly through the bounds placed on the error metrics as explained above.

Chapter 4

Vehicle Simulator

To test the premise that command display technology can be of assistance in teleoperation, a suitable teleoperation task was necessary. Thus, a six degree of freedom computer flight simulator of SCAMP SSV was developed. This is an interactive dynamic simulation of SSV which includes the physical characteristics and handling qualities of the actual vehicle.

Sections included in this chapter describe the physical characteristics of SSV, the teleoperation task, the simulation interface and development of the automatic trajectory generation routine which is used for comparison with human performance.

4.1 SCAMP SSV Physical Characteristics

SCAMP SSV pictured in Figure 4.1 is a second generation teleoperated underwater camera platform designed and built in the Space Systems Laboratory at the University of Maryland. It is 26-sided with a 26.5 inch span from thruster to thruster and a mass of 76.2 kg. The inertias were calculated using a simplified

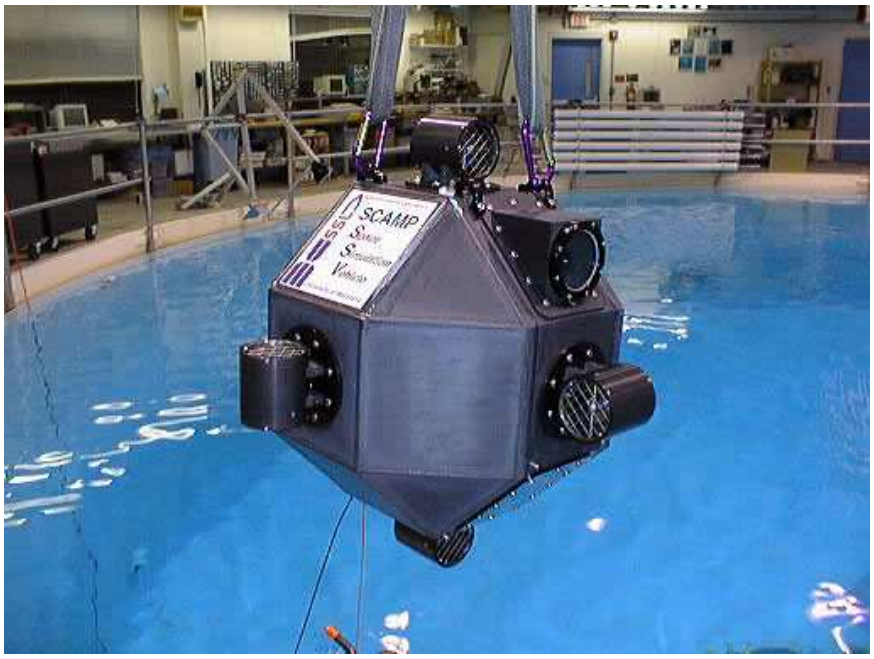

Figure 4.1: Scamp SSV.

model in IDEAS and are listed below.

$$\boldsymbol{H} = \begin{bmatrix} 1.63765 & -0.00126 & 0.00038 \\ -0.00126 & 1.61554 & -0.00003 \\ 0.00038 & -0.00003 & 1.87114 \end{bmatrix} Nm.$$

Since the Space Systems Lab does not currently have the capability of directly measuring the drag parameters of an underwater vehicle, it was necessary to estimate C_d. These estimates were determined using the dynamic equations of motion, addressing translation and rotation separately. Several assumptions concerning the vehicle were made for these calculations including that the vehicle was operating at terminal velocity and that the vehicle was depth neutral. In additon, it was assumed that vehicle translation or rotation occurring along one

axis at a time. Using these simplifications the dynamics can be rewritten as

$$m\dot{v} \simeq f - C_{d_v} v^2. \tag{4.1}$$

Since it is known that for SSV

- $f = f_{max} = 0.75 lb_f \simeq 3.336N$ (per thruster),
- $v = v_{max} \simeq 0.127\, m/s$ and
- $\dot{v} = 0$

at terminal velocity, Equation (4.1) can be rewritten in terms of C_{d_v} as

$$C_{d_v} \simeq \frac{2 f_{max}}{v_{max}^2}$$

noting that there are two thrusters in each direction. The maximum velocity of SSV was determined using the amount of time it took SSV to cross the 50' diameter tank in the lab. Although the propellers used on SSV provide approximately half the thrust in the reverse direction as in the forward direction, the simulation assumed equivalent thrust levels along both directions. Thus it can be seen that for the model above,

$$\boldsymbol{C}_{d_v} \simeq \begin{bmatrix} 413.685 & 0 & 0 \\ 0 & 413.685 & 0 \\ 0 & 0 & 413.685 \end{bmatrix} \frac{kg}{m}.$$

Similarly, the rotational dynamic equation can be manipulated to solve for C_{d_ω} at terminal velocity via

$$C_{d_\omega} \simeq \frac{\tau_{max}}{\omega_{max}^2}$$

where

- $\omega_{max} \simeq 1.34 \frac{rad}{sec}$ from Hossaini (2000),
- $\tau_{max} = 2 f_{max} l$,
- $l = 0.3$ m is the distance from the origin of the body coordinates to the thruster and
- $f_{max} \simeq 3.336$ N as determined above

such that

$$\boldsymbol{C}_{d_\omega} \simeq \begin{bmatrix} 1.114 & 0 & 0 \\ 0 & 1.114 & 0 \\ 0 & 0 & 1.114 \end{bmatrix} kg\, m.$$

It is difficult to balance an underwater vehicle so that it is completely neutral. Therefore the simulation includes an initial buoyancy offset. Since SSV tends to be somewhat light the offset buoyancy force $\Delta B = -0.5$ N was chosen corresponding to $B = 748.05$ Nm. To ascertain where the center of buoyancy might reside, a preferred vehicle orientation as reported during a typical test in Hossaini (2000) was utilized. Using the steady state quaternion (which has been normalized)

$$\boldsymbol{q}_{ss} \simeq \begin{bmatrix} 0.8335 \\ -0.4777 \\ -0.0407 \\ -0.2746 \end{bmatrix},$$

the center of buoyancy as measured in the body coordinate system can be calculated via

$$\boldsymbol{r}_b = |\boldsymbol{r}_b|\, \boldsymbol{R}_{bi}(\boldsymbol{q}_{ss}) \hat{\boldsymbol{k}}_b,$$

where the assumption of a depth neutral vehicle results in

$$|\boldsymbol{r}_b| = B/2$$

and $\hat{\boldsymbol{k}}_b$ is the unit vector along the $\boldsymbol{z}_b$ axis. The resulting offset vector between the buoyancy force acting on the vehicle and the center of gravity of the vehicle is approximately

$$\boldsymbol{r}_b = \begin{bmatrix} -0.2206 \\ -0.280 \\ -0.5655 \end{bmatrix} mm,$$

causing an estimated buoyancy moment of

$$B\boldsymbol{r}_b = \begin{bmatrix} -0.165 \\ -0.209 \\ -0.423 \end{bmatrix} Nm.$$

During initial trials with the simulation, it was determined that the current vehicle rates were too slow to permit repeated testing in a reasonable interval without fatiguing the subjects. Therefore, the nominal vehicle parameter estimates remain as calculated above but the achievable velocities were adjusted. The maximum translational velocity capability of the vehicle was increased to 0.33 m/s. In an attempt to avoid thruster saturation the maximum allowable translational velocity was capped at 75% of the capability (0.25 m/s). In addition, the maximum allowable rotational velocity was capped at 0.5 rad/s. These new velocities were used to estimate the maximum parameter values used in adaptive controller explained below.

$$\boldsymbol{v}_{max_{all}} = \begin{bmatrix} \pm 0.25 \\ \pm 0.25 \\ \pm 0.25 \end{bmatrix} \frac{m}{s}$$

$$\boldsymbol{\omega}_{max_{all}} = \begin{bmatrix} \pm 0.5 \\ \pm 0.5 \\ \pm 0.5 \end{bmatrix} \frac{rad}{s}.$$

4.1.1 Thruster Saturation

All physical systems are limited in the amount of control authority they are capable of delivering. The control actuators on SSV consist of six thrusters distributed such that two thrusters lie parallel to each of the principle axes of the vehicle as seen in Figure 4.1. These thrusters are used to move SSV on command and also to maintain position and orientation when required. Thruster saturation levels are included in the dynamic simulation of SSV to provide a more realistic representation of the control available during operation. The thruster saturation levels were determined using the physical parameters above, and the new maximum translational velocity levels, not the allowable levels.

$$f_{max} = C_{d_v} v_{max}^2 = \pm 45.965\, N \,(\text{per thruster pair})$$

$$\tau_{max} = 2 f_{max} l = \pm 13.7895\, Nm \,(\text{per thruster pair})$$

It can bee seen that ω_{max} as calculated from τ_{max} above corresponds to an even faster rotational rate than the original rate which was deemed overly responsive. Therefore, $\omega_{max_{all}} = 0.5\, \frac{rad}{sec}$ as discussed in the previous section.

4.1.2 Parameter Limits

When the adaptive nonlinear controller is used, the controller estimates for the vehicle parameters are adjusted during operation by the controller as it attempts to "learn" these parameters to achieve better control of the vehicle. As mentioned

previously, unless the system is in a state of persistent excitation, the parameter values determined by the controller will not necessarily correspond to the actual vehicle parameters. Parameter limits have been implemented in the simulation to prevent parameter estimation runaway. Table 4.1 shows the parameters that were chosen for adaptation, their nominal values, as well as the minimum and maximum levels allowed.

Knowledge of the actual physical system was used in an attempt to set reasonable parameter limits without constraining them too tightly. For instance, the mass was easily determined by weighing the vehicle. A lumped model was used to determine the inertial parameters so these were fairly well defined. SSV is a fairly depth neutral vehicle. When in the water, only a few nuts and bolts are used during the balancing procedure to compensate for the air mass contained in the vehicle. Therefore it was decided that ΔB, the nominal difference between the mass and buoyancy forces would be set at -0.5N indicating that the vehicle is positively buoyant. The vehicle buoyancy changes slightly from day to day due to changes in air conditions so the limits were fairly narrow for ΔB.

Since the translational drag parameter, C_{d_v}, had the largest degree of uncertainty, it was restrained less than the other variables. A lower limit corresponding to no drag was assumed and the upper limit was calculated as follows.

$$C_{d_{v\,max}} = \frac{f_{max}}{v^2_{max_{all}}} \simeq 735 \simeq 800$$

As with translational drag, the lower limit for C_{d_ω} assumed no drag. The upper limit for C_{d_ω} was limited to 5 kg-m.

As mentioned in Section 3.2.4.1, controller adaptation is temporarily halted if the magnitude of the translational and rotational portions of the error metric, $||\boldsymbol{\sigma}_t||$ or $||\boldsymbol{\sigma}_r||$ become too large. The limits placed on the error metrics for this

Parameter Type	**"True" Value** a_i	**Minimum Value** $\hat{a}_{i,min}$	**Maximum Value** $\hat{a}_{i,max}$
H_{xx} (Nm)	1.63765	0	5
H_{xy} (Nm)	-0.00126	-0.5	5
H_{xz} (Nm)	0.00038	-0.5	5
H_{yy} (Nm)	1.61554	0	5
H_{yz} (Nm)	-0.00003	-0.5	5
H_{zz} (Nm)	1.87114	0	5
C_{d_ω} (kg m)	1.114	0	5
$B\,r_{b_x}$ (Nm)	$\simeq -0.165$	-2.64	2.64
$B\,r_{b_y}$ (Nm)	$\simeq -0.209$	-2.64	2.64
$B\,r_{b_z}$ (Nm)	$\simeq -0.423$	-2.64	2.64
C_{d_v} (kg/m)	413.685	0	800
ΔB (N)	-0.5	-1.5	1.5
m (kg)	76.2	50	100

Table 4.1: Parameter Values and Limits for Adaptive Estimates. Refer to Equation 3.2.4.1.

study are listed below.

$$\begin{aligned} ||\boldsymbol{\sigma}_t|| &> \boldsymbol{\sigma}_{t,max} = 0.015 \\ ||\boldsymbol{\sigma}_r|| &> \boldsymbol{\sigma}_{r,max} = 0.08. \end{aligned}$$

4.2 Task and Hoop Course

In order to test the underlying hypotheses of this thesis it was necessary to design a task that would require coupled motion in six degrees of freedom. In addition the task must be repeatable as subjects would be required to test over separate sessions. One such task would be to have SSV fly through an obstacle course in the tank. This course could consist of way points marked by hoops that SSV would have to successfully pass through before proceeding to the next hoop/obstacle. Unfortunately there are several implementation problems with this strategy. First, it requires that the tank have a positioning system so that the trajectory of the vehicle can be recorded; such a system is not currently available at SSL. Second, there are several problems associated with a hoop course. It would be almost impossible to ensure that the hoops remain in the same position and orientation throughout the study. Other diving operations might require movement of the hoop and unless the hoops are rigidly mounted to some hard point in the tank there will be some resulting movement of the hoop due to the filtration system, divers, or even the vehicle running into the hoop. As a result of these physical limitations, it was decided to use a computer simulation of SSV so that the task would be as repeatable as possible throughout testing.

It was desired to require the human test subjects to exercise both hand controllers while flying the hoop course. Thus, all course designs are of an irregular

"S" shape and include hoops at varying depths and orientations. During the first iteration of course design, a nine hoop course was conceived that required more varied movements of the hand controllers, but took experienced pilots around three minutes to complete. Since each test condition would require repeated runs, it was decided that this duration would prove too fatiguing to the test subjects and a shorter five hoop test course was designed. The automatic trajectory generator or an experienced pilot can cover this course in less than a minute, thereby allowing for more trials to be completed per test session without fatigue. In addition, during the pilot study a separate three hoop course was utilized for training. This is explained in more detail in Chapter 5.

Schematics of hoop locations for the three hoop training course used only in the pilot study, and the five hoop course used in both the pilot study and the main study are shown in Figure 4.2. The starting point of each course, delineated by an "S", is also indicated. Figures 4.3 and 4.4 show enlarged pictures of the global course views available in the lower left corner of the screen during operation and are included to provide an indication of hoop orientation throughout the course. The hoops were designed as cylinders having a height and thickness of one inch and an inner radius of 18 inches. This allows a 4.75 inch ring of clearance about all the thrusters if SSV were to fly through the center of the hoop. The hoops are numbered in consecutive order and subjects were required to successfully fly through the current hoop before proceeding to the next one.

The hoop course was designed so the operator would have visual indication of the position of the next hoop while flying through the current hoop. This would prevent the subject accruing time while searching for a hoop which might influence results. This was accomplished using two methods; the first was to

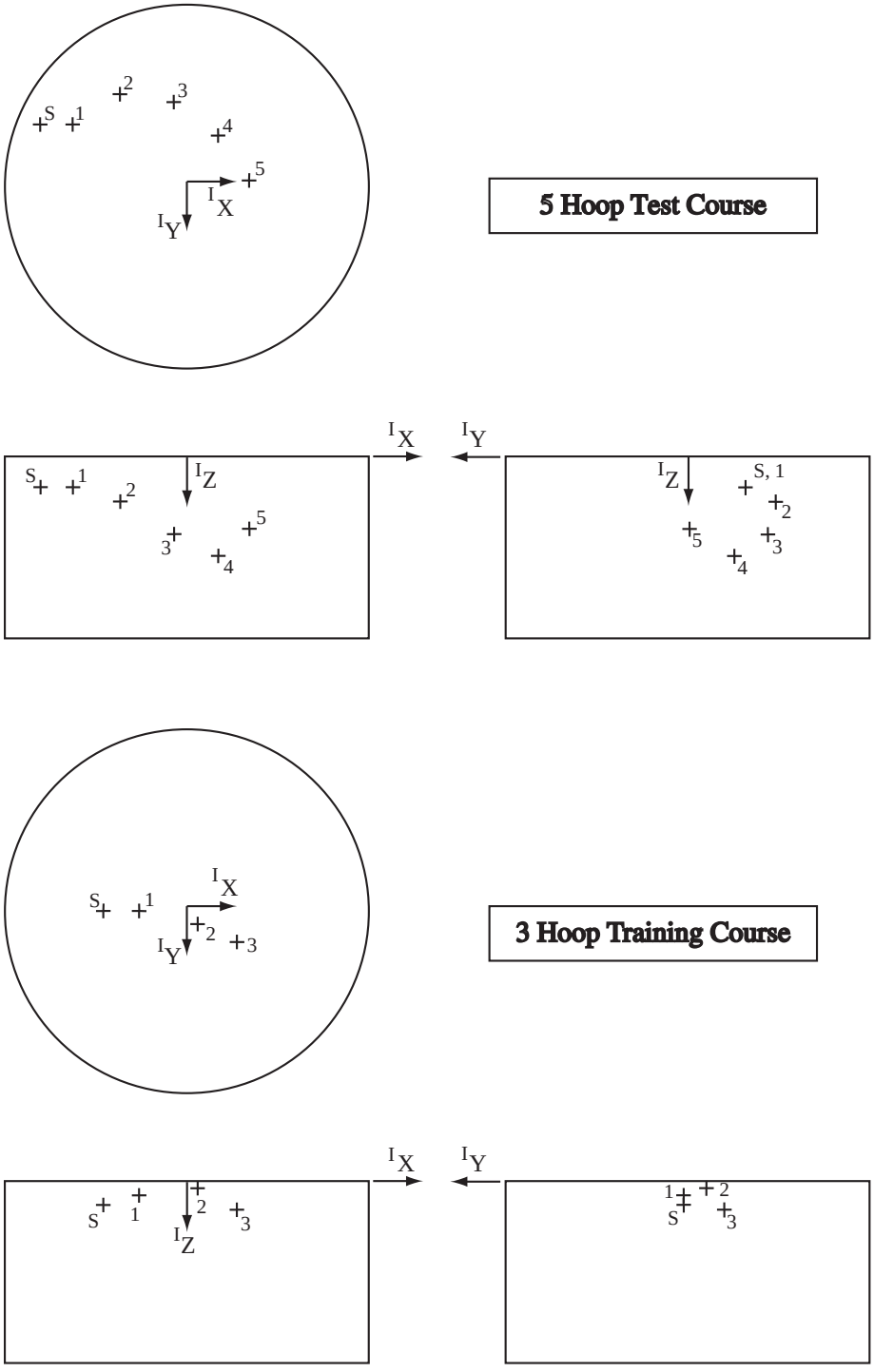

Figure 4.2: 3 Views of Hoop Positions in Tank.

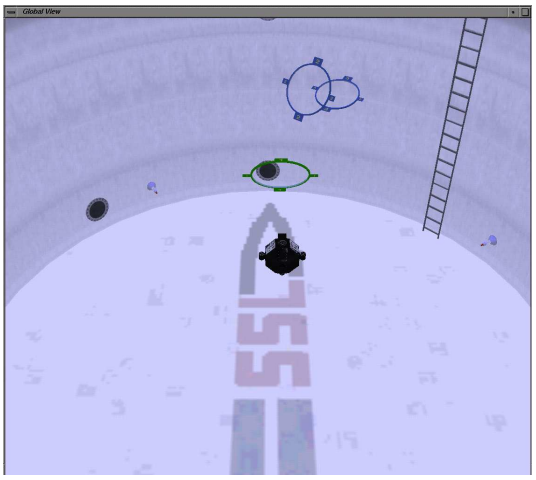

Figure 4.3: Global View of 3 Hoop Training Course Used in Pilot Study.

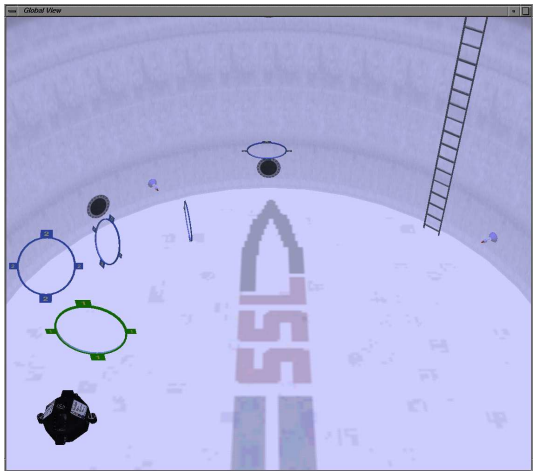

Figure 4.4: Global View of 5 Hoop Testing Course Used in Pilot and Main Studies.

include a window containing the entire test course on the computer monitor, the second was to design the course so that at least part of the next hoop is visible to the operator as they were flying through the current hoop in one or more of the camera views. This feature is demonstrated in Figure 4.5 where the upper right window on the screen shows the view seen by the onboard camera of SSV as it approaches Hoop 3 and the lower left window on the screen shows the entire test course. In addition, the hoops are color coded to assist the operator in determining when he has successfully maneuvered through the current hoop. The current hoop the subject is interacting with is colored green while all remaining hoops are gray. After the center of SSV has passed through the back plane of the current hoop, that hoop shifts back to gray and the next hoop changes to green. The course is considered finished once the center point of SSV has passed through the back plane of the last hoop.

Figure 4.5: SSV Simulation Approaching Hoop 3.

4.2.1 Collisions

To create a simulation environment that more closely resembles the real world, the dynamic simulation of SSV includes the possibility of collision with objects in the virtual environment. For the collision routine SSV was modeled as a sphere with a diameter equal to that of SSV's thruster span. A collision is modeled as a linear spring

$$f = -k\Delta x \tag{4.2}$$

where Δx, the depth of penetration into the ring, corresponds to the length of the spring. The determination of the location and magnitude of the forces and torques acting upon SSV during a collision is computed as follows. There are three frames which must be accounted for in modeling collisions, as shown in

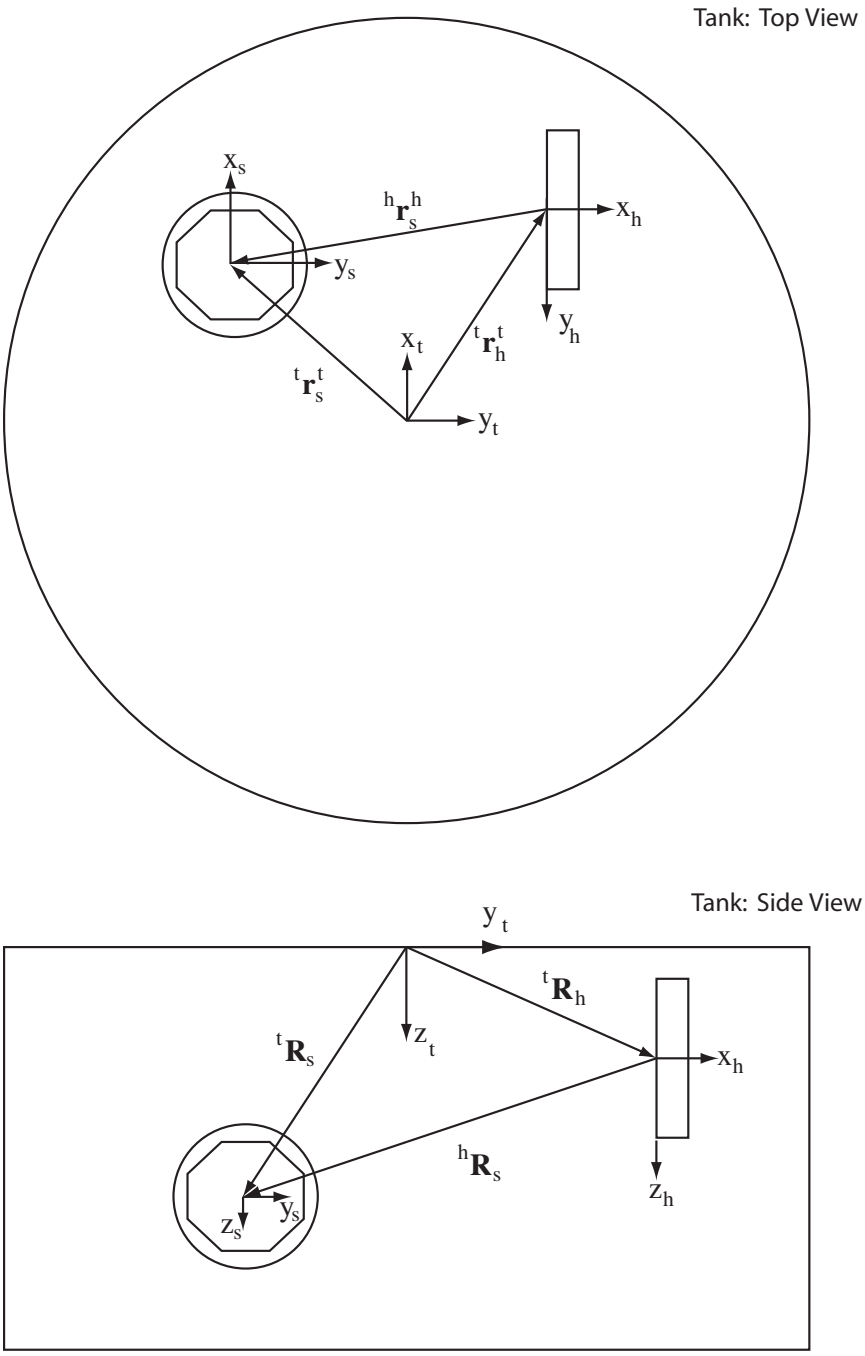

Figure 4.6: Frames of Reference Used for Collision Determination.

Figure 4.6. The tank frame, denoted with a t, corresponds to the inertial frame for the dynamics as developed in Chapter 3. The SSV frame, denoted by an s, corresponds to the body frame in Chapter 3. The third frame which must be taken into account is that corresponding to a hoop. Each hoop has its own frame. The origin of a hoop frame is the center of the front plane of the hoop with the x coordinate facing towards the back of the hoop. For clarity, the top view of the tank in Figure 4.6 describes the vectors associated with the location of objects in the tank, while the rotation matrices involved between each frame are noted along the vectors in the side view of the tank. The notation is as follows.

- ${}^{a}\boldsymbol{r}_{b}^{c}$ describes the vector $\boldsymbol{r}$ of b with respect to c in the a coordinate frame
- ${}^{a}\boldsymbol{R}_{b}$ describes the rotation from frame b to a

For example

${}^{t}\boldsymbol{r}_{h}^{t} =$ the distance of the hoop frame from the tank frame in tank coordinates

and

${}^{t}\boldsymbol{R}_{s} =$ the rotation matrix describing the orientation between the SSV frame and the tank frame.

Collision determination is available at all times for the tank boundaries and for the hoop closest to the vehicle. ${}^{h}x_{s}^{h}$, the distance in the x direction between the hoop coordinate origin and SSV coordinate origin measured with respect to the hoop, determines whether SSV is in contact with the hoop. To determine if SSV is colliding with a hoop the following procedure is used. r_s indicates the radius of the circle used as the SSV model in collision and h_t is the hoop thickness.

- $-r_s < {}^{h}x_{s}^{h} < r_s + h_t$ indicates a possible collision

- $r_{s,eff} = \sqrt{r_s^2 - ({}^h x_s^h)^2}$ is the effective radius of SSV in the yz plane of the hoop as shown in Figure 4.7

- ${}^h \boldsymbol{r}_{s,yz}^h = \sqrt{({}^h y_s^h)^2 + ({}^h z_s^h)^2}$

- $r_{h_i} - r_{s,eff} < |{}^h \boldsymbol{r}_{s,yz}^h| < r_{h_o} + r_{s,eff}$ indicates a collision

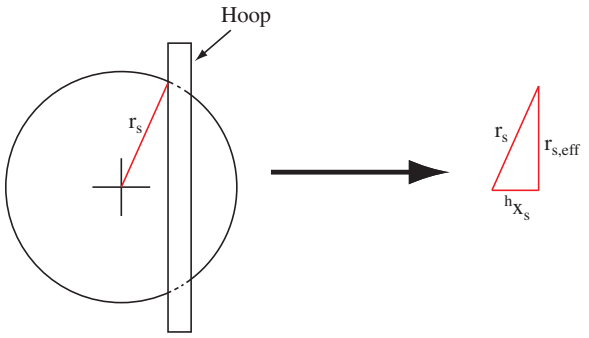

Figure 4.7: Determination of $r_{s,eff}$ for Hoop Collision.

If it is determined that there is contact between SSV and a hoop, it is necessary to determine which face of the hoop is being contacted.

- ${}^h x_s^h < 0 \Rightarrow$ contact with the front face of the hoop

- $h_t < {}^h x_s^h < r_s + h_t \Rightarrow$ contact with back face of hoop

- otherwise the collision is with SSV through the side of the hoop in the yz coordinate plane

If the point of contact is with either the front or the back face of the hoop, the routine then determines where the center of SSV is in relation to the hoop.

- $|{}^h \boldsymbol{r}_{s,yz}^h| \leq r_{h_i} \Rightarrow$ the center of SSV is inside the inner radius of the hoop as shown in Figure 4.8

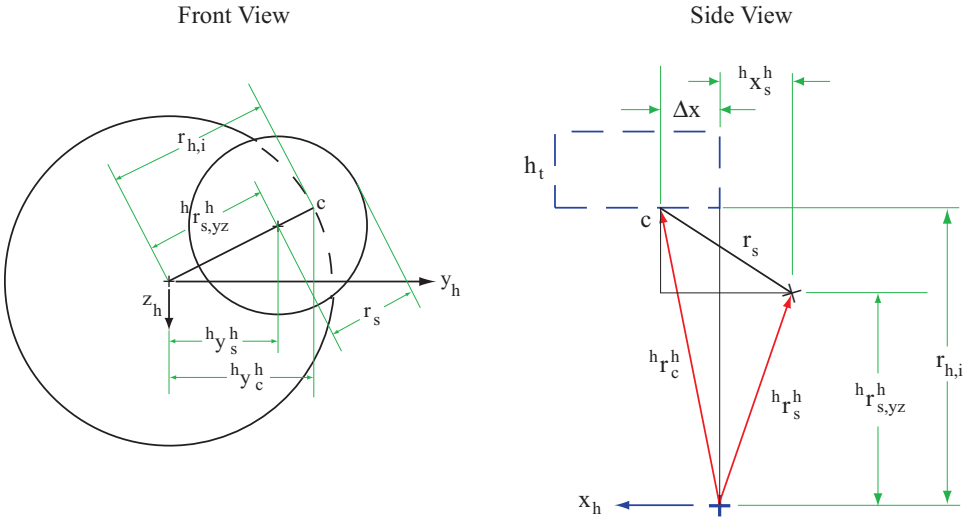

Figure 4.8: Collision with Front Face of Hoop with Center of SSV Inside Inner Radius of Hoop.

- $r_{h_i} < |{}^h\boldsymbol{r}^h_{s,yz}| < r_{h_o} \Rightarrow$ center of SSV is between the inner and outer radii of the hoop as shown in Figure 4.9

- $|{}^h\boldsymbol{r}^h_{s,yz}| \geq r_{h_o} \Rightarrow$ center of SSV is outside the outer radius of the hoop as shown in Figure 4.10

If the point of contact between SSV and the hoop occurs on either the front or back face of the hoop, the method of determining the forces and torques acting upon the vehicle is similar. Therefore, the procedure will be detailed only for a collision with the front face.

The force on SSV in the hoop coordinate frame for all front face collisions is defined as

$$\boldsymbol{f}_h = -k \begin{bmatrix} {}^h x^h_c \\ 0 \\ 0 \end{bmatrix}$$

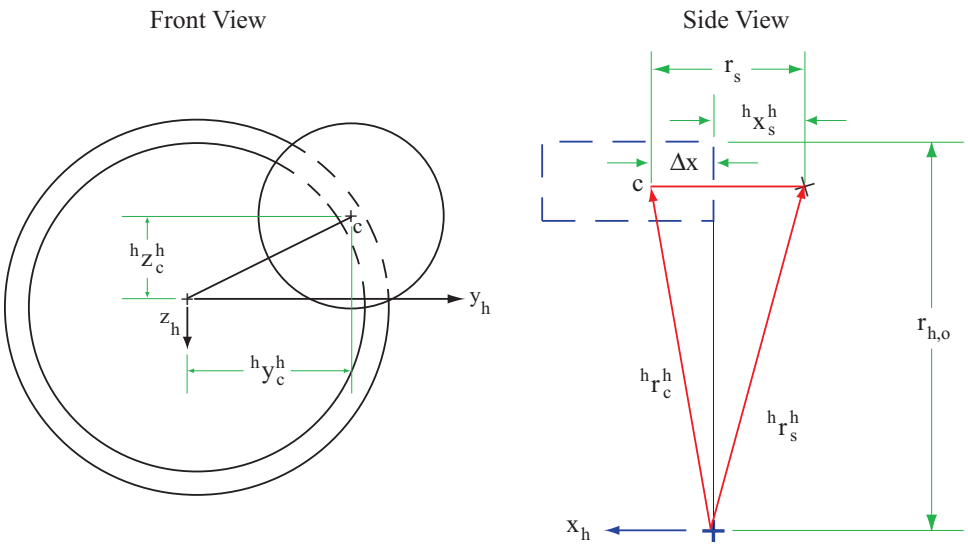

Figure 4.9: Collision with Front Face of Hoop with Center of SSV Between the Inner and Outer Radii of Hoop.

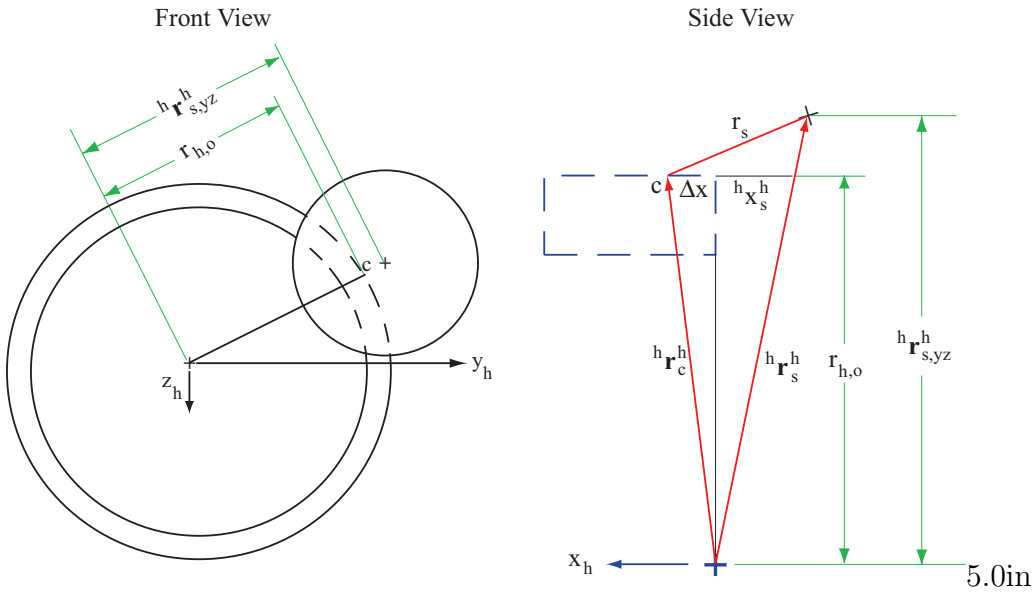

Figure 4.10: Collision with Front Face of Hoop with Center of SSV Outside the Outer Radius of Hoop.

This force is then transformed into the SSV coordinate frame via the rotation matrix as shown in Figure 4.6 so that

$$\boldsymbol{f}_s = ({}^h\boldsymbol{R}_s)^T \boldsymbol{f}_h \tag{4.3}$$

The torques acting upon the vehicle may then be determined by

$$\boldsymbol{\tau}_s = {}^s\boldsymbol{r}_c^s \times \boldsymbol{f}_s = \boldsymbol{S}({}^s\boldsymbol{r}_c^s)\boldsymbol{f}_s \tag{4.4}$$

where

$${}^s\boldsymbol{r}_c^s = ({}^h\boldsymbol{R}_s)^T \, {}^h\boldsymbol{r}_c^s \tag{4.5}$$

and

$${}^h\boldsymbol{r}_c^s = {}^h\boldsymbol{r}_c^h - {}^h\boldsymbol{r}_s^h \tag{4.6}$$

Calculation of ${}^h\boldsymbol{r}_c^h$ depends on where the center of SSV is in relation to the hoop. Table 4.2 provides for the calculation of the impact point Δx and ${}^h\boldsymbol{r}_c^h$ for all three types of collisions as defined above. If the point of contact is with the

Item		Position of SSV Center with Respect to yz Plane of Hoop		
		$\left\|{}^h\boldsymbol{r}_{s,yz}^h\right\| \leq r_{h,i}$	$r_{h,i} < \left\|{}^h\boldsymbol{r}_{s,yz}^h\right\| < r_{h,o}$	$\left\|{}^h\boldsymbol{r}_{s,yz}^h\right\| \geq r_{h,o}$
Δx		$\sqrt{r_s^2-(r_{h,i}-\left\|{}^h\boldsymbol{r}_{s,yz}^h\right\|)^2} + {}^h x_s^h$	$r_s - \left\|{}^h x_s^h\right\|$	$\sqrt{r_s^2-(\left\|{}^h\boldsymbol{r}_{s,yz}^h\right\|-r_{h,o})^2} + {}^h x_s^h$
${}^h\boldsymbol{r}_c^h$	${}^h x_c^h$	Δx	Δx	Δx
	${}^h y_c^h$	${}^h y_s^h \left(\frac{r_{h,i}}{\left\|{}^h\boldsymbol{r}_{s,yz}^h\right\|}\right)$	${}^h y_s^h$	${}^h y_s^h \left(\frac{r_{h,o}}{\left\|{}^h\boldsymbol{r}_{s,yz}^h\right\|}\right)$
	${}^h z_c^h$	${}^h z_s^h \left(\frac{r_{h,i}}{\left\|{}^h\boldsymbol{r}_{s,yz}^h\right\|}\right)$	${}^h z_s^h$	${}^h z_s^h \left(\frac{r_{h,o}}{\left\|{}^h\boldsymbol{r}_{s,yz}^h\right\|}\right)$

Table 4.2: Location of Contact Point for Collision with Front Face of Hoop.

back face of the hoop the force $\boldsymbol{f}_h$ becomes

$$\boldsymbol{f}_h = -k \begin{bmatrix} -{}^h x_c^h \\ 0 \\ 0 \end{bmatrix} = k \begin{bmatrix} {}^h x_c^h \\ 0 \\ 0 \end{bmatrix}$$

and Equations (4.3) - (4.6) can be applied as before where Table 4.3 describes depth of penetration and ${}^h\boldsymbol{r}_c^h$. It is also possible for SSV to skim the side of the

Item		Position of SSV Center with Respect to yz Plane of Hoop		
		$\lvert {}^h\boldsymbol{r}_{s,yz}^h \rvert \leq r_{h,i}$	$r_{h,i} < \lvert {}^h\boldsymbol{r}_{s,yz}^h \rvert < r_{h,o}$	$\lvert {}^h\boldsymbol{r}_{s,yz}^h \rvert \geq r_{h,o}$
Δx		$\sqrt{r_s^2 - (r_{h,i} - \lvert {}^h\boldsymbol{r}_{s,yz}^h \rvert)^2} - {}^h x_s^h + h_t$	$r_s + h_t - \lvert {}^h x_s^h \rvert$	$\sqrt{r_s^2 - (\lvert {}^h\boldsymbol{r}_{s,yz}^h \rvert - r_{h,o})^2} - {}^h x_s^h + h_t$
${}^h\boldsymbol{r}_c^h$	${}^h x_c^h$	$h_t - \Delta x$	$h_t - \Delta x$	$h_t - \Delta x$
	${}^h y_c^h$	${}^h y_s^h \left(\frac{r_{h,i}}{\lvert {}^h\boldsymbol{r}_{s,yz}^h \rvert} \right)$	${}^h y_s^h$	${}^h y_s^h \left(\frac{r_{h,o}}{\lvert {}^h\boldsymbol{r}_{s,yz}^h \rvert} \right)$
	${}^h z_c^h$	${}^h z_s^h \left(\frac{r_{h,i}}{\lvert {}^h\boldsymbol{r}_{s,yz}^h \rvert} \right)$	${}^h z_s^h$	${}^h z_s^h \left(\frac{r_{h,o}}{\lvert {}^h\boldsymbol{r}_{s,yz}^h \rvert} \right)$

Table 4.3: Location of Contact Point for Collision with Back Face of Hoop.

hoop as it is passing through. Equations (4.3) - (4.6) are again applicable, with $\boldsymbol{f}_h$ now determined as

$$\boldsymbol{f}_h = -k \begin{bmatrix} 0 \\ \Delta\, {}^h y_{c,yz}^h \\ \Delta\, {}^h z_{c,yz}^h \end{bmatrix} = -k \begin{bmatrix} 0 \\ {}^h y_s^h \left(\frac{{}^h r_{s,yz}^h + r_s - r_{h,i}}{{}^h r_{s,yz}^h} \right) \\ {}^h z_s^h \left(\frac{{}^h r_{s,yz}^h + r_s - r_{h,i}}{{}^h r_{s,yz}^h} \right) \end{bmatrix}$$

where $\Delta\, {}^h y_{c,yz}^h$ and $\Delta\, {}^h z_{c,yz}^h$ represent the amount of penetration into the hoop along the y and z directions of the hoop respectively.

Interaction with SSV is fairly benign. If the actual vehicle comes into contact with anything in the environment, it tends to bump off rather gently rather

than careen off in another direction. The spring constant, k, was determined by running the simulated vehicle into a hoop using a variety of values of k. A value of $k = 750\,Nm$ was found to provide similar performance to observed recoils of the actual SSV vehicle. Thus while no explicit deformation of the hoop was modeled, the spring is fairly compliant to represent such a collision.

It should be noted that since SSV was modeled as a sphere for the collision routine having a diameter equal to that of the thruster span, there is a remote possibility that the collision routine could indicate an impact when one had not really occurred.

4.3 Control Station

A schematic of the control station is presented in Figure 4.11. The pilot receives visual feedback of system performance via the monitor which provides views of the vehicle/simulated vehicle and its surrounding environment. The pilot then responds to these visual cues by issuing commands using two three degree of freedom hand controllers, one translational and one rotational. These hand controller instructions are read by a Silicon Graphics Inc. (SGI) O2 175 MHz computer which transmits them to the SGI Octane where they are converted into the desired rates and the desired vehicle state is determined. If the command display is in use, the desired vehicle state is sent simultaneously to the dynamic simulation as well as the graphical simulation where it is transmitted to the monitor immediately regardless of transmission delays. With no command display, the desired vehicle state is delivered only to the dynamic simulation and the pilot may receive possibly time delayed information from the graphical simulation if there is time delay. Note the time delays discussed here are not associated with

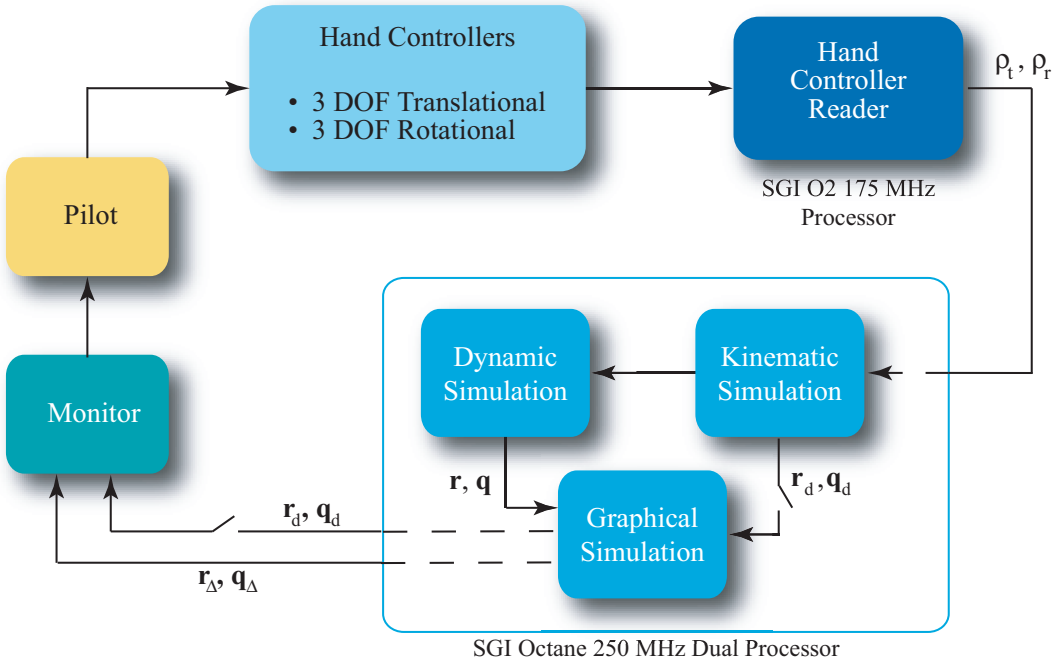

Figure 4.11: Control Station Schematic.

any computing time required, rather they are the transmission signal delays that are being addressed by this thesis. The kinematic, dynamic and graphical simulations are run on an SGI Octane 250 MHz dual processor. A picture of the control station interface is shown in Figure 4.12. In it the twenty-one inch monitor and two hand controllers are displayed. The left controller is the translational hand controller, while the right controller is the rotational hand controller.

The elements contained in the display window and the hand controllers will be discussed in the following sections. The kinematic simulation is discussed with the hand controllers. Lane (2000) developed the graphical models database used here while completing his PhD and the graphical simulation was adapted from one written by Henshaw using a combination of SGI and Open GL graphics.

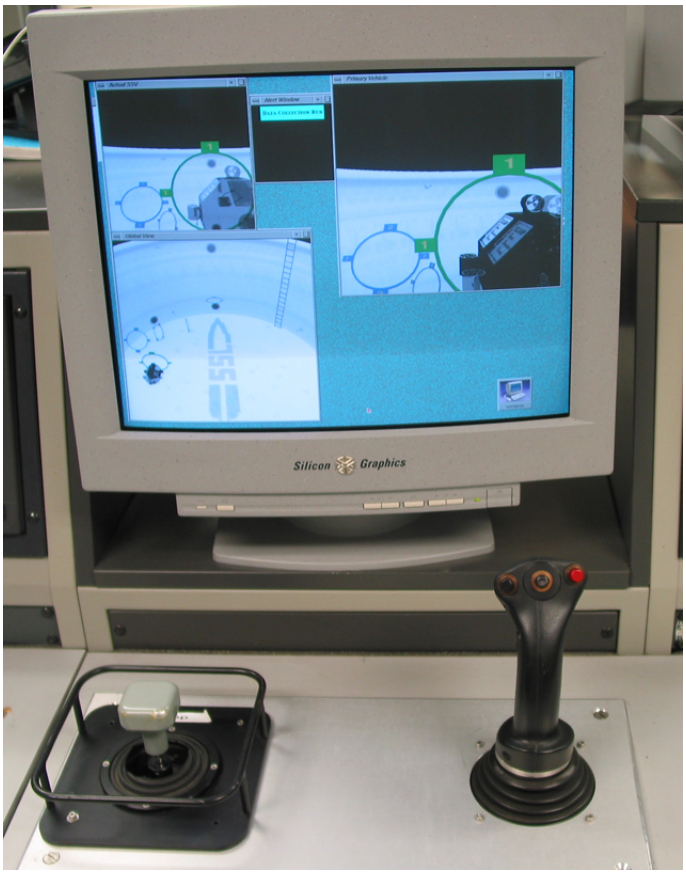

Figure 4.12: Control Station.

4.3.1 Control Station Graphics

In order to provide adequate information for subjects concerning the vehicle environment, the control station display was designed with several individual windows. A snapshot of the display layout is shown in Figure 4.13. The individual windows are explained in more detail below.

Primary Flight Window

This window, located in the upper right portion of the screen is the main window through which the pilot interacts with the vehicle. When the command display

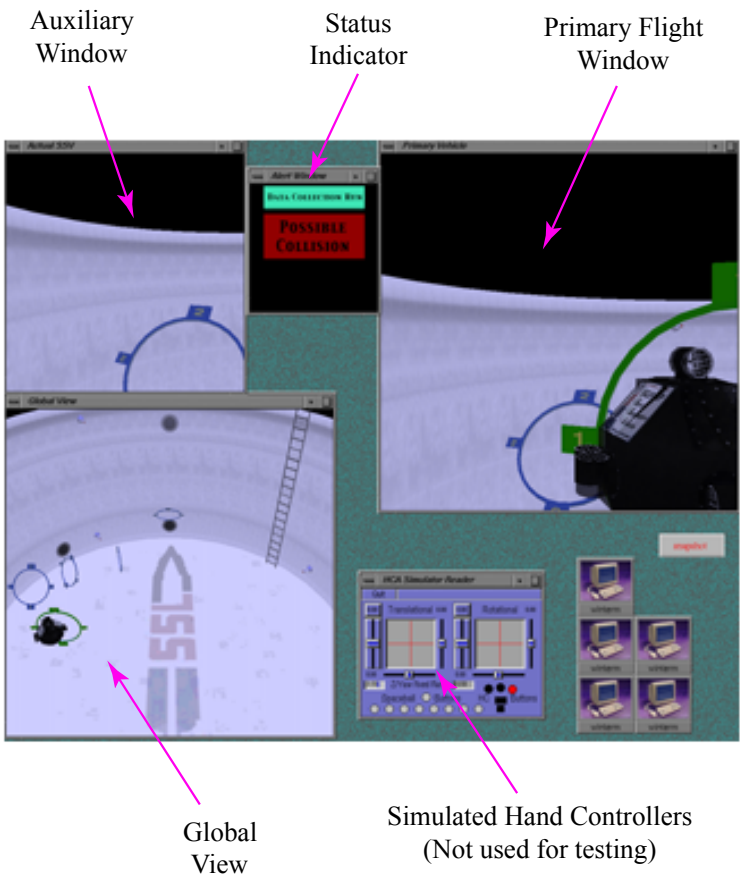

Figure 4.13: Sample Control Station Display for Command Display.

is available, there are two vehicles visible in this window. The desired vehicle, whose trajectory results from the kinematic simulation, is shaded black, while the actual vehicle is shadowed. It was reasoned that the vehicle being commanded should be the most immediately visible vehicle on the screen. When a command display is unavailable, the only vehicle displayed in this window is the actual vehicle. It becomes shaded black to make it more apparent to the pilot.

There are three separate camera views available in this window. The cameras are attached to whichever vehicle is being flown: the desired vehicle when the command display in use and the actual vehicle when there is no command display.

These camera views are discussed in more detail in a following section.

Auxiliary Window

This window is located in the upper left corner of the monitor. It provides dedicated views of the actual vehicle. It is available only during operations with a command display and is black for operations with no command display. The same three camera views available in the primary window are also provided here. They are attached to the actual vehicle.

Global View

This window in the lower left portion of the screen provides a more global view of the environment and hoop course. As with the primary window both vehicles are portrayed if command display is used and the actual vehicle is the transparent vehicle while the desired vehicle is black. Only the actual vehicle is shown for tests with no command display and it is shaded black.

Status Indicator

This primary purpose of this window is to indicate when a collision is detected by the simulation. A large red box flashes intermittently when the vehicle "senses" forces and torques as a result of contact. In addition, the top box in the window indicates whether a test is taking place or a practice session. This indicator was used during the pilot study when training was conducted separately from testing.

4.3.2 Camera Views

Camera views are of great importance whether piloting a vehicle in the tank or in space. Indeed, the driving force behind the development of the first generation SCAMP vehicle was to provide a maneuverable camera platform to supply auxiliary camera views to pilots of teleoperated vehicles in the lab. On vehicles with fixed cameras, the entire workspace may not be visible to the teleoperator, or another perspective may be useful for completing a task.

The decision of which camera views should be available to an operator is difficult. For instance, in this application, if camera views similar to those available in the tank are used, there would be a limited number of options available to an operator trying to maneuver through the tank. There are two fixed cameras located in portholes opposite one another on the north and south sides of the tank approximately three feet from the top of the tank. These cameras can be adjusted in a limited fashion; they can be rotated and their field of view can be changed to provide a more close in shot, but in most instances they are still too far away to provide the detail required for many tasks. They are more suited for supplying a global perspective of an environment such as the one available in the lower left window of the control station display used in this work. In addition, any adjustments to these cameras must be performed manually at a video control station located in the control room. Since most of the vehicle control stations currently reside outside the control room some sort of radio communication is required when these cameras need to be refocused. This could add a secondary source of time delay into the system particular to tank operations in the Space Systems Lab which might artificially affect results.

Additional views of operations in the actual tank must come from whatever

camera suite a particular vehicle may have or from an auxiliary platform such as SCAMP or SCAMP SSV. SSV's onboard camera is located on the upper forward panel as can be seen in Figure 4.1. This camera has a field of view (FOV) of about 45°. During development it was discovered that with this FOV, the operator might assume they had successfully passed through the hoop when in reality they hadn't yet reached it. One way around this would be to use another SCAMP type vehicle to provide auxiliary views, but the difficulties associated with this are similar to those with the porthole cameras. A separate operator is necessary to control the additional vehicle. The required communication between the two vehicle operators would result in delays in action taken by the test subject. An alternative solution is to provide the operator with a number of simulated camera views. If the world is well modeled in the simulation these additional views can provide the necessary auxiliary information.

Once it was decided to provide additional camera views, it was necessary to decide which ones would be of the most assistance to the pilot without overwhelming them. An entire thesis could be devoted to determining which camera views are optimal but this would be a very task-specific study. For example, views which might be helpful in maneuvering a vehicle such as SSV might not be desirable for satellite servicing. After a variety of combinations were considered, it was decided to make three views available: the onboard camera described above and shown in Figure 4.14; an over the left shoulder view as shown in Figure 4.15; and a view looking at the left side of the vehicle as shown in Figure 4.16 (such a view could result from a second camera platform vehicle looking at SSV). These camera views can be selected by the operator via the rotational hand controller and will explained in more detail in the hand controller section.

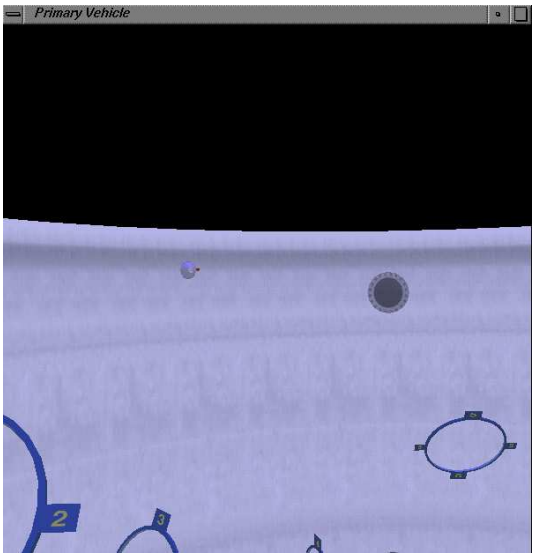

Figure 4.14: View Through Onboard SSV Camera.

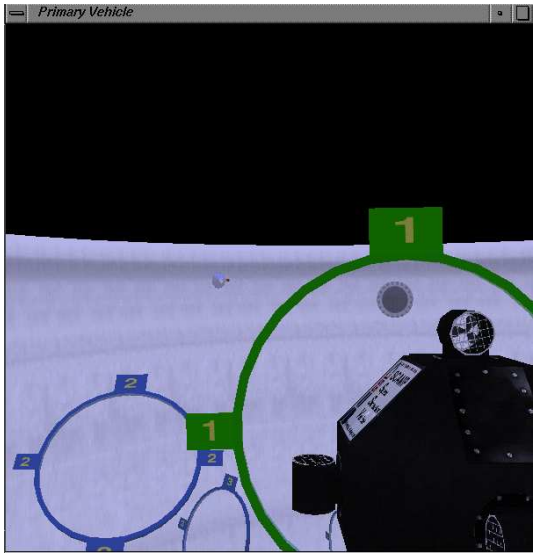

Figure 4.15: View Over Left Shoulder of SSV.

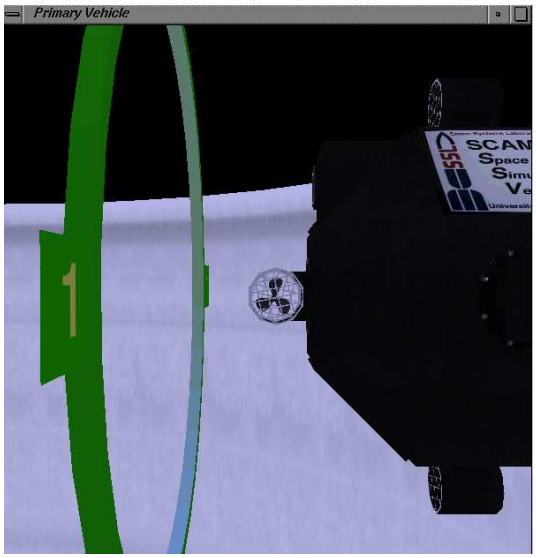

Figure 4.16: View of Left Side of SSV.

4.3.3 Hand Controllers

The interface to the graphical simulation includes a pair of Measurement Systems 3 DOF hand controllers as seen in Figure 4.17. The translational hand controller is located on the left, the rotational controller on the right. The rotational controller includes several programmable switches. These include three switches which are distributed across the upper portion of the front face and can be implemented using the thumb. There is also a trigger located along the back stem of the rotational hand controller which can be depressed. For this simulation the hand controller switches were programmed as follows.

- Left button: Changes the camera view in the upper left window on the computer screen which displays only the actual vehicle. It is applicable only for tests in which the command display is in use.

- Middle button: Allows the pilot to remove and replace the actual vehicle in the upper right window on the monitor. This can be helpful for tests with time delay when the actual vehicle may block part of the desired vehicle. It works only during tests implementing the command display.

- Right button: Useful in collision situations. This button can assist the vehicle operator to recover from a tumble due to a collision. In essence, depressing this button snaps SSV back to a stored snapshot of the desired vehicle taken before the collision.

- Trigger: This button cycles through the three available camera views in the main window. The cameras are attached to the desired vehicle during tests with the command display and to the actual vehicle during tests with no command display.

Figure 4.17: Hand Controllers.

4.3.4 Trajectory Generation With Hand Controllers

Deflections of the hand controllers cause readings ranging from [-1, 1] along each axis. These raw readings are multiplied by a gain which transforms them into the properly scaled velocities. For this study the gains were set so that

$$\boldsymbol{h}_t = 0.25\,\boldsymbol{h}_{t,raw}\,\frac{m}{s} \tag{4.7}$$

$$\boldsymbol{h}_r = 0.50\,\boldsymbol{h}_{r,raw}\,\frac{rad}{sec}. \tag{4.8}$$

These transformed hand controller readings are placed through a low pass filter to calculate the desired accelerations of the vehicle. This filtering of the hand controller readings rejects any high-frequency noise which tends to be amplified through direct computation of derivatives Sheridan and Ferrell (1974).

$${}^{I}\dot{\boldsymbol{v}}_d = \alpha_t(\boldsymbol{R}_{bi}^T\,\boldsymbol{h}_t - {}^{I}\boldsymbol{v}_d) \tag{4.9}$$

$${}^{D}\dot{\boldsymbol{\omega}}_d = \alpha_r(\boldsymbol{h}_r - {}^{D}\boldsymbol{\omega}_d) \tag{4.10}$$

where $\alpha_t = 2$ and $\alpha_r = 12$ are gains which affect the hand controller dynamics. This set of gains has been used with these hand controllers on several different lab vehicles. A trapezoidal algorithm is used to integrate the desired accelerations resulting in

$$^I\dot{\boldsymbol{r}}_d = {}^I\boldsymbol{v}_d \tag{4.11}$$

$$\dot{\boldsymbol{q}}_d = \boldsymbol{J}(\boldsymbol{q}_d)\,\boldsymbol{\omega}_d. \tag{4.12}$$

The above equations provide the desired state of the vehicle at each time step. This trajectory is sent to the actual vehicle as well as the kinematic simulation.

4.4 Automatic Trajectory Generator

To provide a baseline for comparison against human performance, an automatic trajectory generator was developed to describe an idealized path through the hoop course. Although a purely translational trajectory could be conceived in which the vehicle remained in the same orientation with respect to the tank/inertial reference frame, this wouldn't provide a legitimate comparison to human performance; humans are most likely to fly with the velocity vector out of the nose of the vehicle where the camera is located. Hence the generator must also provide a method for determining the correct vehicle orientation throughout the path. The development of the translational and rotational portions of the trajectory generator are described in detail in the following sections.

4.4.1 Translational Trajectory Generation

In order to prescribe the motion of the vehicle through the course, it is necessary to specify a number of way points between the start and finish positions of the

course. The origins of each individual hoop coordinate system were selected as these way points. A schematic of the course is shown in Figure 4.2 and the coordinate system for an arbitrary hoop is shown in Figure 4.6.

A trajectory describes a time history of the position, velocity, and acceleration of the vehicle. Because smooth operation of the vehicle is desirable the equations which describe the trajectory should be continuous and have continuous first and second derivatives. While the more commonly used cubic spline allows for continuous first and second derivatives, only the positions of each way point may be specified in this method. For this application, it was also a requirement that the velocity and accelerations be specified at each way point. Thus, a quintic/fifth order spline fit was applied to each successive set of way points to determine the corresponding smooth trajectory. Note that the position, velocity and accelerations determined from the spline fits are described relative to the tank/inertial frame. Thus, the equations describing the time history of the position of the vehicle with respect to the tank frame is as follows.

$$\begin{aligned} x(t) &= a_{15}t^5 + a_{14}t^4 + a_{13}t^3 + a_{12}t^2 + a_{11}t + a_{10} \\ y(t) &= a_{25}t^5 + a_{24}t^4 + a_{23}t^3 + a_{22}t^2 + a_{21}t + a_{20} \\ z(t) &= a_{35}t^5 + a_{34}t^4 + a_{33}t^3 + a_{32}t^2 + a_{31}t + a_{30} \end{aligned} \tag{4.13}$$

The velocity and acceleration profiles can be determined by taking the first and second time derivatives of the position profile.

In order to solve the above system for each portion of the trajectory, it is necessary to have some knowledge about the system at each of the way points. This knowledge is generally provided through constraints placed on vehicle performance. The first constraint involves definition the way point positions. Since for this application, the center of the front face of each hoop defines the way

point, three coefficients can be determined immediately through inspection.

$$x(0) = a_{10}$$

$$y(0) = a_{20}$$

$$z(0) = a_{30}$$

Boundary conditions at each point require that the velocity have maximum magnitude at each endpoint. Since the orientation of each hoop is known with respect to inertial coordinates, the velocity of the vehicle at each way point can be determined. Thus, the velocity constraints at the starting point of each spline section dictate that

$$\dot{x}(0) = a_{11}$$

$$\dot{y}(0) = a_{21}$$

$$\dot{z}(0) = a_{31}.$$

Because the velocity is constrained to be the maximum value at each way point it follows that the desired acceleration at each boundary point is equal to zero resulting in

$$\ddot{x}(0) = 0 = a_{12}$$

$$\ddot{y}(0) = 0 = a_{22}$$

$$\ddot{z}(0) = 0 = a_{32}.$$

Since the beginning of each intermediate spline section is the endpoint of the previous spline, the position, velocity and acceleration conditions at the endpoint

of each spline section are also known, reducing the equations to

$$\begin{aligned} a_{15}t_f^5 + a_{14}t_f^4 + a_{13}t_f^3 &= x(t_f) - x(0) - \dot{x}(0)t_f \\ a_{25}t_f^5 + a_{24}t_f^4 + a_{23}t_f^3 &= y(t_f) - y(0) - \dot{y}(0)t_f \\ a_{35}t_f^5 + a_{34}t_f^4 + a_{33}t_f^3 &= z(t_f) - z(0) - \dot{z}(0)t_f \end{aligned} \tag{4.14}$$

$$\begin{aligned} 5a_{15}t_f^4 + 4a_{14}t_f^3 + 3a_{13}t_f^2 &= \dot{x}(t_f) - \dot{x}(0) \\ 5a_{25}t_f^4 + 4a_{24}t_f^3 + 3a_{23}t_f^2 &= \dot{y}(t_f) - \dot{y}(0) \\ 5a_{35}t_f^4 + 4a_{34}t_f^3 + 3a_{33}t_f^2 &= \dot{z}(t_f) - \dot{z}(0) \end{aligned} \tag{4.15}$$

$$\begin{aligned} 20a_{15}t_f^3 + 12a_{14}t_f^2 + 6a_{13}t_f &= 0 \\ 20a_{25}t_f^3 + 12a_{24}t_f^2 + 6a_{23}t_f &= 0 \\ 20a_{35}t_f^3 + 12a_{34}t_f^2 + 6a_{33}t_f &= 0 \end{aligned} \tag{4.16}$$

By scaling time such that $t_f = 1$ for each segment, the equation becomes linear.

$$\begin{bmatrix} 1 & 1 & 1 & 0 & 0 & 0 & 0 & 0 & 0 \\ 0 & 0 & 0 & 1 & 1 & 1 & 0 & 0 & 0 \\ 0 & 0 & 0 & 0 & 0 & 0 & 1 & 1 & 1 \\ 3 & 4 & 5 & 0 & 0 & 0 & 0 & 0 & 0 \\ 0 & 0 & 0 & 3 & 4 & 5 & 0 & 0 & 0 \\ 0 & 0 & 0 & 0 & 0 & 0 & 3 & 4 & 5 \\ 3 & 6 & 10 & 0 & 0 & 0 & 0 & 0 & 0 \\ 0 & 0 & 0 & 3 & 6 & 10 & 0 & 0 & 0 \\ 0 & 0 & 0 & 0 & 0 & 0 & 3 & 6 & 10 \end{bmatrix} \begin{bmatrix} a_{15} \\ a_{14} \\ a_{13} \\ a_{25} \\ a_{24} \\ a_{23} \\ a_{35} \\ a_{34} \\ a_{33} \end{bmatrix} = \begin{bmatrix} x(1) - x(0) - t_s\dot{x}(0) \\ y(1) - y(0) - t_s\dot{y}(0) \\ z(1) - z(0) - t_s\dot{z}(0) \\ t_s(\dot{x}(1) - \dot{x}(0)) \\ t_s(\dot{y}(1) - \dot{y}(0)) \\ t_s(\dot{z}(1) - \dot{z}(0)) \\ 0 \\ 0 \\ 0 \end{bmatrix} \tag{4.17}$$

It is now an easy matter to create a program which solves for the unknown coefficients for each spline section given that all the variables on the right hand

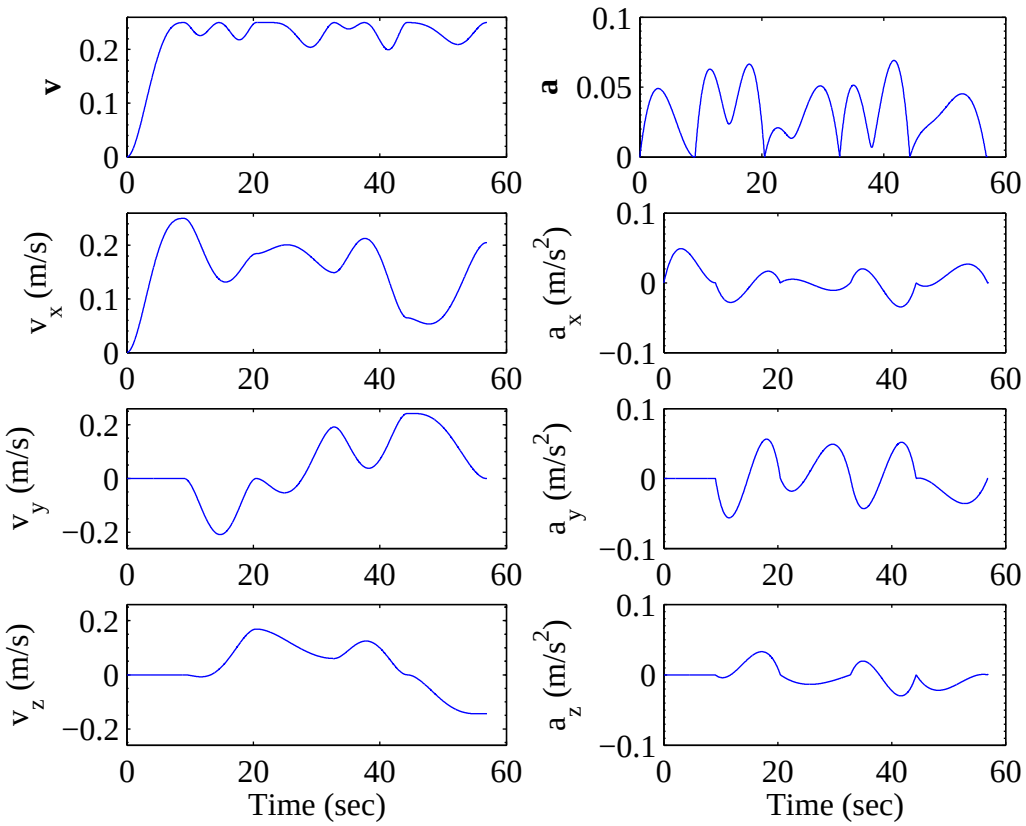

Figure 4.18: Velocity and Acceleration Profiles Generated by the Automatic Trajectory Generator with Respect to the Inertial Frame.

side of Equation (4.17) are known except for t_s, the time required for the vehicle to maneuver through each segment. The equations can be solved iteratively for t_s such that the maximum velocity and maximum acceleration constraints are satisfied throughout the section. The resulting velocity and acceleration profiles are shown in Figures 4.18.

4.4.2 Orientation Generation

As previously stated, while it is possible to devise an automatic trajectory which completes the obstacle course while remaining in the same orientation with re-

spect to the tank/inertial frame, this is a less than optimum choice for comparing with human performance. Humans tend to fly where they can see; if the main camera view is out the nose of the vehicle, they will tend to keep the course visible in front of that camera, using the camera to guide them through it. While an inexperienced pilot may resort to decoupling the rotational and translational degrees of freedom available from the hand controllers, i.e. if the pilot gets too close to an obstacle, they may resort to purely translational motion to extract themselves from the difficulty, a more experienced pilot will tend to use a smoother combination of rotation and translation to guide themselves through the course. Thus, it was determined that it would be appropriate to design a trajectory generator which maintains the velocity vector of the vehicle pointed out the nose of the vehicle. In other words,

$$\begin{bmatrix} \dot{x} \\ 0 \\ 0 \end{bmatrix}_b = \boldsymbol{R_{bi}} \begin{bmatrix} \dot{x} \\ \dot{y} \\ \dot{z} \end{bmatrix}_i$$

$\boldsymbol{R}_{bi}$, the rotation matrix which relates the vehicle frame to the inertial frame is equivalent to the direction cosine matrix (DCM). First the angle α, the rotation of the velocity vector about the $\boldsymbol{z}$-axis is determined. Then the angle β, the rotation about the new $\boldsymbol{y}$-axis is determined. These rotations, illustrated in Figure 4.19 result in

$$\begin{aligned} \boldsymbol{R}_{bi} &= \boldsymbol{R}_\beta \boldsymbol{R}_\alpha \\ &= \begin{bmatrix} \cos\alpha\cos\beta & \sin\alpha\cos\beta & \text{-}\sin\beta \\ \text{-}\sin\alpha & \cos\alpha & 0 \\ \cos\alpha\sin\beta & \sin\alpha\sin\beta & \cos\beta \end{bmatrix} \end{aligned} \tag{4.18}$$

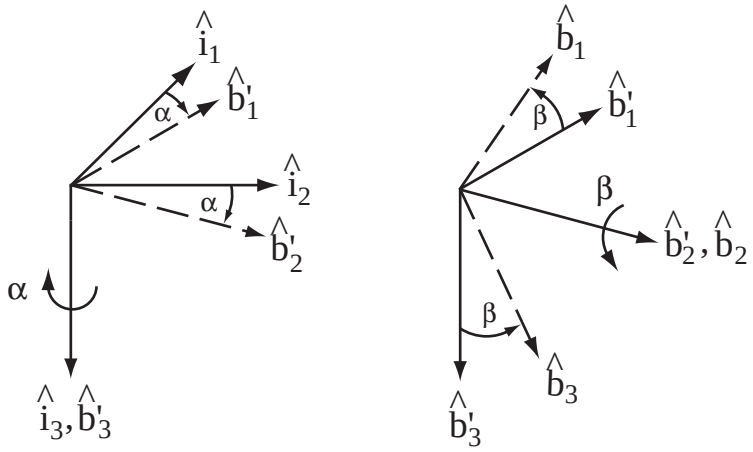

Figure 4.19: Rotations from Inertial Frame to Body Frame.

The required rotation angles α and β were determined using the desired translational velocity vectors as measured in the I-frame. α, the angle of rotation about the $\hat{\boldsymbol{i}}_3$-axis was determined using v_{d_x} and v_{d_y} while β, the angle of rotation about the $\hat{\boldsymbol{b}}_2$ axis was found via $v_{d_{xy}}$ and v_{d_z} with

$$v_{d_{xy}} = \sqrt{{}^I v_{d_x}^2 + {}^I v_{d_y}^2}. \tag{4.19}$$

The method to determine the quaternion from the DCM parallels that described in Shepperd (1978). This is by no means the only method available for deriving the quaternion from the DCM; others include, but are certainly not limited to, Grubin (1970, 1979) and Klumpp (1976). The algorithm developed by Grubin (1970) encounters a singularity when the rotation is 180°; this was addressed by Grubin (1979) where a second algorithm is developed for angles of rotation surrounding 180°, however, this necessitates the use of separate algorithms depending upon how close the rotation is to 180°. While neither of the methods developed in Klumpp (1976) and Shepperd (1978) encounter the singularity at 180°, Shepperd's algorithm is more straightforward and so was selected

for this application. Note that while the development of the following algorithm parallels that described by Shepperd, his definition of a quaternion differs by a minus sign in the vector portion from the one given in Chapter 3. Thus the resulting equations obtained here are slightly different than those presented in his paper.

Recall the definition of the quaternion given in Chapter 3 is as follows.

$$\boldsymbol{q} = \begin{bmatrix} \boldsymbol{\epsilon} \\ \eta \end{bmatrix} = \begin{bmatrix} \boldsymbol{a} \sin \frac{\varphi}{2} \\ \cos \frac{\varphi}{2} \end{bmatrix} = \begin{bmatrix} q_1 \\ q_2 \\ q_3 \\ q_4 \end{bmatrix}$$

The DCM can be rewritten in terms of the quaternion components resulting in

$$\boldsymbol{M} = \begin{bmatrix} q_4^2 + q_1^2 - q_2^2 - q_3^2 & 2(q_1 q_2 + q_3 q_4) & 2(q_1 q_3 - q_2 q_4) \\ 2(q_1 q_2 - q_3 q_4) & q_4^2 - q_1^2 + q_2^2 - q_3^2 & 2(q_2 q_3 + q_1 q_4) \\ 2(q_1 q_3 + q_2 q_4) & 2(q_2 q_3 - q_1 q_4) & q_4^2 - q_1^2 - q_2^2 + q_3^2 \end{bmatrix}. \tag{4.20}$$

In addition, recall that the quaternion also satisfies the condition that

$$q_1^2 + q_2^2 + q_3^2 + q_4^2 = 1. \tag{4.21}$$

Equations (4.20) and (4.21) provide the basis for determining the correct orientation of the vehicle at each time step in terms of quaternions from the DCM. It should be noted that there exists an ambiguity in the solution of the above equations; they are satisfied not only by the quaternion, but also by its negative. Usually, the q_4 term is chosen so that it is positive when corresponding to a rotation of less than 180°. The alternative is to use the negative, corresponding to a rotation of $360° - \varphi$ in the opposite direction.

4.4.3 Angular Velocity

The method for specifying the desired angular velocity of the vehicle follows Kane et al. (1983) and Creamer (2000). It is possible to exploit the fact that the body and inertial frames are moving relative to one another resulting in a time varying direction cosine matrix to determine the angular velocity between the two frames. Referring back to Figure 4.19 it can be seen that

$$\hat{\boldsymbol{b}} = \boldsymbol{R}_{bi}\hat{\boldsymbol{i}}. \tag{4.22}$$

The time rate of change of $\hat{\boldsymbol{b}}$ is then

$${}^{I}\dot{\hat{\boldsymbol{b}}} = \dot{\boldsymbol{R}}_{bi}\hat{\boldsymbol{i}}. \tag{4.23}$$

But ${}^{I}\dot{\hat{\boldsymbol{b}}}$ can also be written as

$${}^{I}\dot{\hat{\boldsymbol{b}}} = {}^{I}\boldsymbol{\omega}_b \times \hat{\boldsymbol{b}} = -\boldsymbol{S}(\boldsymbol{\omega})\hat{\boldsymbol{b}} \tag{4.24}$$

where

$${}^{I}\boldsymbol{\omega}_b = \omega_1\hat{\boldsymbol{b}}_1 + \omega_2\hat{\boldsymbol{b}}_2 + \omega_3\hat{\boldsymbol{b}}_3.$$

Equating (4.23) and (4.24) and substituting (4.22) results in

$$-\boldsymbol{S}(\boldsymbol{\omega}) = (\boldsymbol{R}_{bi})^T\,\dot{\boldsymbol{R}}_b i. \tag{4.25}$$

Recalling that

$$\boldsymbol{S}(\boldsymbol{\omega}) = \begin{bmatrix} 0 & -\omega_3 & \omega_2 \\ \omega_3 & 0 & -\omega_1 \\ -\omega_2 & \omega_1 & 0 \end{bmatrix},$$

$\boldsymbol{\omega}$ can be determined from the direction cosine matrix as defined in (4.18) to be

$$\boldsymbol{\omega_d} = \begin{bmatrix} \dot{\beta}\sin\alpha \\ -\dot{\beta}\cos\alpha \\ -\dot{\alpha} \end{bmatrix}. \tag{4.26}$$

In order to complete the calculation of the angular velocity of the vehicle in Equation (4.26), it is necessary that $\dot{\alpha}$ and $\dot{\beta}$ be known. From the geometry of the rotations, it can be seen that in general

$$\begin{aligned} \alpha &= \tan^{-1}\left(\frac{{}^{I}v_{d_y}}{{}^{I}v_{d_x}}\right) \\ \beta &= \tan^{-1}\left(\frac{{}^{I}v_{d_z}}{{}^{I}v_{d_{xy}}}\right) \end{aligned}$$

where ${}^{I}v_{d_{xy}}$ corresponds to the velocity component in the xy plane as defined in Equation (4.19). Equation (4.27) permits calculation of $\dot{\alpha}$ and $\dot{\beta}$.

$$\frac{d}{dt}\tan^{-1}u = \frac{1}{1+u^2}\frac{du}{dt} \tag{4.27}$$

$$\dot{\alpha} = \frac{{}^{I}v_{d_x} \cdot {}^{I}a_{dy} - {}^{I}v_{d_y} \cdot {}^{I}a_{d_x}}{{}^{I}v_{d_{xy}}^2}$$

$$\dot{\beta} = \frac{{}^{I}v_{d_z}\left({}^{I}v_{d_x} \cdot {}^{I}a_{d_x} + {}^{I}v_{d_y} \cdot {}^{I}a_{d_y}\right) - {}^{I}a_{d_z} \cdot {}^{I}v_{d_{xy}}^2}{{}^{I}v_{d_{xy}}({}^{I}v_{d_x}^2 + {}^{I}v_{d_y}^2 + {}^{I}v_{d_z}^2)}$$

Figure 4.20 shows the desired rotational velocity ($\boldsymbol{\omega}_d$) and acceleration ($\dot{\boldsymbol{\omega}}_d$) profiles computed by the automatic trajectory generator.

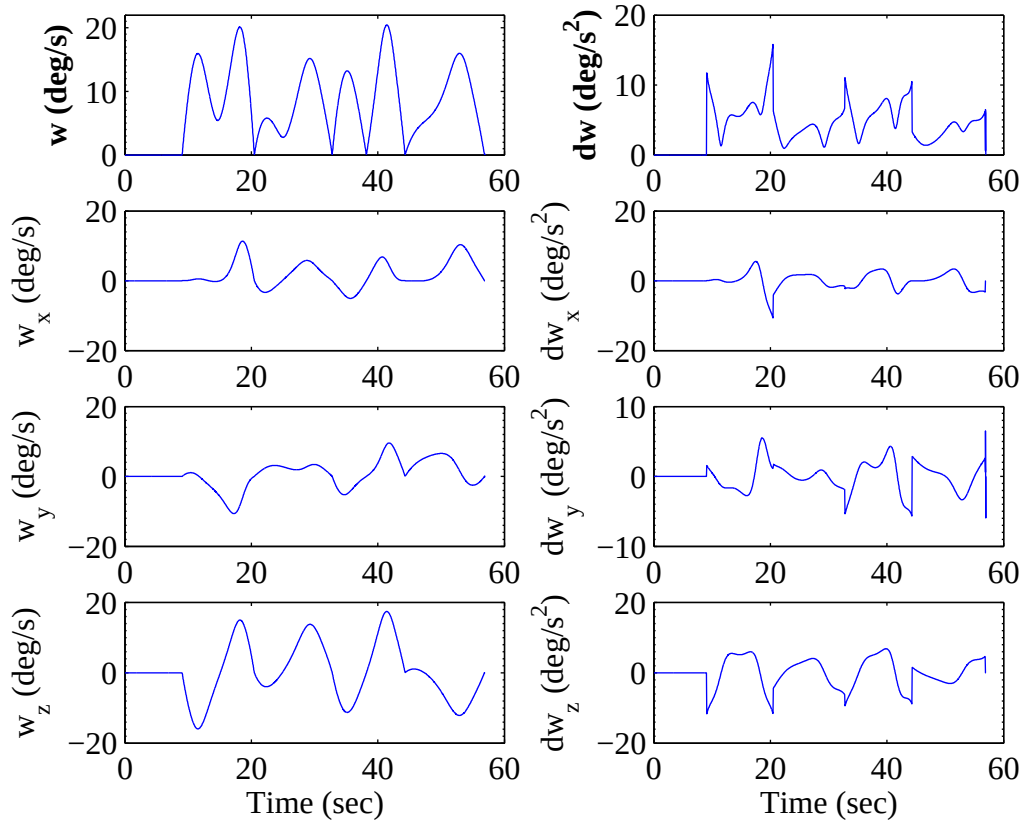

Figure 4.20: Rotational Velocity and Acceleration Profiles Generated by the Automatic Trajectory Generator.

Chapter 5

Pilot Study

5.1 Goals

A wide variety of factors may contribute to the effectiveness of a particular method for remote teleoperation of space vehicles. Therefore, an initial pilot study was performed to best determine the combination of factors to be examined in the primary study to follow. The goals of the pilot study included

- determining the range of time delays to be examined,
- establishing the amount of parameter uncertainty that should be used to initiate the adaptive controller,
- evaluating the controller gains and
- checking the simulation and testing procedure.

5.2 Methodology

Two subjects were selected to participate in the pilot study. Each person signed the consent form in Appendix A.1 and filled out the questionnaire in Appendix A.2

designed to determine experience in areas thought to affect performance. This included video game playing as well as flying lab vehicles, remotely piloted vehicles and private planes. Since all lab vehicles currently operate with the same type of three-axis translational and rotational hand controllers, experience with lab vehicles would indicate exposure to these hand controllers. Questions about the type and frequency of computer games played were also included, the hypothesis being that the skill set of someone who plays first person games such as "Doom" frequently might adapt to the simulator more quickly than a person who either infrequently plays computer games or plays non-first person games such as "Solitaire" or "Tetris". Subject A had no experience flying the lab vehicles and hence no experience with the hand controllers, but was a first person gamer. Subject B, the second person chosen to participate in this study had considerable experience flying lab vehicles but was not a computer game player. Time constraints forced subject B to drop out of the study, but an interesting trend was noticed in subject B's data. Subject B's completion times were longer than those of subject A, the gamer. This was somewhat surprising, since it had been surmised that someone with considerable flight experience on lab vehicles would produce the quickest completion times. Subject C, the replacement for subject B, was chosen for their lack of experience with both first person games and lab vehicles since it was thought that this might indicate a boundary of the performance envelope. All three test subjects were volunteers. The study was approved by the institutional review board (IRB) at the University of Maryland, College Park.

The goal of the pilot study was to obtain information on a number of factors to determine which were most relevant and merited further exploration during

the primary study. Hence, a 2x4x8 test matrix was developed with the following criteria:

- Display modes (2): The first display type consists of a dynamic model of the actual vehicle position and orientation portrayed on the screen. This model includes vehicle dynamics and reacts to hand controller inputs in much the same way as the actual vehicle would. In fact, if an actual vehicle were available, the dynamics of this model could be replaced by the state vector of the vehicle during operations. This display type is abbreviated as NCD throughout the rest of this thesis referring to no command display. The second display mode combines the display of the actual dynamic vehicle response with a second kinematic vehicle model representing the current desired configuration of the vehicle. While the actual dynamic vehicle performance can be affected by time delays in the communications loop, this kinematic model responds immediately to operator commands regardless of time delay. This display, in which both kinematic and dynamic models are available to the pilot, is termed a Command Display (CD).

- Time Delays (4): 0, 0.5,1.0, and 1.5 seconds. These are round trip delays inserted into the communication loops to simulate delays associated with uplink and downlink of information to and from the vehicle. The amount of delay is divided equally between the uplink and downlink.

- Controller combinations (8):

  - 'PD' Controller: has no knowledge of vehicle physical parameters
  - Nonlinear Controller (NL): assumes perfect knowledge of vehicle parameters

– Nonlinear + Adaptive Controller (AD): begins with some level of knowledge of vehicle parameters and then has the capability of changing these parameters to allow better controller performance. This controller was implemented by either assuming zero percent initial knowledge in one of the three parameter categories (mass/inertial, drag or buoyancy) while assuming full knowledge in the other two parameter categories, or else with 50 percent intitial knowledge of one parameter type at a time while assuming full knowledge of the other two.

The various combinations of display, time delay and controllers resulted in a sixty-four cell test matrix for each test subject. Each combination of controller, display and time delay was assigned a number as indicated in Table 5.2. The test was conducted in a completely randomized fashion. The order in which each subject tested each particular combination was determined using the random number generator available in Microsoft® Excel and can be found in Appendix B.

5.3 Pilot Study Gainsets

There are two gainsets that must be tuned before testing can begin. The first gainset includes the gains in the 'PD' portion of each controller. In order to tune the 'PD' gains the dynamics were decoupled and linearized. Buoyancy terms were ignored as these can be considered external forcing functions. In addition, the off diagonal terms of the $\boldsymbol{H}$ matrix for SSV are several magnitudes smaller than the diagonal terms so a diagonal $\boldsymbol{H}$ matrix was assumed. The linearized

Controller Type	Initial Parameter Uncertainty (%)	Uncertainty Type	Display Type	Combination Number			
				Time Delay - 1 way (sec)			
				0	0.25	0.50	0.75
PD	100	–	NCD	1	2	3	4
AD	100	Mass/Inertia	NCD	5	6	7	8
AD	100	Drag	NCD	9	10	11	12
AD	100	Buoyancy	NCD	13	14	15	16
AD	50	Mass/Inertia	NCD	17	18	19	20
AD	50	Drag	NCD	21	22	23	24
AD	50	Buoyancy	NCD	25	26	27	28
NL	0	–	NCD	29	30	31	32
PD	100	–	CD	33	34	35	36
AD	100	Mass/Inertia	CD	37	38	39	40
AD	100	Drag	CD	41	42	43	44
AD	100	Buoyancy	CD	45	46	47	48
AD	50	Mass/Inertia	CD	49	50	51	52
AD	50	Drag	CD	53	54	55	56
AD	50	Buoyancy	CD	57	58	59	60
NL	0	–	CD	61	62	63	64

Table 5.1: Pilot Study Parameter Arrangement.

translational dynamic equations can be written along a single axis as

$$m\ddot{x} + 2C_{d_t}\dot{x}_{ref}\dot{x} = u_{pd_t}.$$

With $\dot{x}_{ref} = 0.25\frac{m}{s}$ corresponding to the maximum allowable velocity for this vehicle, the above equation simplifies to

$$m\ddot{x} + \frac{1}{2}C_{d_t}\dot{x} = u_{pd_t}.$$

If the controller input, u_{pd_t}, is specified as

$$u_{pd_t} = -K_{d_t}\dot{\tilde{x}} - K_{d_t}\lambda_t\tilde{x} + m\ddot{x}_d + \frac{C_{d_t}}{2}\dot{x}_d$$

the closed loop dynamics become

$$m\ddot{\tilde{x}} + \left(\frac{C_{d_t}}{2} + K_{d_t}\right)\dot{\tilde{x}} + K_{d_t}\lambda_t\tilde{x} = 0. \tag{5.1}$$

This is equivalent to the standard second order dynamic equation found in any introductory control book such as Ogata (1990)

$$\ddot{x} + 2\zeta\omega_n\dot{x} + \omega_n^2 x = 0 \tag{5.2}$$

where ζ is the damping ratio and ω_n is the natural frequency. By matching coefficients it can be seen that

$$K_{d_t} = 2\zeta\omega_n m - \frac{C_{d_t}}{2}$$

and

$$\lambda_t = \frac{m\omega_n^2}{K_{d_t}}.$$

The rotational plant dynamics may be linearized in a similar manner such that

$$I\ddot{\theta} + 2C_{d_r}\dot{\theta}_{ref}\dot{\theta} = u_{pd_r}$$

which simplifies to

$$I\ddot{\theta} + C_{d_r}\dot{\theta} = u_{pd_r}$$

since $\dot{\theta}_{ref} = \omega_{max_{all}} = 0.5\frac{rad}{sec}$. Specifying u_{pd_r} the controller input as

$$u_{pd_r} = -K_{d_r}\dot{\tilde{\theta}} - K_{d_r}\lambda_r\tilde{\theta} + I\ddot{\theta}_d + \frac{C_{d_r}}{2}\dot{\theta}_d$$

results in closed loop dynamics

$$I\ddot{\tilde{\theta}} + \left(\frac{C_{d_r}}{2} + K_{d_r}\right)\dot{\tilde{\theta}} + K_{d_r}\lambda_r\tilde{\theta} = 0. \tag{5.3}$$

and the coefficients can be matched with those of Equation (5.2) in a manner similar to that of the translational dynamics.

There were several criteria used to tune the 'PD' gains. It was desirable to keep the errors at a reasonable level: around five centimeters for position and approximately a degree for orientation. Since the hand controllers have some associated dynamics which are discussed in more detail in Section 4.3.3, it was not necessary to tune the 'PD' gains such that the system would respond faster than the hand controllers. Therefore, the above linearized equations were used as a starting point, and then the gain sets were refined using the step inputs from the actual hand controllers and dynamics. The resulting values and the corresponding performance parameters (rise times, settling times and maximum overshoot) are given in Table 5.2.

The second gainset consists of the learning gains used in the adaptive controller. Due to the nonlinearity of the adaptive process, techniques analogous to the semiclassical procedures available when tuning 'PD' gains do not exist for tuning learning gains. Thus the adaptive learning gains were tuned using an iterative process and the automatic trajectory generator described in Section 4.4 to obtain consistent performance. Each parameter was tuned separately; the

DOF	K_d	λ	t_r (sec)	$M_p(\%)$	t_s (sec)
x, y, z	250	1.5	2.31	-	4.21
roll	12	4.5	0.354	6	1.05
pitch	12	4.5	0.354	5.81	1.04
yaw	14	4.5	0.351	5.84	1.04

Table 5.2: Pilot Study: PD Gainset and Resulting Performance Criteria.

parameter being tuned was set to 50% of its actual value and all other parameter values were completely known. Appendix C contains plots which display the normed errors of potential gains for each parameter. The resulting adaptive learning gains which allow translational tracking convergence for the automatic trajectory within 20 seconds are located in Table 5.3.

5.4 Test Procedure

Prior to testing, each subject signed the consent form and was given a short questionnaire to fill out (see Appendix A.1). Then the hand controllers and simulation were explained and demonstrated to the subject. As in Lane (2000), each test session was limited to one hour in duration so that the subjects would not become overly fatigued. A subject was permitted to complete two test sessions per day at most.

For this pilot study, there were three modes of operation:

- General training mode (G), in which the operator had the opportunity to fly the actual test course with the kinematic simulation only. This provided a method of introducing the operator to the hand controllers and simulation

Parameter Estimates $\hat{a}_i$	**Learning Gain** Γ_i
$\boldsymbol{H}$	1,000
$\boldsymbol{C}_{d_\omega}$	1,000
$B\,\boldsymbol{r}_b$	100
$\boldsymbol{C}_{d_v}$	40,000
ΔB	100
m	10,000

Table 5.3: Pilot Study: Adaptive Learning Gains, Γ, for Parameter Estimates $\hat{\boldsymbol{a}}$. See Equation (3.44).

environment without skewing performance toward any particular controller combination. In addition, it allowed them to become familiar with the actual test course. Pilots flew in the general training mode six times at the beginning of the study, and then twice before each new testing period to become reacquainted with the system.

- Cell training mode (C) in which the operator was introduced to the particular combination of controller, parameter uncertainty, display type and time delay to be tested in the next cell. This mode used a different three hoop course from the five hoop training/testing course to permit the operator to become somewhat familiar with the vehicle handling characteristics assigned to that test cell while not skewing results by allowing practice with test parameters on the actual test course. Subjects flew this course three times.

- Testing mode (T) in which the subject tested the particular combination indicated by the test matrix on the actual five hoop test course. Each test was repeated five times in succession.

In a particular test session a subject might complete up to six test cells depending upon the level of experience and the particular demands placed on the subject during that test period. For instance, if a subject was required to perform a series of experiments in which only the actual display was available combined with a significant time delay, their test completion times would be longer and hence fewer test cells could be completed in the time allotted. An example of test session 3 from subject C is as follows:

- 2 runs of general training (G) on the kinematic simulator,
- 3 runs of C47 (command display, adaptive controller with no initial knowlege of the buoyancy parameters, and 1.0 second round trip time delay),
- 5 runs of T47,
- 3 runs of C32 (actual display, nonlinear controller, 1.5 second round trip time delay),
- 5 runs of T32,
- 3 runs of C56 (command display, adaptive controller with 50% knowledge of the drag parameters, 1.5 second round trip time delay),
- 5 runs of T56

(In the above, the letters C and T indicate cell training/testing modes and the number immediately following the C or T indicates the test cell being completed

as described above in Table 5.2). The full breakdown of test sessions for subjects A and C are listed in Table B.1 and Table B.2 located in Figure **??**.

5.5 Results

5.5.1 Average Run Time

Figure 5.1 shows the average run times (of the 5 repetitions completed for each test cell) and standard deviations (1σ) for subject A by display type. Runs completed with no command display are shown in the upper plot, while those conducted with a command display are shown in the lower plot. The results for subject C are shown in Figure 5.2. Of immediate notice is that when no command display (NCD) was available, the results appear to be stratified by time delay; they are independent of vehicle controller type. Runs with no time delay are completed the most rapidly. As the time delay increases, so does the average run time. In addition, there is greater variation in performance for those runs with larger time delay, as demonstrated by the error bars. Both subjects exhibit some evidence of learning as seen through decreasing run times as test number increases. This is much more apparent for subject C, who had no previous experience, especially for time delays of 0.50 and 1.0 second where a much greater decrease in completion time is seen as testing progresses. In addition, there appears to be a separate learning curve associated with each level of time delay.

While the completion times were delineated by time delay when no command display was available, there appears to be a single well defined learning curve for each test subject when the command display was used. Subject performance is independent of time delay. Rather, the performance of a subject with a particular

controller/time delay combination is dependent upon where in the test series a particular test occurs. Those tests that occur later are much more likely to approach the test subject's individual best performance level than those that occur earlier.

While the results shown in Figures 5.1 and 5.2 indicate a delineation in completion times for the task when time delay is present and no command display is available, they provide no insight into the amount of time delay required before performance suffers. To quantify the amount of time delay necessary to observe a performance degradation for the teleoperation task considered in this thesis, the completion times of both subjects were averaged for all controller combinations and display types. As can be seen in Figure 5.3, with no command display available, completion time appears invariant to time delay until around 1 to 1.5 seconds. Thus, it was decided to consider time delays of 0 and 1.25 seconds for the main study.

The average completion times for both subjects for tests with the command display are shown in Figure 5.4. Note that with the command display, the completion times were much less affected by the amount of transmission delay present in the system.

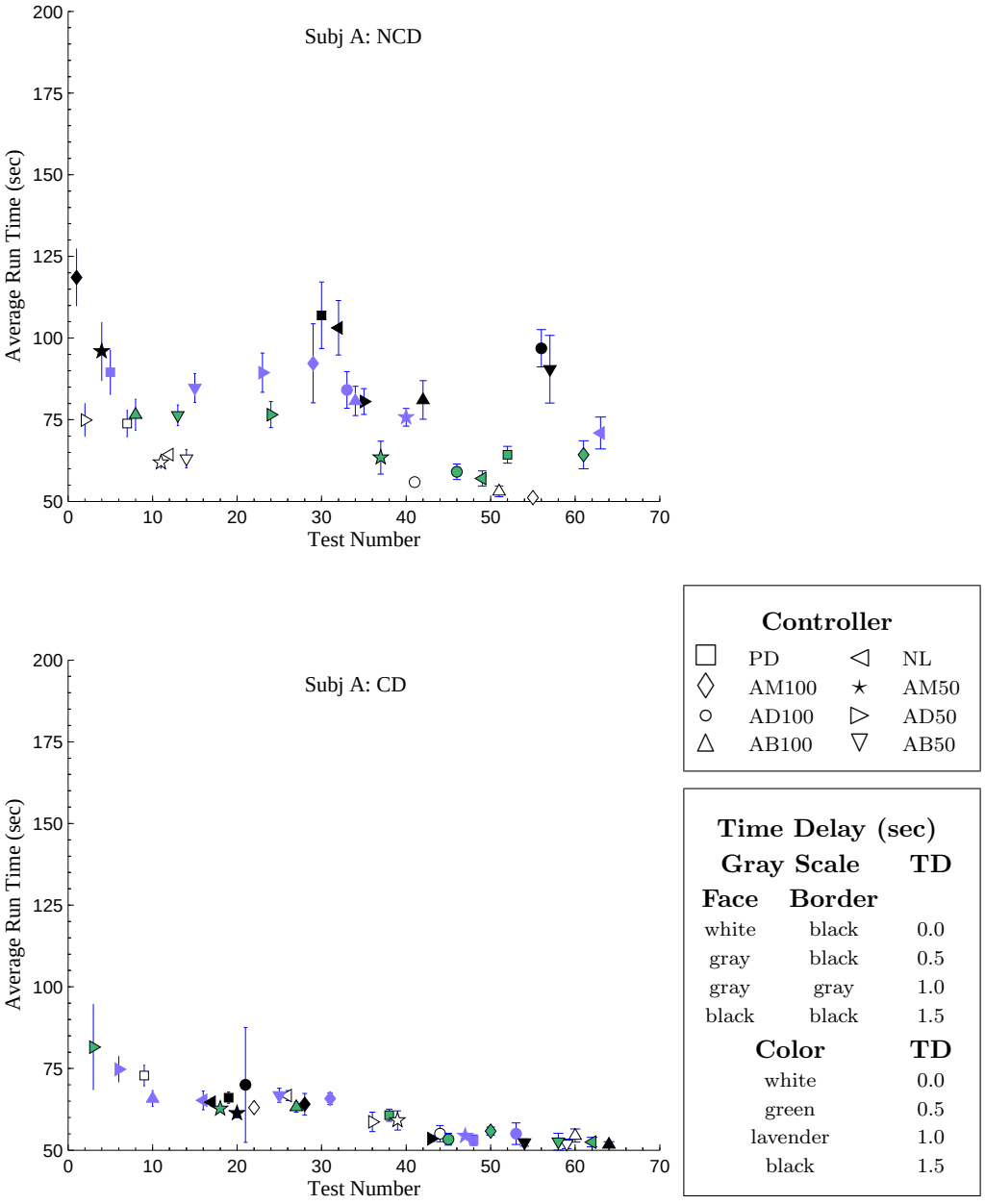

Figure 5.1: Pilot Study: Subject A Average Run Times by Display Type. (See Table 5.2 for Explanation of Controller Type).

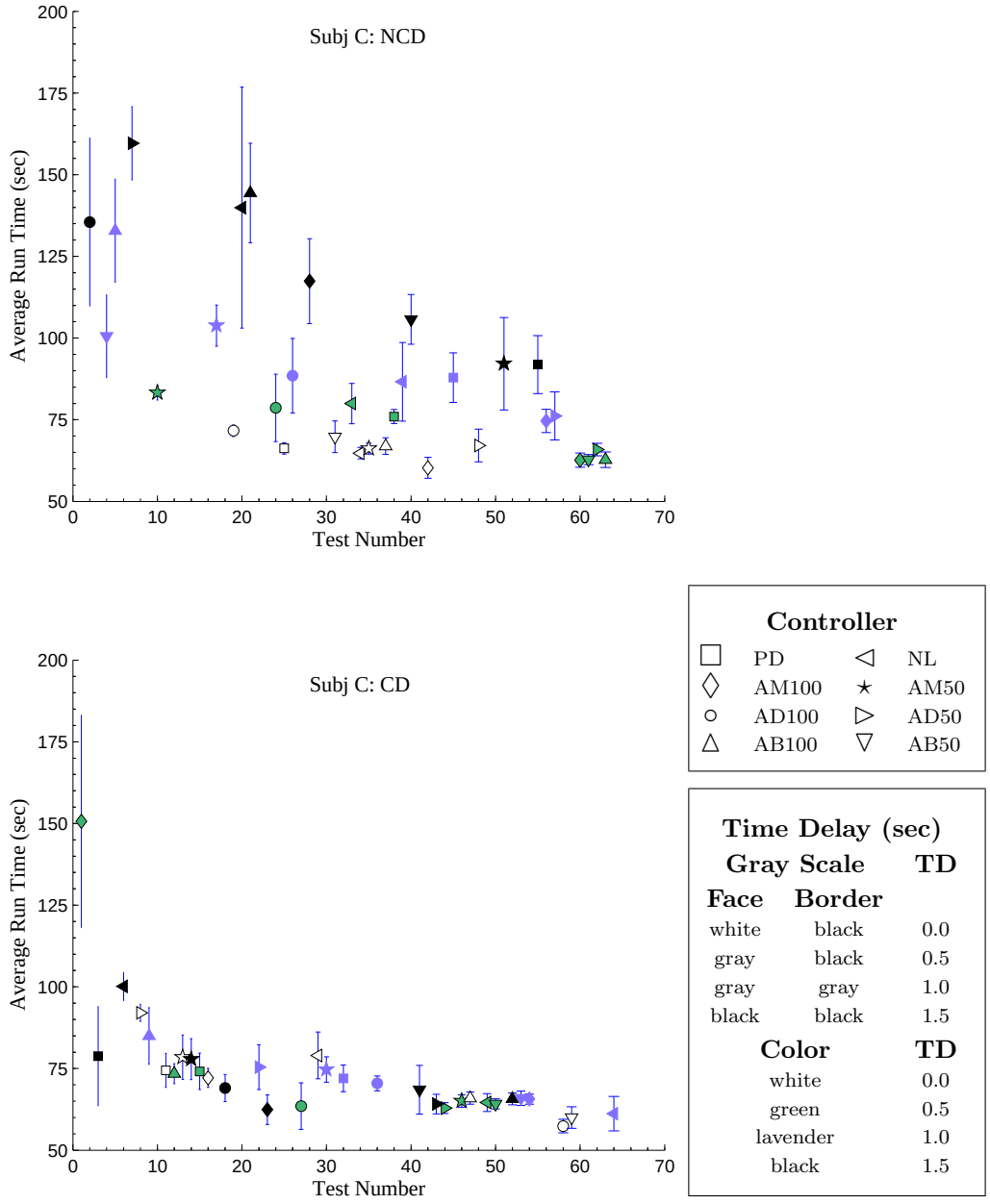

Figure 5.2: Pilot Study: Subject C Average Run Times by Display Type. (See Table 5.2 for Explanation of Controller Type).

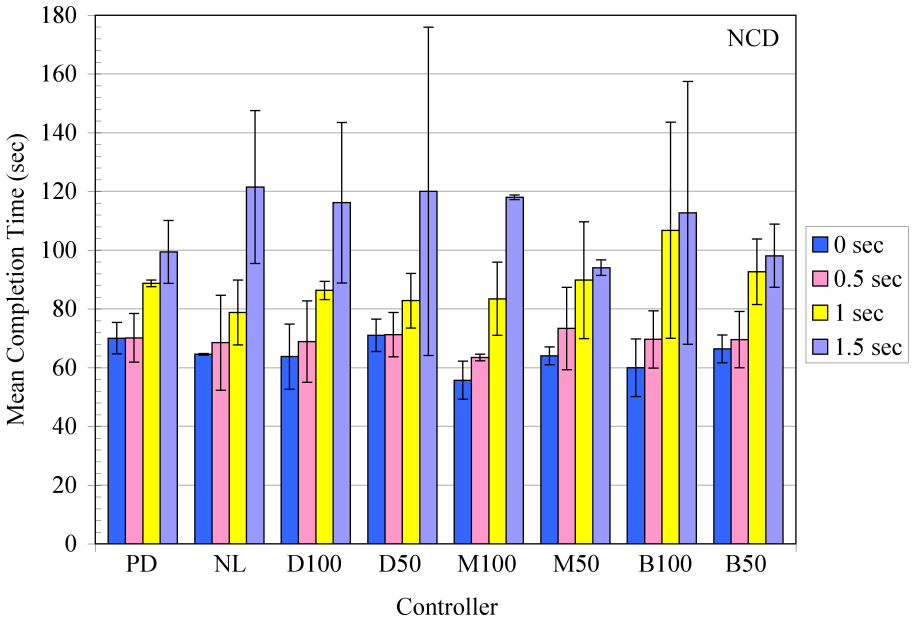

Figure 5.3: Pilot Study: Effect of Time Delay, Controller Type and No Command Display on Completion Times. (See Table 5.2 for Explanation of Controller Type).

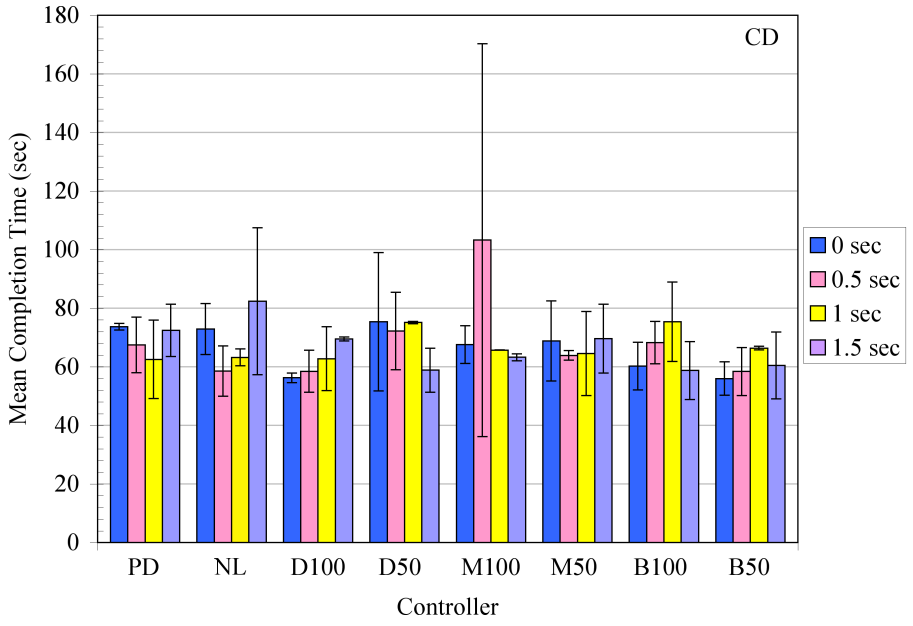

Figure 5.4: Pilot Study: Effect of Time Delay, Controller Type and Command Display on Completion Times. (See Table 5.2 for Explanation of Controller Type).

5.5.2 Average Controller Errors

The first metric used to measure controller performance was the average controller error as shown below where $\tilde{\mathbf{x}}$ and $\tilde{\mathbf{q}}$ are as defined in Chapter 3.

$$E_{avg_{trans}} = \frac{1}{T}\int_0^T ||\tilde{\mathbf{x}}(t)||_2 \, dt$$

$$E_{avg_{rot}} = \frac{1}{T}\int_0^T ||\tilde{\mathbf{q}}(t)||_2 \, dt$$

A cubic spline was used to interpolate the data followed by spline quadrature to determine the area under the curve. The procedure and accompanying program can be found in Van Loan (2000).

In order to reduce clutter on the graphs, the average error of the five runs is displayed along with the standard deviation. In each of the ensuing discussions the results for subject A are displayed in the top two graphs and those for subject C are in the bottom two graphs. The left hand graphs show results for all applicable runs; enlarged views of the vertical scale are located on the right to enable better analysis of results at the low end of the scale.

5.5.2.1 Average Translational Controller Error

Figure 5.5 shows the translational controller errors averaged over both subjects by time delay and controller type for runs with no command display while Figure 5.6 presents the errors for runs in which the command display was available. Of note is that the accuracy achievable with both display types appears to be driven by controller type; time delay has no effect. The 'PD' controller has the largest error ($\sim$5 cm) as would be expected, since it includes no direct knowledge of the vehicle parameters. Also of interest is the fact that the accuracy achievable with the

adaptive controller appears to be invariant to the initial amount of uncertainty in that parameter. This can be seen by comparing the accuracy between the initial uncertainty levels of any particular parameter. Take for example, drag. The accuracy appears to be the same whether there is 100% uncertainty in the initial amount of drag (D100) or 50% uncertainty (D50). This suggests that the adaptive controller estimates were reaching their steady state values well before the test ended. In fact, during tuning runs which were done with the automatic trajectory generator, the controller was reaching its steady state values in around 20 seconds. The accuracy achieved by the adaptive controller with uncertainty in the drag parameter is approximately 1 cm. If the mass/inertial parameters are uncertain, the accuracy is around 0.2 cm and less than that if the buoyancy terms are unknown. The nonlinear controller is accurate to within 0.3 cm. Since the nonlinear controller contains full knowledge of vehicle parameters it should exhibit the greatest accuracy. That it was somewhat less accurate than the adaptive controller may be attributable to discretization.

For all the adaptive controllers, the deciding factor on controller error appears to have been the magnitude of the parameter being adapted. The translational drag parameter was by far the largest parameter on this vehicle at about 414 kg/m (note these are not the unitless drag parameters often encountered in aerodynamics), whereas the mass of the vehicle was 76.2 kg and the vehicle was made 0.5 N buoyant. The larger the magnitude of the parameter, the larger the error.

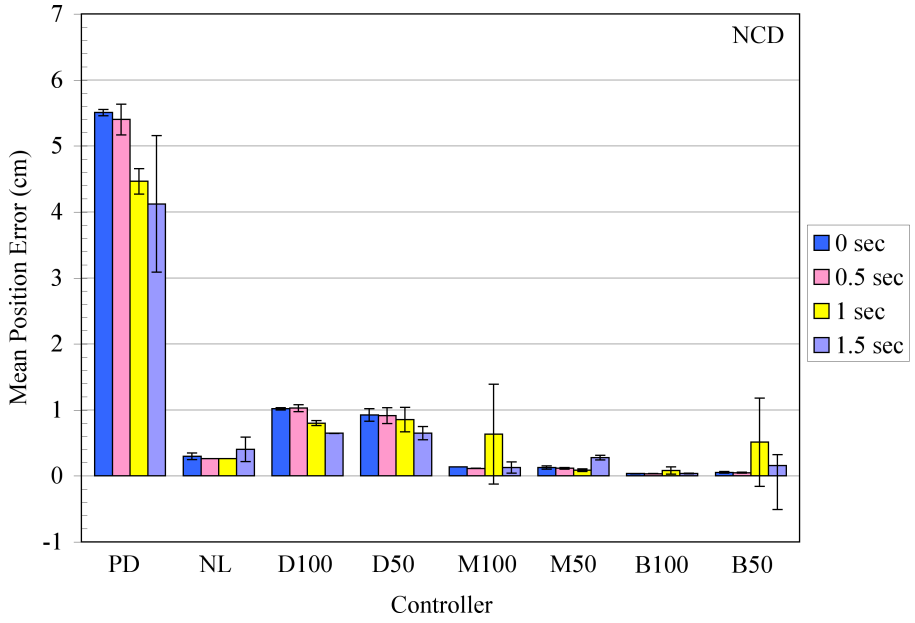

Figure 5.5: Pilot Study: Effect of Time Delay, Controller Type and No Command Display on Vehicle Position Error. (See Table 5.2 for Explanation of Controller Type).

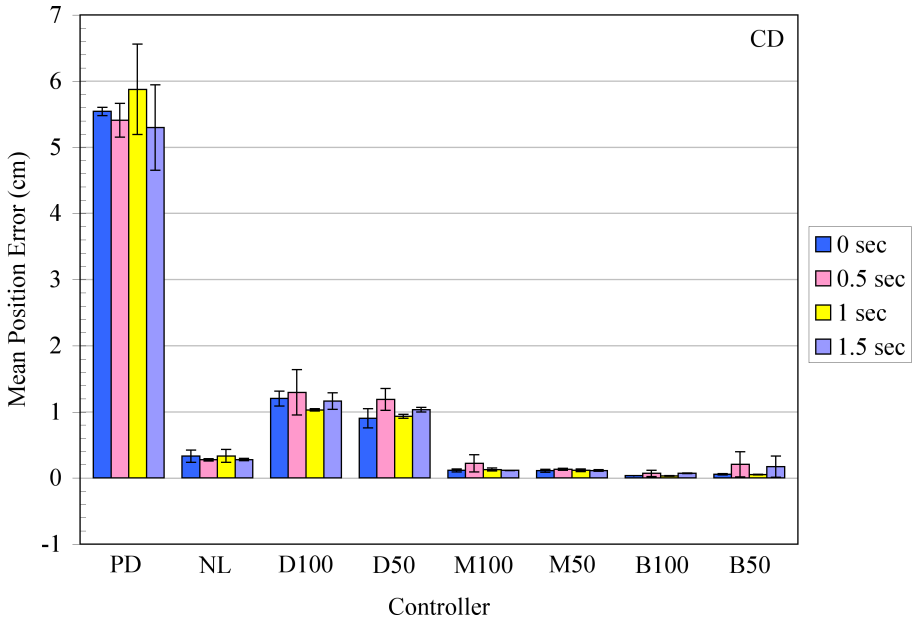

Figure 5.6: Pilot Study: Effect of Time Delay, Controller Type and Command Display on Vehicle Position Error. (See Table 5.2 for Explanation of Controller Type).

5.5.2.2 Average Rotational Controller Error

The orientation errors were also averaged over both subjects and are shown in Figure 5.7 for runs with no command display and Figure 5.8 for runs in which a command display was used. As with the translational errors discussed previously, the average error is indicated for each controller type and time delay. The rotation errors are quite small. Even the least accurate controller, the 'PD' controller, has an accuracy of approximately 0.5 degrees. The remainder of the controllers appear to have an accuracy at least an order of magnitude less than that of the 'PD' controller.

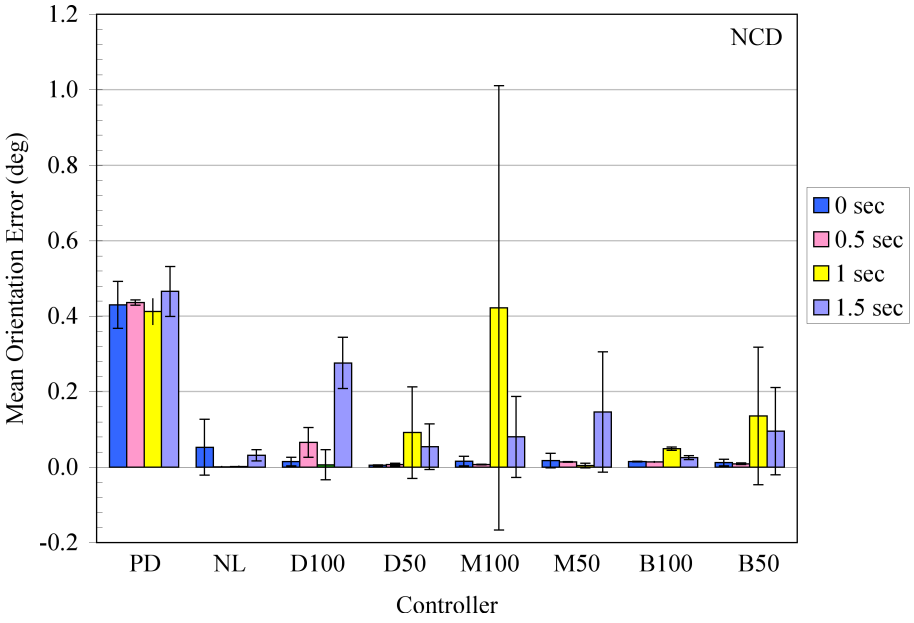

Figure 5.7: Pilot Study: Effect of Time Delay, Controller Type and No Command Display on Vehicle Orientation Error. (See Table 5.2 for Explanation of Controller Type).

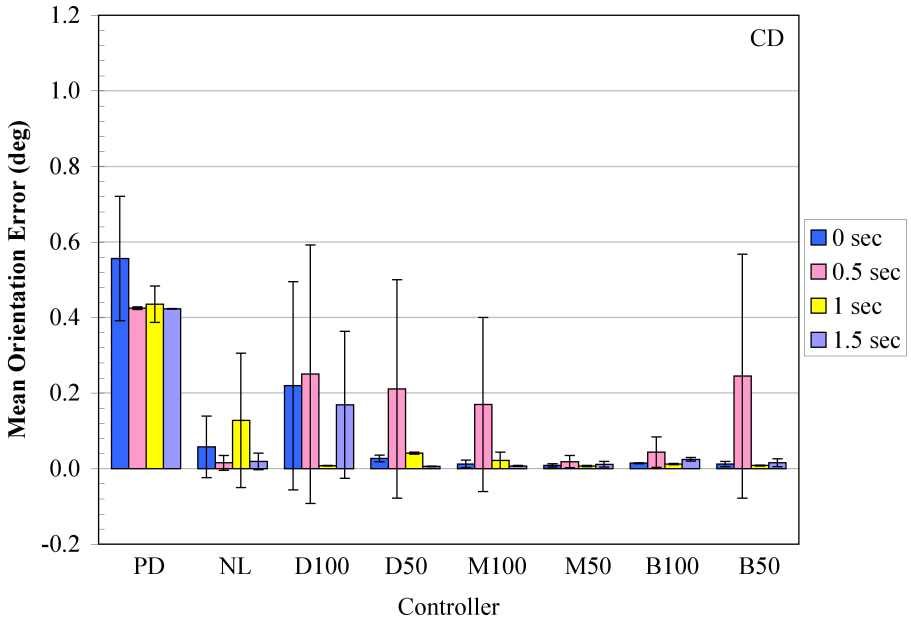

Figure 5.8: Pilot Study: Effect of Time Delay, Controller Type and Command Display on Vehicle Orientation Error. (See Table 5.2 for Explanation of Controller Type).

5.6 Summary of Results

This pilot study was conducted to better define which treatment combinations should be examined in the main study. Thus several combinations of possible treatments were studied. These included

- 4 time delays: 0, 0.5, 1, 1.5 seconds round trip,
- 8 vehicle controllers including a 'PD', nonlinear, and adaptive in which the initial amount of parameter uncertainty in the adaptive controller was varied, and
- 2 display types: no command display and command display.

The results of the pilot study yielded the following conclusions:

- With no command display, completion times were relatively unaffected for time delays less than 1 second in duration (see Figure 5.3). Therefore, only two levels of time delay will be examined in the main study: 0 and 1.25 seconds. A time delay of 1.25 seconds was chosen to attempt to ensure that all subjects would be adversely affected with no command display; Lane (2000) found that some subjects were still able to teleoperate effectively with one second of delay in the system.
- The amount of parameter uncertainty initially present in the adaptive controller does not influence the vehicle controller performance (see Figure 5.5 - Figure 5.8). Thus, the main study will use an adaptive controller that starts as a 'PD' controller, i.e. with no initial knowledge of any of the vehicle parameters. This will reduce the number of controller combinations from eight to three.

- Errors in vehicle rotation are quite small. The least accurate vehicle controller, the 'PD' controller, is accurate to within 0.5 degrees. The remaining controllers are at least a magnitude of order more accurate (see Figures 5.7 - 5.8). Thus, the gains in the rotational portion of the 'PD' controller will be detuned for the main study. The guidelines used to retune these gains remains the same as for the pilot study: reasonable accuracy and little to no overshoot. The values utilized in the main study along with the resulting performance parameters are shown in Table 5.4.

- The subjects were comfortable with the testing protocol and teleoperation interfaces.

.

DOF	K_d	λ	t_r (sec)	$M_p(\%)$	t_s (sec)
x, y, z	250	1.5	2.31	-	4.21
roll	8 (12)	2.5 (4.5)	0.652	2.93	1.65
pitch	8 (12)	2.5 (4.5)	0.653	2.79	1.63
yaw	9 (14)	2.5 (4.5)	0.647	3.26	1.68

Table 5.4: Main Study: PD Gainset and Resulting Performance Criteria (Pilot Study Gains in Parentheses).

Because the 'PD' gains are being retuned in order to make the vehicle less responsive in rotation it is necessary to adjust the learning gains used for the adaptive controller. The new learning gains to be used during the main study are located in Table 5.5 and plots showing controller performance for candidate gains are located in Appendix D. The criterion used for retuning the learning

Parameter Estimates $\hat{a}_i$	**Learning Gain** Γ_i
$\boldsymbol{H}$	5,000 (1,000)
$\boldsymbol{C}_{d_\omega}$	5,000 (1,000)
$B\,\boldsymbol{r}_b$	500 (100)
$\boldsymbol{C}_{d_v}$	250,000 (40,000)
ΔB	500 (100)
m	250,000 (10,000)

Table 5.5: Main Study: Adaptive Learning Gains, Γ, for Parameter Estimates $\hat{\boldsymbol{a}}$ Defined in Equation (3.44). (Pilot Study Gains in Parentheses).

gains was the same as that used to tune the learning gains in the pilot study: to provide translational tracking convergence for the automatic trajectory within 20 seconds.

Chapter 6

Main Study

6.1 Overview

This chapter details the primary study. Initial sections discuss the study design and testing procedure. Results include average run time, accuracy, pilot effort, hand controller readings, mean flight path, and a discussion of camera views used. Performance with the automatic trajectory generator is compared to that of human test subjects. The chapter ends with an interpretation of the results arising from this study.

6.2 Experiment Design

The pilot study was designed such that each test subject received each treatment in a completely randomized fashion. Because there were 64 treatment combinations (refer to Table 5.2), subjects tested multiple treatments within a test session. This resulted in varying numbers of test sessions per test subject. The main study was designed to make the testing process more standardized for each subject. It was decided that two extraneous sources of variation should be blocked: first,

subject experience level and second, external events that might affect subject performance on any given day such as lack of sleep the preceding night. Thus, a Latin square design was used. Latin square designs are variance balanced meaning that all treatments are considered equally precisely (Jones and Kenward, 1989, pg. 192). Two classes of Latin square designs include the orthogonal Latin square and the combinatorially balanced Latin square. Combinatorially balanced Latin square designs are typified by Jones and Kenward (1989, pg. 194-195) such that

- Each treatment occurs once with each subject.
- Each treatment occurs the same number of times within each test session.
- The number of subjects who receive treatment i in a test session followed by treatment j in the next test session is the same for all $i \neq j$.

While orthogonal designs achieve maximum efficiency in the absence of carry-over effects, they have several drawbacks that made them less than ideal candidates for this experiment. First, they are not as efficient as balanced designs in estimating direct treatment effects. Second, they require more subjects than is necessary to achieve balance as shown by Williams (1949). If more than three treatments are involved, the designs suggested by Williams require fewer subjects than those based on complete sets of orthogonal squares (Jones and Kenward, 1989, pg. 197). Sheehe and Bross (1961) provide a simple algorithm based on Williams to make a combinatorially balanced Latin square design. This combinatorial Latin square algorithm outlined in Jones and Kenward (1989, pg. 197-198) is implemented for the main study and is located in Table 6.1 where the treatment combinations of display and controller type are denoted by the letters A-F.

Group	Test Session					
	1	2	3	4	5	6
1	A	F	B	E	C	D
2	B	A	C	F	D	E
3	C	B	D	A	E	F
4	D	C	E	B	F	A
5	E	D	F	C	A	B
6	F	E	A	D	B	C

Table 6.1: Balanced Latin Square Design.

Combinations of display and controller type were randomly assigned to a treatment before each study. Table 6.2 lists the combinations used for Study 1 and Table 6.3 for Study 2.

Because there were six test sessions, it was necessary to use six groups. Eighteen test subjects were recruited to participate. They were randomly assigned to one of the six groups such that each group contained three test subjects. Prior to the second study, subjects were randomly reassigned to groups such that Study 2 contained different subject/group combinations than did Study 1. These subject/group divisions can be seen in Table 6.4 and Table 6.5.

6.3 Test Procedure

As with the pilot study, each test subject filled out the questionnaire and signed the informed consent form located in Appendix A.1. The equipment and sim-

Study 1: No Time Delay		
Letter	**Display**	**Controller**
A	CD	PD
B	CD	NL
C	NCD	AD
D	NCD	PD
E	NCD	NL
F	CD	AD

Table 6.2: Testing Combinations for No Transmission Delay.

Study 2: 1.25 Second Delay		
Letter	**Display**	**Controller**
A	NCD	NL
B	CD	PD
C	CD	AD
D	NCD	AD
E	NCD	PD
F	CD	NL

Table 6.3: Testing Combinations for 1.25 Second Transmission Delay.

Study 1: No Time Delay			
Group	**Subject Number**		
1	1	2	15
2	3	4	16
3	5	6	13
4	7	8	14
5	9	10	18
6	11	12	17

Table 6.4: Main Study 1: Subject Groupings, No Time Delay.

Study 2: 1.25 Sec Delay			
Group	**Subject Number**		
1	4	5	12
2	8	15	18
3	2	11	14
4	6	9	17
5	1	7	13
6	3	10	16

Table 6.5: Main Study 2: Subject Groupings, 1.25 Second Time Delay.

ulation were then explained and demonstrated to the test subjects. Subjects were instructed to fly as quickly and cleanly through the course as possible with accuracy being of primary importance. To become familiar with the simulation interface and hand controllers, each subject completed one pretest session using the nonlinear controller with command display and no time delay on the full five hoop course. If it appeared that the subject had not yet reached the bottom of the learning curve in this introductory session, they were allowed to continue in following sessions until their run times had leveled off. The training sessions for subject 8 are shown in Figure 6.1 where it can be seen that a second session was required before familiarization with the system was complete. In addition, to assist in determining when subject performance was leveling off during either a training or testing session, a running average of the five most recent runs was plotted. The results for the training session of subject 8 are shown in Figure 6.2. During each test session, the subject tested on the single controller/display combination indicated in Table 6.1 throughout the session on the five hoop course. Since training occurred during testing, only the five hoop course was utilized in the main study. Run time data was plotted during the test session to allow the test director to determine when to halt testing for a particular session. Testing continued until it appeared that either the learning curve had leveled out (see Figure 6.3) or there was evidence of subject fatigue as seen by an increase in completion time as indicated in Figure 6.4. If testing ceased due to subject fatigue, it was assumed that the subject had reached their trained performance level in previous runs and so testing was considered concluded for this controller/display combination. Subjects were not allowed to test with the same display/controller combination in subsequent test sessions as they were for the initial pretest train-

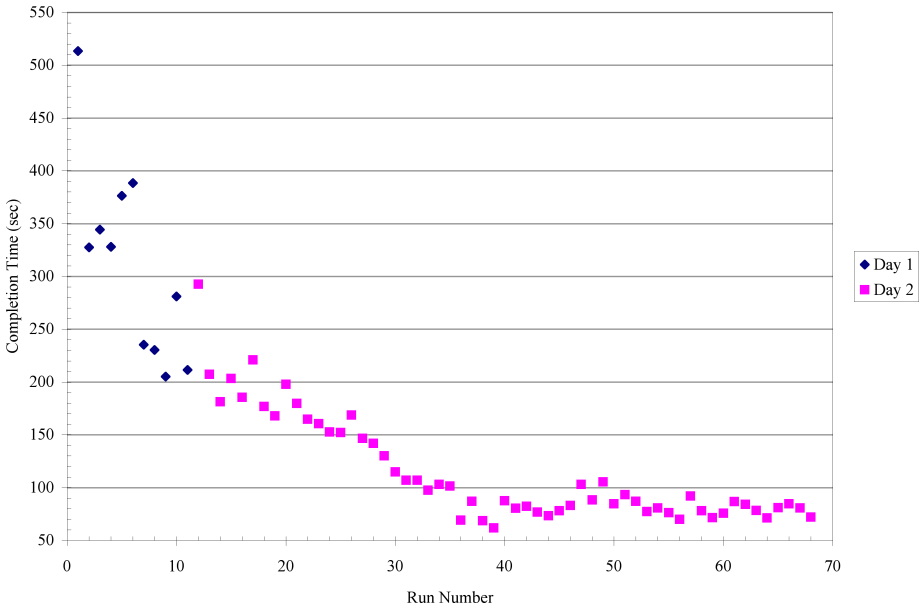

Figure 6.1: Training Session Course Completion Times for Subject 8.

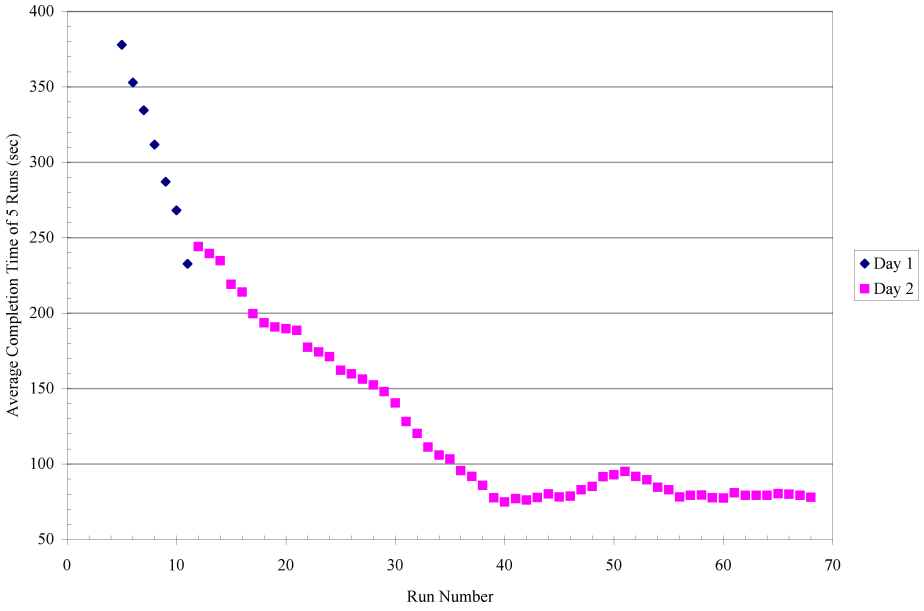

Figure 6.2: Subject 8 Training Session Running Average (5 Runs).

ing.

The main study was conducted over a period of seven weeks with approximately 5,500 runs being completed by the eighteen test subjects. 20GB of information was collected including time, desired and actual states of the vehicle and error data. Collision information included a time stamp of collisions as well as indicating run and hoop number. In addition, camera view usage, hand controller data and button press data was recorded.

6.4 Data Analysis

Since training with each display/controller combination occurred during testing, it was necessary to examine each subject's run time data file to determine which runs were most representative of that subject's performance during the test session. Figures E.1 - E.18 in Appendix E.1 display complete run time data for each test subject when there is no time delay. Appendix E.2 contains the course completion plots for each test subject with 1.25 second round trip time delay. All runs are plotted and those runs chosen for analysis are indicated. Any outliers within a chosen string of runs were not eliminated because it was reasoned that perhaps they might be indicative of an individual's performance. In other words, perhaps every so often the test subject lost concentration during a run. This might be peculiar to that subject's method of operation and the data should reflect it.

A mixed model was used to analyze the data statistically where

$$y_{ijklm} = \mu + \alpha_i^{disp} + \alpha_j^{contr} + \alpha_k^{grp} + \alpha_l^{ts} + a_{m(k)}^{subj} + e_{ijklm} \tag{6.1}$$

with effects

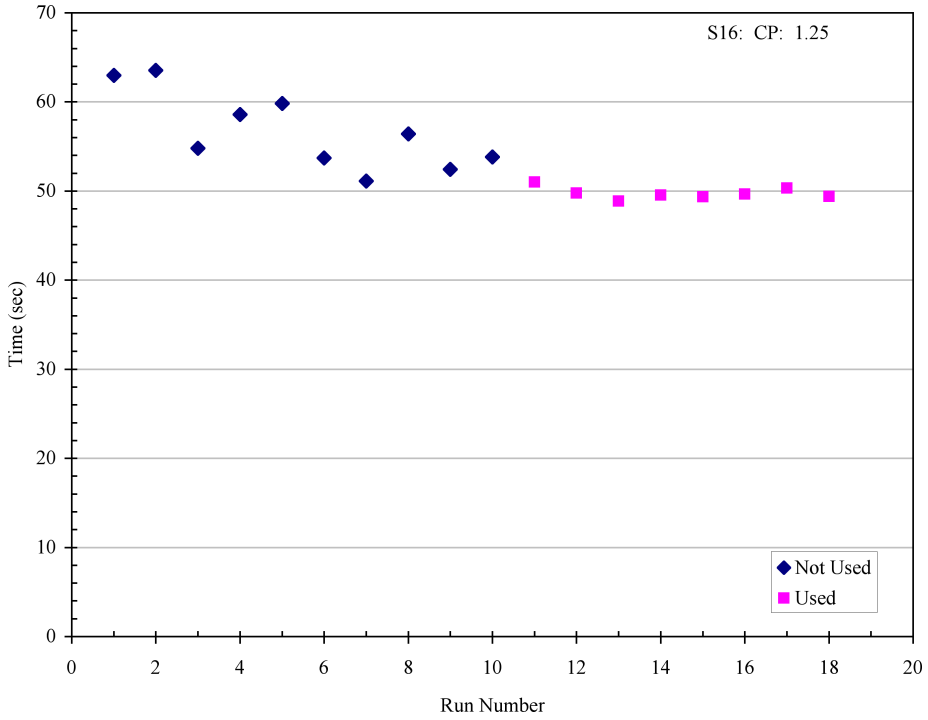

Figure 6.3: Course Completion Times for Subject 16 with 1.25 Seconds of Command Display and 'PD' Controller.

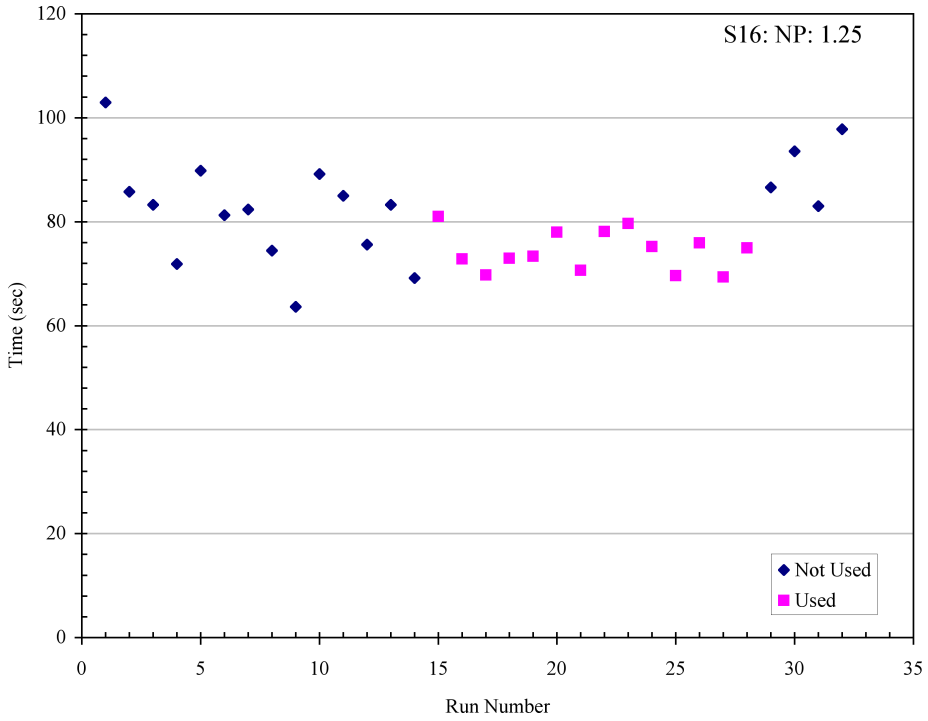

Figure 6.4: Running Average (5 Runs) of Course Completion Times for Subject 16, 1.25 Second Time Delay, No Command Display and 'PD' Controller .

- μ: unknown overall mean for response variable
- α_i^{disp}: fixed effect corresponding to the ith level of display type (i = 1,2)
- α_j^{contr}: fixed effect corresponding to the jth level of controller type (j = 1-3)
- α_k^{grp}: fixed effect corresponding to kth group (k = 1-6)
- α_l^{ts}: fixed effect corresponding to the lth test session (l = 1-6)
- $a_{m(k)}^{subj}$: random effect corresponding to the mth subject nested within kth group (m = 1-3)
- e_{ijklm}: residual error not accounted for by the model

If an effect, such as display type, appeared to impact subject performance, linear contrasts were used to investigate the extent of the effect. Linear contrasts provide a method for making comparisons among population means. More on this subject can be found in Ott and Longnecker (2001, pg. 431-437).

A quick note about statistical significance is mentioned here. When performing hypothesis testing for effects, it is common to consider a Type I error, or the probability that we reject the null hypothesis when in fact it is true. The probability of a Type I error is denoted as α. One drawback of reporting results in this manner is that if other researchers wish to apply the results of a study with some other value of α than reported, they must recalculate rejection regions. An alternative method of hypothesis testing involves using a level of significance or (P-value). Basically, the P-value is compared with the researcher's desired α. If P $\leq \alpha$ the probability that the effect is due to chance is small and the null hypothesis should be rejected; if P $> \alpha$ there is not enough evidence to reject

the null hypothesis. For instance, a result with P = 0.001 indicates that there is a 0.1% likelihood that the result is due to chance. A more complete discussion of this can be found in Ott and Longnecker (2001, pg. 224). In all graphs that follow, P-levels which are below the value $\alpha = 0.05$ level are indicated on graphs.

6.5 Results

6.5.1 Average Run Time

The average run time of each subject for each test session was calculated and entered into the mixed model described above. The statistical package SAS® was used to determine the P-levels for each hypothesis. Results from SAS® indicate that when no time delay is present, display type and controller type both impact subject performance. However, with 1.25 seconds of time delay, the only factor affecting subject performance is display type. In addition, there is evidence of a linear learning effect between test sessions one through six when no time delay is present ($P < 0.0001$) but no such trend with time delay.

The difference in course completion times by display type for both studies is displayed in Figure 6.5 while the average completion times are listed in Table 6.6. Figure 6.5 compares completion time between runs utilizing a command display (CD) with runs in which the command display is not available (ND). Results for both levels of time delay are included. In studies with no time delay, completion times are 7.4% (4.7 seconds) faster without the command display than with the display. With a 1.25 second transmission delay present in the system however, the command display is of great assistance as can be seen in the 32% decrease in completion times for tests implementing the command display. Completion

times were about 29.3 seconds faster when the command display was available than with no display, and were slightly faster than for the tests with no time delay and no display as can be seen in Table 6.6. The effect of display type on completion time is significant ($P < 0.0001$) for both time delay levels tested indicating a strong probability that they are not due to chance.

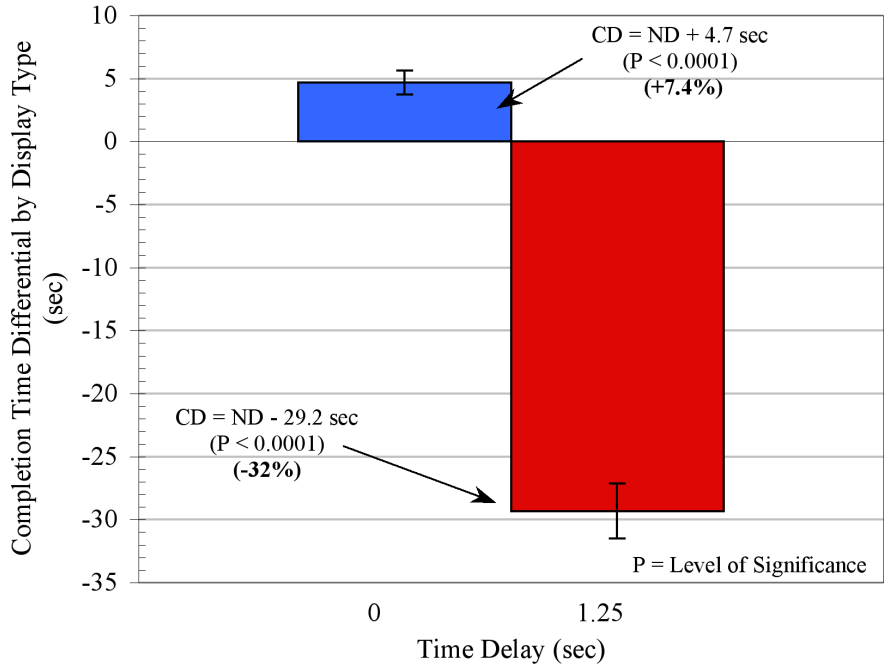

Figure 6.5: Effect of Display Type on Average Completion Time.

The effect of controller type on completion time is shown in Figure 6.6 and Table 6.7. Figure 6.6 shows the difference in performance between controller types for both levels of time delay while Table 6.7 lists the average course completion times for all time delay and controller combinations. With no transmission delay in the system, subject completion times were shorter with both the nonlinear and adaptive controllers than with the 'PD' controller. There was a 6.4% (4.3 second)

Average Run Time (sec)		
Time	**Display Type**	
Delay	**ND**	**CD**
0	63.5	68.2
1.25	91.1	61.8

Table 6.6: Average Run Times by Time Delay and Display Type.

Average Run Time (sec)			
Time	**Controller Type**		
Delay	**PD**	**NL**	**AD**
0	68.1	63.8	65.7
1.25	78.6	76.0	74.7

Table 6.7: Average Run Times by Time Delay and Controller Type.

decrease with the nonlinear controller vs. the 'PD' controller (P = 0.0003) while completion times with the adaptive controller were about 3.6% (2.5 seconds) less than those of the 'PD' controller (P = 0.0356). No statistically significant difference in performance between the nonlinear and adaptive controllers was found for tests with no time delay. While Figure 6.6 demonstrates slightly faster performance with the nonlinear controller than with the adaptive controller, the standard deviation is too large in comparison to the difference to be able to assert statistical significance.

Figure 6.6 indicates that completion times improve with either of the advanced controllers over the 'PD' controller when 1.25 seconds of time delay is present. This is most likely attributable to the additional model information contained in both the nonlinear and adaptive controllers. Unfortunately, although these trends are suggested, the standard deviation is so large in comparison to the estimates that true differences are impossible to detect. Testing with a larger subject pool might enable determination of whether or not these results are indeed significant.

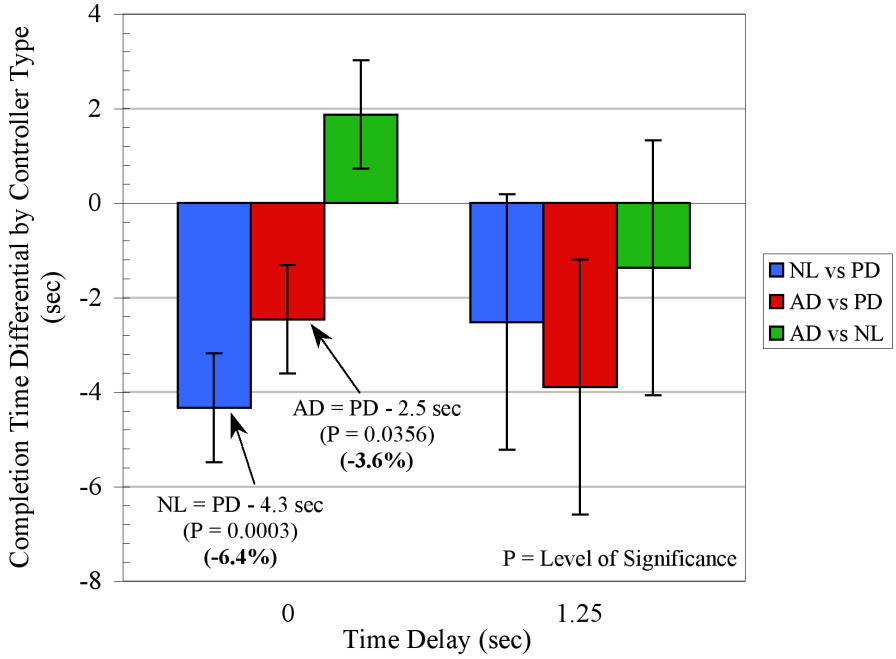

Figure 6.6: Comparison of Controller Effects on Average Completion Time.

6.5.2 Average Number of Hoops Hit Per Run

In order to evaluate the accuracy with which the subjects were able to fly through the hoop course, two metrics were used. The first, discussed in this section, was the average number of hoops that were hit per run by each test subject. The second was the ability of subjects to complete the course cleanly, without any collisions and will be discussed in the next section. Results from SAS indicate that while both display and controller types affect the average number of hits that occur per run when there is no time delay in the system, display is again the only effect with statistical significance when time delay is present.

Figure 6.7 compares accuracy between display types for both time delay levels. As evidenced by completion time results discussed previously, the command display may slightly hinder subject performance when no time delay is present in the system. For tests with no transmission delays, subjects were slightly more likely to hit a hoop while using the command display than without ($P = 0.0073$). With 1.25 seconds of time delay present, however, the command display was of benefit to the test subjects, decreasing the average number of hoops hit by 0.5 hits per run ($P < 0.0001$). The effect of the display type on subject accuracy was statistically significant for both time delays as indicated by the P-levels.

Examination of Table 6.8, which lists the average number of hits that occurred for all display and time delay combinations, permits some additional conclusions to be drawn. From this table, several trends can be inferred:

- with no time delay, subjects were about 50% more likely to hit a hoop with the command display than without it;
- with a 1.25 second delay in the system, subjects were more than three

Average Hoop Hits		
Time	**Display Type**	
Delay	**ND**	**CD**
0	0.19	0.28
1.25	0.77	0.24

Table 6.8: Average Number of Hoops Hit Per Run by Time Delay and Display Type.

Average Hoop Hits			
Time	**Controller Type**		
Delay	**PD**	**NL**	**AD**
0	0.30	0.23	0.19
1.25	0.54	0.48	0.50

Table 6.9: Average Number of Hoops Hit Per Run by Time Delay and Controller Type.

times as likely to hit a hoop with no command display as they were with the command display

- with no command display, subjects were over three times more likely to hit a hoop with 1.25 seconds of time delay than when no time delay was present;

- the command display permitted subjects to fly through the course with the same level of accuracy regardless of time delay level.

While display type affects subject accuracy significantly, controller type appears to have less impact, according to statistical analysis. An examination of Table 6.9 indicates that the addition of time delay appears to increase the likelihood of a hoop hit regardless of controller type. Figure 6.8 shows the adaptive controller to be more accurate than the 'PD' controller when there is no time delay in that it results in fewer hoop hits. The magnitude of the standard error is too large for all other controller/time delay combinations to permit any meaningful conclusions to be drawn concerning number of hoops hit per run.

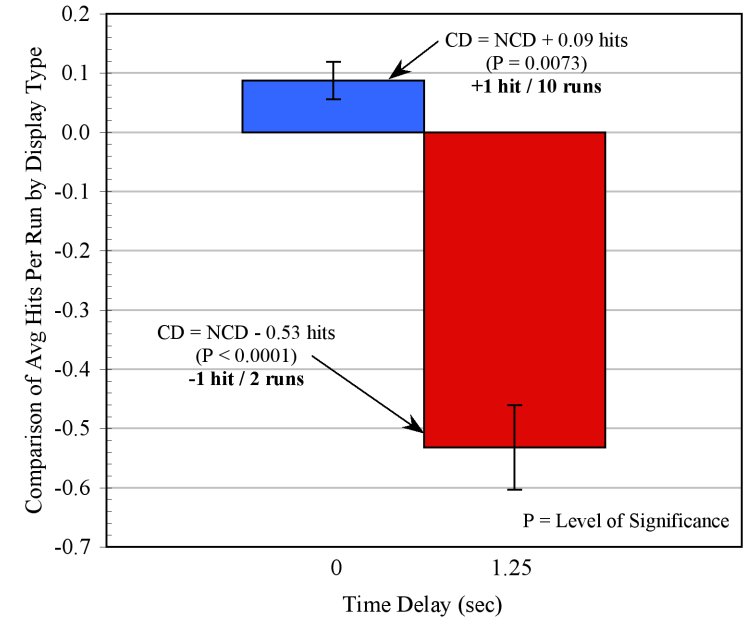

Figure 6.7: Effect of Display Type on Average Number of Hoops Hit Per Run.

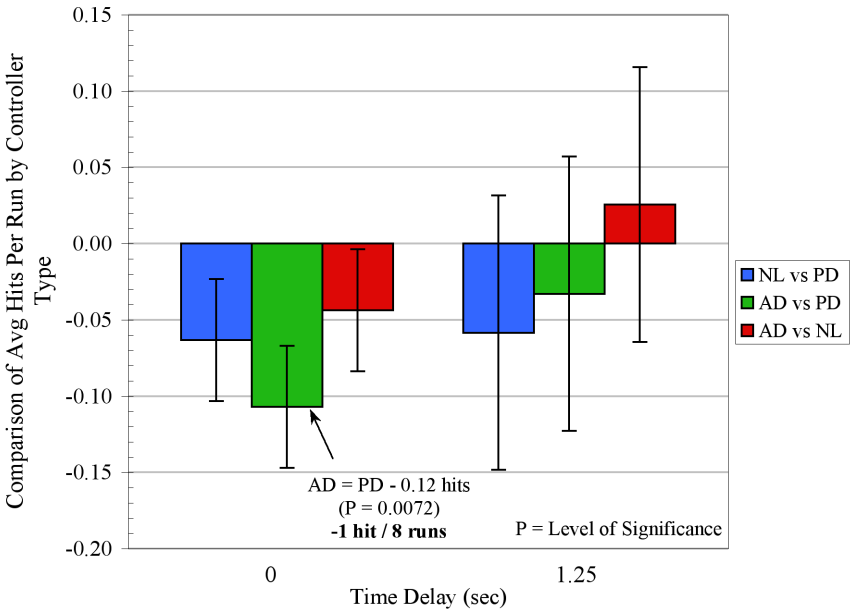

Figure 6.8: Comparison of Controller Effects on Average Number of Hoops Hit Per Run.

Figure 6.9 displays the average number of hits by hoop for each display/controller combination averaged over all subjects for tests with no time delay while Figure 6.10 shows the same information for tests with 1.25 seconds of transmission delay. These figures are shown to provide some suggestion about the difficulty of the course. For both levels of time delay studied, it appears as if hoop 5 provided the most difficulty for subjects while hoop 1 was the least difficult. It is also apparent that hoop hits increased when the command display was unavailable for tests with time delay.

6.5.3 Ability to Complete Runs Cleanly

The second metric used to evaluate subject accuracy was the ability of subjects to complete a run cleanly, that is without any hoop collisions. When no time delay was present in the system approximately 77% of the runs were collision free; with 1.25 seconds of time delay 65% of the runs had no collisions.

While previous response variables have been continuous, this response is binary, i.e. either a run was completed cleanly or else one or more collisions occurred during the run. Logistic regression analysis is used to study the association between a binary response and the set of explanatory variables (such as display or controller type). The response variable y, can take one of two values; for this analysis, either the run was completed cleanly ($y = 1$), or a collision occurred ($y = 0$). If $\boldsymbol{x}$ is a vector containing the explanatory variables, p, the probability that a run was completed cleanly given the particular explanatory variables is

$$p = Pr(y = 1|\boldsymbol{x}).$$

To relate p to a linear combination of independent/explanatory variables, the

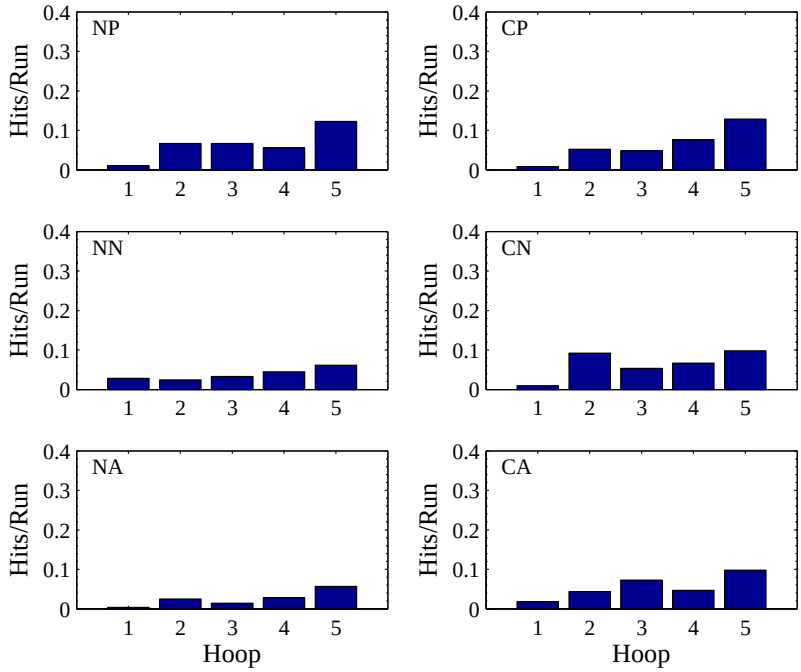

Figure 6.9: Mean Hits Per Run for Each Hoop by Display Type and Controller Type for Tests with No Time Delay.

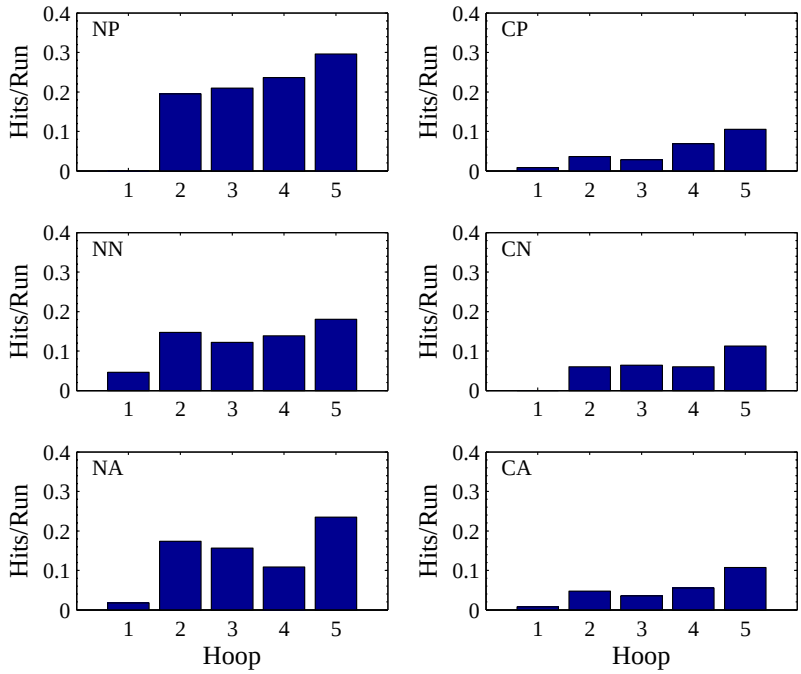

Figure 6.10: Mean Hits Per Run for Each Hoop by Display Type and Controller Type for Tests with 1.25 Second Time Delay.

logistic regression model is

$$\text{logit}(p) \equiv \ln\left(\frac{p}{1-p}\right) = \alpha + \boldsymbol{\beta}'\boldsymbol{x}.$$

The above discussion was derived from SAS (1999) and Ott and Longnecker (2001). For this analysis, the vector $\boldsymbol{x}$ of explanatory variables consisted of:

- x_1: display type
- x_2: controller type
- x_3: group
- x_4: test session
- x_5: subjects nested within groups
- x_6: interaction of display and controller

The effect of display type on the ability to fly the course cleanly can be seen in Figure 6.11. This figure indicates the likelihood that a subject will complete an error free run while using a command display versus when no command display is available. With no time delay, subjects were slightly more likely to hit a hoop during the run with the command display than without ($P < 0.0001$), but when time delay was present subjects were over twice as likely to have an error free run with the command display than when one was not available ($P < 0.0001$).

Figure 6.12 shows the effect of controller type on the ability to fly an error free run. With no time delay, subjects were approximately 1.5 times more likely to complete the course cleanly with the adaptive controller than with either the 'PD' ($P = 0.0001$) or nonlinear controllers ($P = 0.0093$). There was no difference in performance between the nonlinear and 'PD' controllers. When time delay is

present in the system, vehicle controller type has no statistically significant effect on the ability of subjects to maneuver through the course cleanly. This is evident when the odds ratios between controller types are examined in Figure 6.12; they are all approximately equal to one.

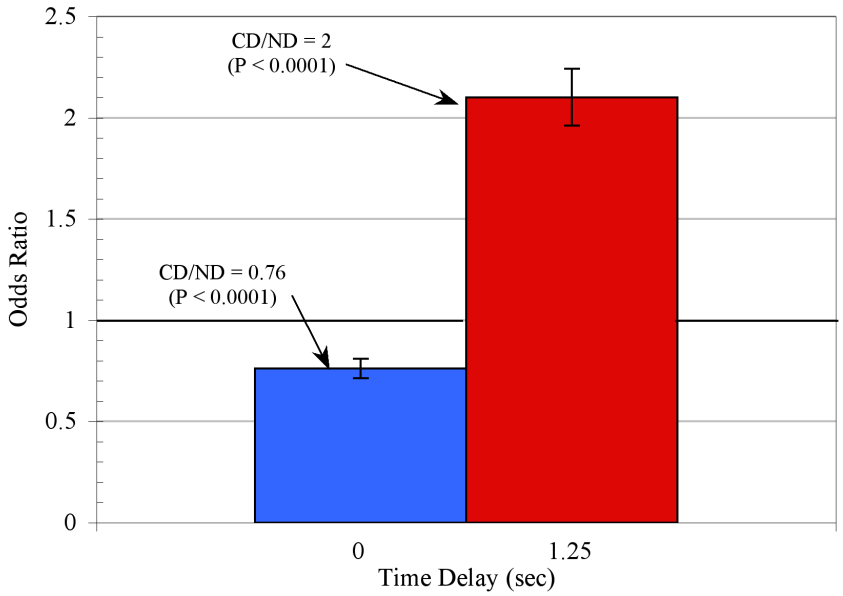

Figure 6.11: Effect of Display Type on the Probability of Completing Run With No Collisions.

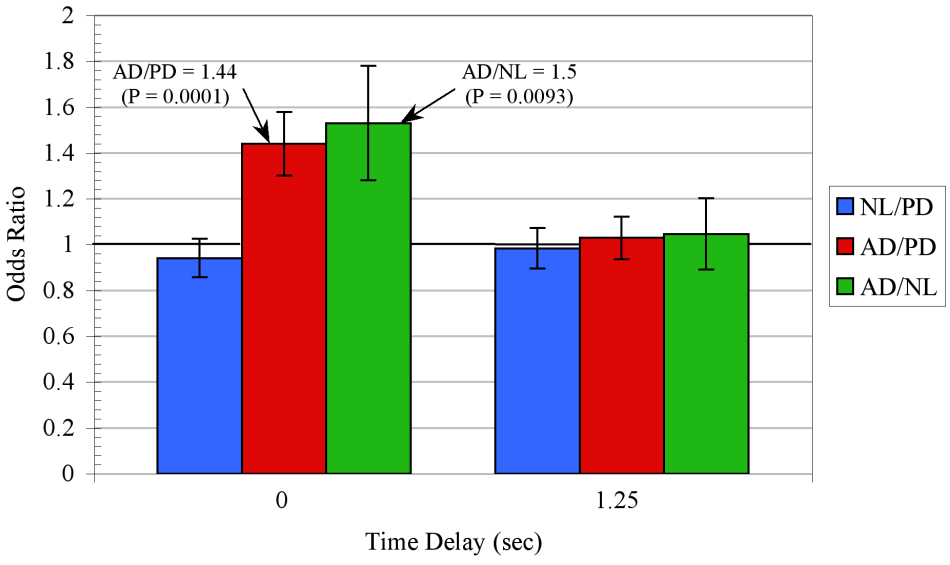

Figure 6.12: Comparison of Controller Effects on the Probability of Completing a Run with No Collisions.

6.5.4 Pilot Effort

Two separate metrics were chosen to provide an indication of the level of effort expended by subjects during testing. These include the percentage of test time each hand controller degree of freedom was used and the variance in deflection for each hand controller degree of freedom. It was reasoned that it would prove more interesting to measure the hand controller effort, not by the mere deflection of the hand controller, but by the variations in hand controller deflection from its mean value. For example, if a subject maintained the x degree of freedom of the translational hand controller in the full on position for the entire time of the test, not much effort was really required. However, if the subject moved the x DOF back and forth throughout the test, more effort was expended. In this analysis, each of the six hand controller degrees of freedom was considered separately. The effort for each degree of freedom was determined by calculating a type of impulsive variance of the hand controller usage whereby only the time a particular hand controller was utilized was used for the calculation. The effort for each hand controller was determined as follows

$$E_{ff_i} = \frac{1}{T}\sum_{k=1}^{n-1}(h_{i,k} - \bar{h}_i)^2 \Delta t_k \tag{6.2}$$

where for a particular hand controller degree of freedom i ($i = 1, ..., 6$), T represents the total run time, k represents a particular data point in time, n represents the total number of data points recorded in a run, $h_{i,k}$ is the raw hand controller reading of DOF i at time k, Δt_k the increment of time between points k and $k+1$ and $\bar{h}_i$ the mean level of deflection of DOF i during a particular test. The equations for the calculation of mean hand controller deflection and usage time

with each hand controller degree of freedom are shown below.

$$\bar{h}_i = \frac{1}{T_{o_i}} \sum_{k=1}^{n-1} (h_{i,k}) \Delta t_k \tag{6.3}$$

$$T_{o_i} = \sum_{\substack{k=1 \\ h_{i,k} \neq 0}}^{n-1} \Delta t_k \tag{6.4}$$

Figure 6.13 compares of the percentage of time that each hand controller degree of freedom was used according to display type for both time delay levels tested and Figure 6.14 compares the variance in each hand controller degree of freedom between display types for both time delays. As mentioned previously, due to camera position the x dof is the primary degree of freedom used for vehicle translation. Thus, this tends to be the degree of freedom most affected by changes in variables. Examining results for the x dof in Figure 6.13 and Figure 6.14 it can be seen that with no time delay in the system the x dof is used less with the command display than without ($P < 0.0001$) but the variance in deflection is greater with the command display than without it ($P < 0.0001$). This provides a strong indication that subjects were using the x dof in a more intermittent fashion when the command display was implemented in the system with no time delay. The opposite is true when a 1.25 second time delay is introduced into the system. Table 6.10 shows the level of usage of the x dof increases 24% with the command display ($P < 0.0001$) and actually reaches the same level (84%) as the system with no time delay and no command display while Table 6.11 indicates the variance in the x dof deflection drops dramatically to match the low level (0.122) obtained under conditions of no time delay and no display ($P < 0.0001$). These results provide evidence that the command display is counteracting the move and wait strategy adopted by subjects when time delay is present and no

command display is available. While the percentage of x dof usage increased, the decrease in variance suggests that the pilots were able to utilize the x dof more consistantly.

The effect of display type on the other hand controller degrees of freedom is not so dramatic. Indeed, for tests with no time delay all remaining dofs are used less and exhibit a decreased variance of hand controller deflection when the command display is available. Results are statistically significant for the y and z dofs for both percent usage ($P < 0.0001$; $P = 0.002$) and variance in deflection ($P = 0.0007$; $P = 0.0211$). As with the x dof, the opposite trend is observed when time delay is introduced into the system. The remaining hand controller degrees of freedom are used more with the command display than without (all significant to $P < 0.0001$) and the variance in hand controller deflection also increases, although only the yaw dof is statistically significant ($P = 0.0055$).

As with other performance metrics the impact that vehicle controller type has on hand controller effort is not obvious. There is a statistically significant effect on pilot effort about two degrees of freedom when effort levels between the nonlinear and 'PD' controllers are examined. The first indicates that the x dof is used more with the nonlinear controller than with the 'PD' controller ($P = 0.0127$) with no time delay as can be seen in Figure 6.15. Since Figure 6.16 indicates no statistical difference in variance between the nonlinear and 'PD' controllers about the x dof, once can conclude that the subjects may exert less effort about the x dof with the nonlinear controller than with the 'PD' controller in the absence of time delay.

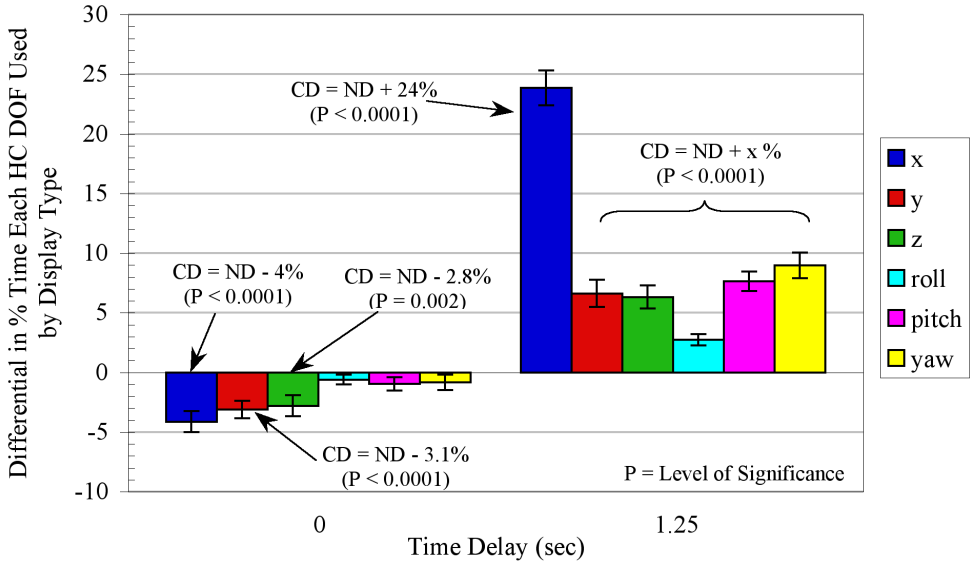

Figure 6.13: Effect of Display Type on Percentage of Time Hand Controllers Used.

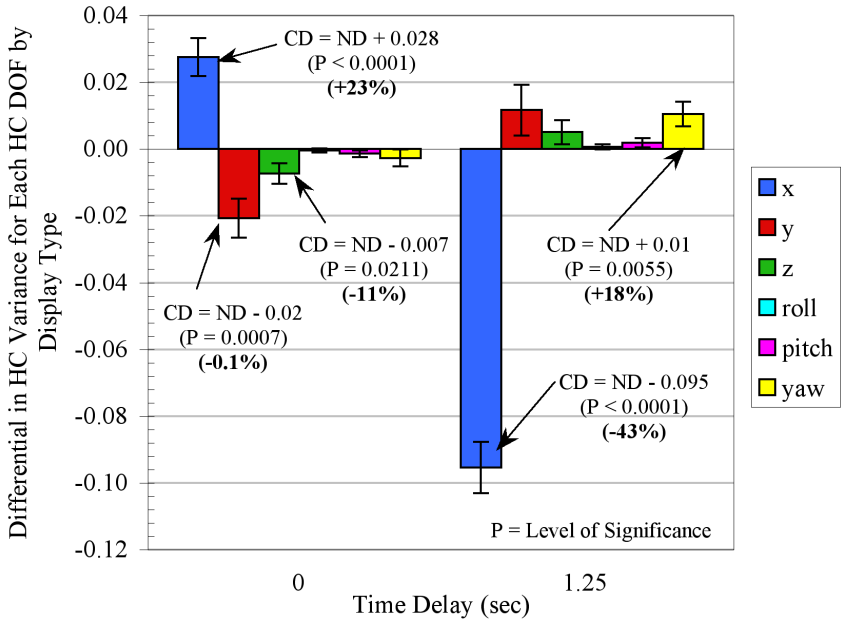

Figure 6.14: Comparison of Display Effects on Hand Controller Variance.

		Time Delay (sec)			
		0		1.25	
Display		ND	CD	ND	CD
H	x	83	79	60	84
C	y	40	37	27	34
	z	25	22	13	19
D	roll	8	7	3	6
O	pitch	22	21	12	19
F	yaw	25	24	13	22

Table 6.10: Mean Percentage of Time Each Hand Controller DOF Used by Time Delay and Display Type.

		Time Delay (sec)			
		0		1.25	
Display		ND	CD	ND	CD
H	x	0.122	0.150	0.219	0.124
C	y	0.218	0.197	0.169	0.181
	z	0.066	0.059	0.048	0.053
D	roll	0.0070	0.0066	0.0057	0.0063
O	pitch	0.028	0.027	0.028	0.030
F	yaw	0.064	0.062	0.058	0.069

Table 6.11: Mean Variance in Each Hand Controller DOF by Time Delay and Display Type.

The second degree of freedom in which controller type affects effort levels is the pitch dof. Once again, time delay is not present. Figure 6.16 indicates that the variance in the pitch dof increases with the nonlinear controller ($P = 0.007$). Since Figure 6.15 indicates no difference in time the pitch dof was used between the 'PD' and nonlinear controllers, one can conclude that more effort is expended about the pitch dof when the nonlinear controller is used than when the 'PD' controller is used.

There is no indication that the controller type has any effect on pilot effort regardless of time delay for any other combination of controllers. Figure 6.17 and Figure 6.18 present the results comparing hand controller metrics between 'PD' and adaptive controllers while Figure 6.19 and Figure 6.20 compare nonlinear with adaptive controllers. They provide little assistance in determining any patterns in hand controller usage but are presented for completeness.

Table 6.12 which compares time usage of each hand controller degree of freedom for all combinations of time delay and controller type and Table 6.13, which compares the variance in hand controller deflection for each dof by time delay and controller type were examined to determine if there might be some trends in hand controller performance. It can be seen in Table 6.12 that all hand controller degrees of freedom are used less when time delay is present than with no time delay. In addition, an examination of Table 6.13 reveals an increase in the variance in deflection for the x dof regardless of controller type when there is time delay in the system. This, coupled with the decrease in percentage of use, indicates that more effort is expended with the x dof for conditions of time delay regardless of controller type. It is much more difficult to distinguish any patterns in usage for the remaining hand controllers. While remaining hand controller degrees of

freedom were used less when time delay was present, the variance in deflection for the y and z dofs also decreased but remained approximately the same for the rotational degrees of freedom regardless of display type or time delay.

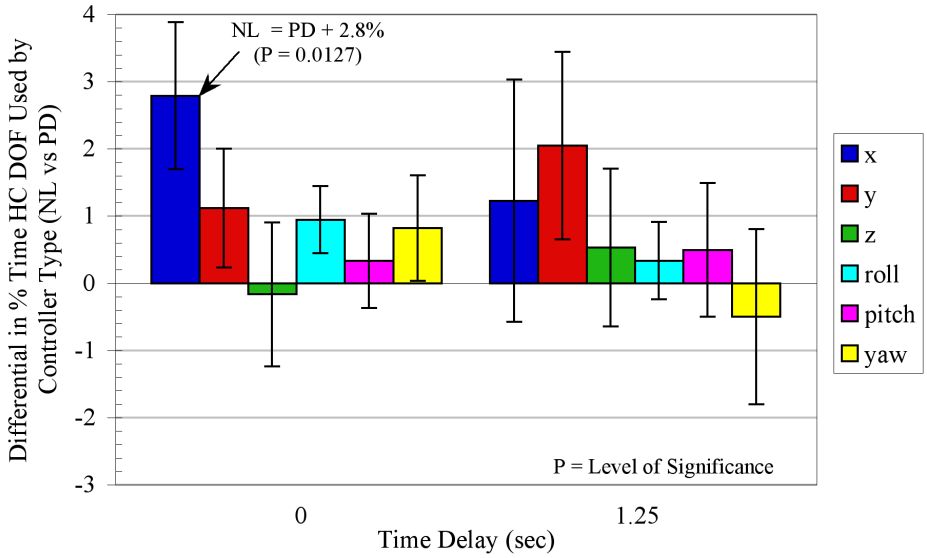

Figure 6.15: Differential in Percent of Time HC DOFs Used between Nonlinear and 'PD' Controllers (NL = PD ± x%).

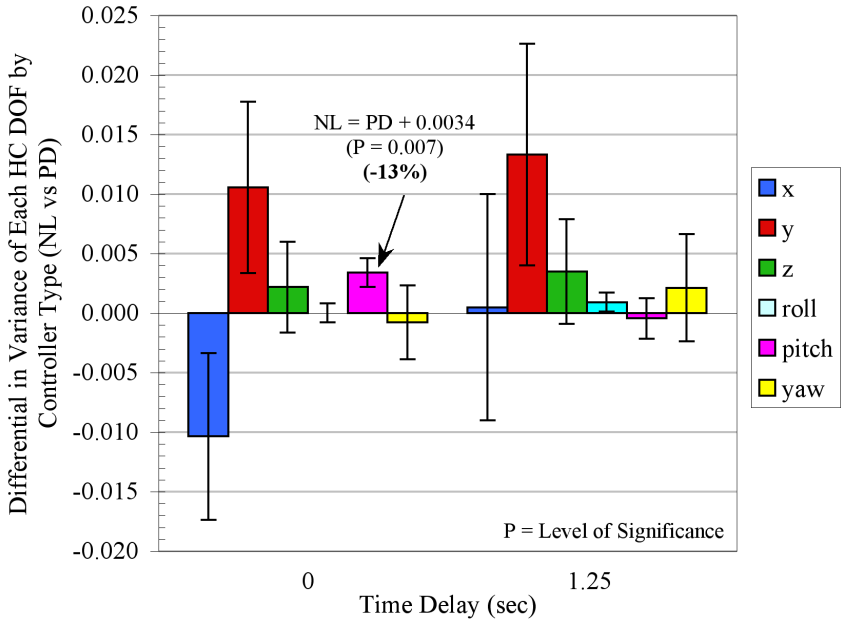

Figure 6.16: Differential in Variance of HC DOFs Used between Nonlinear and 'PD' Controllers (NL = PD± x%).

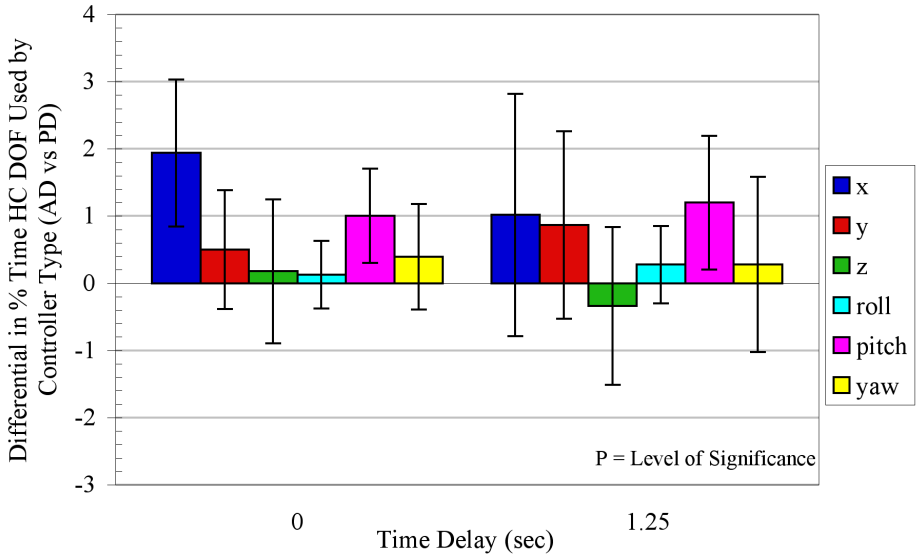

Figure 6.17: Differential in Percent of Time HC DOFs Used between Adaptive and 'PD' Controllers (AD = PD ± x%).

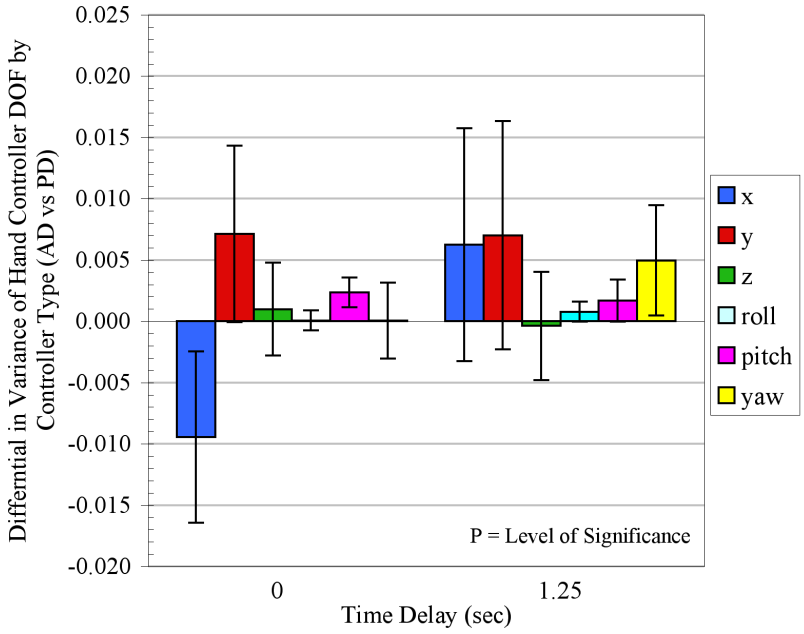

Figure 6.18: Differential in Variance of HC DOFs Used between Adaptive and 'PD' Controllers (AD = PD ± x%).

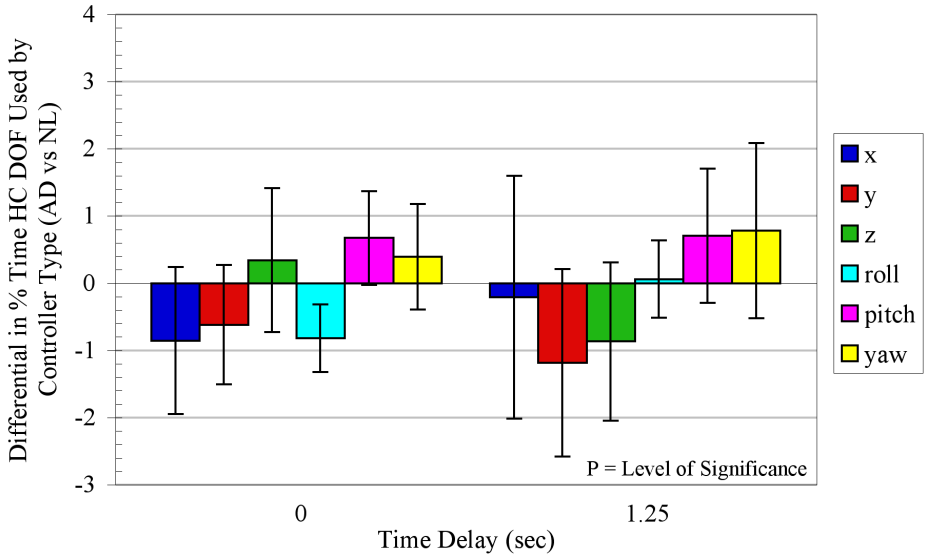

Figure 6.19: Differential in Percent of Time HC DOFs Used between Adaptive and Nonlinear Controllers (AD = NL ± x%).

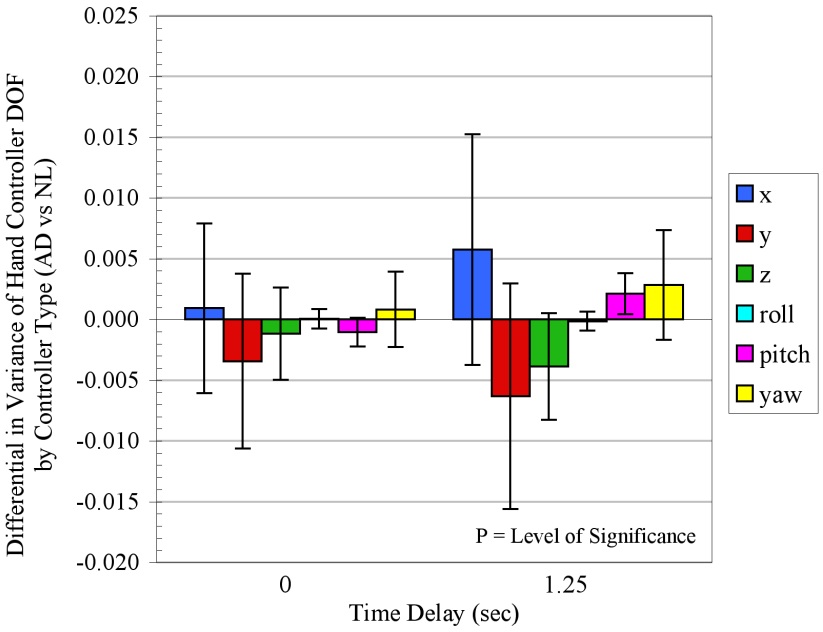

Figure 6.20: Differential in Variance of HC DOFs Used between Adaptive and Nonlinear Controllers (AD = NL ± x%).

		Time Delay (sec)					
		0			1.25		
Controller		PD	NL	AD	PD	NL	AD
H	x	79.8	82.5	81.7	71.1	72.4	72.2
C	y	37.9	39.0	38.4	29.4	31.5	30.3
	z	23.4	23.3	23.6	16.1	16.6	15.8
D	roll	7.4	8.3	7.5	4.3	4.6	4.5
O	pitch	20.9	21.2	21.9	15.0	15.5	16.2
F	yaw	23.6	24.5	24.9	17.2	16.7	17.5

Table 6.12: Mean Percentage of Time Each Hand Controller DOF Used by Time Delay and Controller Type.

		Time Delay (sec)					
		0			1.25		
Controller		PD	NL	AD	PD	NL	AD
H	x	0.142	0.132	0.133	0.170	0.170	0.176
C	y	0.201	0.212	0.209	0.169	0.182	0.176
	z	0.061	0.063	0.062	0.050	0.053	0.049
D	roll	0.0068	0.0068	0.0069	0.0055	0.0064	0.0063
O	pitch	0.025	0.029	0.028	0.029	0.028	0.030
F	yaw	0.063	0.062	0.063	0.061	0.063	0.066

Table 6.13: Mean Variance in Each Hand Controller DOF by Time Delay and Controller Type.

6.5.5 Mean Flight Path

In order to compare the flight paths generated by the test subjects with the flight path resulting from the automatic trajectory generator the mean flight path for each subject during each test session was calculated. To accomplish this, for each run in a test session

- the time data were normalized;
- separate spline functions were fit through the x, y and z data using the normalized time data;
- the resulting spline functions were evaluated at specified times throughout the run.

Finally, the average of these computed values for x, y and z positions were obtained over the test session for each subject. The results were categorized according to group, display/controller combination and time delay, and plotted against the appropriate automatic trajectory data. These plots indicated that there were two distinctly different approaches adopted by test subjects when approaching a hoop. One subset of four to five subjects demonstrated a preference for aligning themselves with a hoop at a much greater distance than the automatic trajectory. This approach is clearly indicated in Figure 6.21 which displays the mean paths taken by group five subjects with a command display, nonlinear controller and 1.25 second time delay. Subjects 1 and 13 swing much further out to align themselves with the hoop face as can be seen in the xy and xz projections than that of the automatic trajectory or subject 7. Most subjects more closely approached the automatic trajectory path as is evident in Figure 6.22 which shows the mean flight path of group six subjects under the same conditions as the previous figure.

These plots are representative of the two types of flight paths adopted by the test subjects. The strategy utilized by each subject was independent of display, controller type or time delay. Rather, the strategy adopted by each subject reflects an innate "preference" of that pilot. The lone exception to this appears in the results of subject 15, whose mean flight path swung wide in tests with no time delay but more closely approximated that of the automatic trajectory for the study with time delay.

Of the five subjects who adopted this approach, only one was experienced. This subject's technique is likely due to the extensive experience obtained on another larger, more powerful lab vehicle used for docking maneuvers. Due to the handling characteristics of this vehicle, there was a greater probability of successfully completing a docking maneuver if the vehicle was aligned with the target when still at a distance from the target. None of the other subjects in the study had experience operating this vehicle.

To determine if flight path type affected any of the performance metrics such as completion time and accuracy, the mixed model analysis was rerun with approach added as an effect. The mean flight path type for each subject was determined for each test condition by examining both the mean flight path plots such as those shown above as well as plots of the first derivatives of the mean flight path. Since it was determined that this contrast might be of interest only after the data had been examined, it is necessary to perform a more conservative comparison to assess if there is in fact any effect on performance due to mean flight path type. Thus, Scheffé's method was implemented Ott and Longnecker (2001). In this procedure, the ratio of the estimate to standard error is compared

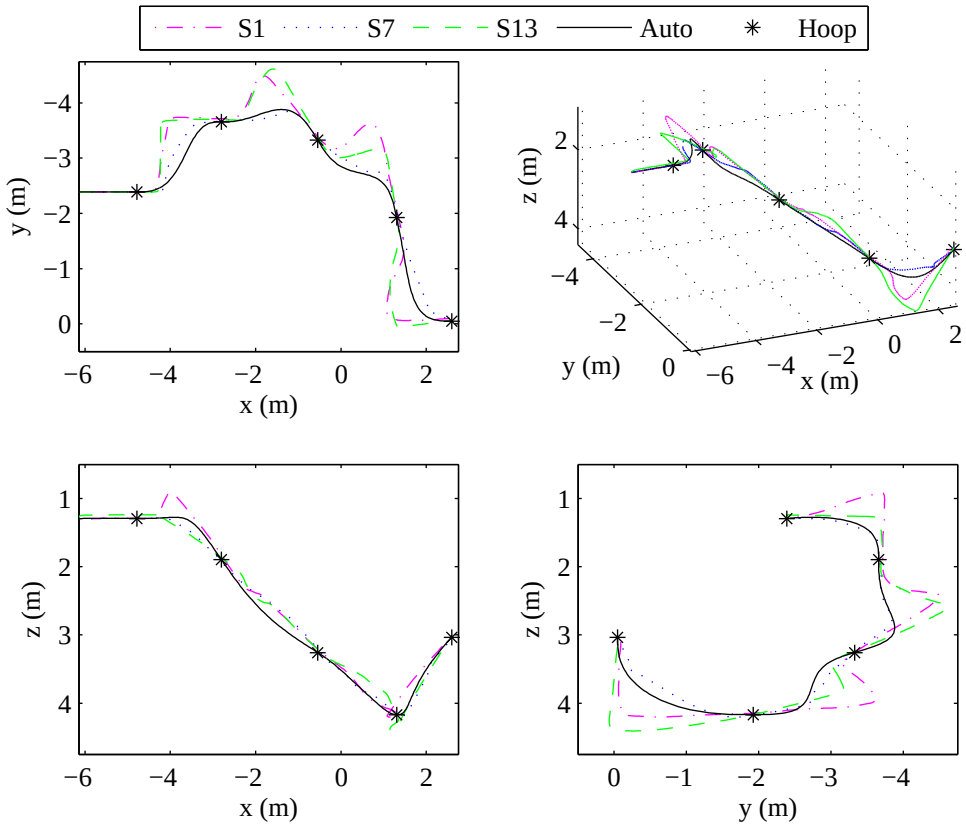

Figure 6.21: Mean Paths of Group 5 Subjects with 1.25 Second Time Delay, Command Display and Nonlinear Controller (upper left: projection of trajectory onto the xy plane, lower left: projection of trajectory onto the xz plane, lower right: projection of trajectory onto the yz plane,upper right: three dimensional plot of trajectory).

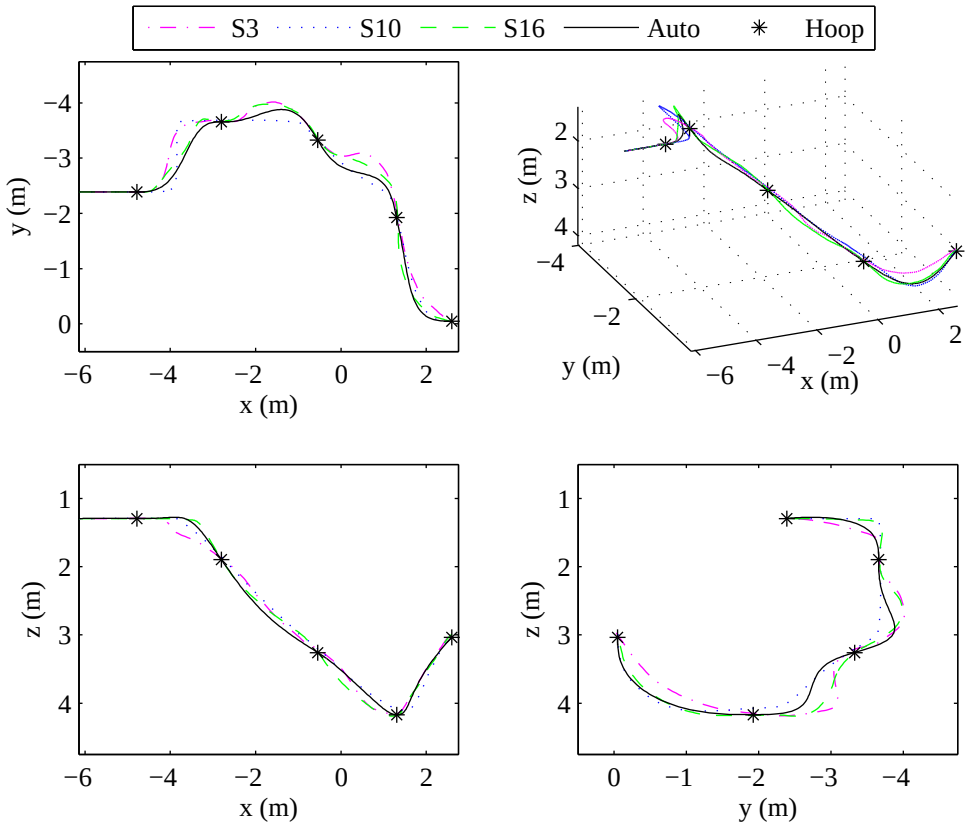

Figure 6.22: Mean Paths of Group 6 Subjects with 1.25 Second Time Delay, Command Display and Nonlinear Controller (upper left: projection of trajectory onto the xy plane, lower left: projection of trajectory onto the xz plane, lower right: projection of trajectory onto the yz plane,upper right: three dimensional plot of trajectory).

to the quantity

$$\sqrt{(n-1)F_{df_1,df_2,\alpha}}$$

where $F_{df_1,df_2,\alpha}$ is the upper α critical value from the F distribution, n is the number of population means, $df_1 = n - 1$ and df_2 is the number of error degrees of freedom for the effect in question. Results from Scheffé's method indicate that hoop approach style has no statistical effect on course completion time or accuracy at the $\alpha = 0.05$ level used for this study.

6.5.6 Comparison of Hand Controller Usage between Automatic Trajectory Generator and Human Subjects

In order to compare hand controller usage of human subjects with the automatic trajectory generator, it was first necessary to determine the equivalent hand controller readings that would have produced the desired trajectory. These raw hand controller readings were determined using the equations describing the kinematic simulation previously detailed in Section 4.3.4.

The raw hand controller readings for each subject during each test session were averaged. Since the time steps were not consistent between runs the time variable was normalized and a spline curve was fit through the data points of each hand controller degree of freedom. The resulting curves corresponding to each run were then evaluated at a set number of points along the trajectory. This data was then averaged over the corresponding number of runs to obtain the mean hand controller commands issued by test subjects throughout a typical run. Typical results from this process are shown in Figure 6.23 for group 1 using a 'PD' controller with no command display and no time delay. These results are representative of performance for all subjects.

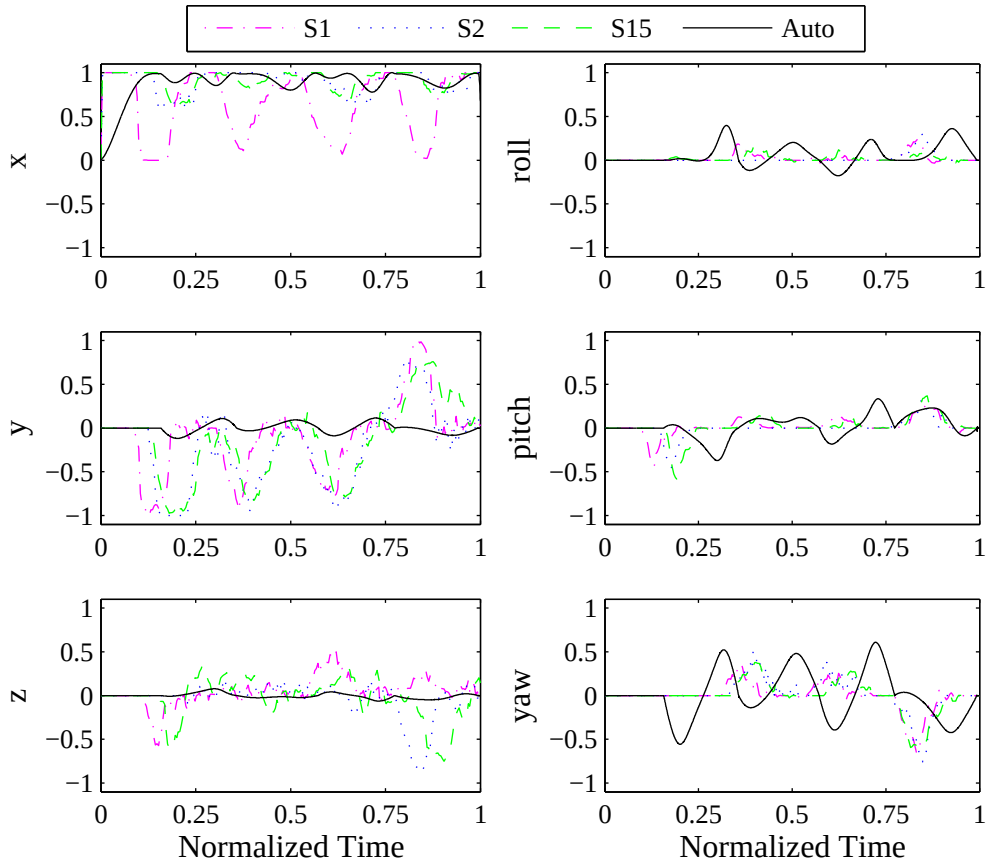

Figure 6.23: Mean Hand Controller Commands Issued by Group 1 Subjects with No Time Delay, No Command Display and 'PD' Controller.

Since completion times for each run were different and it was necessary to normalize the time variable, quantitative measures cannot be performed on this particular data. However, the mean hand controller commands can be used to draw some qualitative comparisons about hand controller performance between the automatic trajectory generator and human subjects. It can be seen that the automatic trajectory generator results in a smooth profile about all hand controller degrees of freedom whereas the profiles from human subjects are more variable. In addition, the plots indicate that humans adopt an alternate strategy to maneuver through the course than the automatic generator. While most human subjects are unable to operate the vehicle at the consistently high level of x deflection exhibited with the automatic generator, they tend to use the y and z dofs much more. In addition, human subjects tend to avoid much use of the roll degree of freedom.

The standard deviation in the mean hand controller deflection can also provide information about hand controller usage. Figure 6.24 and Figure 6.25 compare the standard deviation in the mean hand controller deflection about each degree of freedom for all subjects as well as the automatic trajectory generator for both display options, 'PD' control and 1.25 second time delay. From these representative plots, it can be seen that there is a greater variation in hand controller deflection in human subjects than the automatic trajectory, especially about the translational degrees of freedom. These plots indicate that humans tend to be more comfortable using translation rather than the coordinated rotational and translational motions of the automatic trajectory generator.

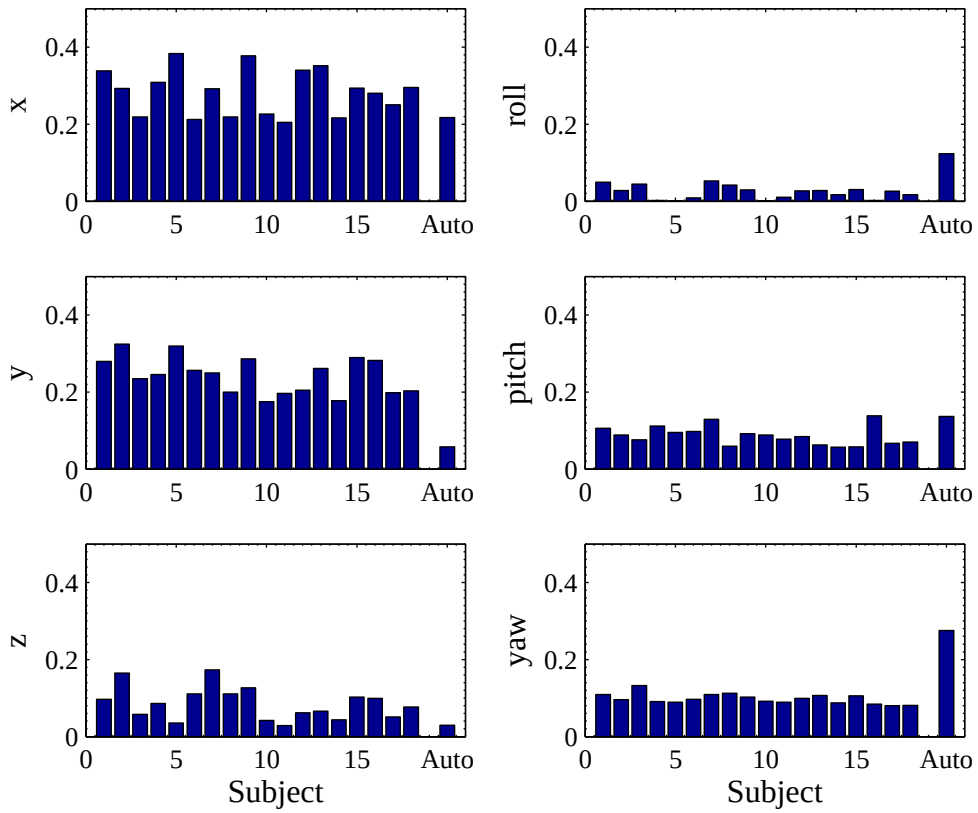

Figure 6.24: Standard Deviation of Mean Hand Controller Commands by Subject for Tests with No Command Display, 'PD' Controller, and 1.25 Second Time Delay.

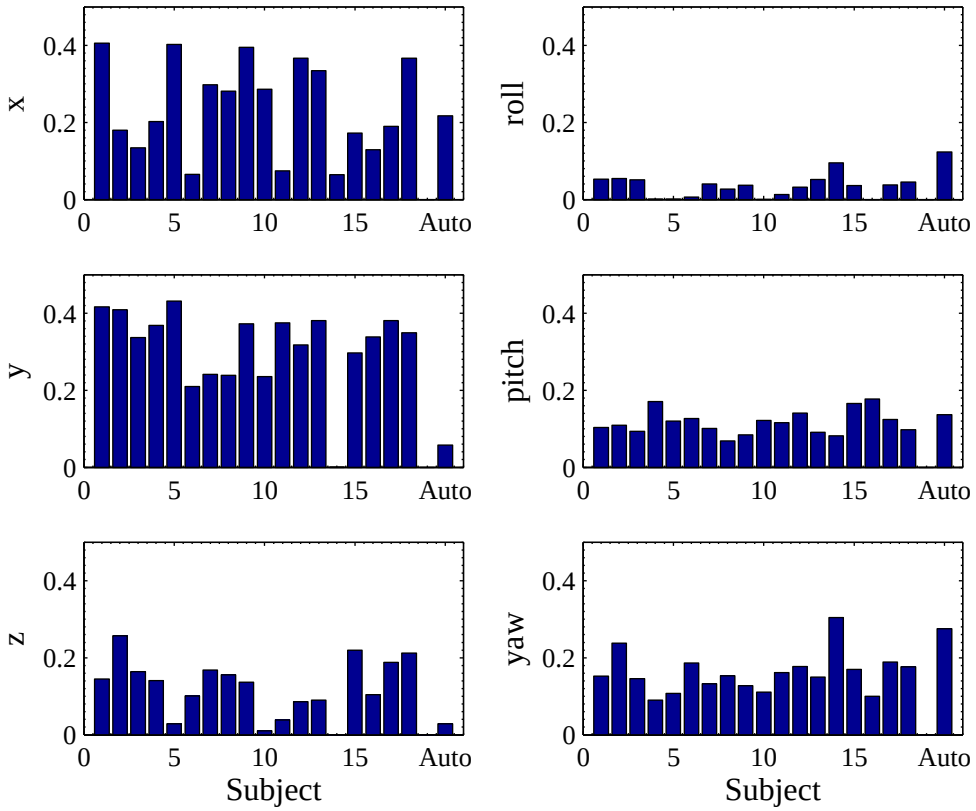

Figure 6.25: Standard Deviation of Mean Hand Controller Commands by Subject for Tests with Command Display, 'PD' Controller, and 1.25 Second Time Delay.

6.5.7 Main Flight Window Camera Views

As detailed in the simulation discussion, test subjects had three camera views available in each view window that they could cycle through at will. These included the SSV onboard camera view, an over the left shoulder of SSV view and a view directed perpendicularly toward the left side of SSV. In an effort to determine if camera view selection in the main window affected subject performance, the amount of time spent by each subject with each camera view during each test session was recorded.

Figure 6.26 displays the average amount of time each subject spent using each camera view in the primary flight control window for each controller type with no time display and no command display. Figure 6.27 presents camera view data for tests in which the command display was available whereas Figure 6.28 and Figure 6.29 show camera view usage for tests with a 1.25 second delay. Several trends are noticeable upon examining these plots. First, the side on view of SSV was used much less than the other views. Most subjects tended to use the shoulder view almost exclusively while about a third of the subjects used a either the onboard camera or some combination of the onboard camera with the shoulder view. Second, most subjects appear to stick with a camera strategy once they find one that works for them. Third, controller type has little effect on choice of camera view. Fourth, display type appears to have little effect on choice of camera for most subjects with the exception of the side on view. The side on view was used by more subjects when no command display was available most likely to provide more information about the position of SSV with respect to a hoop when in the vicinity of a hoop.

Statistical analysis appears to confirm the above mentioned observations re-

garding controller and display type. Figure 6.30 indicates the amount of time a subject spent with either the onboard or over the shoulder camera view is invariant to display type regardless of time delay. However, while the side on view was used less than 5% of the time, the fact that there was a statistically significant difference in usage by display type ($P < 0.0001$) for no time delay indicates that the subjects were using this view to provide additional information when the command display was unavailable. With time delay usage of the side view decreased and the standard error is too large in comparison to conclude any statistical significance.

Figure 6.31, Figure 6.32 and Figure 6.33 examine how camera selection is affected by controller type for the onboard camera, shoulder camera and side on camera respectively. As previously observed in Figures 6.26 - 6.29 the statistics show no evidence that controller type has any effect on camera selection. Indeed, the difference in time spent in any camera view between any controllers is less than 0.1 seconds.

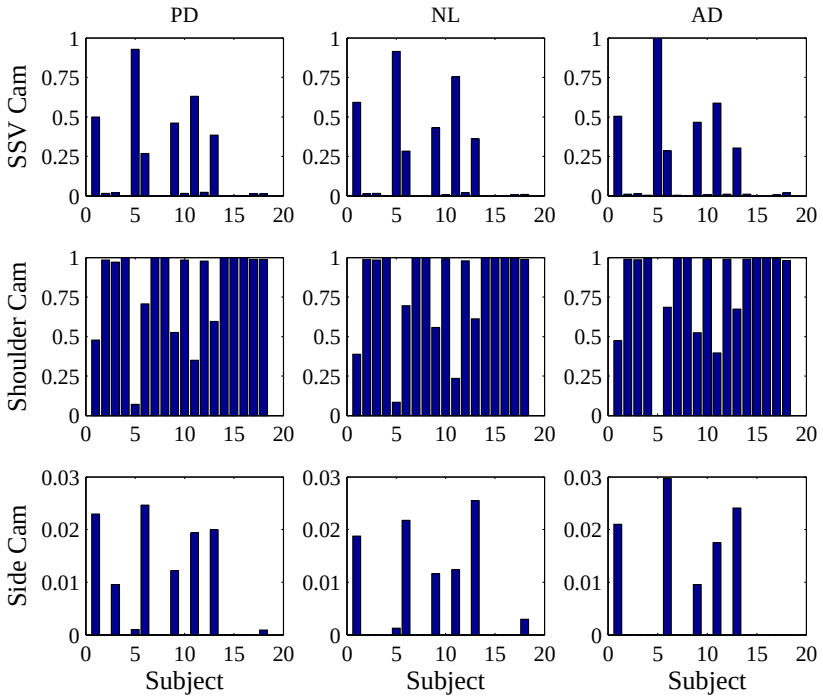

Figure 6.26: Percentage of Time Main Window Camera Views Used by Subjects with No Command Display and No Time Delay.

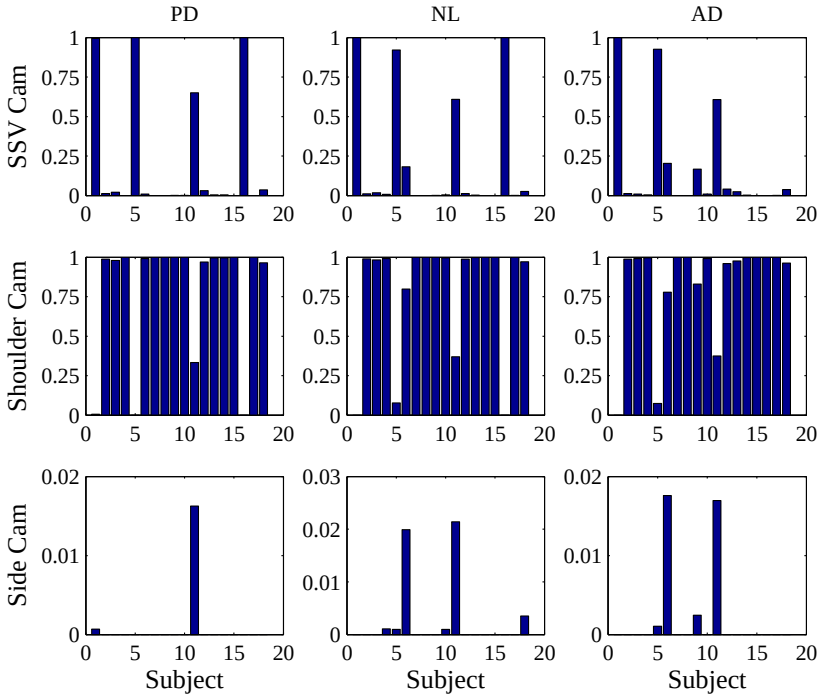

Figure 6.27: Percentage of Time Main Window Camera Views Used by Subjects with a Command Display and No Time Delay.

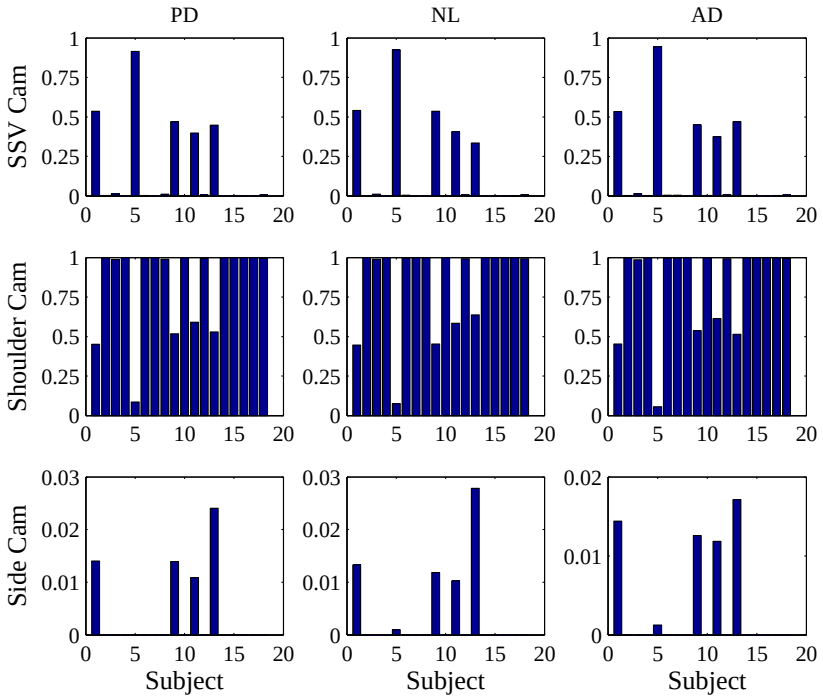

Figure 6.28: Main Window Camera Views Used by Subjects with No Command Display and 1.25 Second Time Delay.

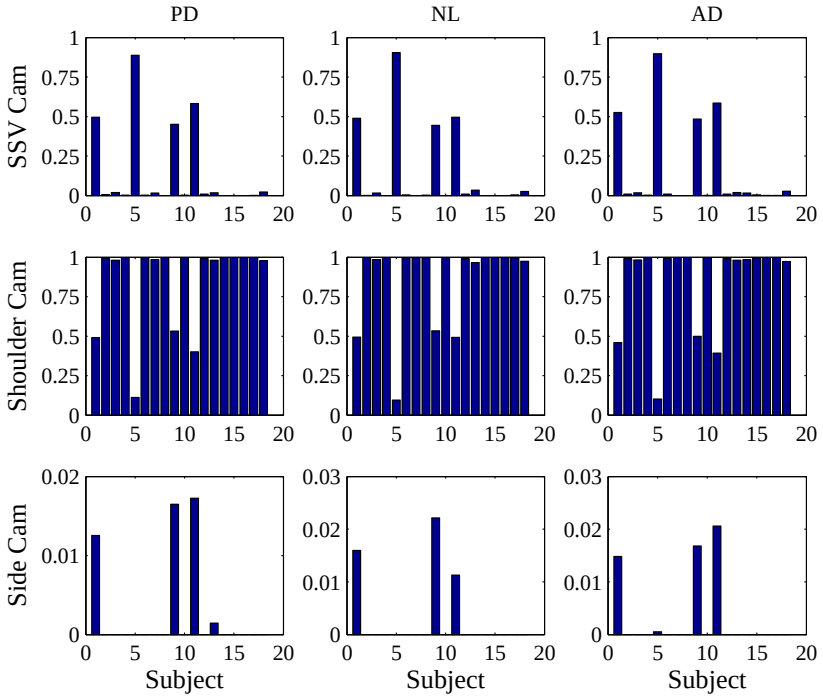

Figure 6.29: Main Window Camera Views Used by Subjects with a Command Display and 1.25 Second Time Delay.

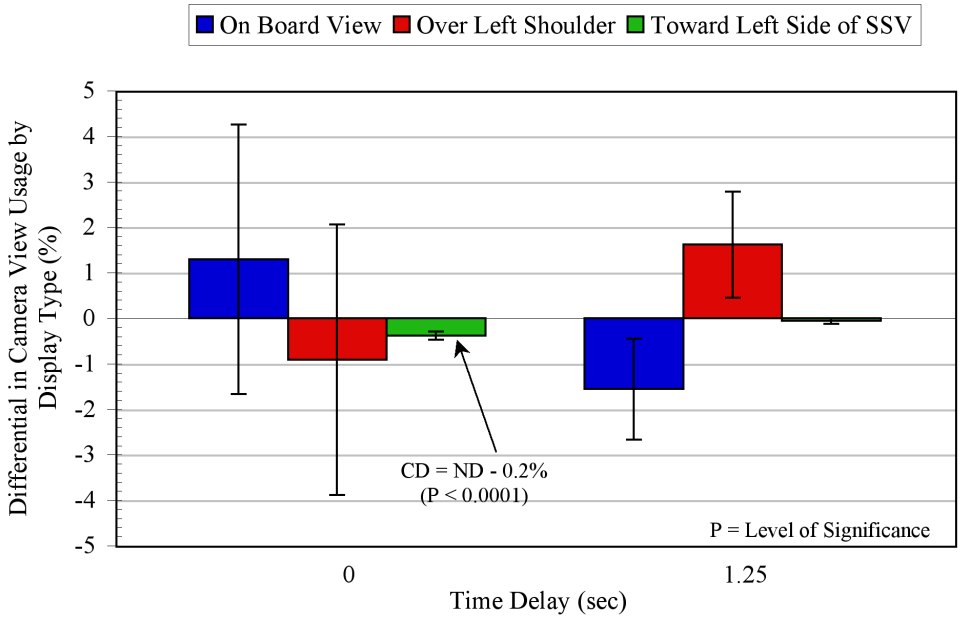

Figure 6.30: Camera Usage in Main Window by Display Type.

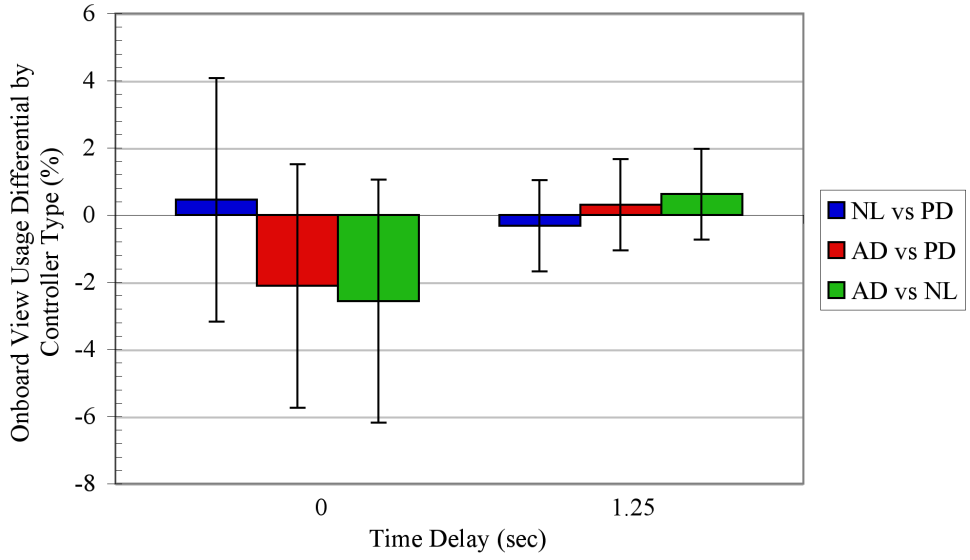

Figure 6.31: SSV Onboard Camera View Usage in Main Window by Controller Type.

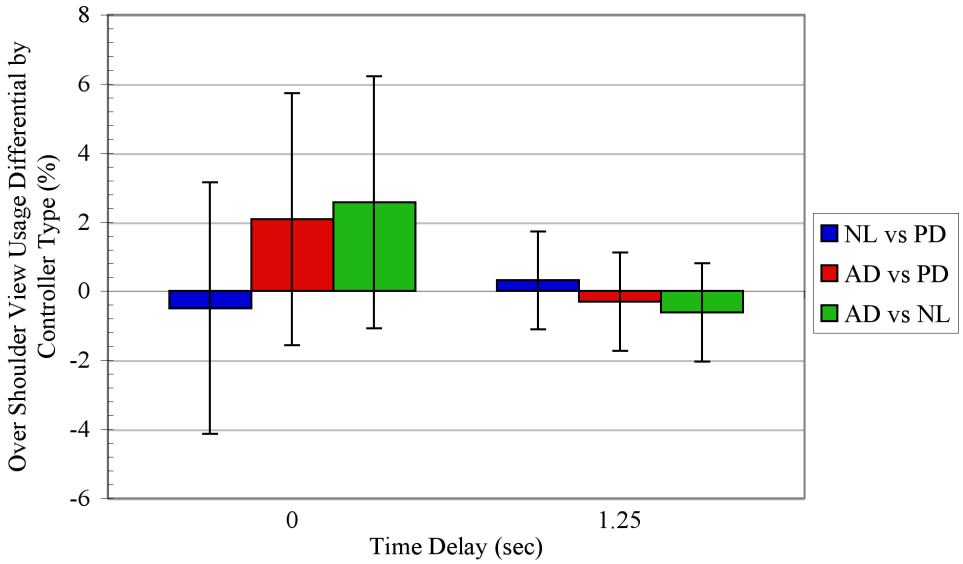

Figure 6.32: Over Left Shoulder Camera View Usage in Main Window by Controller Type.

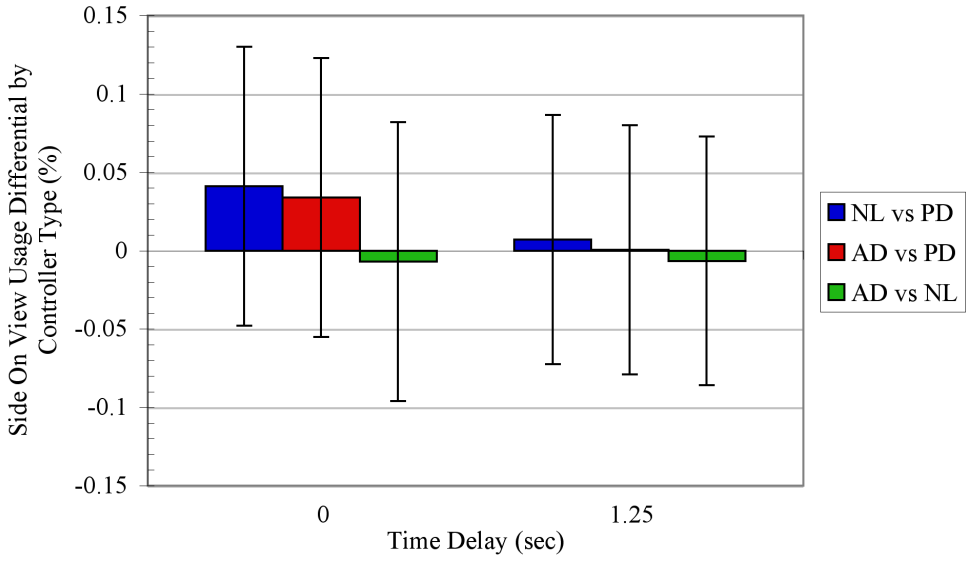

Figure 6.33: Left Side of SSV Camera View Usage in Main Window by Controller Type.

6.5.8 Upper Left Window Camera View Usage

During runs in which the command display was in use, an auxiliary window was available in the upper left corner of the monitor. This window displayed only the actual vehicle. The same three camera views available in the primary flight window were also available to the test subject for this window. Figure 6.34 shows the camera selection distribution by the test subjects during tests with no time delay, while Figure 6.35 indicates views selected for tests with time delay. Most subjects left the window in the default onboard camera view. It is unknown whether this was actually the preferred view or rather whether this window provided little additional value during flight operation. The fact that most subjects selected the shoulder view for the primary window, but the onboard view for this auxiliary window suggests that it may not have been used to any great extent. Since there is no way to actually determine if a subject actually utilized this window, further analysis of this data is not possible and it has been included only for completeness.

6.5.9 Experience

Prior to conducting the experiment and based on the results of the pilot study, it was thought that the experience level of a subject prior to partaking in the experiment might affect performance. Thus, the pretest questionnaire completed by subjects included questions concerning type and frequency of video game playing, previous experience with lab vehicles and ROV's and airplane piloting. Subjects were categorized as experienced if they played first person scenario video games such as Doom for greater than five hours a week, had more than five hours of flight experience with lab vehicles such as SCAMP or SCAMP SSV or piloting

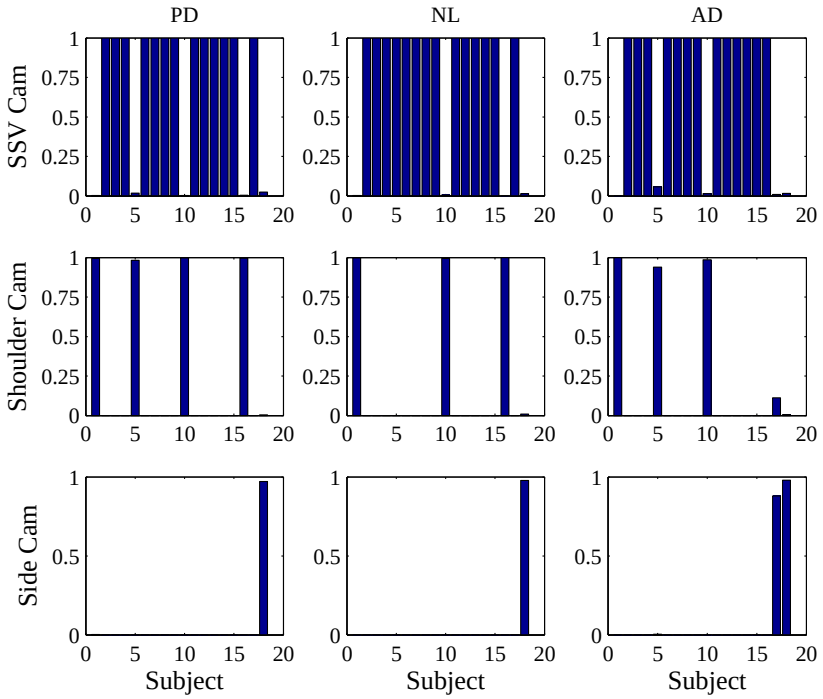

Figure 6.34: Upper Left Window Camera Views Selected by Subjects with a Command Display and No Time Delay.

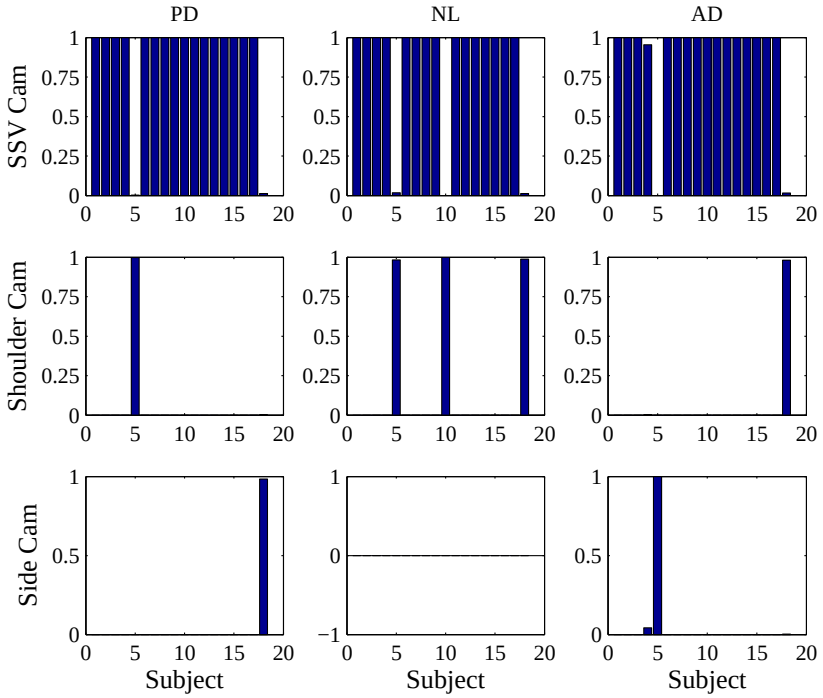

Figure 6.35: Upper Left Window Camera Views Selsected by Subjects with a Command Display and 1.25 Second Delay.

ROV's or were experienced airplane pilots. Statistical analysis indicates no difference in performance regarding prior experience level of subjects. This could be due to several factors. First, it may be that a more detailed investigation is needed to determine what constitutes an experienced subject from an inexperienced one. Second, even though the pilot study suggested that experience level might affect performance it is quite possible that the inexperienced subject was not yet completely trained on the system by the time testing commenced since the pilot study was designed with a specific number of runs for each training session and test session. The primary study was open ended in the sense that subjects flew the course until it appeared they were either becoming fatigued or their completion times had leveled off. Thus, there is more certainty that the runs analyzed in the main study were representative of the capability of each pilot.

6.6 Summary of Results

This experiment was conducted to more fully understand the impact that display and controller type have on the performance of a human pilot under conditions of time delay. One of the central hypotheses being tested in this work was that a more capable controller would result in better performance. Of primary interest was the possible benefit an adaptive controller might provide given that uncertainty might exist in the vehicle model implemented by the controller. This was investigated by comparing subject performance with three controllers: a baseline 'PD' like controller; a nonlinear controller containing full knowledge of model parameters; and an adaptive controller that was initialized with no model information, i.e. to the equivalent 'PD' controller. The results were somewhat

surprising.

- Presence of a command display was instrumental in counteracting the "move and wait" strategy normally adopted under conditions of time delay. This was indicated by the
  - decreased completion times of approximately 32% (29 seconds) with a command display,
  - the likelihood of completing a run cleanly doubled with the command display,
  - the average number of hoop hits per run decreased threefold when the command display was used, and
  - more consistent use of hand controllers, especially the primary flight dof, x indicating alleviation of the move and wait strategy.
- However, use of a command display is actually not as beneficial when no transmission delays are present since
  - completion times increased by 7.4% (4.7 seconds) with the command display,
  - subjects were only 3/4 as likely to complete a run cleanly with the command display than without (see Figure 6.11) and
  - the average number of hoop hits per run increased by 50%.
- With signal transmission delays present in the communications loop performance with the command display is robust to uncertainty in the vehicle model as demonstrated by

  - no evidence of statistically significant performance differences among controller types indicating
  - large amounts of uncertainty in the vehicle model appear not to adversely affect performance.

- When no time delay is present in the system however, controller type *is* significant. This was evident since
  - completion times with the 'PD' controller were around 6.3% (4.3 seconds) greater than with the nonlinear controller and 3.6% (2.5 seconds) greater than the adaptive controller,
  - the average number of hoops hit per run was 1.5 times greater with the 'PD' than with the adaptive controller, and
  - subjects were around 1.5 times as likely to complete a run cleanly with the adaptive controller than with either the 'PD' or nonlinear controller.

- Adaptation does not interfere with command display as indicated by comparable or superior performance levels between the adaptive and other controllers. This can be seen in the course completion time results where there was no statistical difference in performance between the adaptive and nonlinear controllers when no time delay was present.

- Analysis of the mean flight path for each subject indicates that there were two primary strategies adopted by humans. While most subjects had mean flight paths similar to that produced by the automatic trajectory, a subset of subjects aligned themselves with the hoop well in advance of encountering

the hoop. Since this was realized after the study was conducted, much more conservative statistical tests must be conducted to ascertain if performance was affected by flight path type. Still, this could prove an interesting effect to investigate in future testing.

- The hand controller strategy adopted by human test subjects differed from that of the automatic trajectory generator. Humans depended upon the translational degrees of freedom much more than did the automatic trajectory generator which exhibited a smoother, coupled rotation and translation through the course.

- Previous experience levels appeared not to affect performance indicating that subjects were fully trained on the system.

- While the side view of SSV was utilized far less than either of the other views there is statistical evidence that it was used more when no display was available for tests with no time delay most likely to provide additional information about the position of SSV relative to a hoop.

From the above summary it is clear that the evidence does not appear to support the hypothesis that for time delayed teleoperation, an advanced nonlinear model following controller will result in better performance than a simpler linear controller, at least for the range of model uncertainty and vehicle speeds present in this thesis. The results of the study indicate that when time delay is present the command display system is actually quite robust with respect to vehicle controller accuracy. Controller type had little to no effect on any of the performance parameters under conditions of time delay. Rather, display type is the primary factor affecting human teleoperation under conditions of time delay. With time

delay present all performance metrics demonstrated considerable improvement when the command display was available versus when it was unavailable.

An additional surprising outcome of the experiment is the contraindication of a command display with a system in which time delay is not present. Subjects took somewhat longer to complete the course and were less accurate while using the command display. Since controller type affected subject performance when no time delay was present, the observed performance decline with the command display could be attributable to visual interference between the desired and actual vehicles. That this conclusion contradicts the findings of Lane (2000) might be attributable to several things. First, system dynamics were included in this study whereas they were not in Lane. Second, the amount of information displayed to the pilot in each experiment was different. Lane's peg-in-hole task lent itself to a single view pane the size of the entire monitor. The subject could change between three view perspectives at will using the hand controller trigger. Since the task involved in this study involved travel over a significant distance, it was necessary to provide a global view of the course as well as more localized views. Thus there may have been more visual clutter on the control station monitor. Third, it is possible that differences in implementation of the command display overlay also contributed to the contradicting conclusions.

Chapter 7

Conclusions and Further Study

7.1 Conclusions

This thesis combined several recently developed technologies to investigate methods for more effective teleoperation under conditions of time delay. These technologies include

- the command display system first discussed in Lane (2000), and
- advanced nonlinear, model following controllers developed within the last ten years Egeland and Godhavn (1994).

Lane's work with a command display system involved a kinematic model of a robotic arm. This study applied command display technology to a full six degree of freedom free flying vehicle simulation involving coupled dynamics.

Prior to this work, the utility of a command display system as a function of vehicle controller type and amount of prior model information had not been examined. One of the primary goals of this research was to better understand the requirements associated with the vehicle controller in a command display system. How does uncertainty in the vehicle model affect performance? Could an

adaptive controller compensate for model uncertainty? To this end, the system was tested with three controllers. It was reasoned that the 'PD' controller which operates with virtually no knowledge about vehicle parameters would indicate lower boundary performance and the nonlinear controller containing full knowledge about the vehicle would provide an upper boundary on performance against which the adaptive controller could be compared.

Results of the study found insufficient evidence to conclude that controller type affects performance under conditions of time delay, at least for vehicles with physical characteristics and operating speeds similar to SSV. The command display system proved robust to model inaccuracy. Display type did play a significant role in subject performance under conditions of time delay and there is sufficient evidence to conclude that use of a command display enhances human teleoperation under conditions of time delay.

It was also determined that the command display may actually be contraindicated when there is no signal transmission delay present. With no time delay, the difference in position/orientation between the desired and actual vehicle is generally quite small due to capabilities of the vehicle controller. This small discrepancy may result in a blurring of the vehicle edges making it difficult to discern which is the desired vehicle. That this conclusion contradicts the findings of Lane is most likely a result of the inclusion of the system dynamics in this thesis.

7.2 Areas of Future Study

7.2.1 Enlarged Subject Pool

Due to time constraints the subject pool consisted of eighteen participants. It took approximately seven weeks to collect the data with each subject volunteering approximately fifteen hours of time. Some interesting performance trends are observed in the results but the standard deviation is too large to assert statistical significance. One such trend mentioned previously can be observed in Figure 6.5 which compares course completion times by controller type. With 1.25 seconds of delay in the system, it appears that both nonlinear and adaptive controllers result in decreased times when compared to the 'PD' controller. It is possible that additional testing with a larger subject pool may resolve some of these results containing borderline statistical significance.

7.2.2 Larger Uncertainty and Trust Breakdown

Command displays provide immediate visual feedback to operator commands in systems containing signal transmission delays. Implicit in this system is the issue of trust. The teleoperator must have confidence that the actual vehicle will accurately follow the specified time delayed commanded trajectory as shown on the command display. Should this trust break down the operator may revert to the "move and wait" strategy, rendering the command display useless.

The command display system was found to be robust to information about the vehicle model, at least for vehicles moving at the velocity considered in these experiments. Since it was desired to compare realistically tuned systems, hindsight indicates that perhaps the 'PD' portions of the controllers were tuned too

well to identify a regime in which operator trust will begin to break down. An investigation into how much the 'PD' gains must be detuned for the command display paradigm to break down might be useful. For instance, with effectively zero 'PD' gains the vehicle will track so poorly that trust should break down and the move-and-wait strategy will be implemented.

7.2.3 Implementation on a Physical System

To date, teleoperation with a command display system has not been performed on an actual physical vehicle. Lane's work with the Ranger arm involved computer simulation as did this thesis since the required position determination system currently does not exist in the neutral buoyancy tank at the Space Systems Lab. Smithanik (2004) at the University of Maryland recently completed work on a preliminary version of VPS, or Vision Positioning System, a vision-based inertial navigation system developed in the lab for use on an SSV type vehicle in the tank. Reported accuracy with this system is on the cm level and while further enhancements must be added before it can be implemented on a system, it shows promise. When such a system becomes available, it would be interesting to investigate the utility of the command display on a physical system containing real world effects such as sensor noise, limited camera views, and environmental disturbances.

The issue of available camera views is an interesting one. As explained earlier in this thesis, there are a limited number of camera views available in the tank consisting of the two porthole cameras and whatever onboard cameras the vehicle has been outfitted with. A synthetic camera view created on the computer using the sensor data from SSV and VPS may be able to provide additional views to

the operator. The feasibility and utility of such simulated camera views as well as the fidelity required of the virtual environment model for these simulated camera views to be of use should be explored.

7.2.4 Flight Trajectory

Analysis of the mean flight path of each test subject indicated two distinct strategies for maneuvering through the course. A subset of subjects tended to align themselves with the hoop much further from the hoop than most of the subjects, whose flight paths more closely resembled the "just in time" alignment of the automatic trajectory generator. Because this was not an anticipated effect prior to the study, the statistical comparison used for determining significance is required to be much more conservative . Hence, it couldn't be concluded that there was any statistical difference in performance between the two groups due to flight trajectory . Future tests might determine if this phenomenon is indeed a factor in performance, and attempt to further identify the specific cognitive and/or psychological factors which influence the choice of approach.

7.2.5 Display Window

The amount of information displayed to the test subject is complex. Enough information must be conveyed to the teleoperator to allow them to successfully perform the task without being visually overburdened. Several windows were available for subjects to use in this study. Unfortunately, the experiment design precludes any conclusions being drawn as to the utility of the auxiliary view window. A more directed study concentrating on display and usage of visual information could prove extremely useful in avoiding overcluttered displays.

Appendix A

Questionnaires

INFORMED CONSENT FORM

Adaptive Control of Submersible Vehicles With Time Delay Study

I state that I am over 18 years of age, in good physical health, and wish to participate in a program of research being conducted by the Space Systems Laboratory in the Department of Aerospace Engineering at the University of Maryland, College Park, Maryland 20742.

The purpose of this research is to investigate human pilot performance during time delayed teleoperation. I understand that I will be asked to repeatedly fly either SCAMP SSV, a submersible robotic vehicle or a computer simulation of SCAMP SSV using a translational/rotational hand controller pair**. The testing will entail no more than 20 sessions each of which will last no longer than one hour in duration**.

All information collected in the study is confidential, and my name will not be identified at any time.

I understand that operation of the remote control station may result in minor hand and arm fatigue and/or eye strain. I understand that there are normally no long-term effects of this fatigue.

I understand that the experiment is not designed to help me personally, but that the investigator hopes to learn more about human performance in piloting submersible vehicles with time delay. I understand that I am free to ask questions or to withdraw from participation at any time without penalty.

Principal Investigator:

Dr. Robert Sanner
Space Systems Lab
Bldg. 382
University of Maryland
College Park, MD 20742
(301) 405-1928

Printed Name of Subject: _____

Signature of Subject: _____

Date: _____

Figure A.1: Test Subject Informed Consent Form

Demographics Survey

General Information

Subject No: _____

Age: _____

Gender: M: _____ F: _____

Handedness: Left: _____ Right: _____ Ambidextrous: _____

Do you have difficulties distinguishing the following colors? (Check all that apply)
None:_____ Red-Green: _____ Blue-Green: _____ All Color: _____

Do you have corrected vision (wear glasses, contacts)? Yes: _____ No: _____

If you have corrected vision, which of the following are being compensated (Check all that apply)
Near sighted: _____ Far sighted: _____ Astigmatism: _____

Experience

Video Games

Do you play video games? Yes: _____ No: _____

If so, about how many hours a week? _____

What type (mark all that apply): Driving: _____ Flight Simulators: _____

Life Scenario (Doom, etc): _____

Tetris/Solitaire/other non life scenario: _____

What type or types of games do you predominantly play?

Driving: _____ Flight Simulators: _____

Life Scenario (Doom, etc): _____

Tetris/Solitaire/other non life scenario: _____

Lab Vehicles

Do you have experience piloting any vehicles in the lab? Yes: _____ No: _____

Which vehicles: BAT: _____ MPOD: _____ SCAMP: _____ SSV: _____

Approximately how many hours of total flight time do you have? _____

Remotely Piloted Airplanes

Do you have any experience piloting remote controlled airplanes?

Yes: ___ No: ___

If so, how many hours? _____

Airplane Pilot

Do you have experience piloting airplanes? Yes: ____ No: ____

How often do you pilot an airplane? _____

_____

How many hours of piloting do you have? _____

Figure A.2: Test Subject Questionnaire

Appendix B

Pilot Study Information

Table B.1: Pilot Study: Subject A Test Order

Test Session	Test Number	Cell Number	Controller	Uncertainty Type	Percent Uncertainty	Display	Time Delay
1	1	40	NLAD	M	100	A	0.75
	2	53	NLAD	D	50	A	0
	3	22	NLAD	D	50	C	0.25
	4	52	NLAD	M	50	A	0.75
2	5	35	PD	-	-	A	0.5
	6	23	NLAD	D	50	C	0.5
	7	33	PD	-	-	A	0
	8	46	NLAD	B	100	A	0.25
	9	1	PD	-	-	C	0
3	10	15	NLAD	B	100	C	0.5
	11	49	NLAD	M	50	A	0
	12	61	NL	-	-	A	0
	13	58	NLAD	B	50	A	0.25
	14	57	NLAD	B	50	A	0
	15	59	NLAD	B	50	A	0.5
4	16	31	NL	-	-	C	0.5
	17	32	NL	-	-	C	0.75
	18	18	NLAD	M	50	C	0.25
	19	4	PD	-	-	C	0.75
	20	20	NLAD	M	50	C	0.75
	21	12	NLAD	D	100	C	0.75
5	22	5	NLAD	M	100	C	0
	23	55	NLAD	D	50	A	0.5
	24	54	NLAD	D	50	A	0.25
	25	27	NLAD	B	50	C	0.50
	26	29	NL	-	-	C	0

continued on next page

Table B.1: *continued*

Test Session	Test Number	Cell Number	Controller	Uncertainty Type	Percent Uncertainty	Display	Time Delay
6	27	14	NLAD	B	100	C	0.25
	28	8	NLAD	M	100	C	0.75
	29	39	NLAD	M	100	A	0.5
	30	36	PD	-	-	A	0.75
	31	7	NLAD	M	100	C	0.5
7	32	64	NL	-	-	A	0.75
	33	43	NLAD	D	100	A	0.5
	34	47	NLAD	B	100	A	0.5
	35	56	NLAD	D	50	A	0.75
	36	21	NLAD	D	50	C	0
8	37	50	NLAD	M	50	A	0.25
	38	2	PD	-	-	C	0.25
	39	17	NLAD	M	50	C	0
	40	51	NLAD	M	50	A	0.5
	41	41	NLAD	D	100	A	0
	42	48	NLAD	B	100	A	0.75
9	43	24	NLAD	D	50	C	0.75
	44	9	NLAD	D	100	C	0
	45	10	NLAD	D	100	C	0.25
	46	42	NLAD	D	100	A	0.25
	47	19	NLAD	M	50	C	0.5
	48	3	PD	-	-	C	0.5
10	49	62	NL	-	-	A	0.25
	50	6	NLAD	M	100	C	0.25
	51	45	NLAD	B	100	A	0
	52	34	PD	-	-	A	0.25
	53	11	NLAD	D	100	C	0.5
	54	28	NLAD	B	50	C	0.75
11	55	37	NLAD	M	100	A	0
	56	44	NLAD	D	100	A	0.75
	57	60	NLAD	B	50	A	0.75
	58	26	NLAD	B	50	C	0.25
	59	25	NLAD	B	50	C	0
12	60	13	NLAD	B	100	C	0
	61	38	NLAD	M	100	A	0.25
	62	30	NL	-	-	C	0.25
	63	63	NL	-	-	A	0.5
	64	16	NLAD	B	100	C	0.75

Table B.2: Pilot Study: Subject C Test Order

Test Session	Test Number	Cell Number	Controller	Uncertainty Type	Percent Uncertainty	Display	Time Delay
1	1	6	NLAD	M	100	C	0.25
2	2	44	NLAD	D	100	A	0.75
	3	4	PD	-	-	C	0.75
	4	59	NLAD	B	50	A	0.5
3	5	47	NLAD	B	100	A	0.5
	6	32	NL	-	-	C	0.75
	7	56	NLAD	D	50	A	0.75
4	8	21	NLAD	D	50	C	0
	9	15	NLAD	B	100	C	0.5
	10	50	NLAD	M	50	A	0.25
	11	1	PD	-	-	C	0
	12	14	NLAD	B	100	C	0.25
5	13	17	NLAD	M	50	C	0
	14	20	NLAD	M	50	C	0.75
	15	2	PD	-	-	C	0.25
	16	5	NLAD	M	100	C	0
	17	51	NLAD	M	50	A	0.5
6	18	12	NLAD	D	100	C	0.75
	19	41	NLAD	D	100	A	0
	20	64	NL	-	-	A	0.75
	21	48	NLAD	B	100	A	0.75
7	22	23	NLAD	D	50	C	0.5
	23	8	NLAD	M	100	C	0.75
	24	42	NLAD	D	100	A	0.25
	25	33	PD	-	-	A	0
	26	43	NLAD	D	100	A	0.5
	27	10	NLAD	D	100	C	0.25
8	28	40	NLAD	M	100	A	0.75
	29	29	NL	-	-	C	0
	30	19	NLAD	M	50	C	0.5
	31	57	NLAD	B	50	A	0
	32	3	PD	-	-	C	0.5
	33	62	NL	-	-	A	0.25
9	34	61	NL	-	-	A	0
	35	49	NLAD	M	50	A	0
	36	11	NLAD	D	100	C	0.5
	37	45	NLAD	B	100	A	0
	38	34	PD	-	-	A	0.25
	39	63	NL	-	-	A	0.5
10	40	60	NLAD	B	50	A	0.75
	41	28	NLAD	B	50	C	0.75
	42	37	NLAD	M	100	A	0
	43	24	NLAD	D	50	C	0.75
	44	22	NLAD	D	50	C	0.25

continued on next page

Table B.2: *continued*

Test Session	Test Number	Cell Number	Controller	Uncertainty Type	Percent Uncertainty	Display	Time Delay
11	45	35	PD	-	-	A	0.5
	46	18	NLAD	M	50	C	0.25
	47	13	NLAD	B	100	C	0
	48	53	NLAD	D	50	A	0
	49	30	NL	-	-	C	0.25
	50	26	NLAD	B	50	C	0.25
12	51	52	NLAD	M	50	A	0.75
	52	16	NLAD	B	100	C	0.75
	53	27	NLAD	B	50	C	0.5
	54	7	NLAD	M	100	C	0.5
	55	36	PD	-	-	A	0.75
13	56	39	NLAD	M	100	A	0.5
	57	55	NLAD	D	50	A	0.5
	58	9	NLAD	D	100	C	0
	59	25	NLAD	B	50	C	0
	60	38	NLAD	M	100	A	0.25
14	61	58	NLAD	B	50	A	0.25
	62	54	NLAD	D	50	A	0.25
	63	46	NLAD	B	100	A	0.25
	64	31	NL	-	-	C	0.5

Appendix C

Pilot Study Learning GainTuning Information

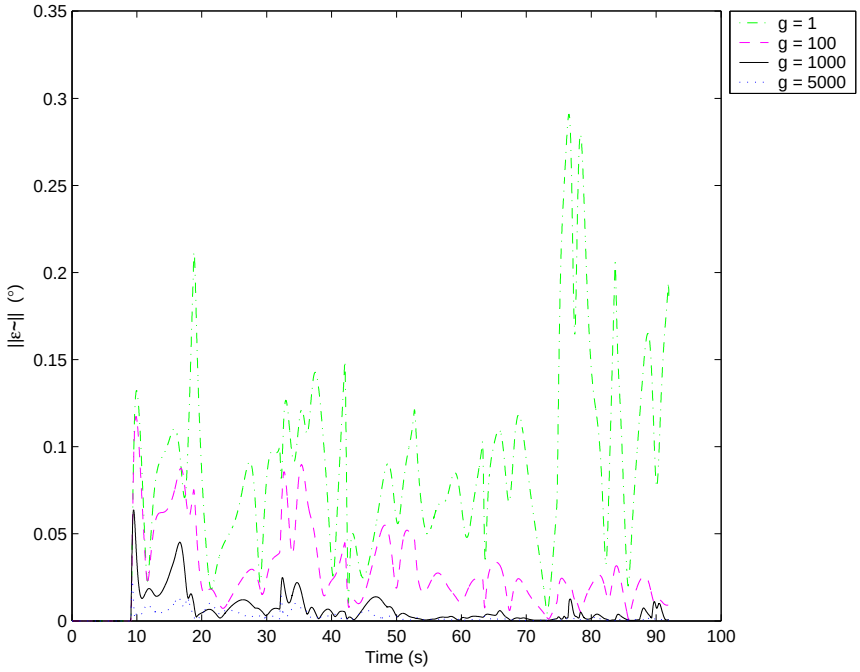

Figure C.1: Pilot Study: Adaptive Learning Gain Tuning for $\boldsymbol{H}$.

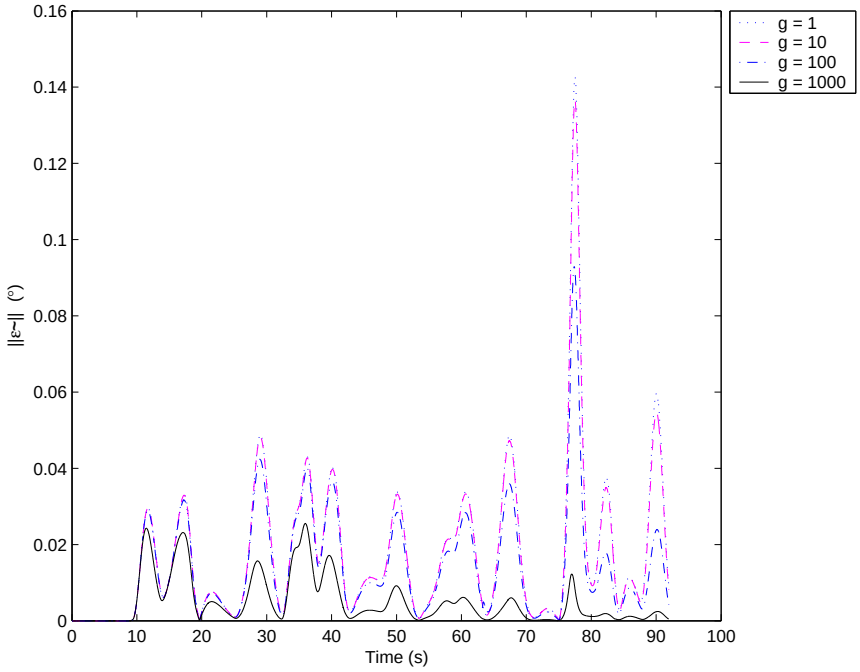

Figure C.2: Pilot Study: Adaptive Learning Gain Tuning for $\boldsymbol{C}_{d_\omega}$.

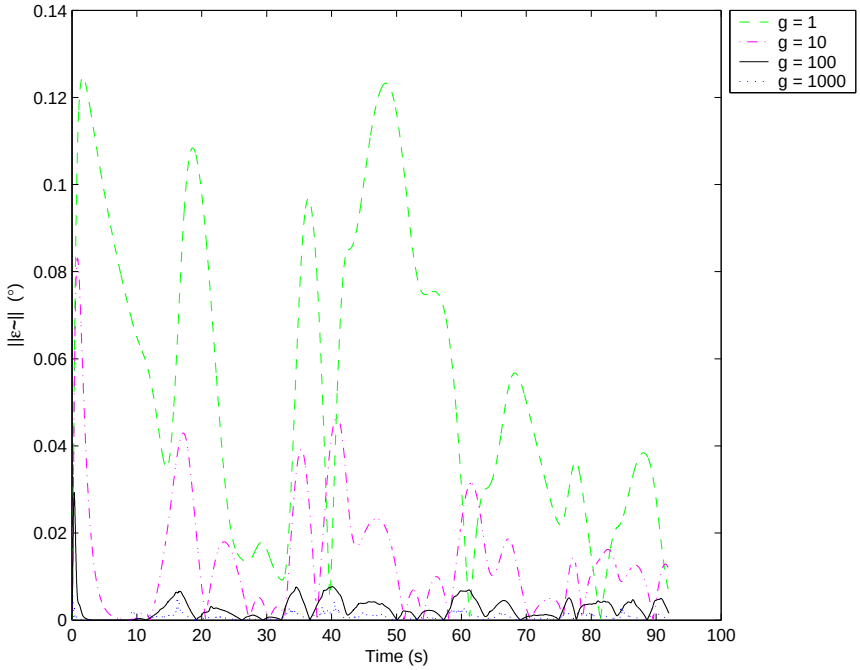

Figure C.3: Pilot Study: Adaptive Learning Gain Tuning for $B\boldsymbol{r}_b$.

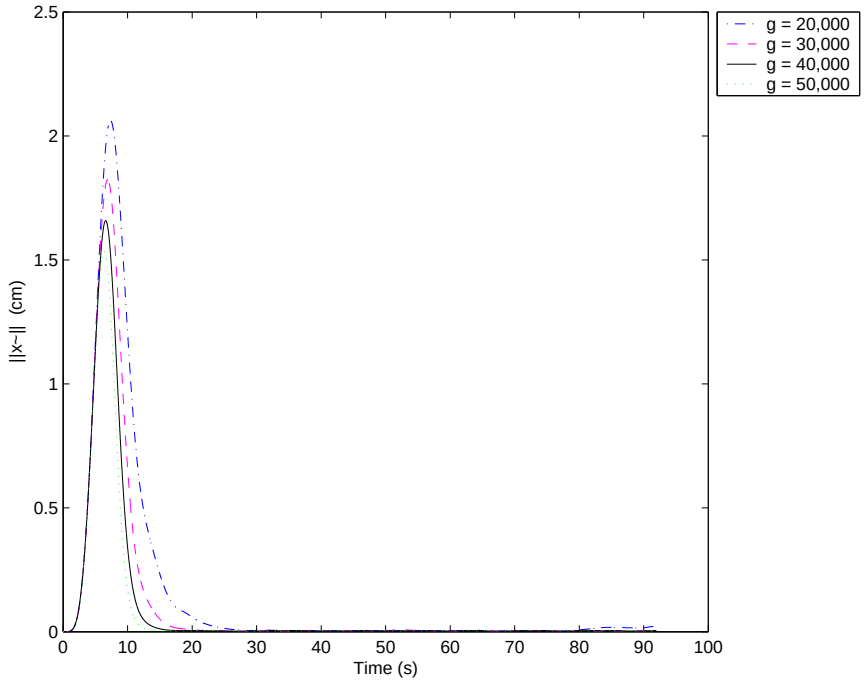

Figure C.4: Pilot Study: Adaptive Learning Gain Tuning for $\boldsymbol{C}_{d_v}$.

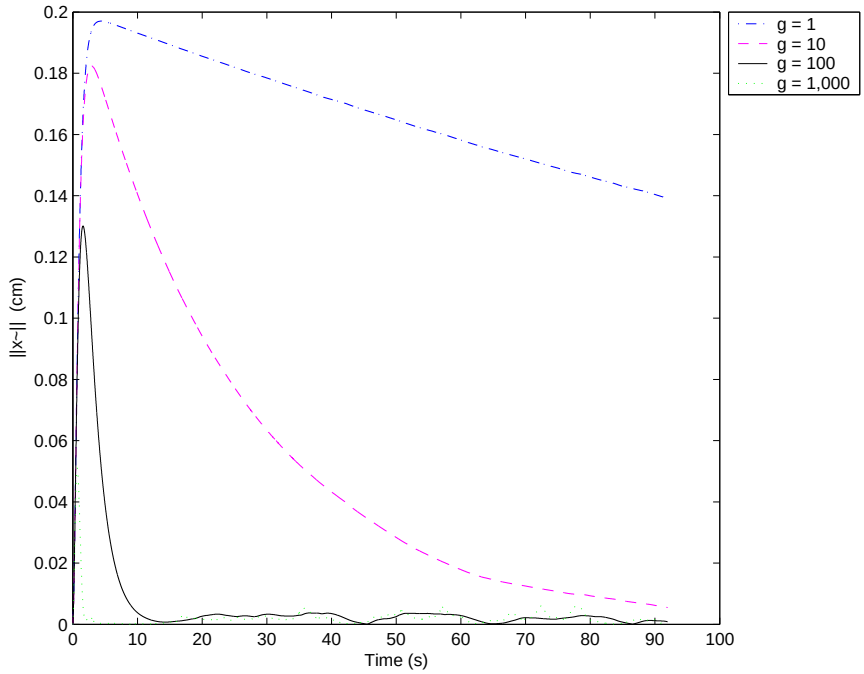

Figure C.5: Pilot Study: Adaptive Learning Gain Tuning for ΔB.

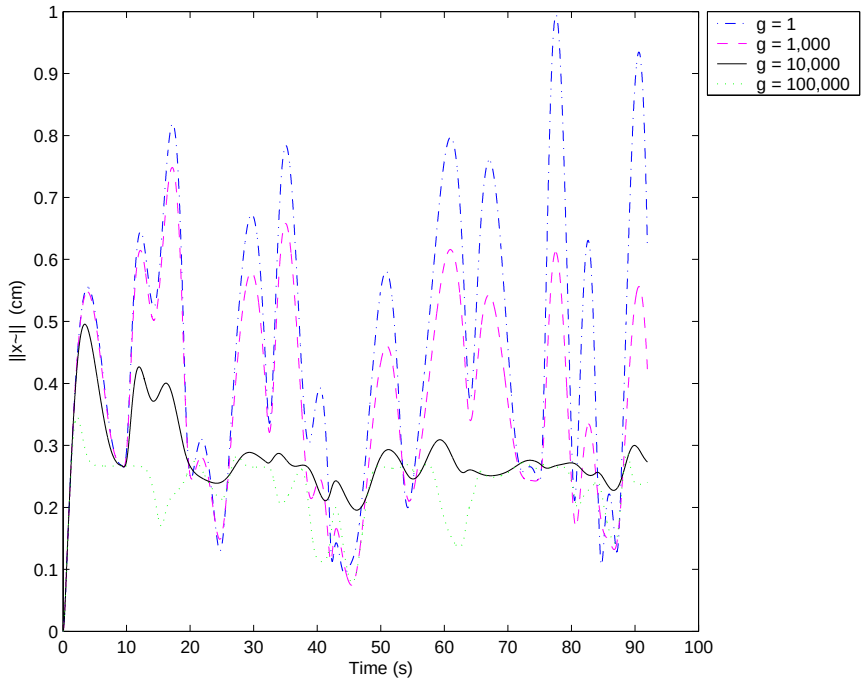

Figure C.6: Pilot Study: Adaptive Learning Gain Tuning for m.

Appendix D

Main Study Learning GainTuning Information

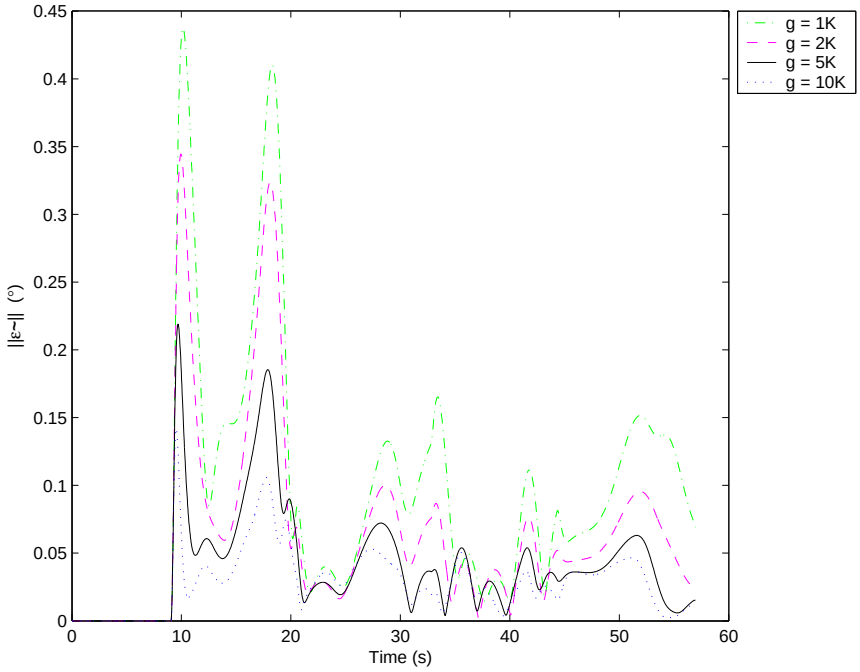

Figure D.1: Main Study: Adaptive Learning Gain Tuning for $\boldsymbol{H}$.

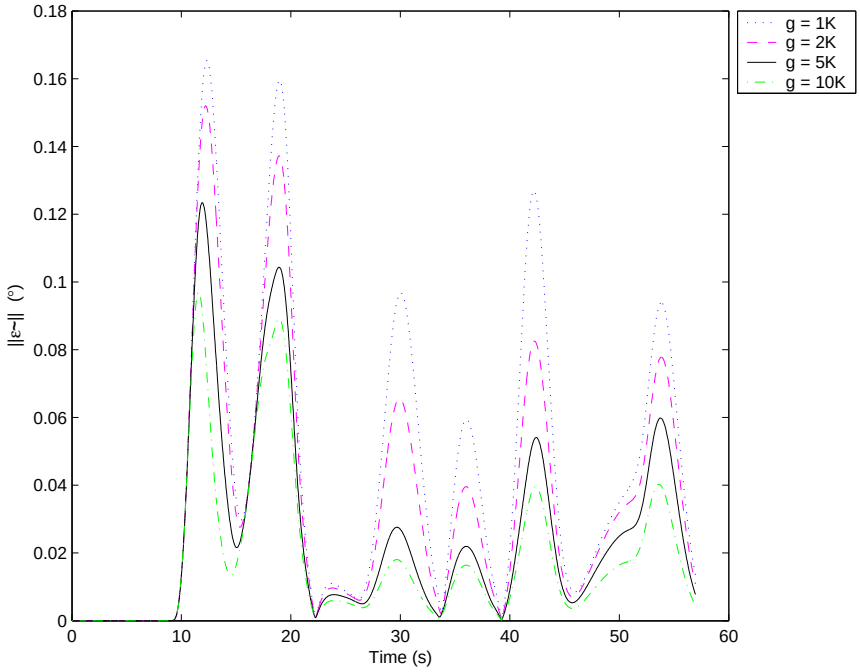

Figure D.2: Main Study: Adaptive Learning Gain Tuning for $\boldsymbol{C}_{d_\omega}$.

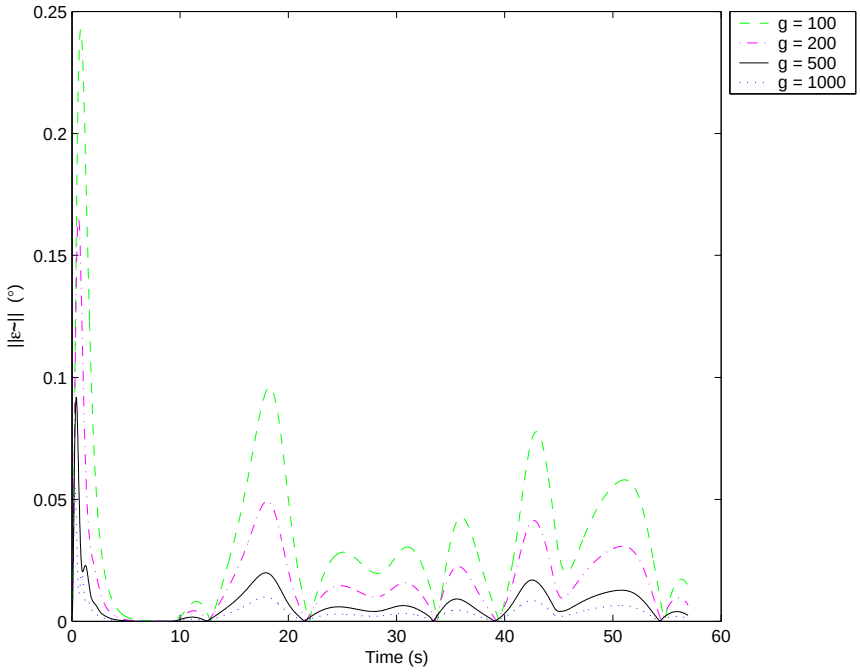

Figure D.3: Main Study: Adaptive Learning Gain Tuning for $B\boldsymbol{r}_b$.

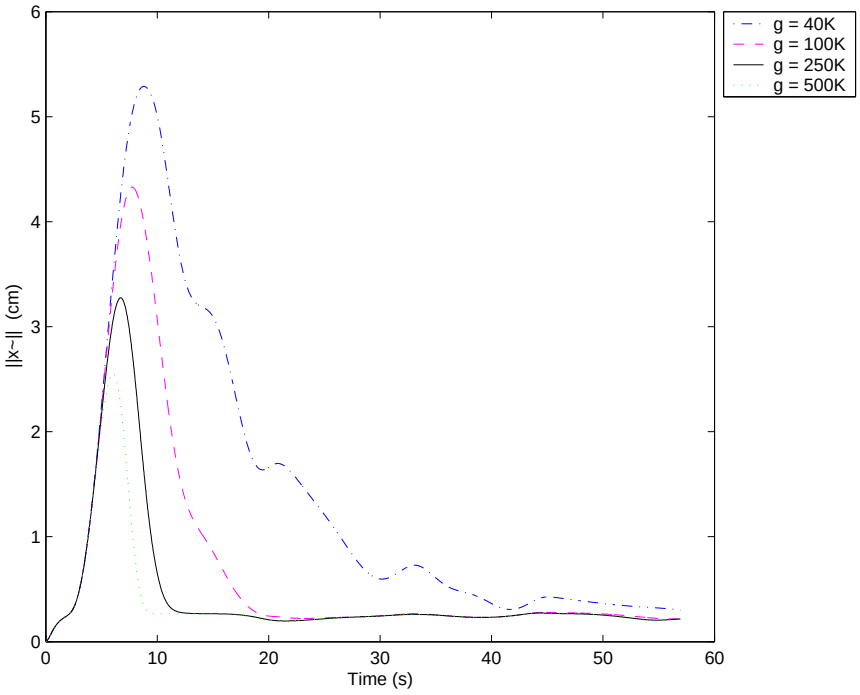

Figure D.4: Main Study: Adaptive Learning Gain Tuning for $\boldsymbol{C}_{d_v}$.

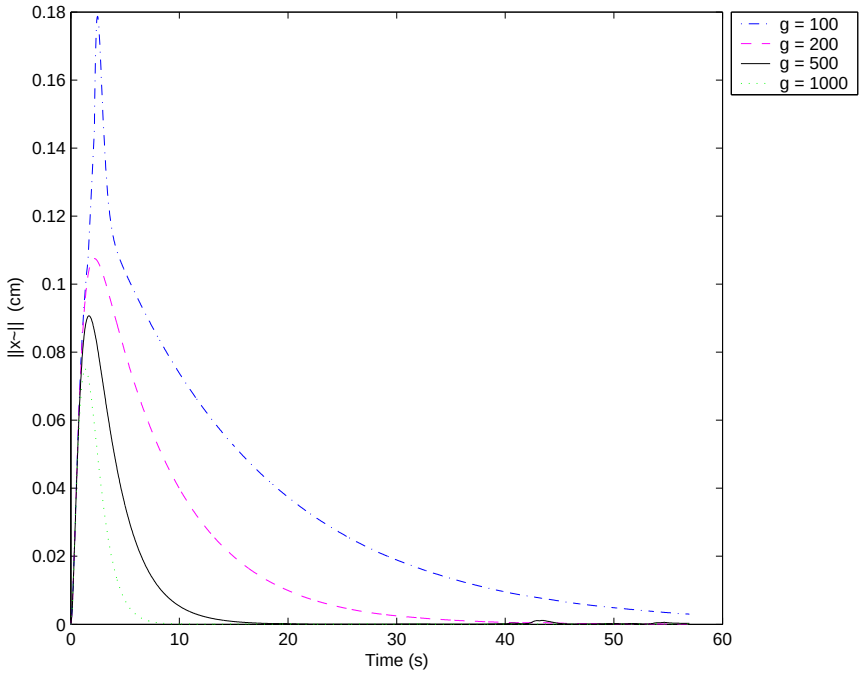

Figure D.5: Main Study: Adaptive Learning Gain Tuning for ΔB.

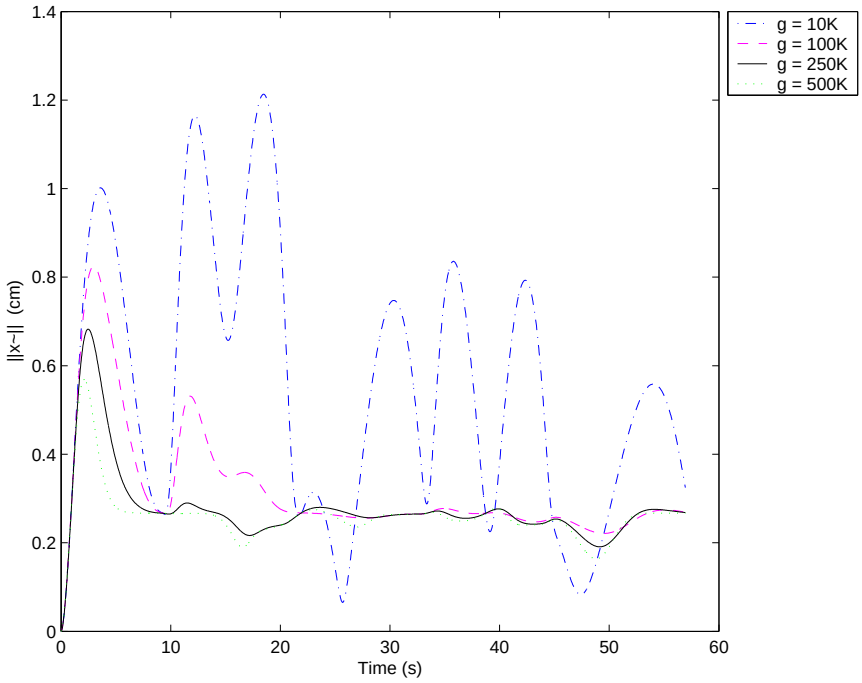

Figure D.6: Main Study: Adaptive Learning Gain Tuning for m.

Appendix E

Pilot Time Data

E.1 Study 1: 0 Second Round Trip Time Delay Run Time Data

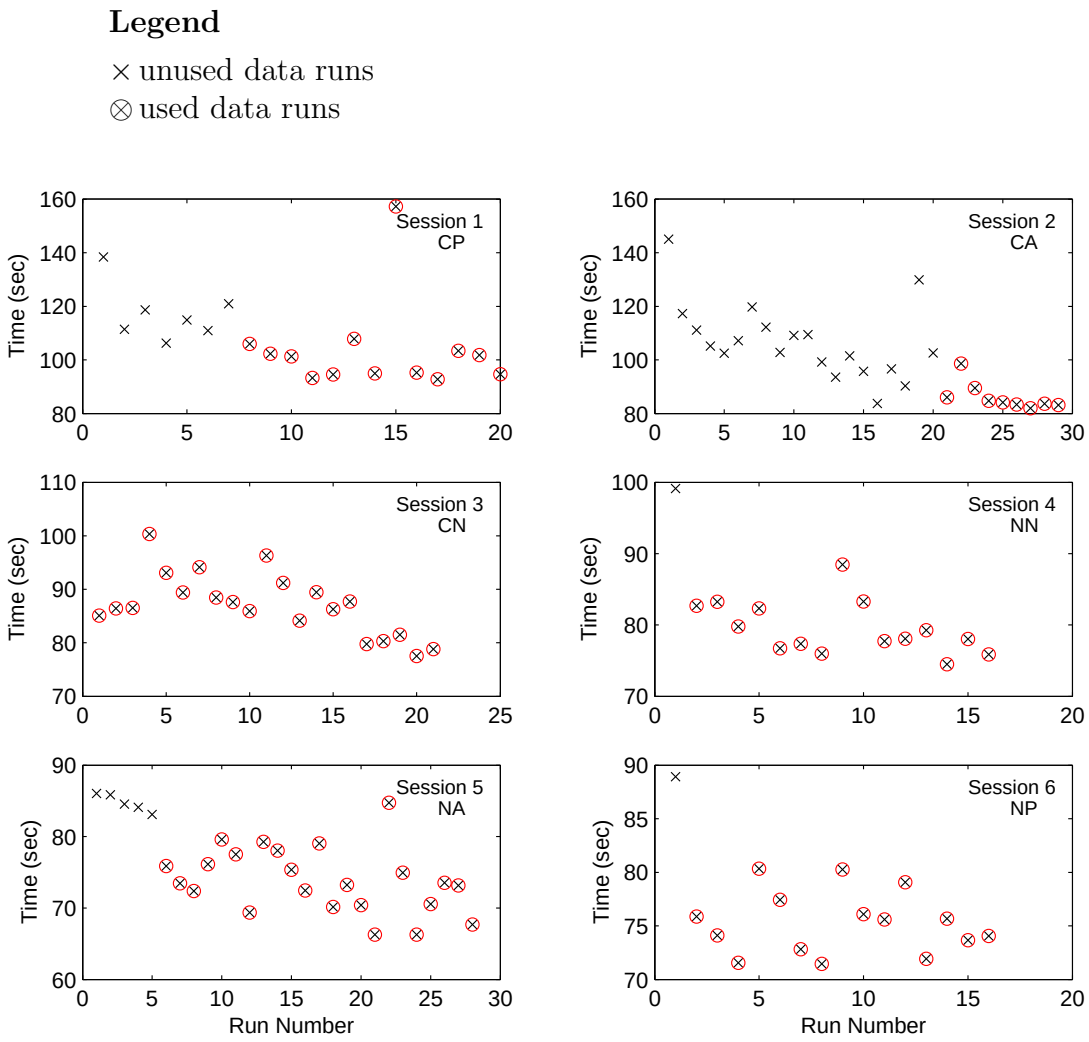

Figure E.1: Study 1: Subject 1 Run Times.

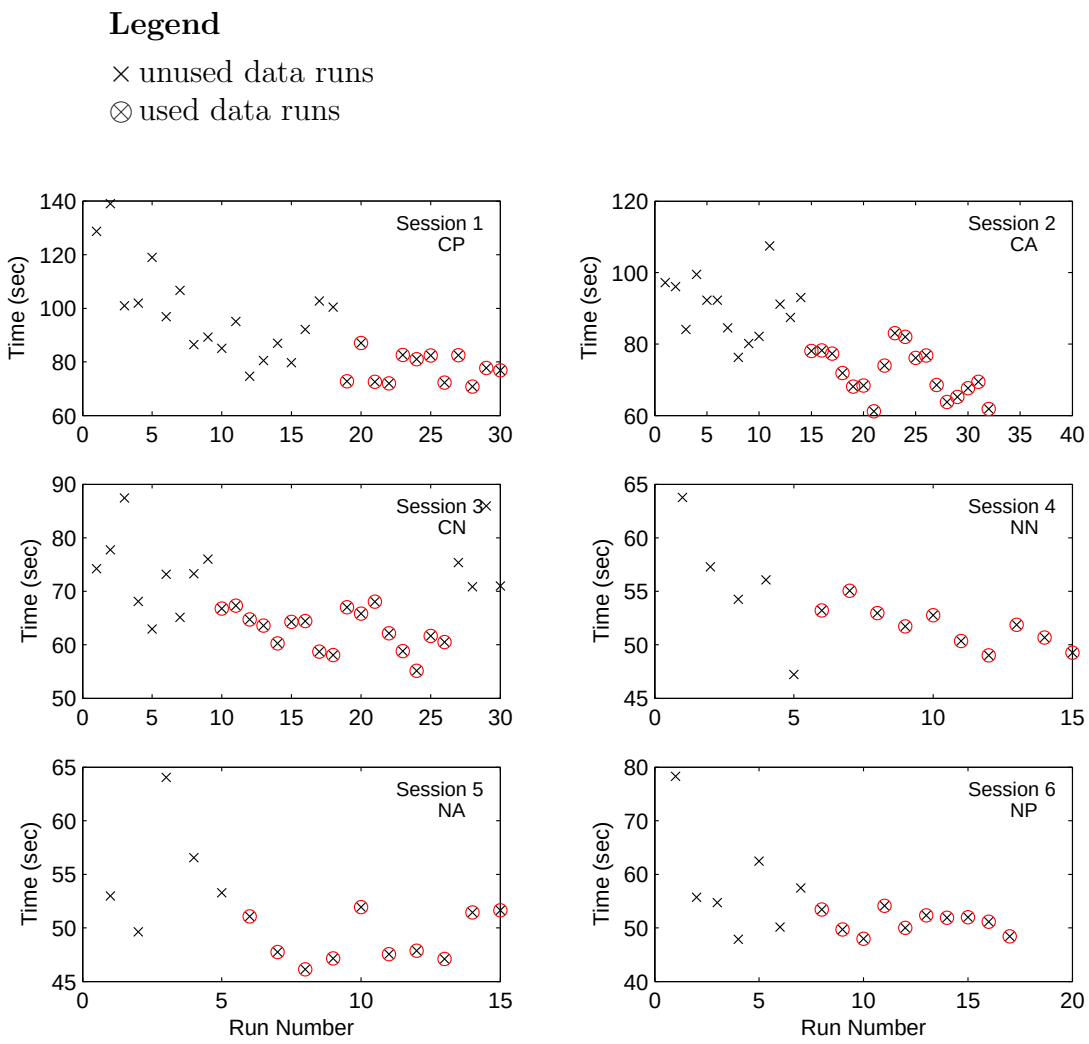

Figure E.2: Study 1: Subject 2 Run Times.

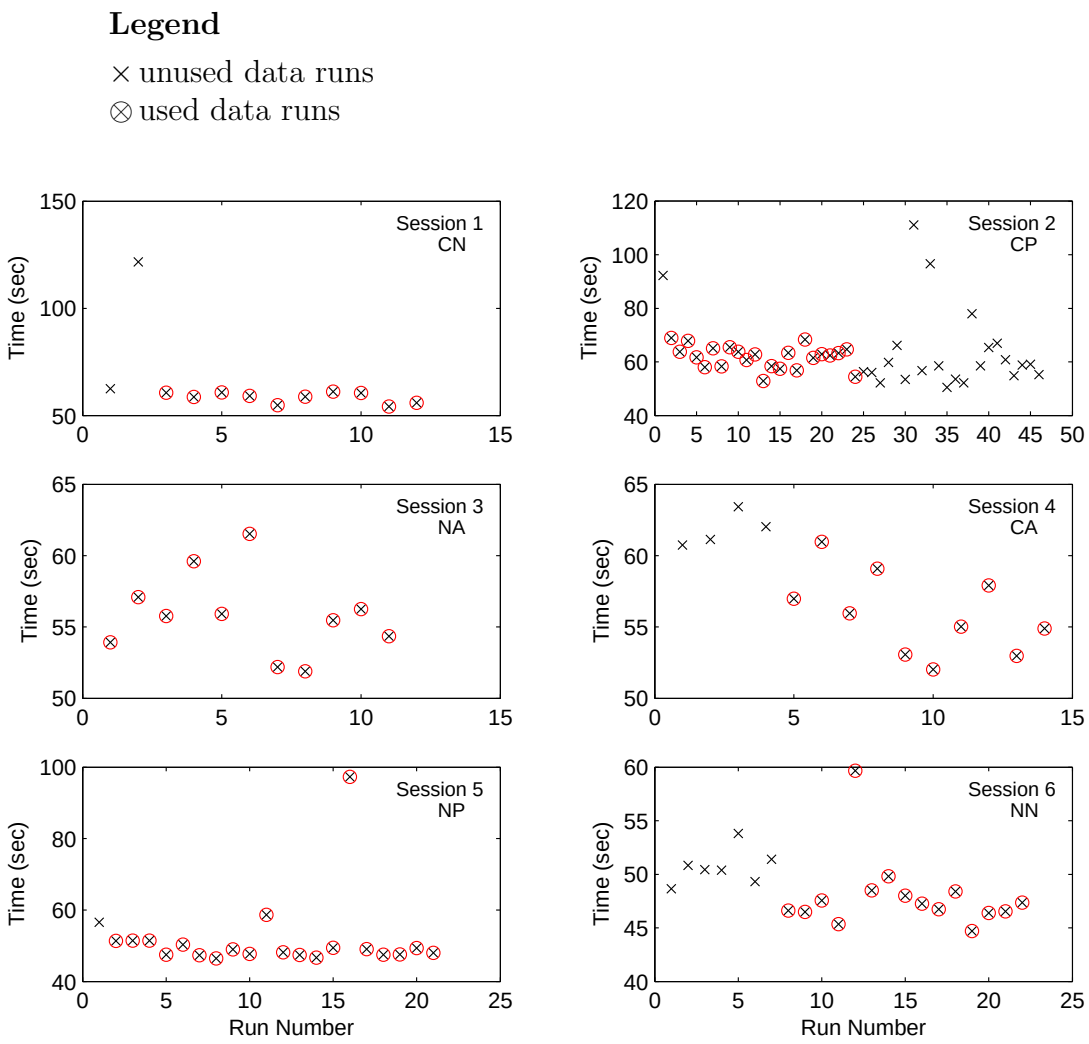

Figure E.3: Study 1: Subject 3 Run Times.

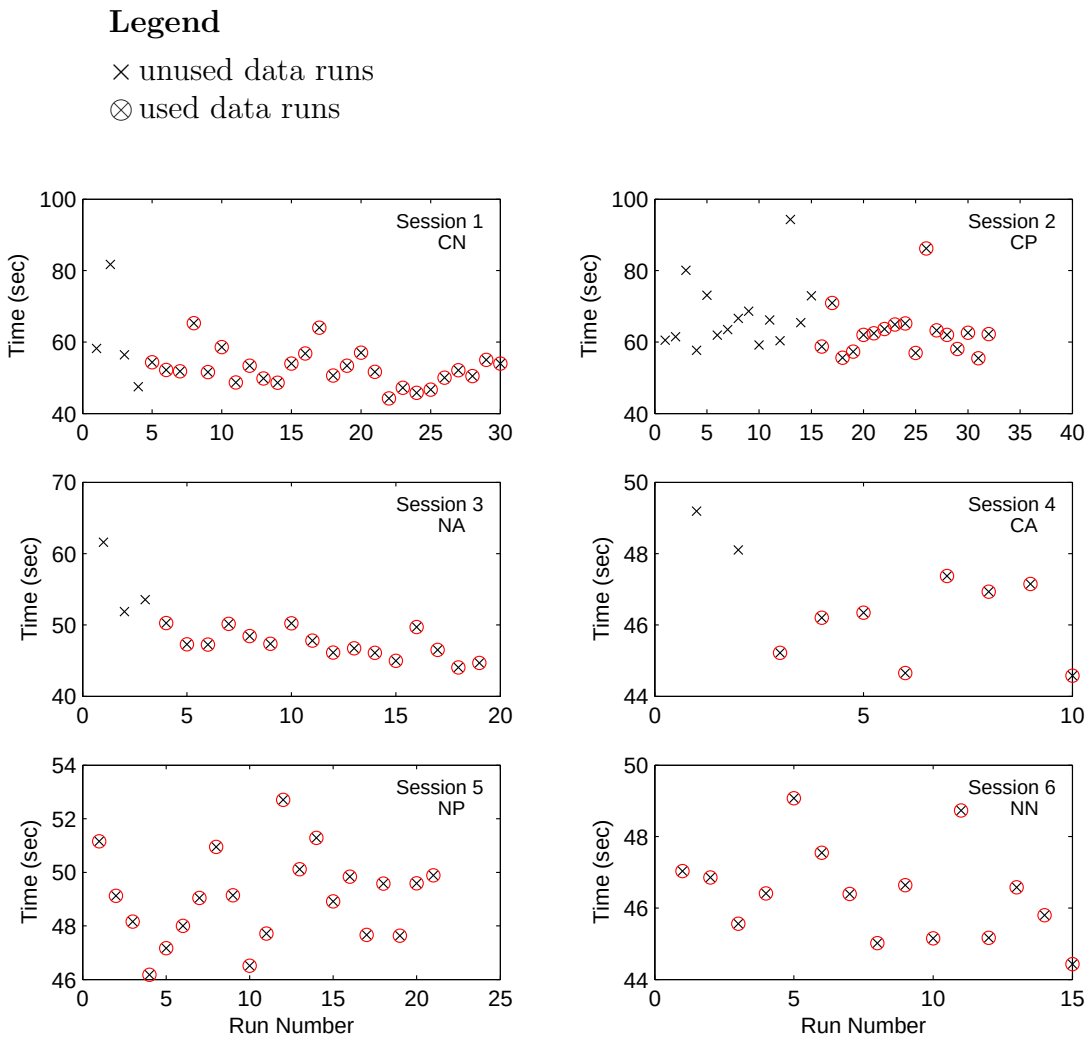

Figure E.4: Study 1: Subject 4 Run Times.

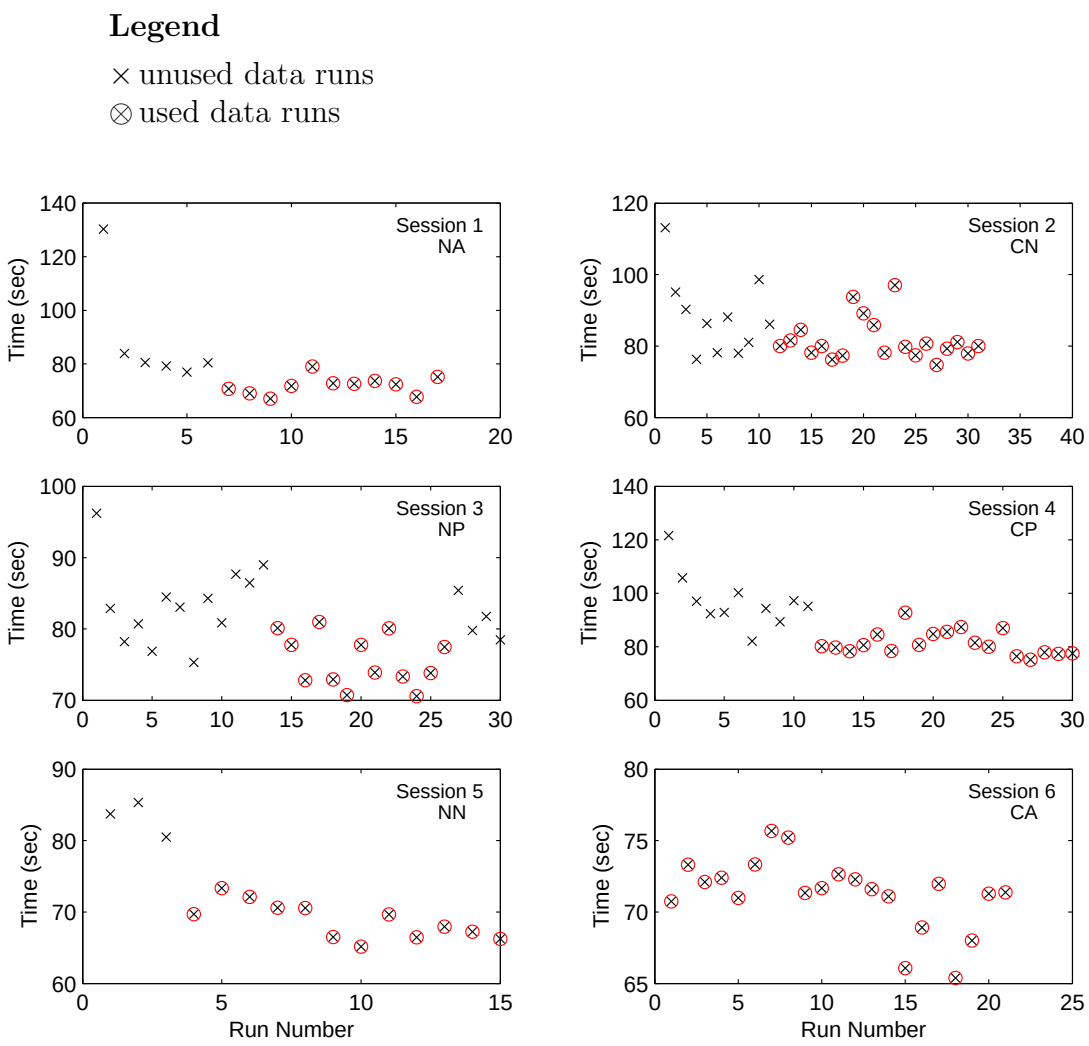

Figure E.5: Study 1: Subject 5 Run Times.

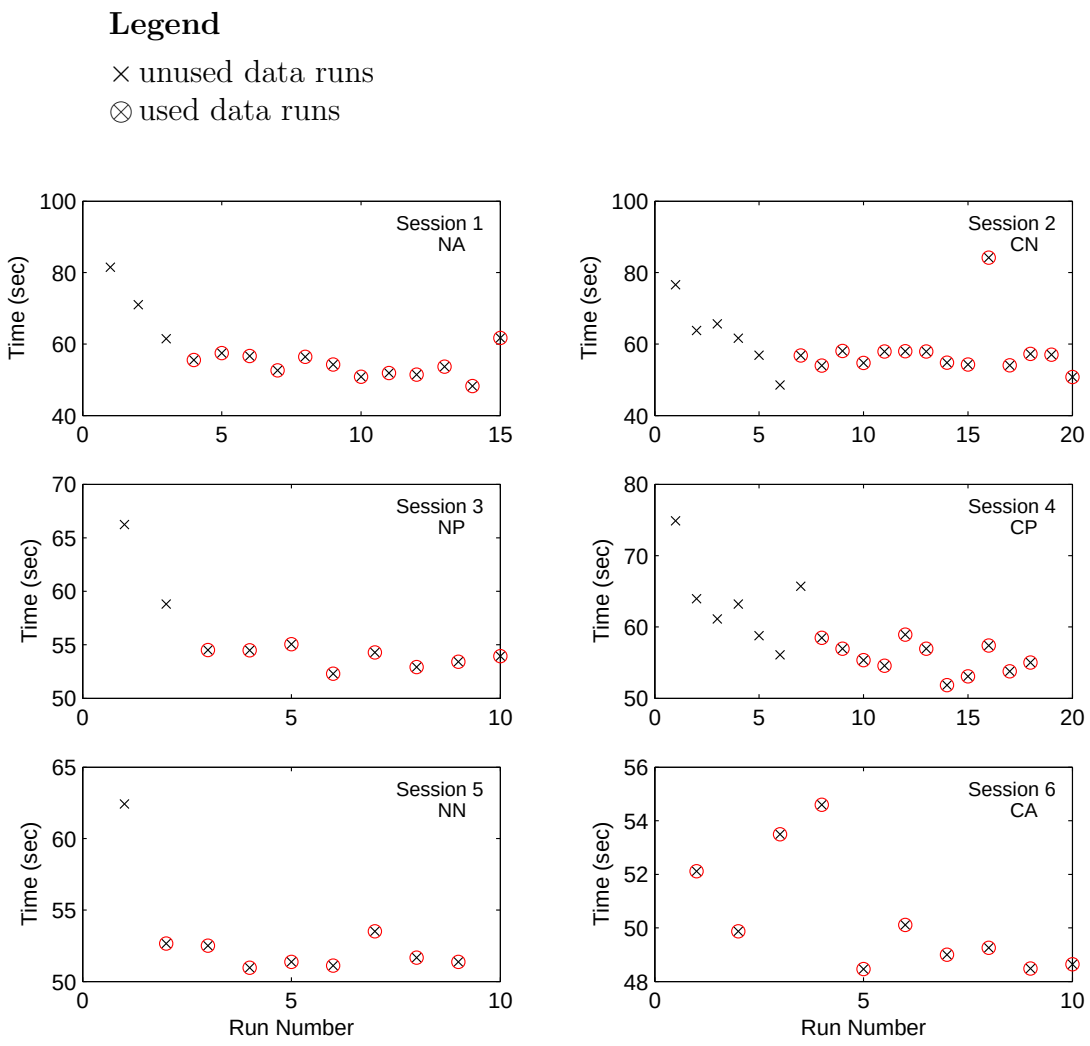

Figure E.6: Study 1: Subject 6 Run Times.

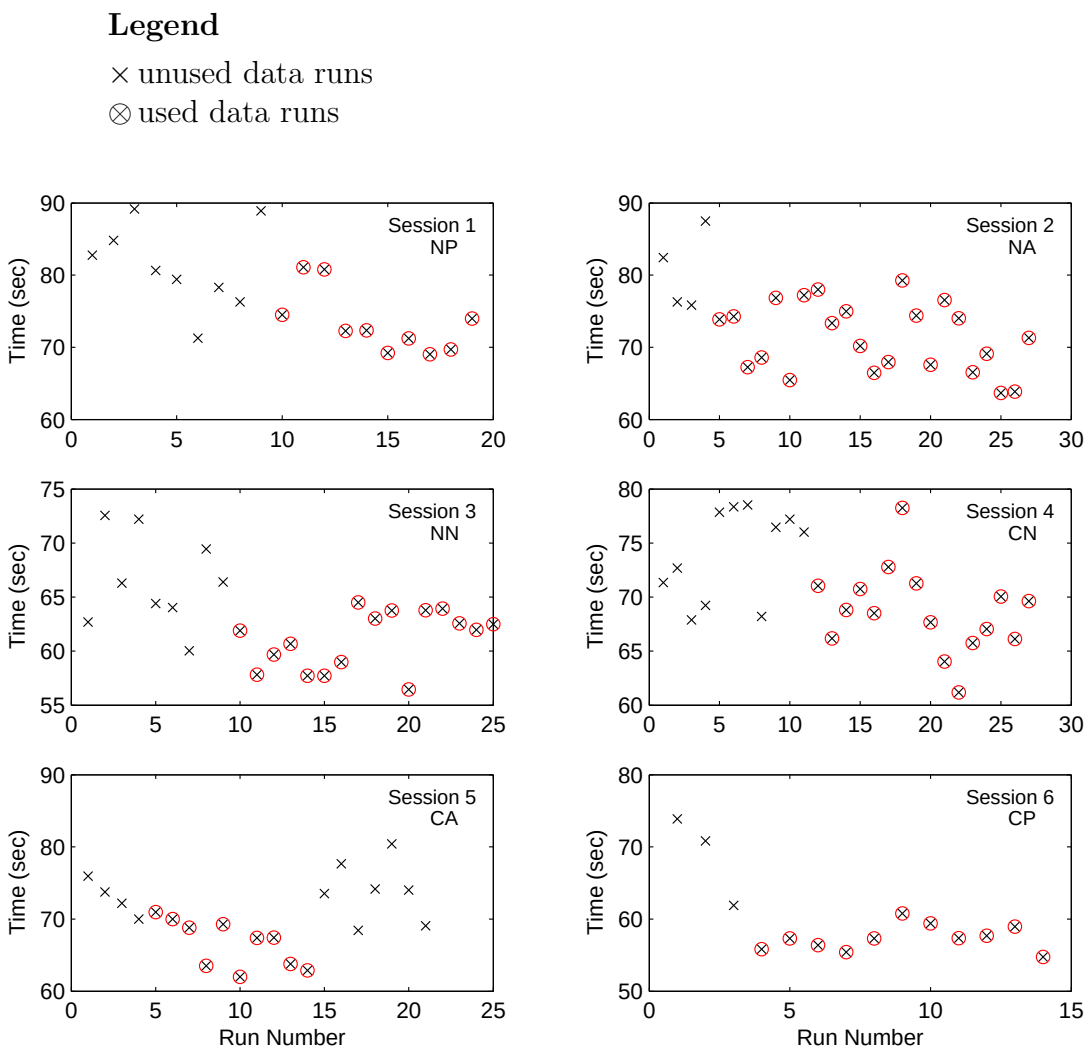

Figure E.7: Study 1: Subject 7 Run Times.

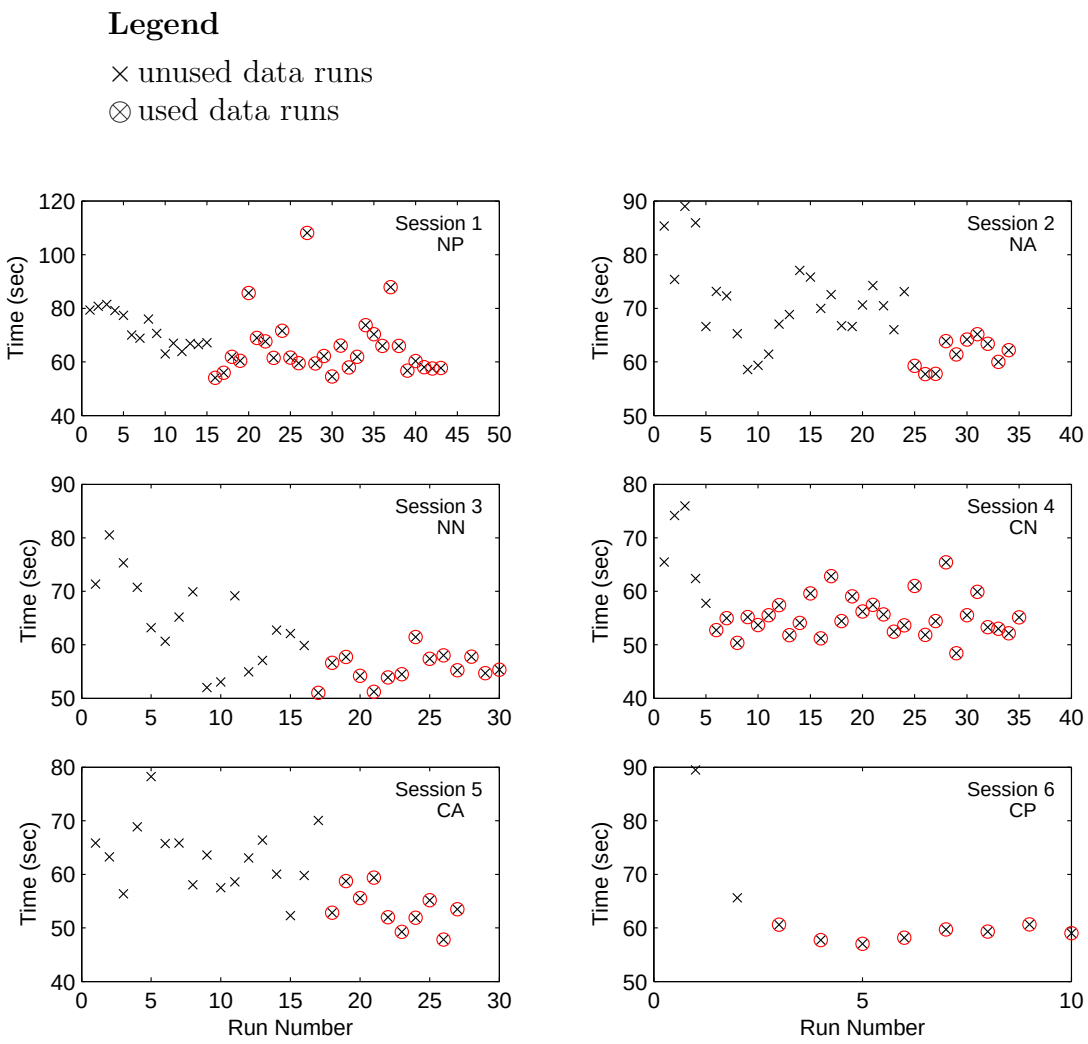

Figure E.8: Study 1: Subject 8 Run Times.

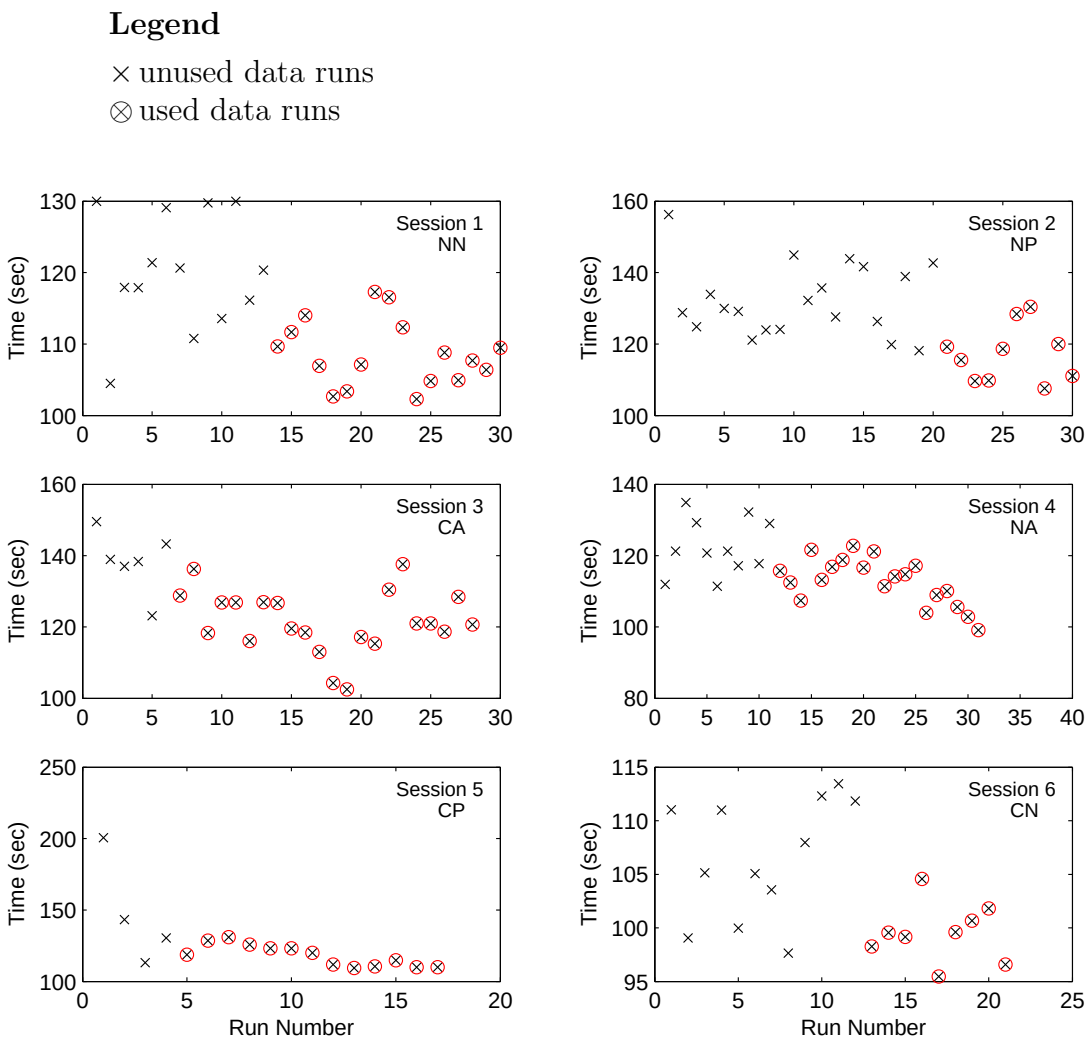

Figure E.9: Study 1: Subject 9 Run Times.

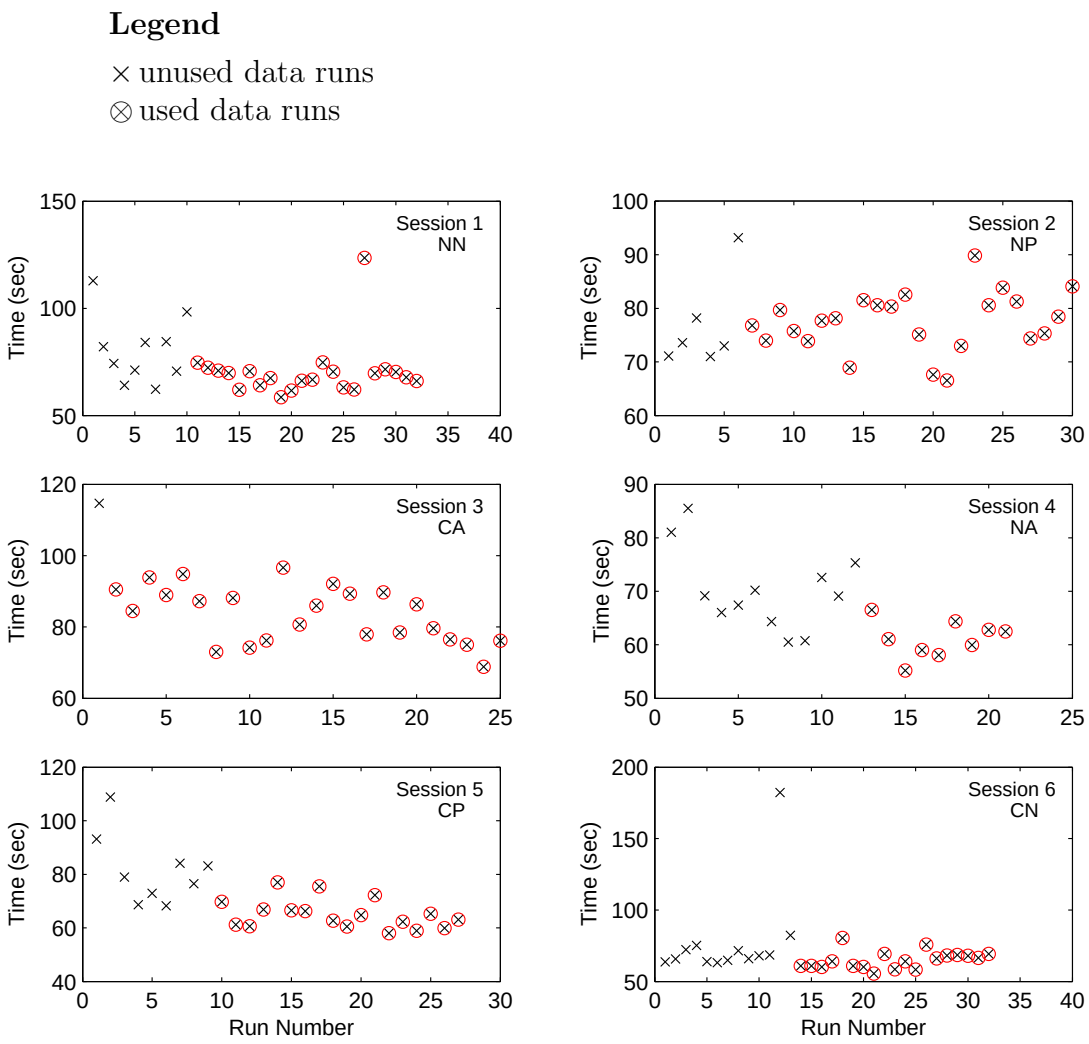

Figure E.10: Study 1: Subject 10 Run Times.

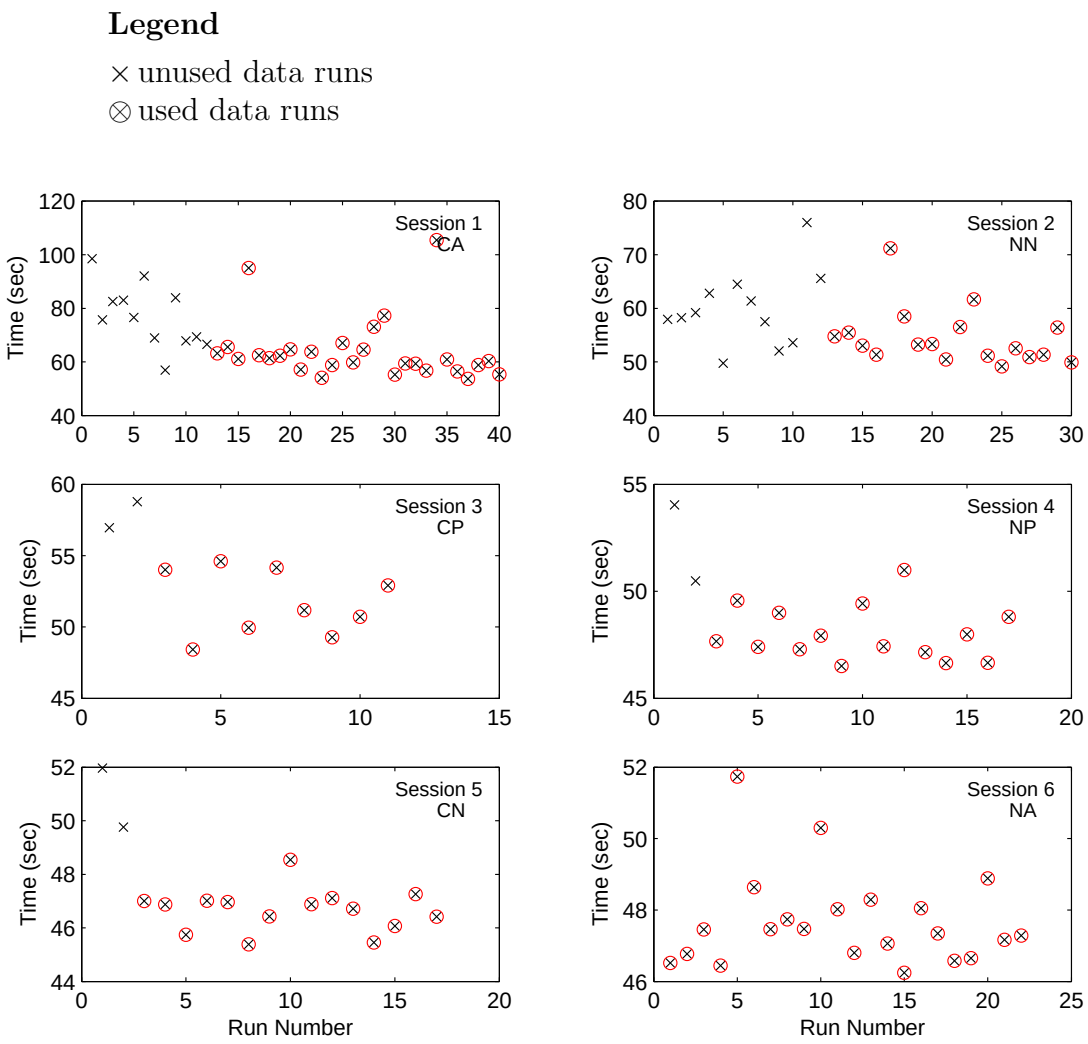

Figure E.11: Study 1: Subject 11 Run Times.

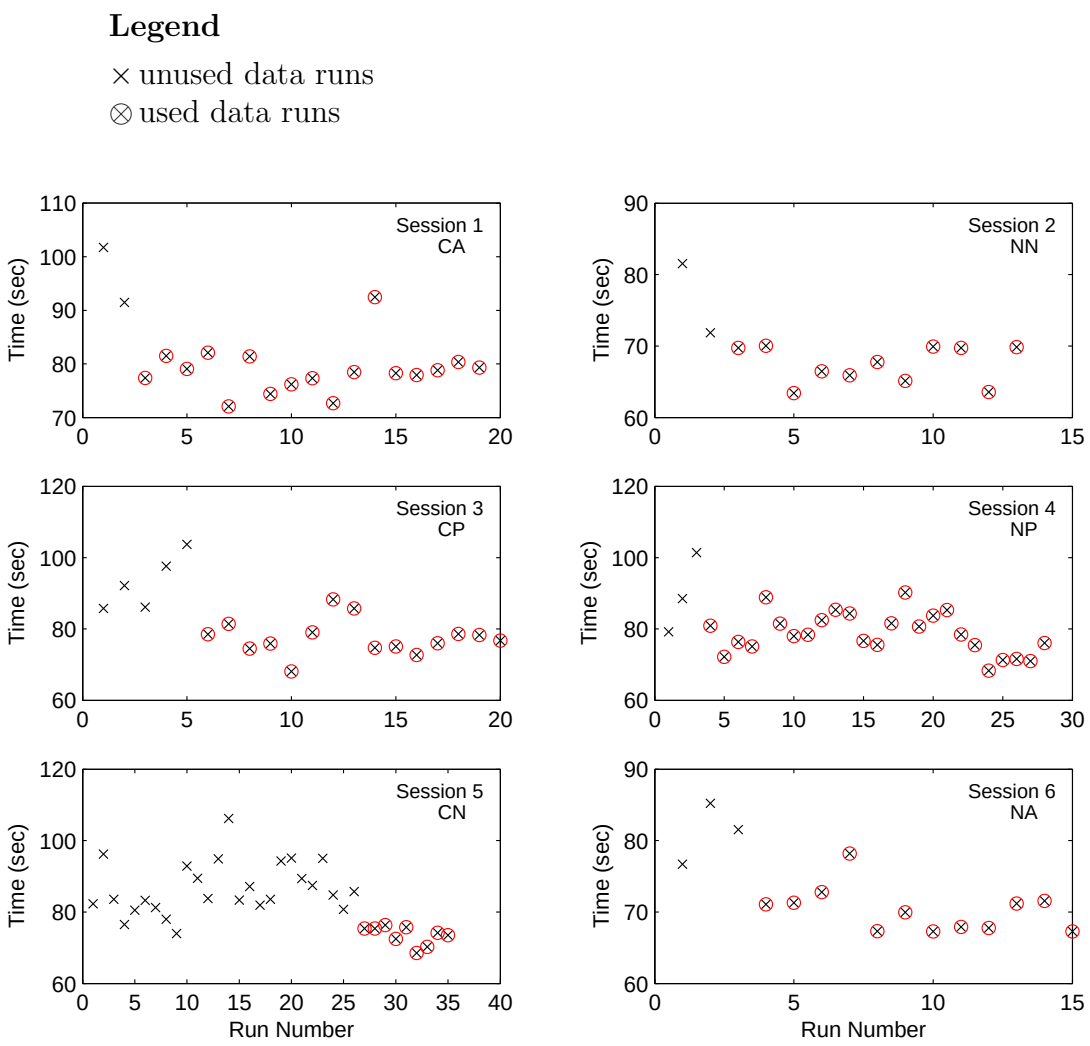

Figure E.12: Study 1: Subject 12 Run Times.

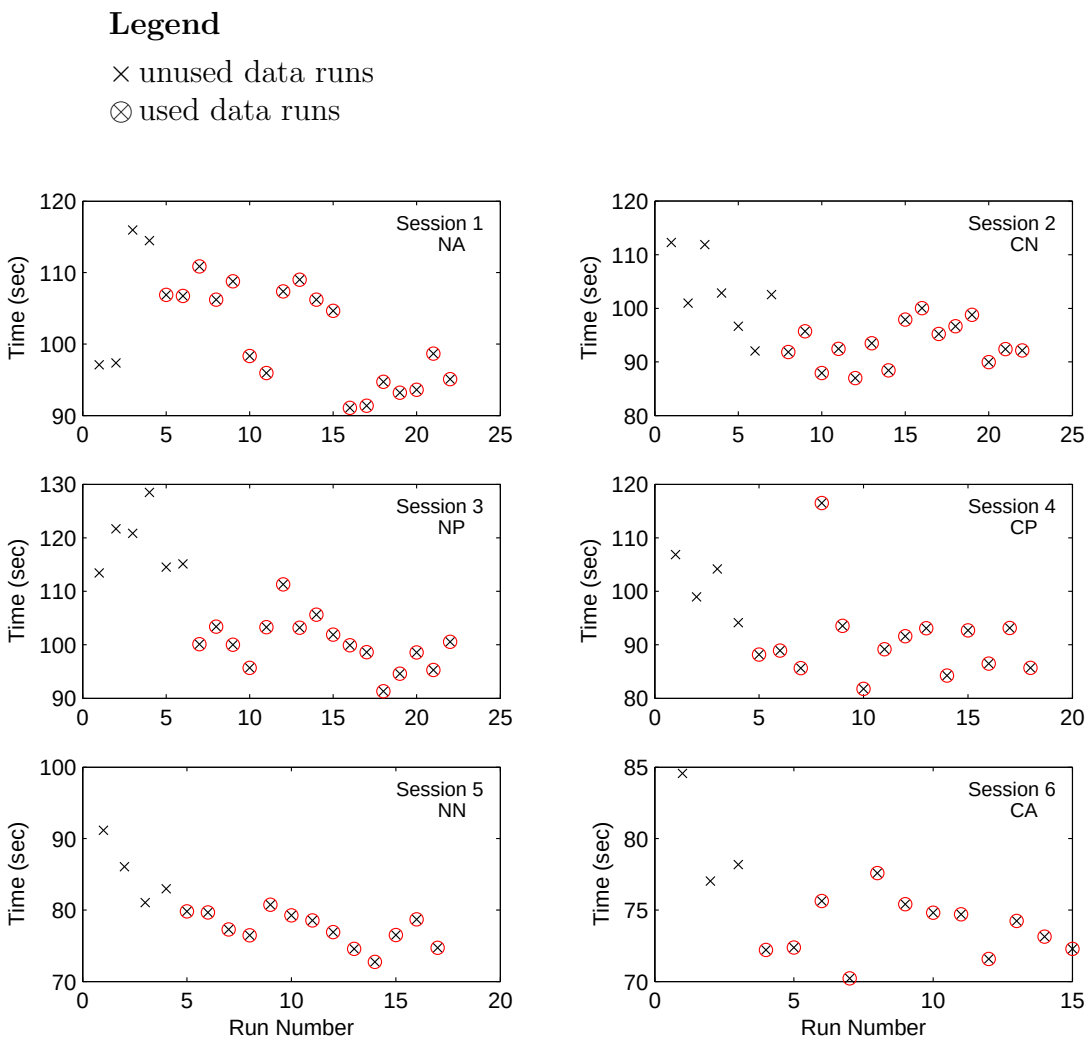

Figure E.13: Study 1: Subject 13 Run Times.

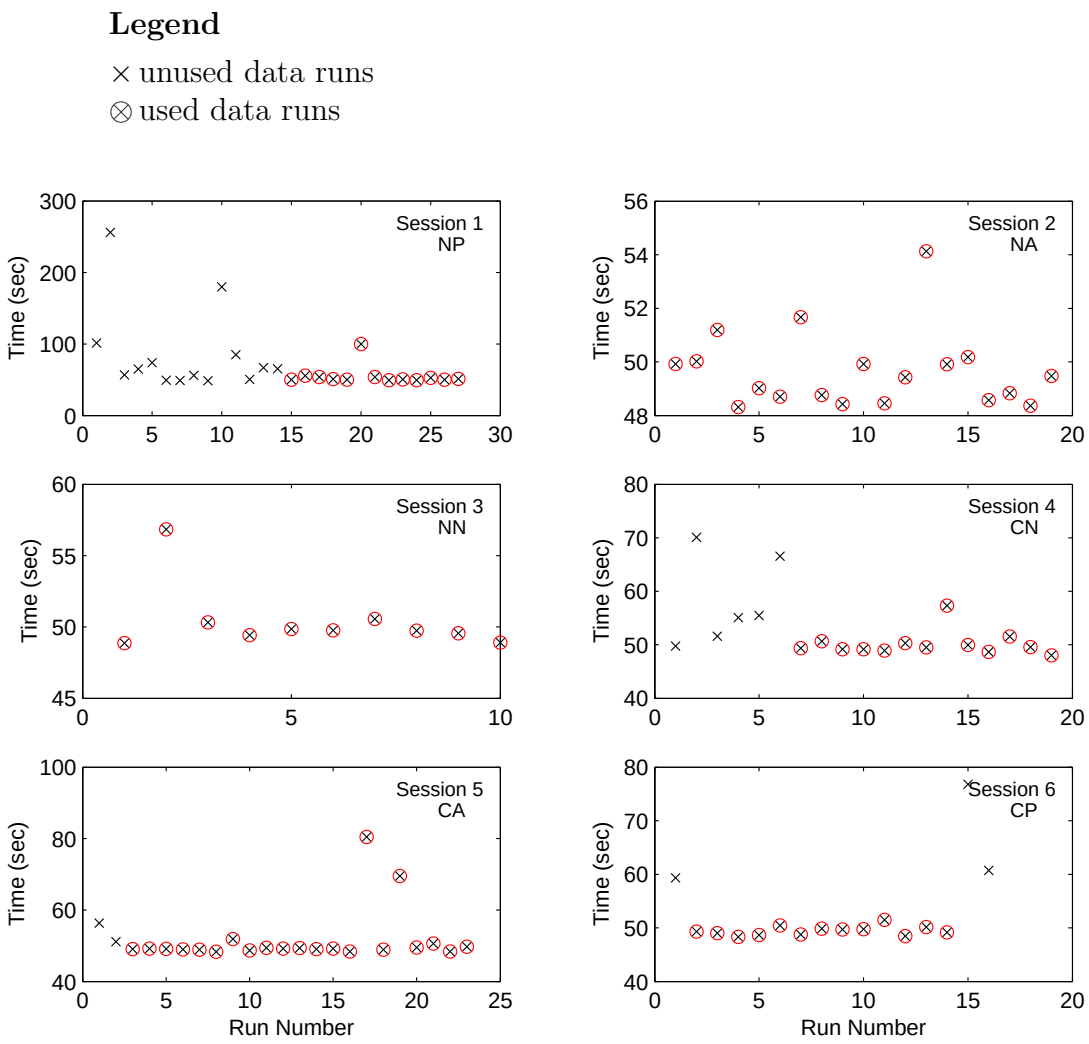

Figure E.14: Study 1: Subject 14 Run Times.

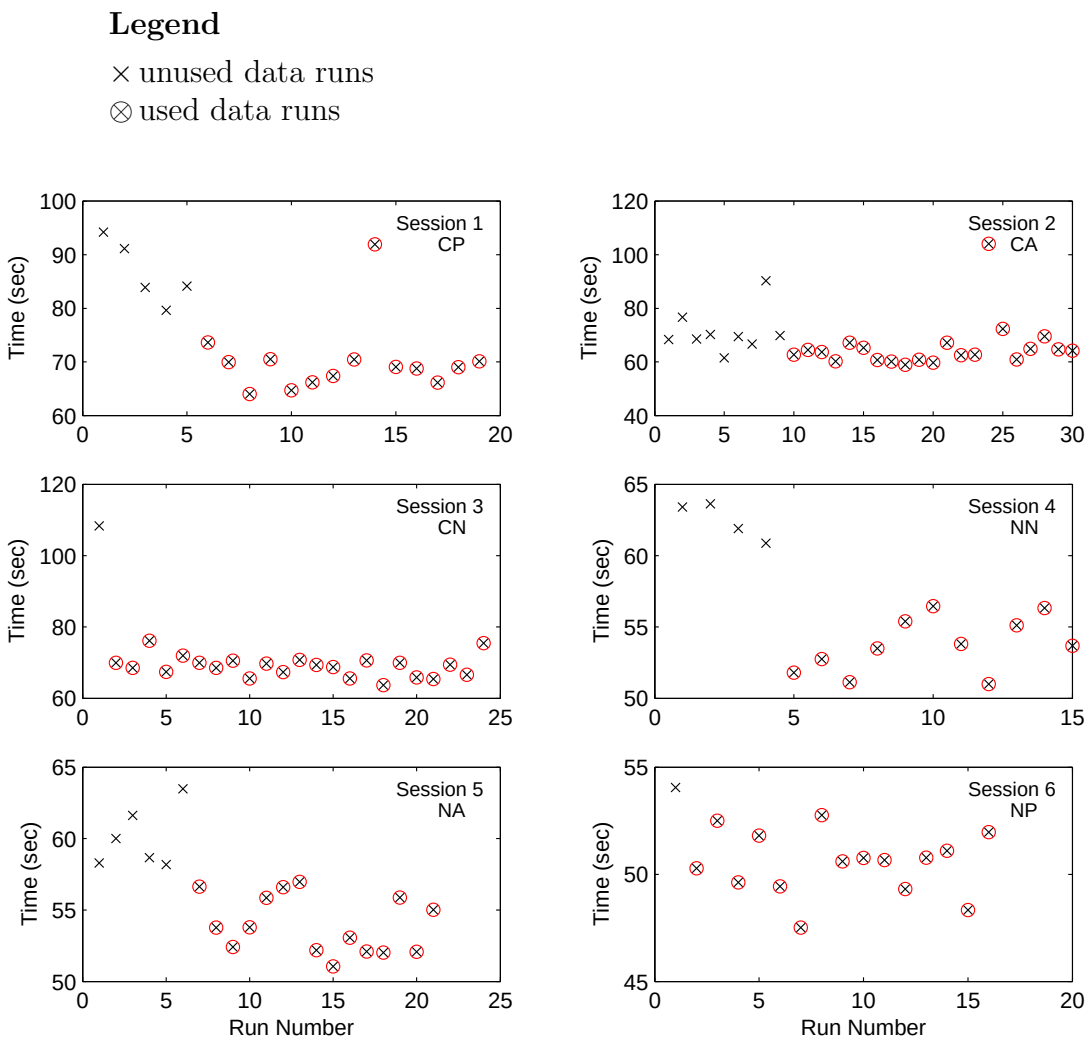

Figure E.15: Study 1: Subject 15 Run Times.

Legend

× unused data runs

⊗ used data runs

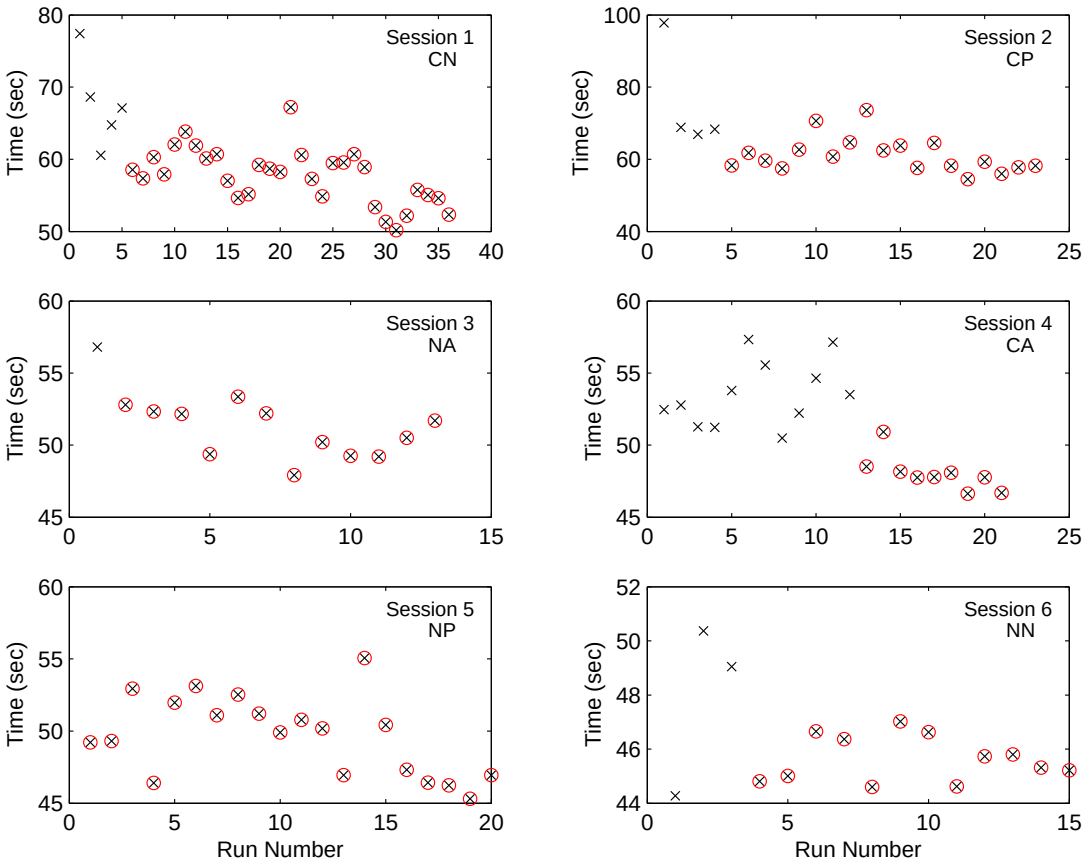

Figure E.16: Study 1: Subject 16 Run Times.

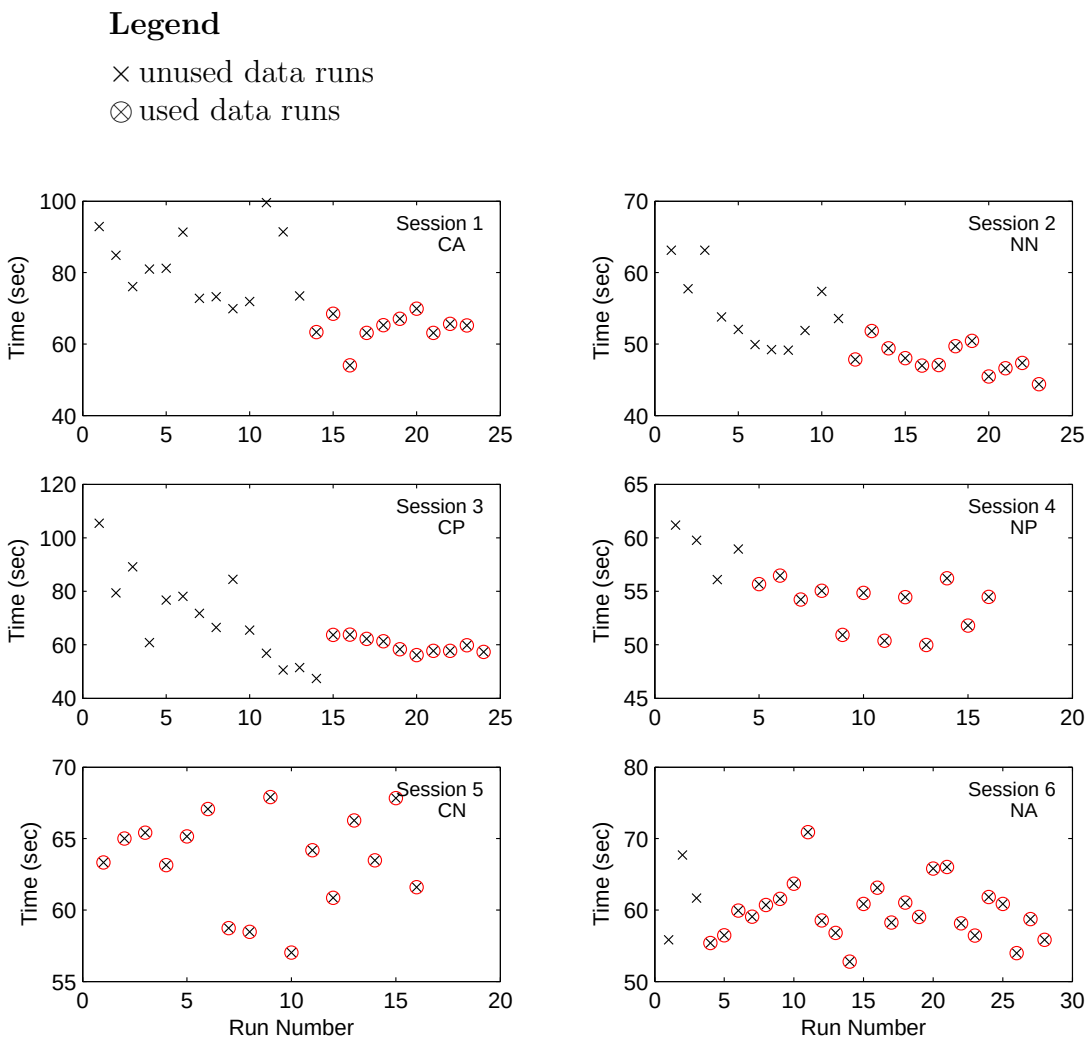

Figure E.17: Study 1: Subject 17 Run Times.

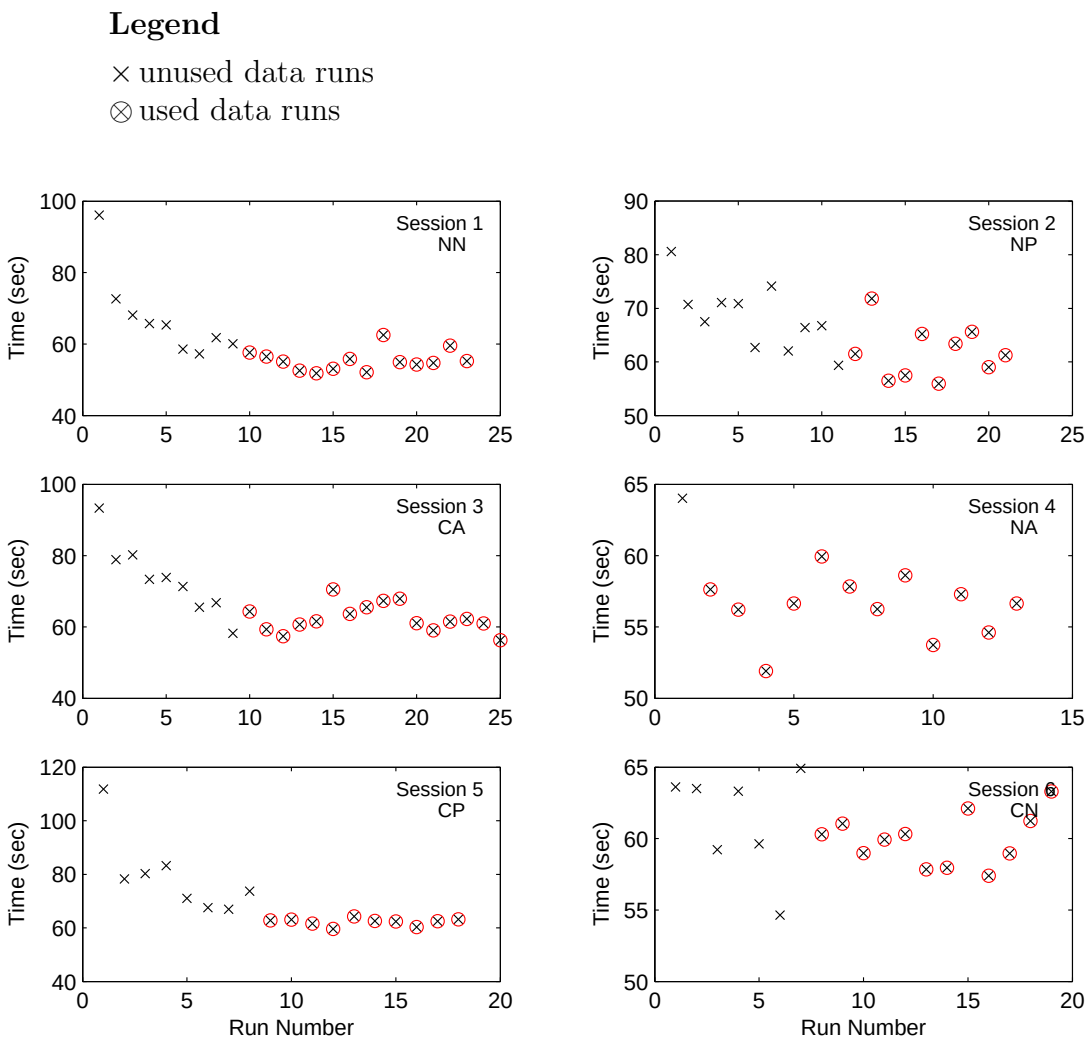

Figure E.18: Study 1: Subject 18 Run Times.

E.2 Study 2: 1.25 Second Round Trip Time Delay Data

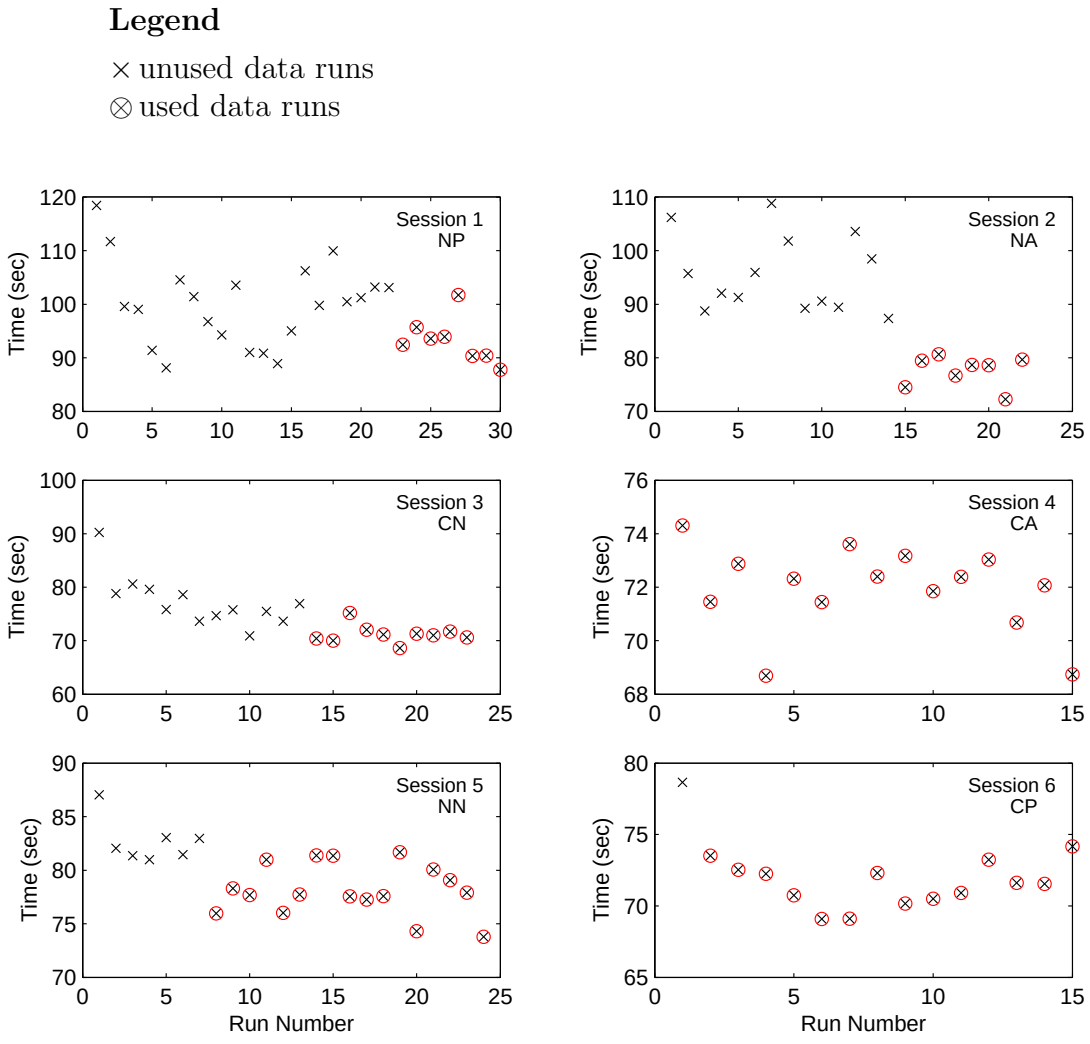

Figure E.19: Study 2: Subject 1 Run Times.

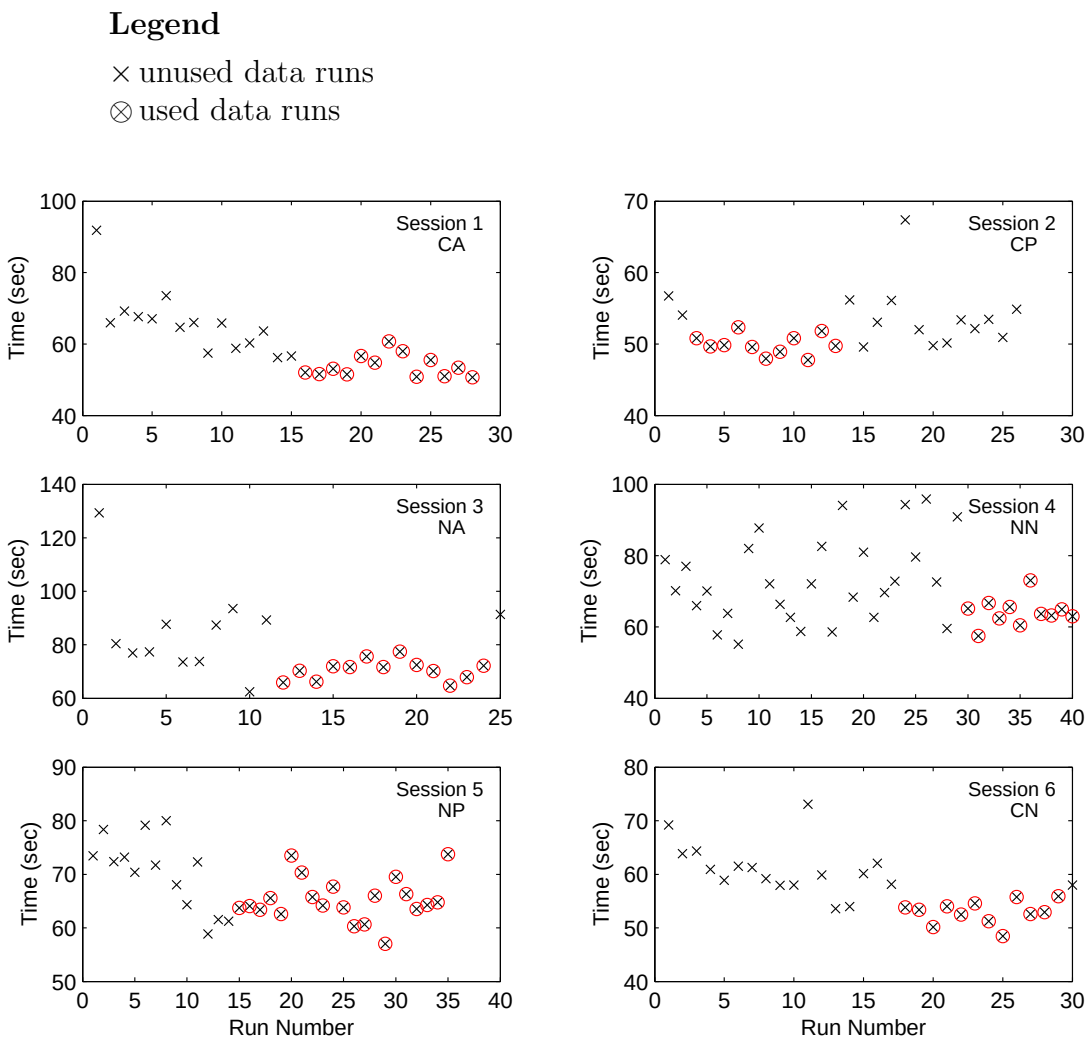

Figure E.20: Study 2: Subject 2 Run Times.

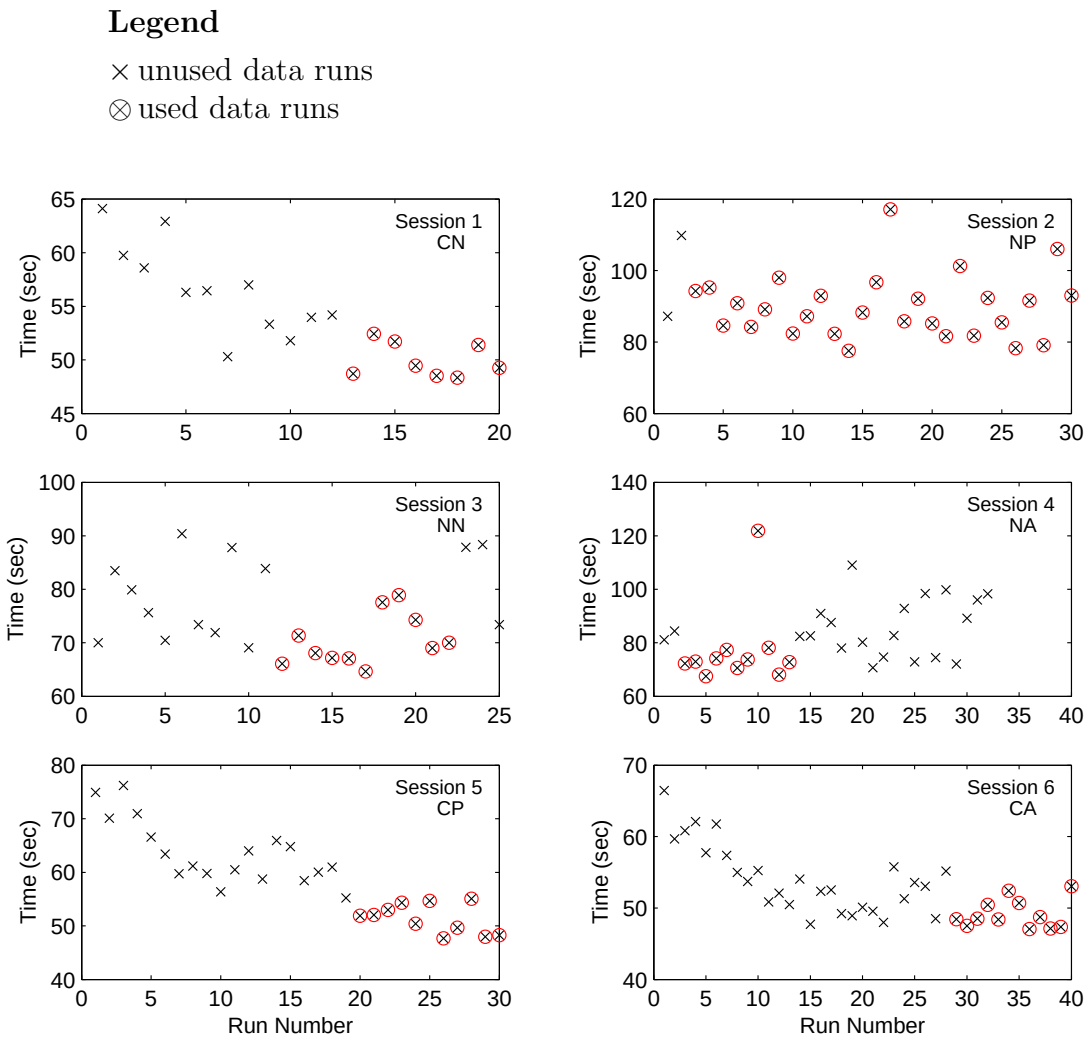

Figure E.21: Study 2: Subject 3 Run Times.

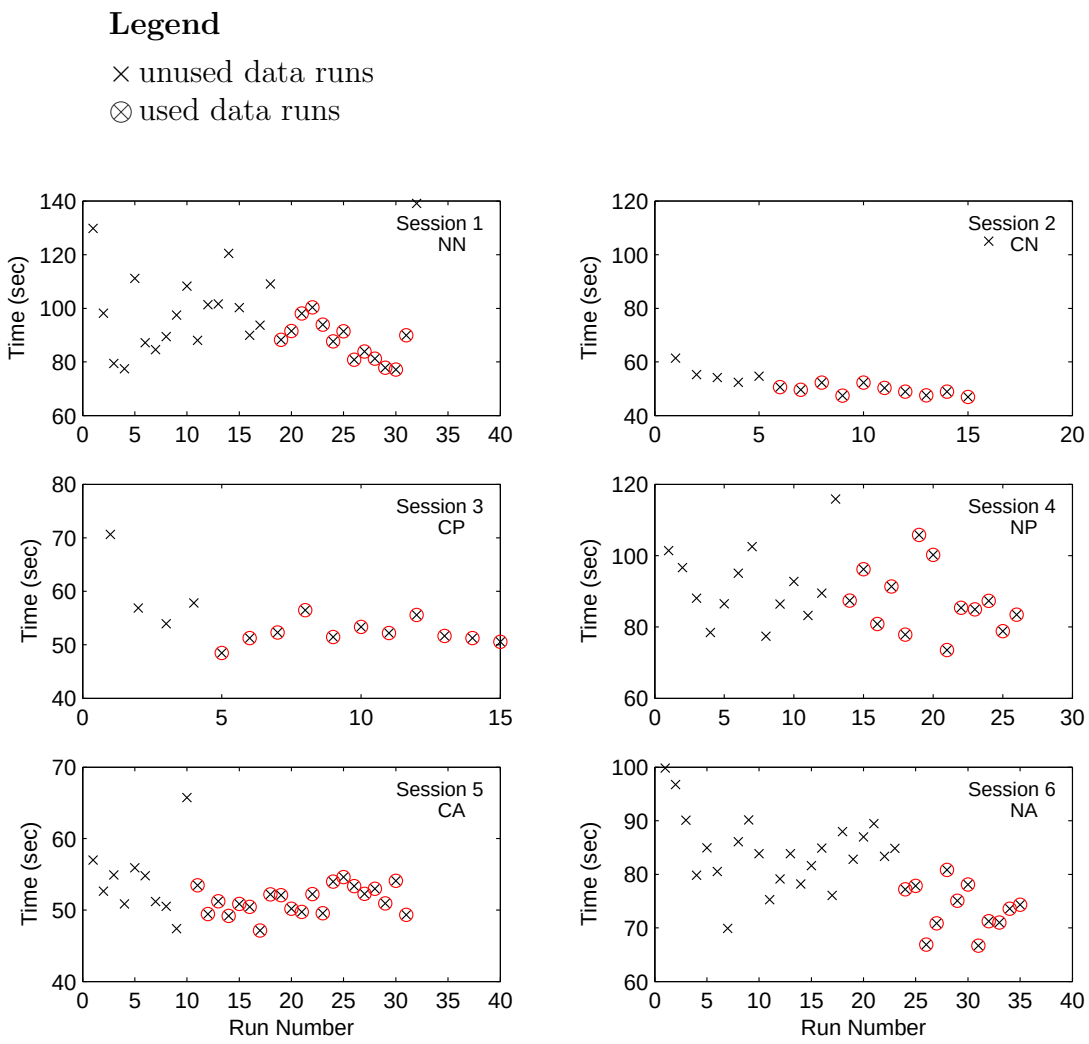

Figure E.22: Study 2: Subject 4 Run Times.

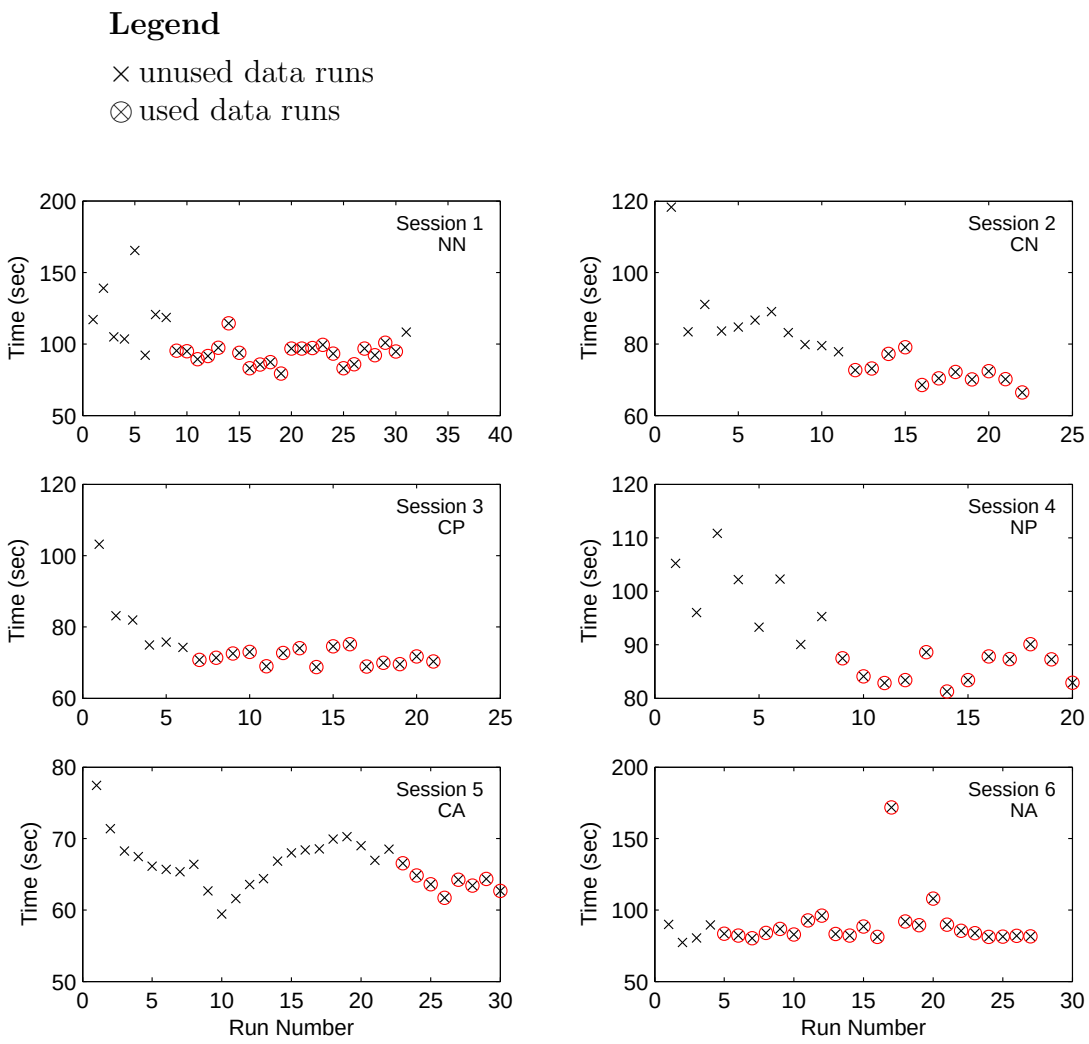

Figure E.23: Study 2: Subject 5 Run Times.

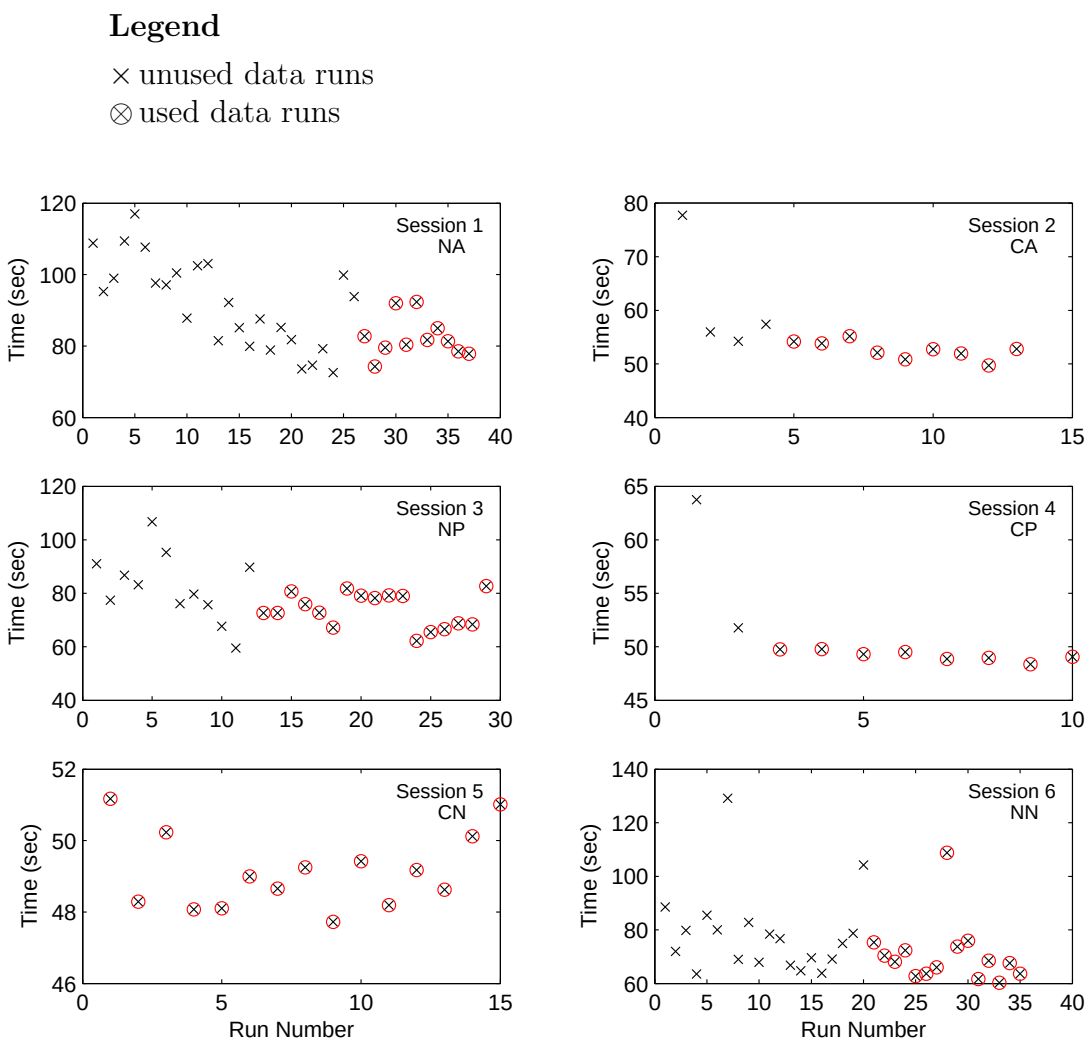

Figure E.24: Study 2: Subject 6 Run Times.

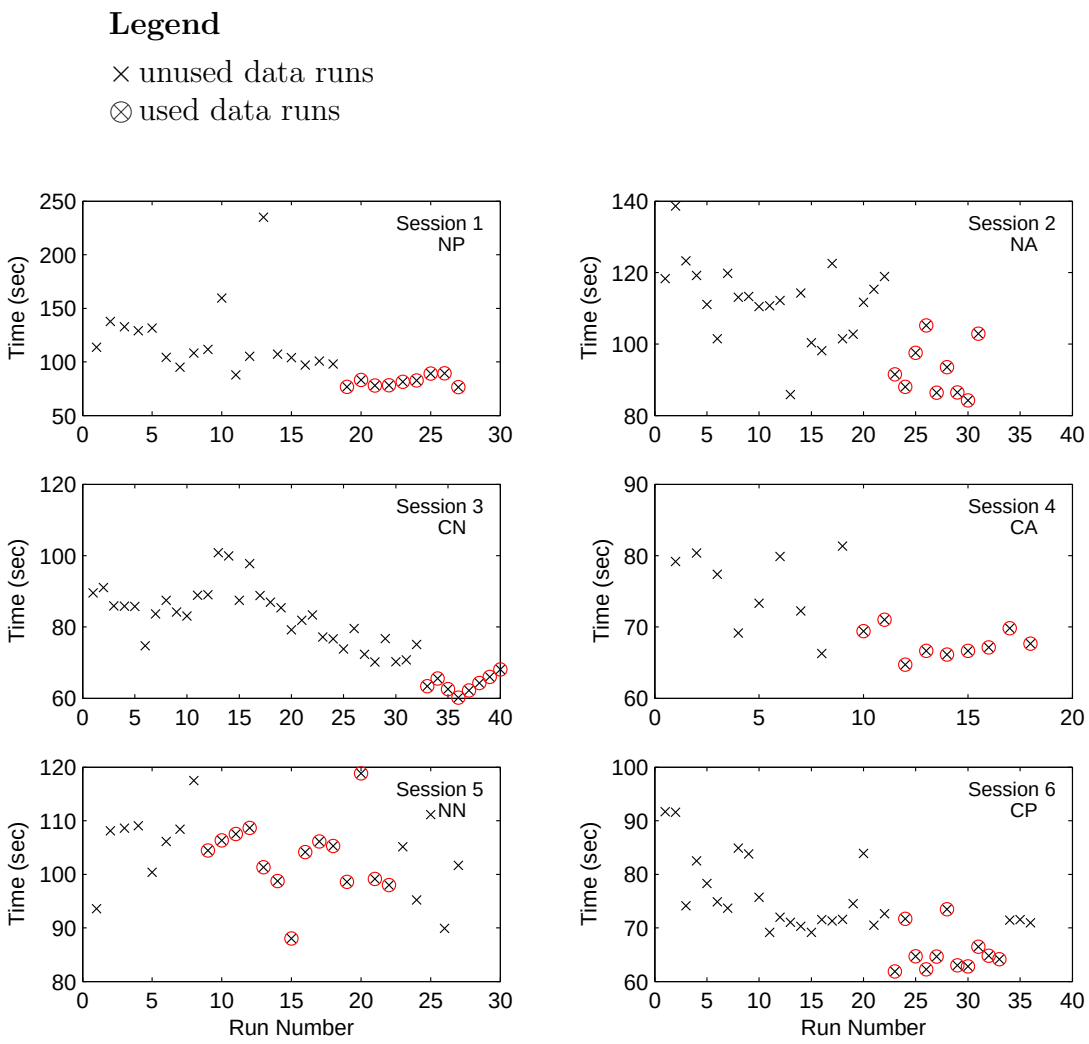

Figure E.25: Study 2: Subject 7 Run Times.

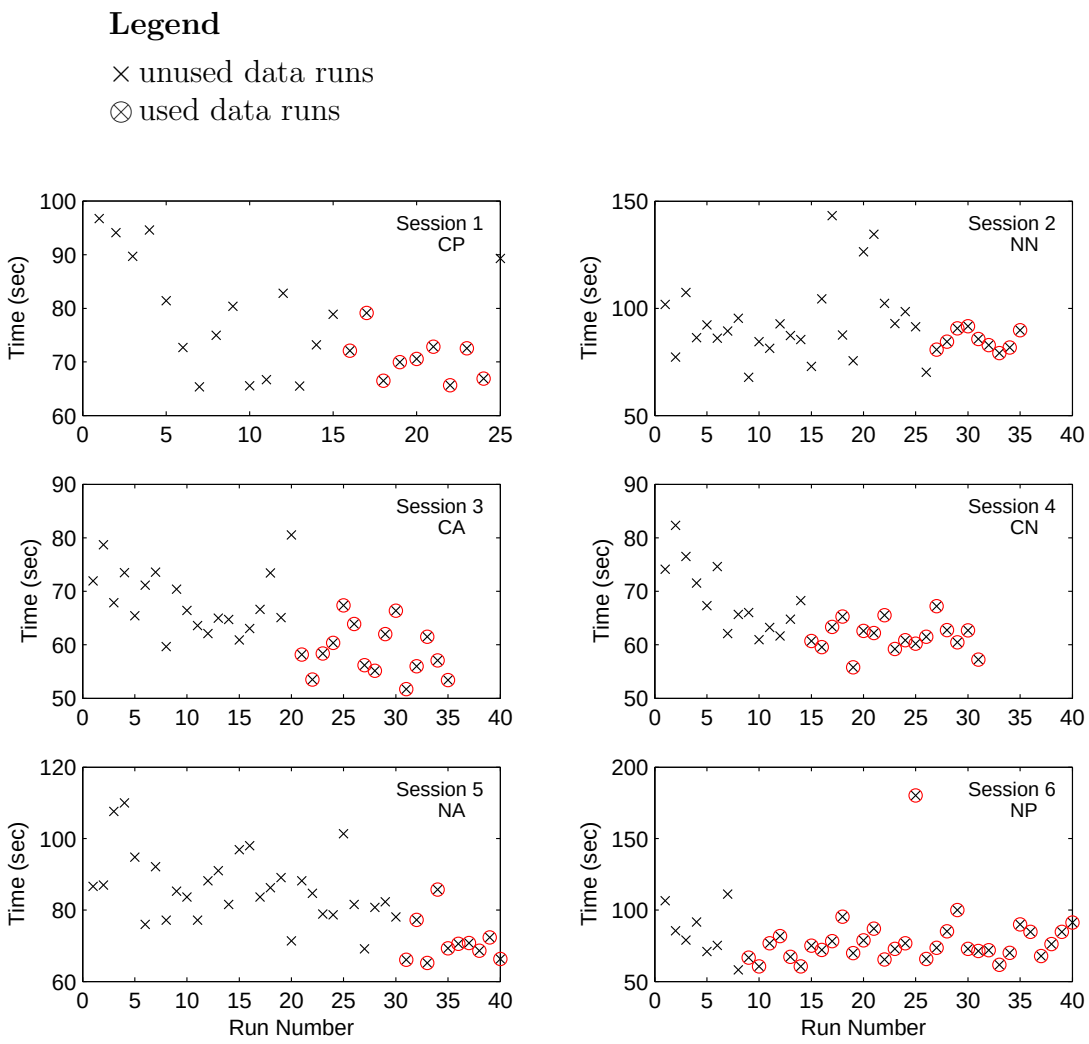

Figure E.26: Study 2: Subject 8 Run Times.

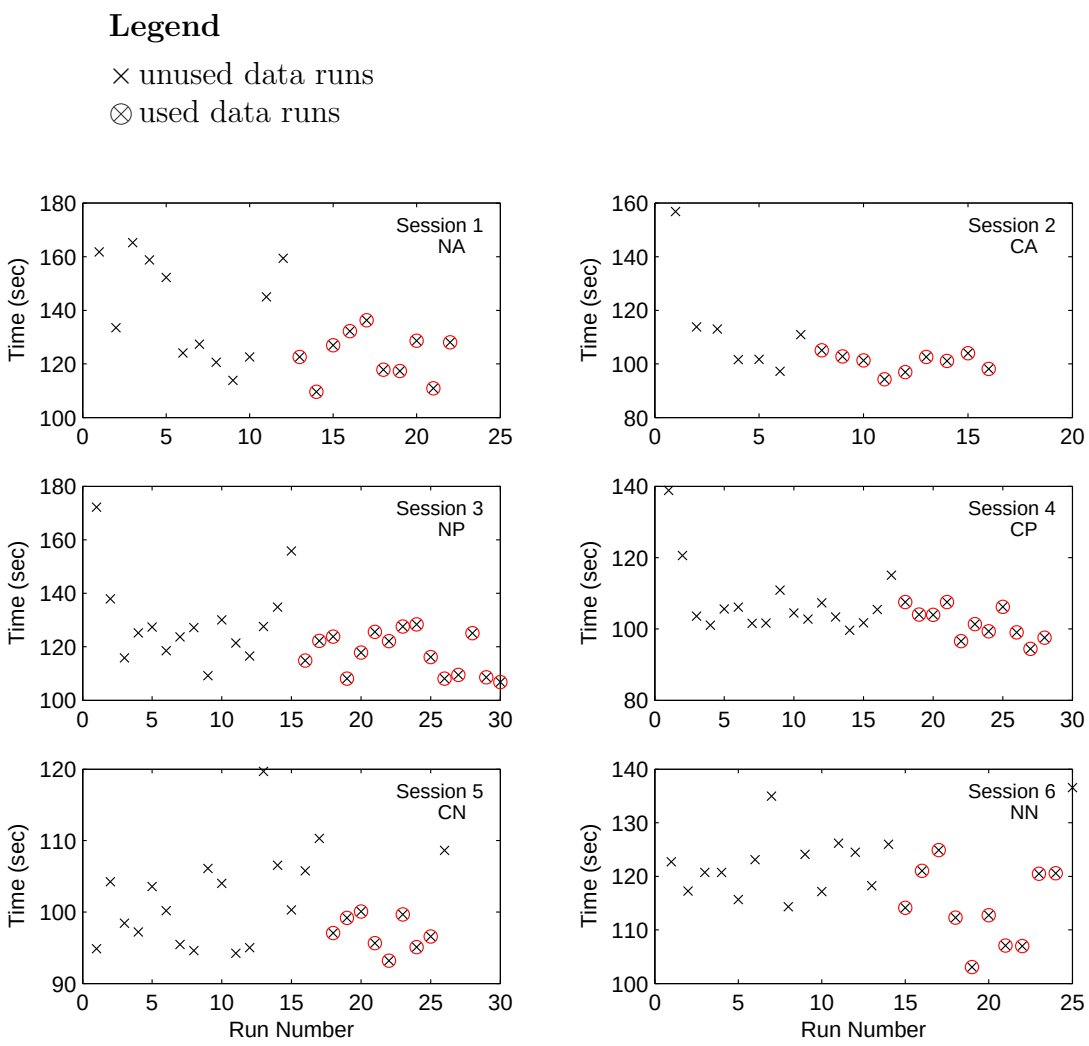

Figure E.27: Study 2: Subject 9 Run Times.

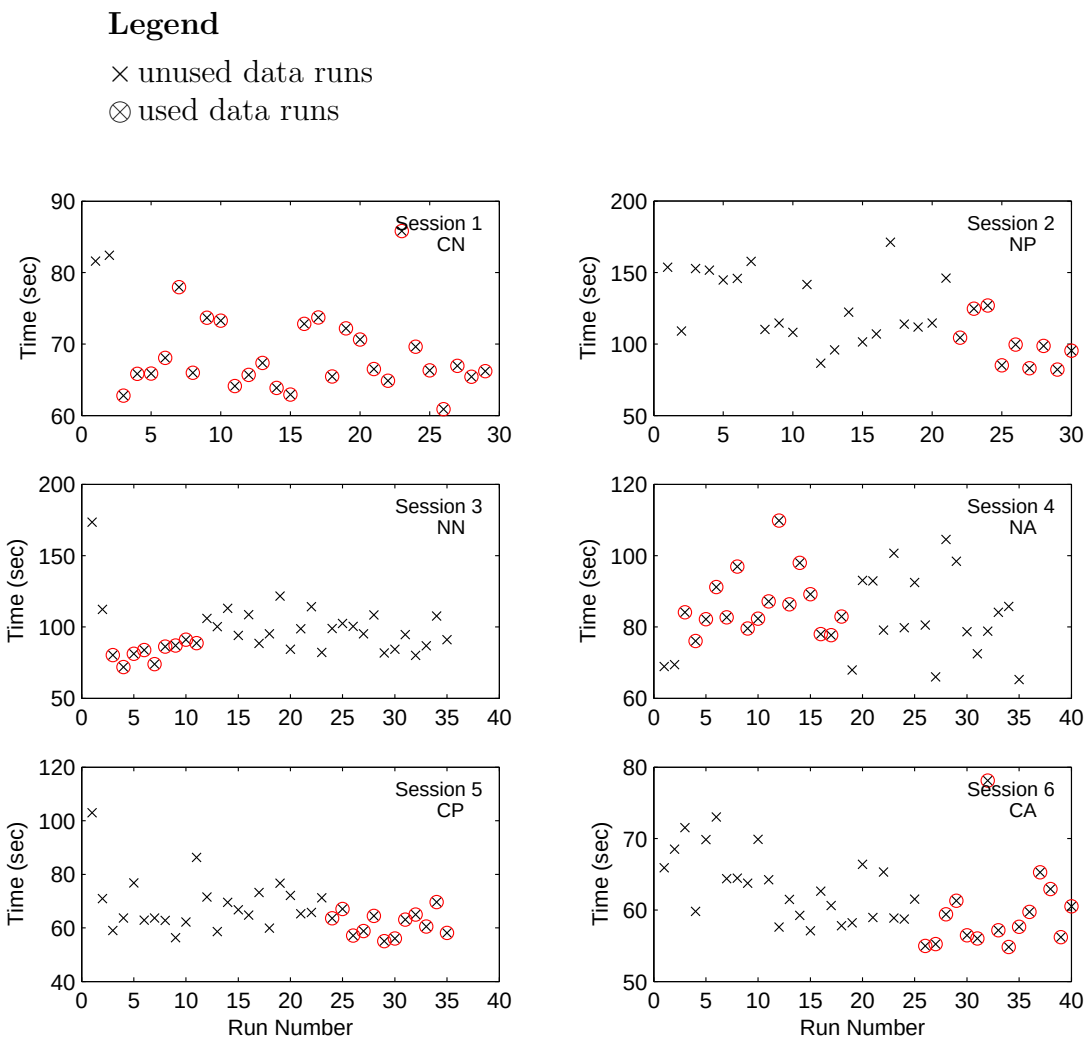

Figure E.28: Study 2: Subject 10 Run Times.

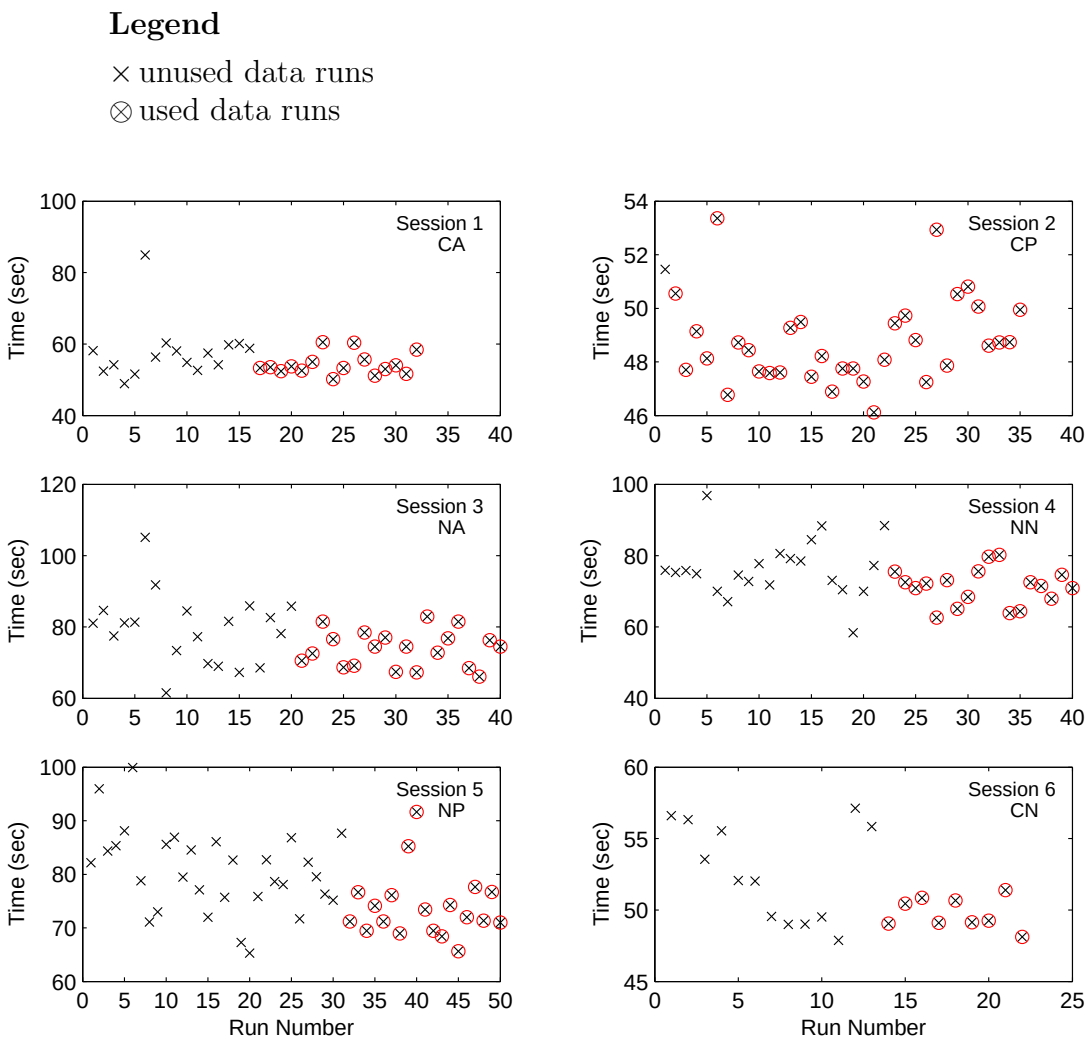

Figure E.29: Study 2: Subject 11 Run Times.

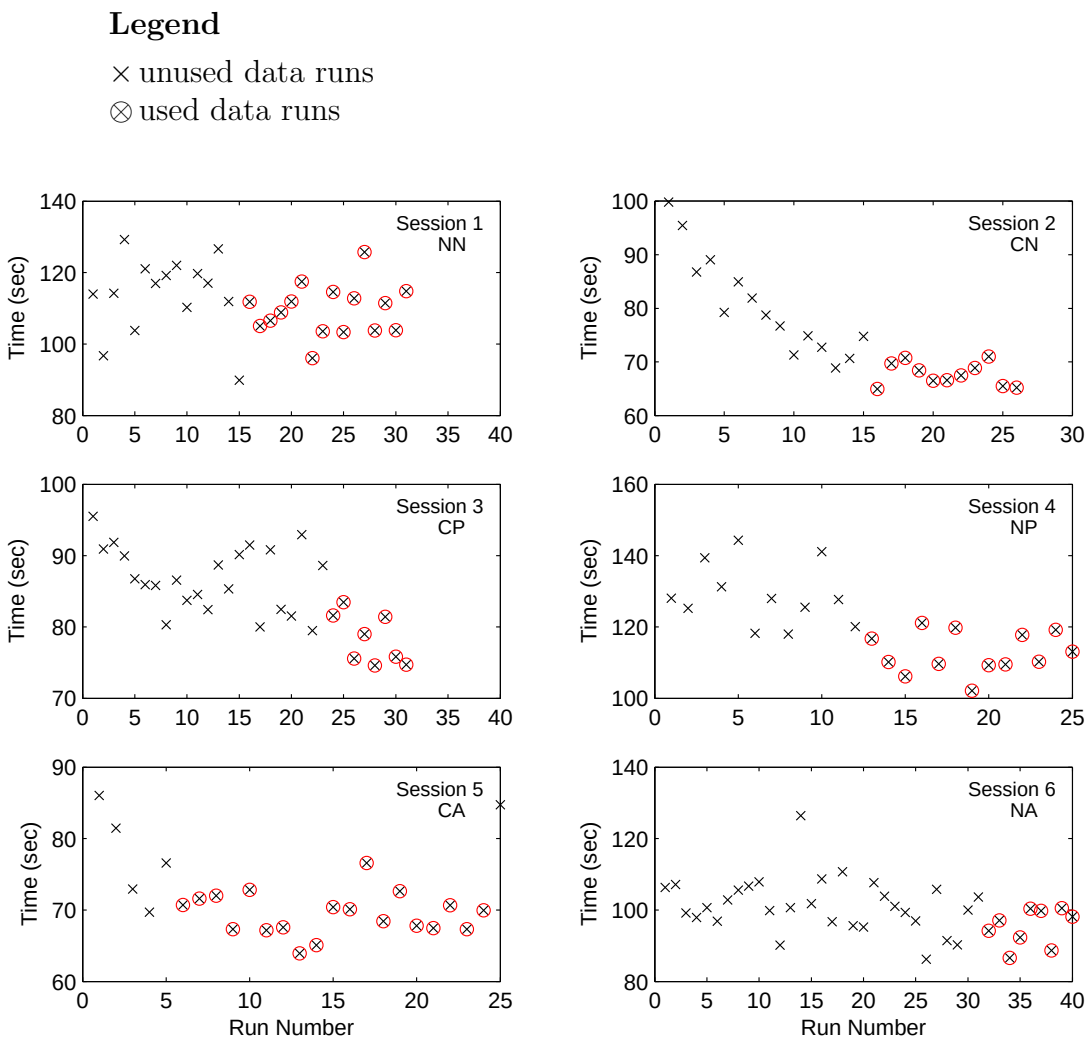

Figure E.30: Study 2: Subject 12 Run Times.

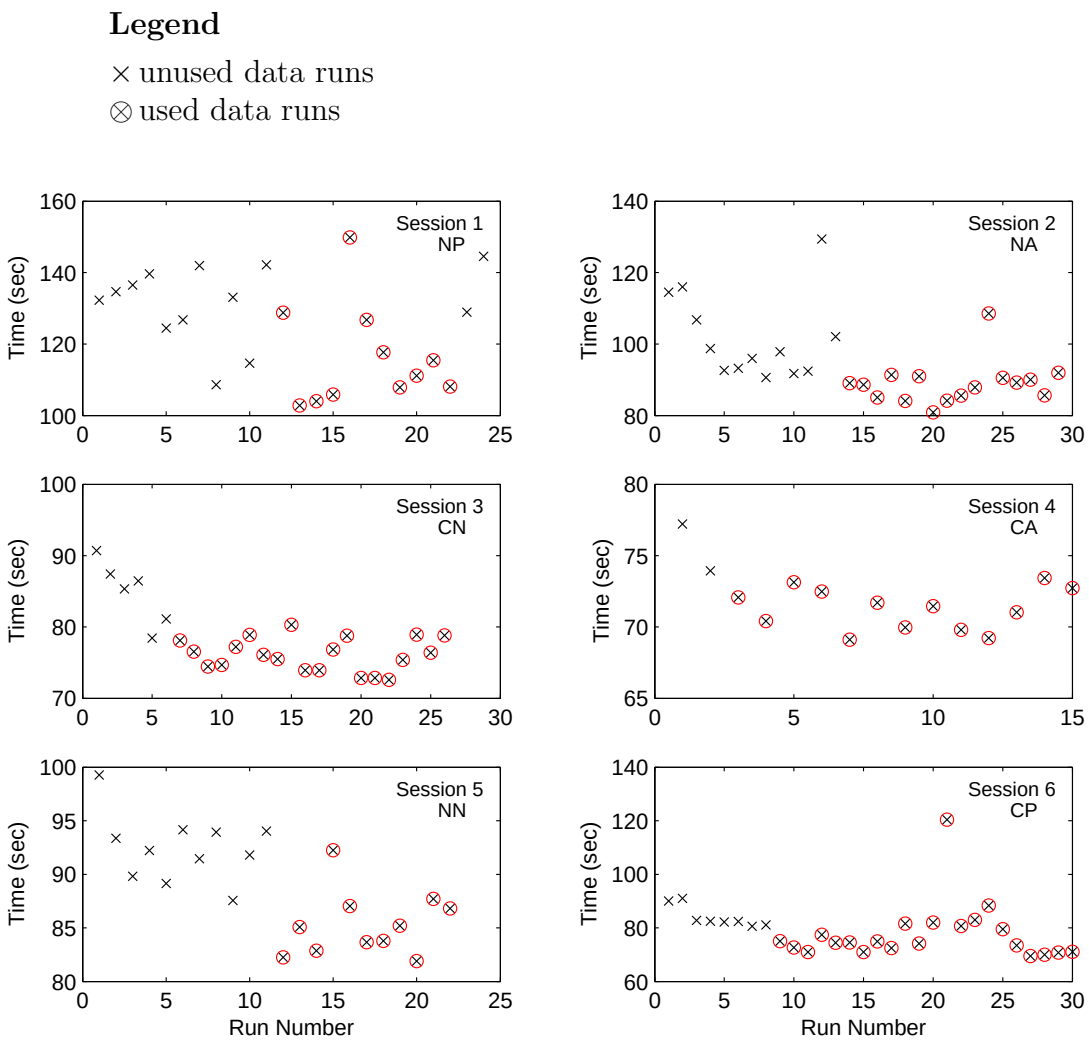

Figure E.31: Study 2: Subject 13 Run Times.

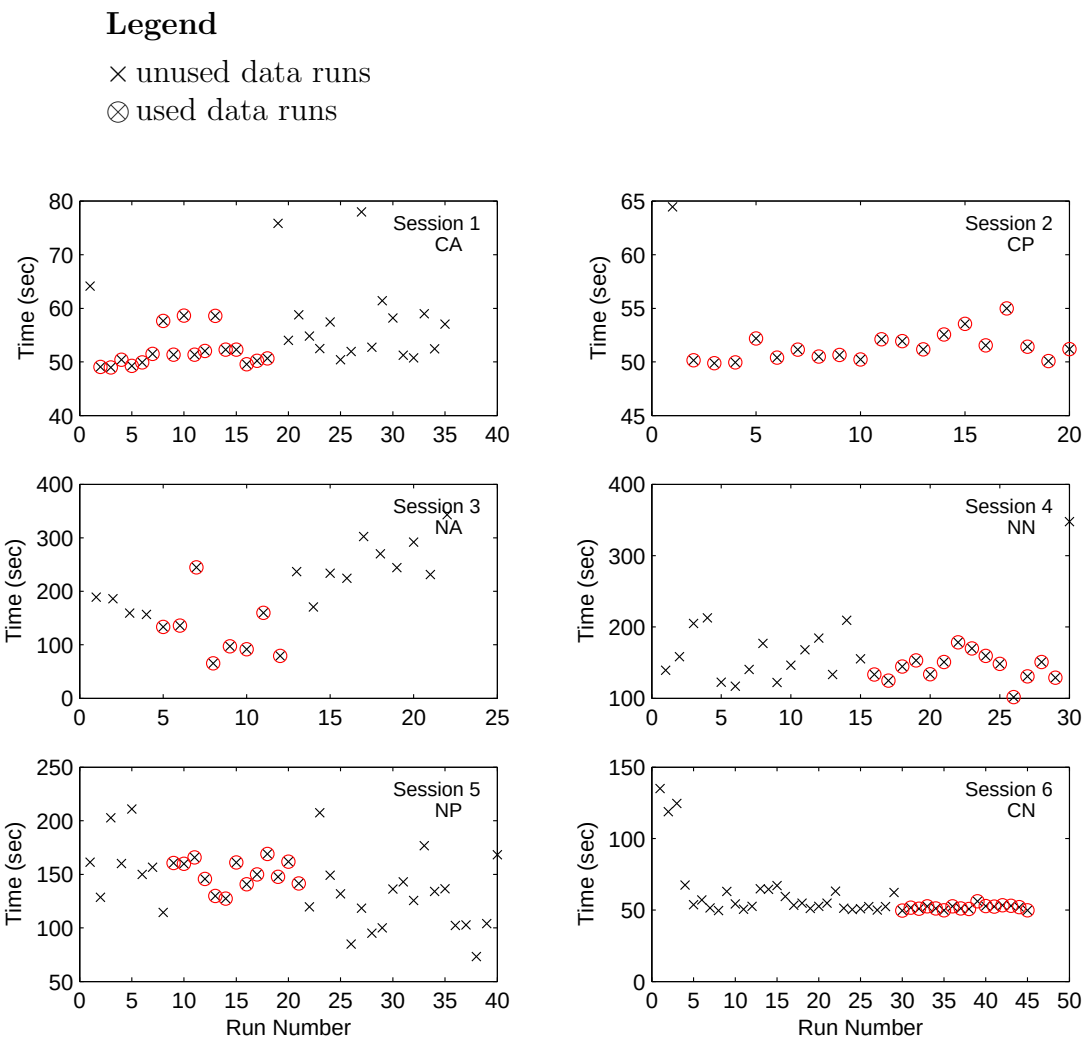

Figure E.32: Study 2: Subject 14 Run Times.

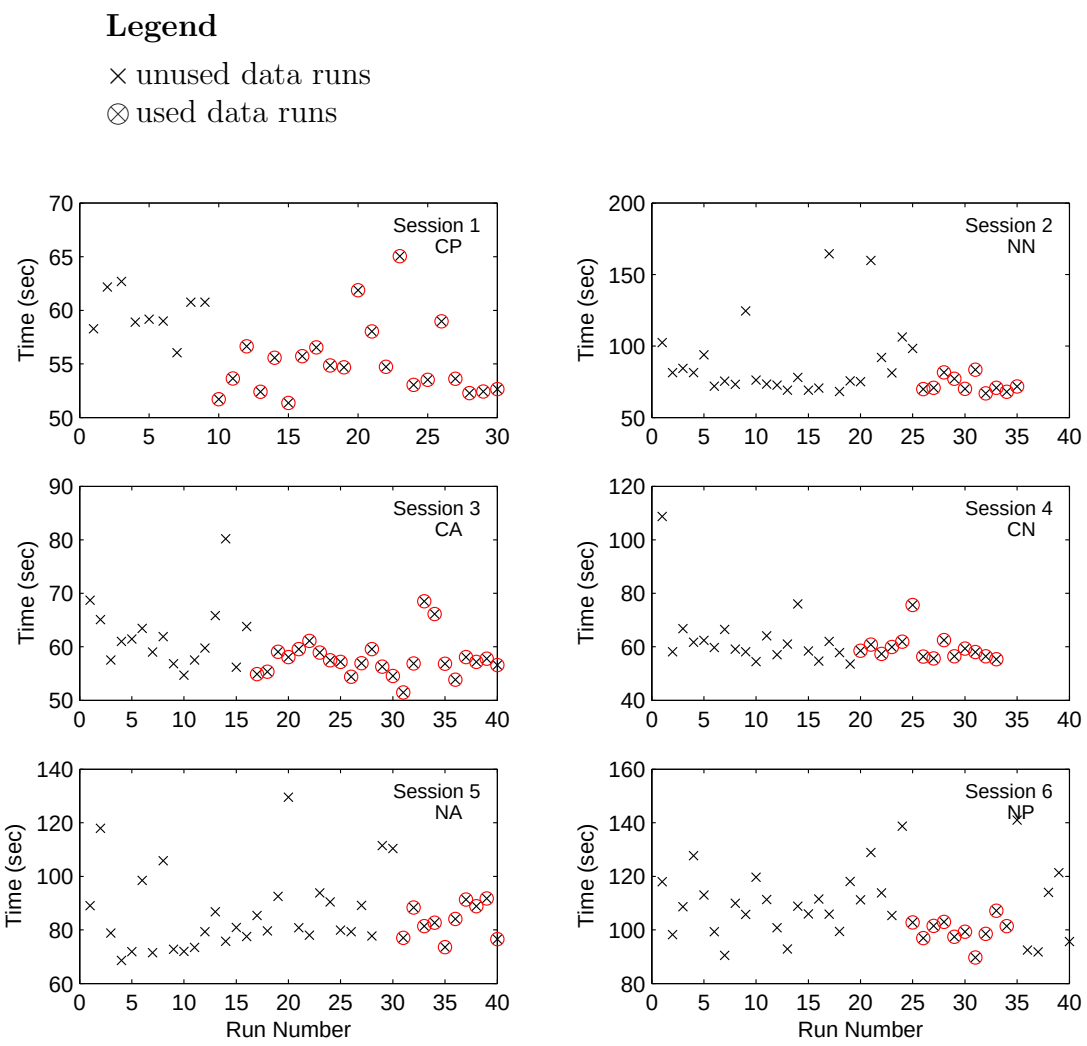

Figure E.33: Study 2: Subject 15 Run Times.

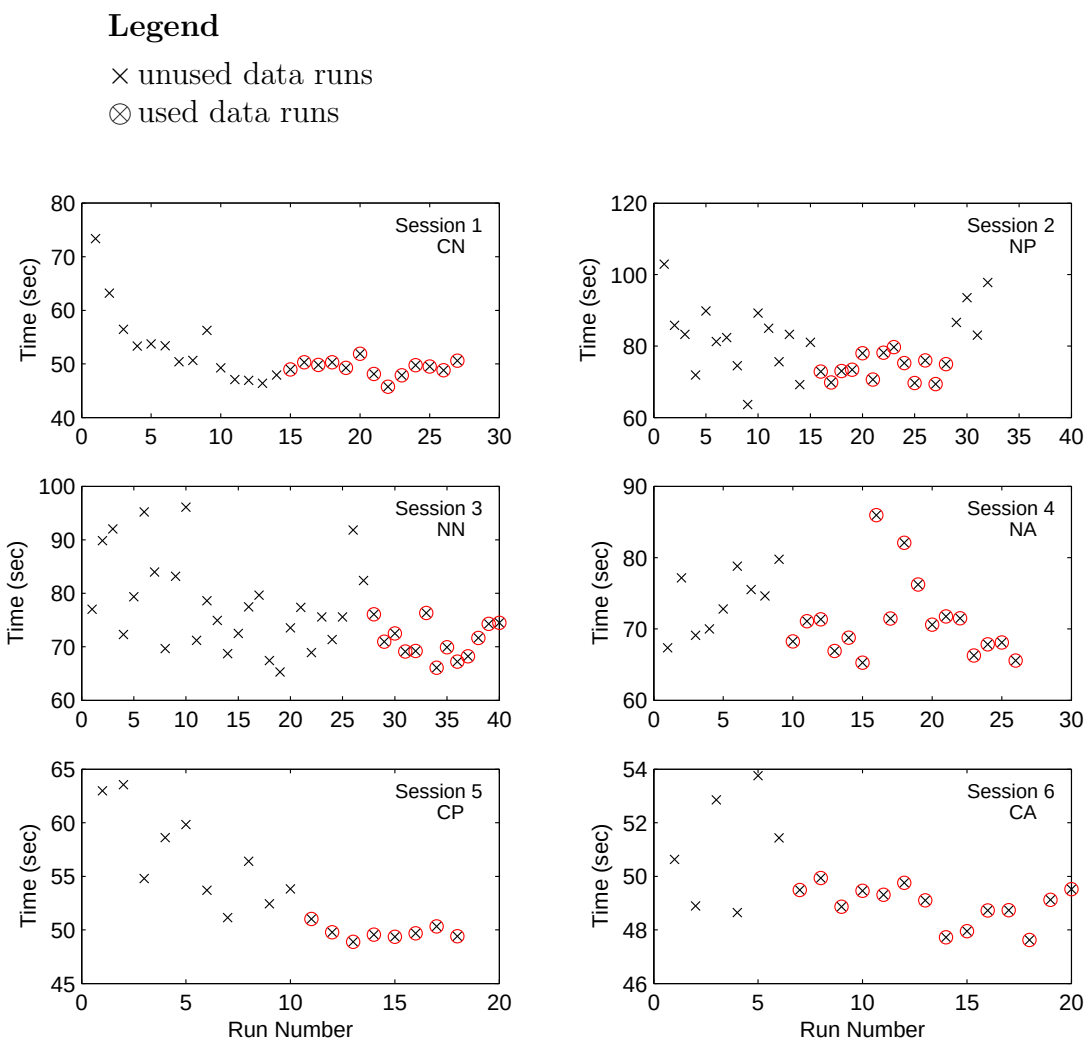

Figure E.34: Study 2: Subject 16 Run Times.

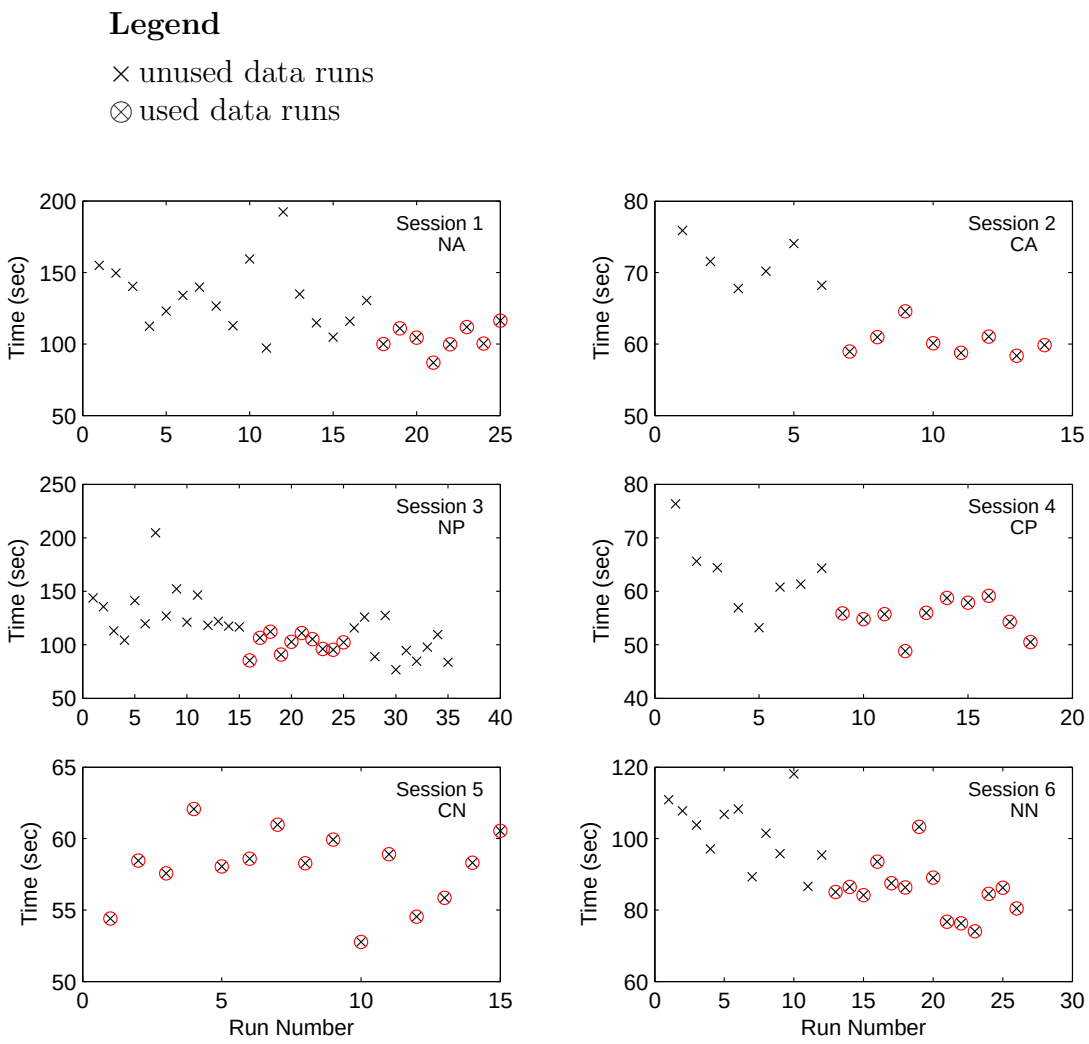

Figure E.35: Study 2: Subject 17 Run Times.

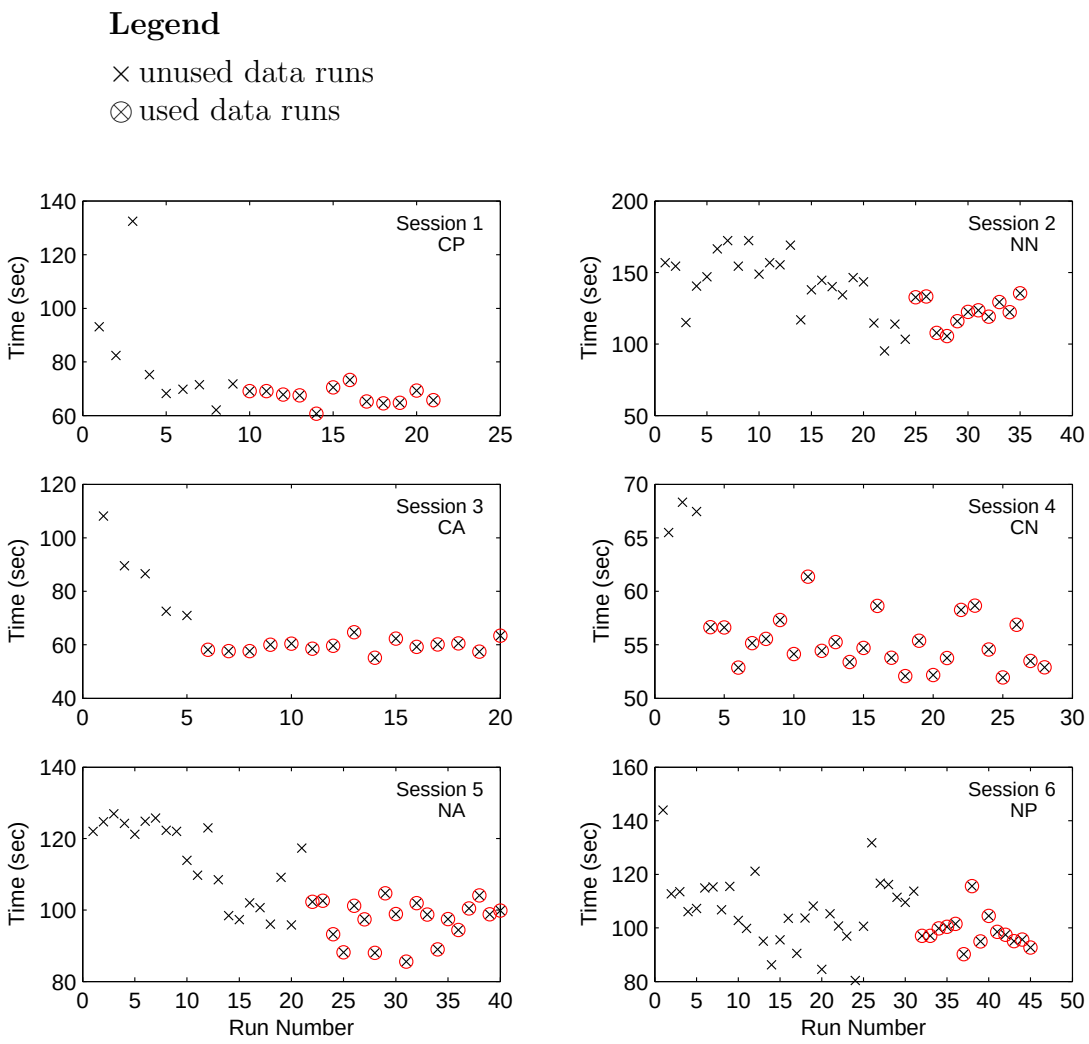

Figure E.36: Study 2: Subject 18 Run Times.

BIBLIOGRAPHY

Adams, J. A. (1961). Human tracking behavior. *Psychological Bulletin*, 58(1):55–79.

Adams, J. L. (1962). *Remote control with long transmission delays*. PhD thesis, Stanford University.

Arnold, J. E. and Braisted, P. W. (1964). Design and evaluation of a predictor for remote control systems operating with signal transmission delays. Technical Report NASA TN D-2229, National Aeronautics and Space Administration, Washington, D.C.

Backes, P. G. (1992). Ground-remote control for space station telerobotics with time delay. In Culp, R. D. and Zietz, R. P., editors, *Guidance and Control 1992: proceedings of the annual Rocky Mountain Guidance and Control Conference*, volume 78 of *Advances in the astronautical sciences*, pages 285–303.

Backes, P. G. (1994). Supervised autonomy for space telerobotics. In Skaar, S. B., Ruoff, C. F., and Seebass, A. R., editors, *Teleoperation and robotics in space*, volume 161 of *Progress in astronautics and aeronautics*, pages 139–158. American Institute of Aeronautics and Astronautics, Washington, D.C.

Backes, P. G., Peters, S. F., Phan, L., and Tso, K. S. (1996). Task lines and motion guides. In *IEEE International Conference on Robotics and Automation*, volume 1, pages 50–57.

Bejczy, A. K., Fiorini, P., Kim, W. S., and Schenker, P. (1995). Toward integrated operator interface for advanced teleoperation under time-delay. In *IROS '94. Proceedings of the IEEE/RSJ/GI International Conference on Intelligent Robots and Systems*, pages 563–570.

Bejczy, A. K. and Kim, W. S. (1990a). Predictive displays and shared compliance control for time-delayed telemanipulation. In *Proceedings of IEEE International Workshop on Intelligent Robots and Systems (IROS '90)*, pages 407–412.

Bejczy, A. K. and Kim, W. S. (1990b). Role of computer graphics in space telerobotics: preview and predictive displays. In de Figueiredo, R. J. P. and

Stoney, W. E., editors, *Proceedings of the Conference on Cooperative Intelligent Robotics in Space*, volume 1387, Bellingham, WA. SPIE-The International Society for Optical Engineering.

Berbert, A. G. and Kelley, C. R. (1962). Piloting nuclear submarines with controls that look into the future. *Electronics*, 35(23):35–39.

Bernotat, R. and Widlok, H. (1966a). Prediction display, a way of easing man's job in integrating control system. In Aseltine, J. A., editor, *Proceedings of the IFAC Symposium on Automatic Control in the Peaceful Uses of Space*, pages 541–549, New York. Plenum Press.

Bernotat, R. and Widlok, H. (1966b). Principles and applications of prediction display. *Institute of Navigation, Journal*, 19:361–370.

Bernotat, R. K. (1971). Prediction displays based on the extrapolation method. In Bernotat, R. K. and Gartner, K. P., editors, *Displays and Controls; the proceedings of the NATO Advanced Study Institute, 1971*, pages 95–114, Amsterdam. Swetz and Zeitlinger.

Black, J. H. (1971). Factorial study of remote manipulation with transmission time delay. Master's thesis, Massachussetts Institute of Technology.

Braisted, P. W. (1964). *Study of a predictor for remote control systems operating with signal transmission delays*. PhD thesis, Stanford University. Published by Dissertation Abstracts International, 25-02, 1113. (University Microfilms No. 64-7621).

Buzan, F. T. (1989). *Control of telemanipulators with time delay: A predictive operator aid with force feedback*. PhD thesis, Massachussetts Institute of Technology.

Cheng, C. (1991). *Predictor displays: Theory development and application to towed submersibles*. PhD thesis, Massachussetts Institute of Technology. Dissertation Abstracts International, 52, 5484B.

Conklin, J. E. (1957). Effect of control lags on performance of a tracking task. *Journal of Experimental Psychology*, 53(4):261–268.

Creamer, G. (2000). Unpublished class notes from ENAE 602: Attitude Space Dynamics and Controls, University of Maryland.

Dey, D. (1969). Prediction displays: A simple way of modeling. *Control Engineering*, 16:82–85.

Dey, D. (1971a). The influence of a prediction displays [sic] on the human transfer characteristics. In Bernotat, R. K. and Gartner, K. P., editors, *Displays and Controls; the proceedings of the NATO Advanced Study Institute, 1971*, pages 483–491, Amsterdam. Swetz and Zeitlinger.

Dey, D. (1971b). Results of the investigation of different extrapolation. In Bernotat, R. K. and Gartner, K. P., editors, *Displays and Controls; the proceedings of the NATO Advanced Study Institute, 1971*, pages 467–481, Amsterdam. Swetz and Zeitlinger.

Egeland, O. and Godhavn, J.-M. (1994). Passivity-based adaptive attitude control of a rigid spacecraft. *IEEE Transactions on Automatic Control*, 39(4):842–846.

Ferrell, W. R. (1965). Remote manipulation with transmission delay. *IEEE Transactions on Human Factors in Electronics*, 6:24–32.

Ferrell, W. R. (1966). Delayed force feedback. *Human Factors*, 8(5):449–455.

Fjellstad, O. and Fossen, T. I. (1994). Singularity-free tracking of unmanned underwater vehicles in 6 dof. In *Proceedings of the 33rd IEEE Conference on Decision and Control*, volume 2, pages 1128–1133.

Fjellstad, O., Fossen, T. I., and Egeland, O. (1992). Adaptive control of rovs with actuator dynamics and saturation. *Modeling, Identification and Control*, 13(3):175–188.

Fossen, T. I. and Sagatun, S. I. (1991). Adaptive control of nonlinear underwater robotic systems. *Modeling, Identification and Control*, 12(2):95–105.

Fossen, T. I. (1994). *Guidance and Control of Ocean Vehicles*. Wiley, New York.

Funda, J. (1991). *Teleprogramming: towards delay invariant remote manipulation*. PhD thesis, University of Pennsylavania.

Gottsdanker, R. M. (1952). The accuracy of prediction motion. *Journal of Experimental Psychology*, 43:26–36.

Gottsdanker, R. M. (1955). A further study of prediction-motion. *American Journal of Psychology*, 68:432–437.

Grubin, C. (1970). Derivation of the quaternion scheme via the euler axis and angle. *Journal of Spacecraft*, 7(10):1261–1263.

Grubin, C. (1979). Quaternion singularity revisited. *Journal of Guidance and Control*, 2(3):255–256.

Hannaford, B. (1994). Ground experiments toward space teleoperation with time delay. In Skaar, S. B., Ruoff, C. F., and Seebass, A. R., editors, *Teleoperation and robotics in space*, volume 161 of *Progress in astronautics and aeronautics*, pages 87–106. American Institute of Aeronautics and Astronautics, Washington, D.C.

Hannaford, B. and Kim, W. S. (1989). Force reflection, shared control, and time delay in telemanipulation. In *Proceedings of the 1989 IEEE International Conference on Systems, Man, and Cybernetics*, volume 1, pages 133–137.

Hayati, S. and Venkataraman, S. (1989). Design and implementation of a robot control system with traded and shared control capability. In *Proceedings of the 1989 IEEE International Conference on Robotics and Automation*, volume 3, pages 1310–1315.

Hossaini, L. S. (2000). The design and analysis of a second generation free flying underwater camera platform. Master's thesis, University of Maryland, College Park.

Ioannou, P. A. and Sun, J. (1996). *Robust Adaptive Control*. Prentice Hall, New Jersey.

Jones, B. and Kenward, M. G. (1989). *Design and Analysis of Cross-Over Trials*. Chapman and Hall, London.

Kane, T. R., Likins, P. W., and Levinson, D. A. (1983). *Spacecraft Dynamics*. McGraw-Hill Inc., New York.

Kelley, C. R. (1958). A predictor instrument for manual control. Appendix A of NTIS No. AD-234494: Developing and testing the effectiveness of the "predictor instrument". Paper presented at the eighth annual Office of Naval Research Human Engineering Conference, Ann Arbor, MI.

Kelley, C. R. (1960a). Developing and testing the effectiveness of the "predictor" instrument. Technical Report NTIS No. AD-234494, Office of Naval Research.

Kelley, C. R. (1960b). Further research on the predictor instrument. Technical Report NTIS NO. AD-253961, Office of Naval Research.

Kelley, C. R. (1962). Predictor instruments look into the future. *Control Engineering*, 9(3):86–90.

Kelley, C. R. (1969). Predictor display for remote roving surface vehicle control. *Proceedings of the SID*, 10(1):51–56.

Kelley, C. R., Mitchell, M. B., and Strudwick, P. H. (1964). Applications of predictor displays to the control of space vehicles. Technical report, NASA Office of Manned Space Flight.

Kelley, C. R., Mitchell, M. B., Wargo, M. J., and Prosin, D. J. (1966). The role of prediction in training with a simulated orbital docking task. Technical Report NTIS No. N66-38396, U.S. Naval Training Device Center, Orlando, FL.

Kelley, C. R. and Prosin, D. J. (1971). Adaptive displays. Technical Report NTIS No. N72-15110, Air Force Office of Scientific Research, Arlington, VA.

Khalil, H. (1996). *Nonlinear Systems*. Prentice Hall, New Jersey. 2nd ed.

Kim, W. S. (1990). Experiments with a predictive display and shared compliant control for time-delayed teleoperation. In *Proceedings of the 12th annual international Conference of the IEEE Engineering in Medicine and Biology Society*, pages 1905–1906.

Kim, W. S. (1996). Virtual reality calibration and preview/predictive displays for telerobotics. *Presence*, 5(2):173–190.

Kim, W. S. and Bejczy, A. K. (1991). Graphics displays for operator aid in telemanipulation. In *Proceedings of the IEEE Conference on Systems, Man, and Cybernetics*, pages 1059–1067.

Kim, W. S. and Bejczy, A. K. (1993). Demonstration of a high-fidelity predictive/preview display technique for telerobotic servicing in space. *IEEE Transactions on Robotics and Automation*, 9(5):698–702.

Kim, W. S., Schenker, P. S., and Bejczy, A. K. (1994). Graphics simulation and training aids for advanced teleoperation. In Skaar, S. B., Ruoff, C. F., and Seebass, A. R., editors, *Teleoperation and robotics in space*, volume 161 of *Progress in astronautics and aeronautics*, pages 182–189. American Institute of Aeronautics and Astronautics, Washington, D.C.

Klumpp, A. R. (1976). Singularity-free extraction of a quaternion from a direction-cosine matrix. *Journal of Spacecraft*, 13(12):754–755.

Lane, J. C. (2000). *Human factors optimization of virtual environment attributes for a space telerobotic control station*. PhD thesis, University of Maryland, College Park.

Leslie, J. M., Bennigson, L. A., and Kahn, M. E. (1966). Predictor aided tracking in a system with time delay, performance involving flat surface, roll, and pitch conditions. Technical Report NASA CR-75399; NTIS No. 66N27533, National Aeronautics and Space Administration, Washington, D.C.

Mar, L. E. (1985). Human control performance in operation of a time-delayed master-slave telemanipulator. Unpublished bachelor thesis, Massachusetts Institute of Technology.

Matsumoto, K. (1992). Space robot telemanipulation experiment using predictive display. In *Proceedings of the Eighteenth International Symposium on Space Technology and Science*, volume 1, pages 1137–1142.

McCoy, Jr, W. K. and Frost, G. G. (1965). Investigation of 'predictor' displays for orbital rendezvous: Program summary. Technical Report AMRL-TR-65-138; NTIS No. N66-21142, Aerospace Medical Research Laboratories, Wright-Patterson Air Force Base, OH.

McCoy, Jr, W. K. and Frost, G. G. (1966). Predictor display techniques for on-board trajectory optimization of rendezvous maneuvers. Technical Report AMRL-TR-66-60; NTIS No. AD-635918, Aerospace Medical Research Laboratories, Wright-Patterson Air Force Base, OH.

McCoy, Jr, W. K. and Frost, G. G. (1967). A predictor display for orbital rendezvous. Technical Report AMRL-TR-67-7; NTIS No. AD-645760, Aerospace Medical Research Laboratories, Wright-Patterson Air Force Base, OH.

McLane, R. C. and Wolf, J. D. (1965). Final research report on the experimental evaluation of symbolic and pictorial displays for submarine control. Technical Report (Honeywell Report No. 1550-FRI; NTIS No. AD-621706, Honeywell, Inc.

McLane, R. C. and Wolf, J. D. (1966). Symbolic and pictorial displays for submarine control. In *Proceedings of the 2nd Annual NASA-University Conference on Manual Control*, pages 213–228.

McLane, R. C. and Wolf, J. D. (1967). Symbolic and pictorial displays for submarine control. *IEEE Transactions on Human Factors in Electronics*, 8(2):148–158.

Noyes, M. V. (1984). Superposition of graphics on low bit rate video as an aid in teleoperation. Master's thesis, Massachusetts Institute of Technology.

Ogata, K. (1990). *Modern Control Engineering*. Prentice Hall, Englewood Cliffs, New Jersey.

Ott, R. L. and Longnecker, M. (2001). *An Introduction to Statistical Methods and Data Analysis*. Duxbury Press, Pacific Grove, California.

Paul, R., Lindsay, T., and Sayers, C. (1992). Time delay insensitive teleoperation. In *Proceedings of the 1992 IEEE/RSJ International Conference on Intelligent Robots and Systems*, pages 247–254.

Pennington, J. E. (1983). A rate-controlled teleoperator task with simulated transport delays. Technical Report NASA TM-85653, National Aeronautics and Space Administration, Washington, D.C.

Poulton, E. C. (1957). On prediction in skilled movements. *Psychological Bulletin*, 54(6):467–478.

Sanner, R. M. (1997). Unpublished class notes from ENAE 743: Nonlinear Control of Aerospace Systems, University of Maryland.

Sanner, R. M. (2001). Unpublished class notes from ENAE 788C: Adaptive and Nonlinear Control of Aerospace Vehicles, University of Maryland.

SAS (1999). *SAS OnlineDoc, Version 8 [On-line]*. Cary, North Carolina. Available: http://v8doc.sas.com/sashtml/.

Sheehe, P. R. and Bross, I. D. J. (1961). Latin squares to balance immediate residual and other effects. *Biometrics*, 17:405–414.

Shepperd, S. W. (1978). Quaternion from rotation matrix. *Journal of Guidance and Control*, 1(3):223–224.

Sheridan, T. B. (1966). Three models of preview control. *IEEE Transactions on Human Factors in Electronics*, 7(2):91–102.

Sheridan, T. B. (1972). Teleoperators and remote control. In Bernotat, R. K. and Gartner, K. P., editors, *Displays and Controls; the proceedings of the NATO Advanced Study Institute, 1971*, pages 215–226, Amsterdam. Swetz and Zeitlinger.

Sheridan, T. B. (1993). Space teleoperation through time delay: Review and prognosis. *IEEE Transactions on Robotics and Automation*, 9(5):592–606.

Sheridan, T. B. and Ferrell, W. R. (1963). Remote manipulative control with transmission delay. *IEEE Transactions on Human Factors in Electronics*, 4:25–29.

Sheridan, T. B. and Ferrell, W. R. (1974). *Man-Machine Systems: Information, Control, and Decision Models of Human Performance*. The MIT Press, Cambridge, Massachussetts.

Slotine, J.-J. E. and Li, W. (1991). *Applied Nonlinear Control*. Prentice Hall, New Jersey.

Smithanik, J. R. (2004). Optimal vision-based position estimation of an underwater space simulation robot. Master's thesis, University of Maryland, College Park.

Van Loan, C. F. (2000). *Introduction to Scientific Computing*. Prentice-Hall, Upper Saddle River, NJ. 2nd ed.

Warner, J. D. (1969). A fundamental study of predictive display systems. Technical Report NASA-CR-1274, National Aeronautics and Space Administration, Washington, D. C.

Warrick, M. J. (1949). Effect of transmission-type control lags on tracking accuracy. Technical report, Aero Medical Laboratory, Wright-Patterson AFB, OH. NASA Tech Rept No. 5916.

Wertz, J. R., editor (1978). *Spacecraft Attitude Determination and Control*. Kluwer Academic Publishers, Dordrecht, The Netherlands.

Williams, E. J. (1949). Experimental designs balanced for estimation of residual effects of treatments. *Australian Journal of Scientific Research*, 2:149–168.

Ziebolz, H. and Paynter, H. M. (1953). Possibilities of a two-time scale computing system for control and simulation of dynamic systems. In *Proceedings of the National Electronics Conference*, volume 9, pages 215–223.